UNIVERSITY OF LONDON THESIS

Degree PhD Year 2005 Name of Author GASTON-MASSUET C.

ROLE OF *ZIC* GENES DURING NEURULATION

Carles Gaston-Massuet

A thesis submitted for the degree of Doctor of Philosophy in the University of London

July 2004

Neural Development Unit
Institute of Child Health
University College London
30 Guilford Street
London
WC1N 1EH

ProQuest LLC
789 East Eisenhower Parkway
P.O. Box 1346
Ann Arbor, MI 48106-1346

DEDICACIÓ

M'agradaria dedicar aquesta tesi a la meva família i a dos bons amics

I would like to dedicate this thesis to my family and two good friends

Xavier Gaston i Maria Teresa Massuet

Emma Gaston i Xavier Cuadrat

Laia Gaston i Pere Canal

Eulàlia Bosch

Joan Carles Fernàndez i Imma Massuet

Aina, Núria, Mireia i Laura Fernàndez

Vincent Goyon i David Paratge

ABSTRACT

Neurulation is the embryonic event that results in formation of the neural tube, the primordium of the central nervous system. Impairment of this process leads to neural tube defects (NTDs), which are among the commonest congenital malformations in humans. *Zic1, 2, 3* and *4* encode a family of 2C2H-like zinc finger transcription factors of which two members, *Zic2* and *Zic3,* have been implicated in the causation of NTDs. The aim of this thesis was to investigate the function of *Zic* genes during neural tube closure in the mouse embryo.

The expression of *Zic* genes was examined at the time of neurulation by *in situ* hybridisation. All 4 *Zic* genes have partially overlapping but distinct expression domains, with *Zic2* and *Zic3* mRNA detected at the posterior neuropore region, consistent with the occurrence of spina bifida and sacral agenesis in *Zic2* and *Zic3* mutants. Expression of *Zic2* was not altered during abnormal neurulation in the mouse mutants *ct*, *Lp* and Sp^{2H}, indicating that *Zic2* does not act downstream of these mutant genes in the production of NTDs. *Zic3* expression was also unaffected in the *ct* and Sp^{2H} mutants but showed downregulation in *Lp* homozygous embryos, suggesting that *Zic3* may be regulated downstream of the *Lp* gene.

A novel ENU-generated mouse model of spina bifida, the *Kumba* mouse ($Zic2^{Ku}$), carries a mutation in the zinc finger domain region of *Zic2*. Morphological analysis of neurulation in $Zic2^{Ku/Ku}$ embryos showed that *Zic2* is required for normal bending of the neural plate. Absence of dorsolateral bending during neural tube closure can explain the subsequent development of spina bifida in $Zic2^{Ku/Ku}$ embryos.

In order to understand the molecular pathway by which Zic2 mediates its function, the yeast two-hybrid system was used to identify protein-binding partners. *Capicua, p53 binding protein 1, Glis2* and *Krox20* were among a series of genes whose protein products were found to interact with Zic2. These protein-protein interactions were confirmed by co-immunolocalisation studies of cultured transfected cells and by glutathione-S-transferase pull-down assays. *In situ* hybridisation studies demonstrated that *Capicua* is expressed in the posterior neuropore region of E9.5 embryos consistent with a role of these proteins in Zic2-dependent spina bifida.

In conclusion, this thesis has established an early embryonic role for Zic2 in low spinal neurulation and has identified several binding proteins that may participate with Zic2 in the regulation of neural tube closure.

ACKNOWLEDGEMENTS

I would like to thank all the people that have been, directly or indirectly, involved in the production of this thesis. Without their help I would not have finished this thesis and therefore I would like to thank them.

Special gratitude goes to my supervisor Dr. Andrew Copp for allowing me to carry out this research in his laboratory, for his patience, encouragement and valuable supervision. Also for their supervision I would like to thank Dr. Deborah Henderson and Dr. Nick Greene, they have always been there to answer my questions and are the pillars of this work.

This work would not have been possible without the help of other scientists that introduced me to the techniques used throughout this thesis. Some of them have left the laboratory to become independent scientists or are working in other laboratories as post-doctoral researchers. A warm thanks goes to Dr. Jennifer Murdoch for teaching me most of the molecular biology techniques and most importantly for transmitting her enthusiasm for science even when the experiments did not work. Thanks to Patricia Cogram for her helpful discussions on science, for teaching me the immunohistochemistry techniques and for being a good colleague that I will always remember. The yeast two-hybrid experiments would not have been possible without the training of Dr. Ania Koziell and Dr. Sugi Hassain that provided me with protocols, advice and reagents. Dr. Caroline Paternotte deserves my gratitude for teaching me how to use the sequencing machine and for her willingness to proof-read this thesis. Thanks also to Dr. Ruth Arkell for providing me with the *Kumba* mice and to Katie Gardener for transferring the *Kumba* embryos to establish the colony.

The beloved and always present "end of 2000 junior crowd" Gemma Brindley, Louisa Dunlevy and Ailish Murray. I will always remember their help when our skills were so poor that we could hardly use a pipette. They have been the best colleagues one

could ever have at work and outside work. I will never forget our B&B breaks to get out of London on a cheap airline.

Simon Lee has also been a great help in teaching me laboratory techniques; he always has a new protocol that he has optimised. Dr. Juan Pedro Martinez-Barbera and Massimo Signore made sure that cloning was not a problem for me and for their always very good advice in laboratory meetings. Thanks to Dr. Clare Faux and Jenny Nixon for developing my radioactive gels when I was too busy and to Dawn Savery for looking after the mouse colony and maintaining the double mutants crosses while I was writing.

I could not forget Brenda Gilliver who was the unit administrator for half of my PhD. Her capacity for multitasking has allowed me to be able to attend international meetings and to meet important deadlines. She will be remembered and missed in the unit for her ability to deal with a hundred things at one time. Also for her support and indispensable help a big thanks goes to Diane Austin, thanks ever so much for autoclaving all my solutions always on time throughout my PhD and for being a good friend.

Thanks to Dr. Patricia Ferretti for providing me with office space for the first year of my PhD and to the DB unit for sharing reagents and advice. To the Friday evening club, Dr. Jean-Marie Delalande, Dr. Gustavo Sajnani, Dr. Sara Reid, Dr. Alan Burns, Dr Patricia Ybot-Gonzalez and Adam Wallace, you have been great fun.

Out of the laboratory I would like to mention a good friend, Roberto Cabarcos. He has genuinely supported me during my thesis, believing in what I do and making sure that I did not isolate myself too much. The last and very important thanks goes to Noraishah Abdul Aziz for her enthusiasm, sanity and insanity in our long hours spent in the lab. To all of them thank you and keep it up.

The British Heart Fundation and the Welcome Trust funded the work in this thesis.

TABLE OF CONTENTS

LIST OF FIGURES

LIST OF TABLES

ABBREVIATIONS

3AT	3-amino-1,2,4-triazole
AA	Amino acid
AD	Activation domain
BLAST	Basic Local Alignment Search Tool
Bp	base pair
BSA	Bovine serum albumin
cDNA	Complementary deoxyribonucleic acid
CIP	Calf intestine phosphatase
DAPI	4'-6-diamidino-2-phenylindole
DBD	DNA binding domain
ddH_20	distilled deionised water
DEPC	Diethyl pyrocarbonate
DIC	Differential interference contrast (Nomarski)
DLHP	Dorsolateral hinge point
DMEM	Dulbecco's Modified Eagle's Medium
DMSO	Dimethyl sulfoxide
DNA	Deoxyribonucleic acid
dNTP	deoxynucleoside triphophate
E	Embryonic day
EDTA	Ethylenediaminetetraacetic acid
EMSA	Electrophoresis mobility shift assay
EST	Expressed sequence tag
Ex	Excencephaly
FCS	Foetal calf serum

GAG	Glycosaminoglycan
GPI	Glycosylphophatidylinositol
GST	Glutathione-S-transferase
HH	Hedgehog
HMG	High mobility group
IPTG	Isopropyl-1-thi-β-D-galactosidase
kb	Kilo base
kD	Kilo Daltons
LB	L-broth
LMP	Low melting point
MHP	Median hinge point
NCBI	Nation Centre for Biotechnology Information
NLS	Nuclear localisation signal
NTDs	Neural tube defects
NTMT	Sodium chloride/Tris/magnesium chloride/Tween buffer
OD	Optic density
PBS	Phosphate buffer saline
PCD	Programmed cell death
PCP	Planar cell polarity
PFA	Paraformaldehyde
PNP	Posterior neuropore region
r	Rhombomere
RPM	rotation per minute
RT	Reverse transcription
Sb	Spina bifida
SD	Synthetic defined medium

SDS	Sodium dodecyl sulphate
SDS-PAGE	Sodium dodecyl sulfate polyacrylamide gel electrophoresis
Shh	Sonic hedgehog
SSC	Sodium chloride
SSCP	Single stranded length polymorphism
SSLP	Simple sequence length polymorphism
TUNEL	Terminal deoxynucleotidyltransferase-mediated UTP end labelling
Xgal	5-bromo-4-chloro-3-indolyl-β-D-galactoside
YPAD	Yeast extract, peptone, adenine and dextrose rich medium
ZFD	Zinc finger domain

CHAPTER 1: GENERAL INTRODUCTION

1.1 INTRODUCTION

The formation of the vertebrate nervous system begins at gastrulation when, during neural induction, a subset of ectodermal cells segregates and thickens to form the neural plate. Soon afterwards, the neural plate undergoes a series of morphogenetic events that ends with the formation of a hollow neural tube characteristic of the chordate phylum, this process being known as neurulation. Impairment of neurulation leads to a range of anomalies known as neural tube defects (NTDs) that are among the commonest congenital malformations in humans.

The embryonic process of neurulation has been well characterised morphologically in different animals models (Colas and Schoenwolf, 2001;Schoenwolf, 1985;Shum and Copp, 1996). Some of the genetic pathways controlling this programme have been identified from the large number of mouse mutants that display NTDs (Juriloff and Harris, 2000;Copp *et al.*, 2003b). However, the underlying molecular mechanisms are still largely unknown. The aim of the work presented in this thesis is to elucidate the function of *Zic* genes, in particular *Zic2*, in the process of neural tube closure. In order to be able to understand the involvement of *Zic2* in the causation of NTDs it is necessary first to consider what is currently known about the normal process of neurulation and the *Zic* gene family.

1.2 THE NORMAL PROCESS OF NEURULATION

Neurulation is divided into two parts: primary and secondary neurulation. Primary neurulation results in the formation of the cranial neural tube and the upper spinal cord rostral to the mid-sacral region, through a process that involves the specification and shaping of the neural plate, followed by the elevation and fusion of the neural folds (Criley, 1969). Initially, the neural plate becomes specified by the underlying mesoderm

and is transformed into a pseudo-stratified columnar epithelium that thickens apicobasally. The edges of the columnar epithelium elevate to form the neural folds that converge in the dorsal midline and fuse, forming the neural tube. Once primary neurulation has occurred and the neural tube has closed, secondary neurulation takes place caudally to the mid-sacral region. At this axial level, the neural tube forms by condensation of mesenchymal cells within the tail bud region which forms an (Criley, 1969)
epithelium that subsequently cavitates, forming the secondary neural tube (Schoenwolf, 1984;Copp and Brook, 1989). Secondary neurulation is a separate autonomous process in relation to primary neurulation, at least in the chick embryo, where if primary neurulation is disrupted experimentally secondary neurulation still occurs normally (Costanzo *et al.*, 1982).

1.2.1 Primary neurulation occurs in a cranio-caudal sequence

During primary neurulation in the mouse embryo, closure of the neural tube starts at three different initiation sites, in a cranio-caudal sequence along the body axis (Fig 1.1) (MacDonald *et al.*, 1989;Copp *et al.*, 1990;Golden and Chernoff, 1993). The first initiation site, Closure 1, occurs in the mouse embryo at the 4-6 somite stage with closure occurring at the cervical/hindbrain region and continuing in a zippering-like fashion caudally along the future spine and rostrally into the hindbrain. By the 12 somite stage, a second site of closure, Closure 2, occurs at the forebrain/midbrain boundary and proceeds caudally into the midbrain and rostrally into the forebrain. At about the same somite stage, a third site of closure, Closure 3, occurs at the rostral extremity of the prosencephalon, and proceeds caudally towards the midbrain. As a result of these three *de novo* sites of closure, three neuropores become apparent. The anterior neuropore (within the forebrain, formed by closure progression from Closures 2 and 3) closes at approximately the 17 somite stage. Soon afterwards, the hindbrain neuropore (formed by progression from Closures 1 and 2) closes, and the zippering

mechanism initiated at Closure 1 spreads caudally, resulting in the closure of the posterior neuropore at the 29 somite stage.

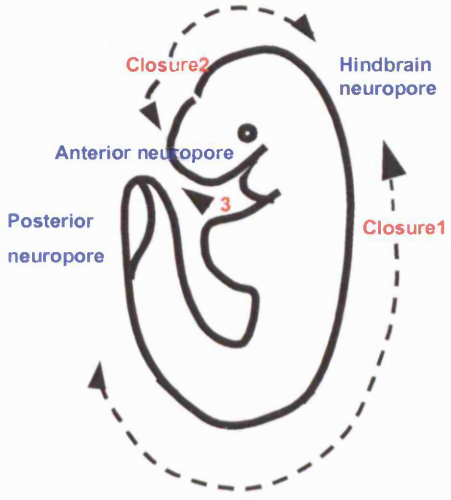

Figure 1.1 Initiation sites of neural tube closure

Diagram to illustrate the three sites of *de novo* initiation of neural tube closure and the three neuropores during primary neurulation. From Copp (1994)

The developmental stage and exact position in which the events of neurulation take place vary between mouse strains (Juriloff *et al.*, 1991). Hence, the site of Closure 2 is polymorphic between mouse strains and its position confers susceptibility to cranial neural tube defects (Fleming and Copp, 2000).

1.2.2 The spectrum of NTDs depends on which of the events of neurulation fail to be completed

The spectrum of NTDs depends on which of *de novo* closure sites or neuropore closures fail to be completed (Fig. 1.2)(Copp and Bernfield, 1994). Hence, failure of initiation of Closures 2 and 3 or incomplete closure of the anterior or hindbrain

neuropores leads to an open cranial neural tube termed exencephaly. The second type of NTD, lumbosacral spina bifida results from failure of the posterior neuropore to complete closure. The size and severity of the lesion depends upon the axial level where closure failed. Hence if closure stops at a more rostral level this results in a more severe phenotype. Cranial NTDs and spina bifida can occur independently or in combination, in humans and in mouse. Failure of initiation of Closure 1 causes craniorachischisis, the most severe form of NTD, in which the hindbrain and spinal neural tube remain open (Fig. 1.2). In the mouse models that display craniorachischisis, Closures 2 and 3 occur, and development of the forebrain and rostral midbrain appear normal (Greene *et al.*, 1998;Murdoch *et al.*, 2001). These observations indicate that the genetic regulation of Closure 1 differs from that of Closures 2 and 3.

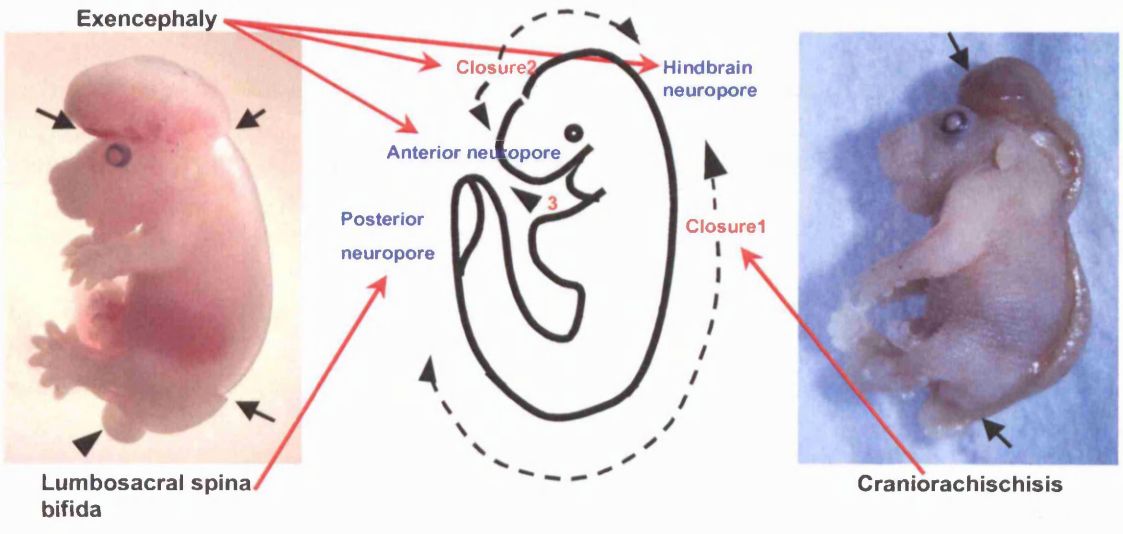

Figure 1.2 The three main subtypes of NTDs

Diagram to illustrate exencephaly, craniorachischisis and lumbosacral spina bifida, which result from failure of closure initiation events or from failure of each neuropore to complete closure. The embryo on the left shows exencephaly and lumbosacral spina bifida whilst the embryo on the right shows craniorachischisis (diagram modified from A. Copp, 1994, note that the black arrowhead shows curled tail).

1.2.3 Morphological changes during primary neurulation: convergent-extension, elevation, bending and apposition

Immediately after its formation, the neural plate elongates rostro-caudally, thickens apico-basally and narrows medio-laterally (Schoenwolf, 1985). Several cellular processes have been implicated in the initial remodelling of the neural plate, including caudal migration of midline cells as the primitive streak regresses, intercalation of neuroepithelial cells in the midline due to convergent-extension movements, and microfilament constriction of neuroepithelial cells (Detrick *et al.*, 1990). As I will describe later, disruption of these initial processes leads to failure of Closure 1 and the most severe form of NTD, craniorachischisis.

The neural folds appear by elevation and bending of the lateral edges of the neural plate at either side of the midline. The morphology that the neural plate acquires during closure differs in the cranial and spinal neural tube. In the midbrain region of the cranial neural tube, the neural folds initially adopt a biconvex shape as they elevate. Subsequently, the lateral edges bend inwards to form the dorsolateral hinge points (DLHPs), which bring the apices of the neural folds into apposition at the dorsal midline (Morriss-Kay, 1981;Morriss-Kay *et al.*, 1994).

As the wave of spinal neural tube closure spreads down the body axis, the morphology of the neural plate at the spinal cord region changes in a stereotypic fashion (Shum *et al.*, 1996). Three distinct morphologies (named Modes of neurulation) have been reported, from the cross-sectional appearance of the neural plate at different axial levels (Fig.1.3). In Mode 1 spinal neurulation, which is seen in the closing posterior neuropore at the 7-15 somite stage, the neural plate bends medially forming the median hinge point (MHP), whilst the lateral edges elevate with straight sides and the neural folds approach each other in the dorsal midline, closing the neural tube to form a slit-like lumen.

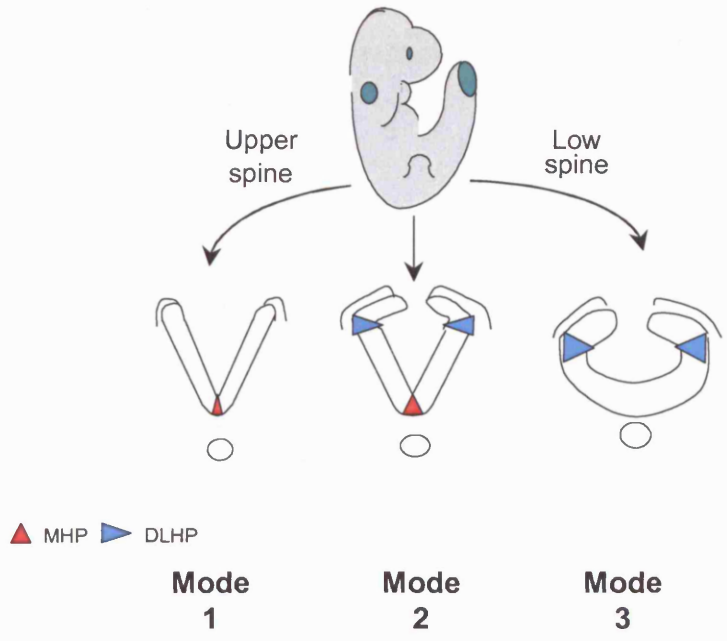

Figure 1.3 Diagram to illustrate the morphology of the neural plate during progressive closure of the posterior neuropore

Mode 1 is characterised by formation of a MHP with straight neural folds apposing each other. In Mode 2 of neurulation the neural plate bends medially to form the MHP and dorsally the neural folds bend bilaterally to form the DLHPs. In Mode 3 of neurulation, closure is solely dependent on DLHPs. Diagram modified from Ybot-Gonzalez (2001)

At the 16-24 somite stage, when Mode 2 spinal neurulation occurs, the neural plate bends not only at the midline, forming the MHP, as in Mode 1, but the dorsal region of each neural fold also bends forming the dorso-lateral hinge points (DLHPs). DLHPs cause the tips of the neural folds to appose in the dorsal midline yielding a closed neural tube with a diamond shaped lumen. At the 25-30 somite stage, in Mode 3 of spinal neurulation, the neural plate does not form a MHP, whereas DLHPs are prominent, closing the neural tube to form a circular shaped lumen. These stereotypical changes in morphology of the spinal neuroepithelium as it closes to form the neural tube have been observed in mouse neurulation. In other models, such as the chick, DLHP formation

occurs in the hindbrain region, and in the spinal level in the most caudal end, although DLHPs are not as prominent as in mouse (Schoenwolf, 1985).

1.3 NTDS IN HUMANS

1.3.1 Types of neural tube defects in humans

NTDs are among the commonest congenital malformation in humans with an average prevalence of 1:1000 live births worldwide (Edmonds and James, 1993). Human NTDs can be divided into open and closed defects. Open NTDs result from failure of the neural tube to close during primary neurulation, whilst closed NTDs results from aberrant secondary neurulation and abnormal axial skeleton development (Lemire, 1988). As in mouse, open NTDs can be grouped depending on which event of closure fails to occur (Van Allen *et al.*, 1993). Exencephaly, open neural tube in the cranial region, can be sub-grouped into three classes. Rostrally, failure of closure 3 at the forebrain region with facial clefting leads to anencephaly. Failure of Closure 2, results in an open midbrain-hindbrain and is named holocrania, whilst failure of closure of the hindbrain neuropore results in merocrania.

As in mouse, spina bifida results from failure of closure of the PNP resulting in an open caudal neural tube that can be exposed (myelocele) or covered by meninges (myelomeningocele). Craniorachischisis is the most severe NTD, and the neural tube remains open along almost the entire rostro-caudal axis.

Neurulation in humans starts at 17-18 days post fertilisation and ends by 26-28 days after fertilisation with closure of the PNP (Campbell *et al.*, 1986). In humans, as in mouse, the initiation of neural tube closure is discontinuous (Van Allen *et al.*, 1993), and sites of initiation equivalent to Closure 1 and Closure 3 have been described (Golden and Chernoff, 1995;Juriloff *et al.*, 2000), although some studies do not identify (Nakatsu et al., 2000)
Closure 2 (O'Rahilly and Müller, 2002). Humans undergo secondary neurulation in the

low sacral and coccygeal region. Despite failure in neural tube closure, neural differentiation and nerve connections can occur (Campbell *et al.*, 1986). However tissue exposure to the amniotic fluid results in degeneration of the open neural tube leading to musculoskeletal, gastrointestinal and urinary dysfunction often associated in NTDs patients (Stark, 1977). This has also been observed in *curly tail* and *Splotch delayed* NTDs mutant mice, were neuronal differentiation occurs normally whilst degeneration occurs at later stages of gestation due to exposure to the environment (Keller-Peck CR, 1996).

1.3.2 Multifactorial aetiology of human NTDs

Human NTDs have multifactorial aetiology, involving genetic and environmental factors (Campbell *et al.*, 1986;Copp *et al.*, 1994;Juriloff *et al.*, 2001). The most important environmental factors are geography, maternal age, socio-economic class, maternal diet and illness.

The relationship between prevalence of NTDs and geography is noticeable. For instance, prevalence of NTDs is higher in the north west of England than in the south east (Carter, 1974). A correlation has also been found between the month of conception and prevalence of NTDs. (Dallaire *et al.*, 1984) Maternal age is also important in prevalence of NTDs since the majority of affected children are born to mothers under 20 years or over 35 years of age. (Bound *et al.*, 1991; Buccimazza *et al.*, 1994) Several studies have shown an association between socio-economic class and the prevalence of NTDs, the prevalence being higher in poor socio-economic backgrounds. This observation prompted investigation on the effects of the diet in prevalence of NTDs. Indeed, supplementing mothers with folic acid or multivitamins has shown a reduction in the prevalence of NTDs (Wald *et al.*, 1991;Czeizel and Dudás, 1992). A correlation has also been found between maternal illness, including higher fever, during the first month of pregnancy and an increase in the risk of NTDs. (Soler *et al.*, 1976; Hunter *et al.*, 1986)

The genetic component of NTDs is supported by family studies showing that siblings of affected individuals have a ten times greater risk of NTDs than the background prevalence (Campbell *et al.*, 1986). In addition, an increased risk is observed in offspring of affected parents (Blatter *et al.*, 1997). However, the inheritance

of NTDs does not follow a pattern of single-gene inheritance, but rather follows a pattern of a multigenic inheritance with strong environmental influence (Campbell *et al.*, 1984;Juriloff *et al.*, 2000). These factors have made the identification of genes for human NTDs difficult. In some cases a mutation in a gene that could be responsible for the NTD phenotype has been found in a patient but also in unaffected relatives, indicating that the mutation may confer susceptibility but is not causative for NTDs. Moreover some of the genetic studies do not take into consideration the phenotypical spectrum of NTDs, and look for linkage or causative mutations within a group of heterogeneous NTDs: spina bifida, exencephaly and craniorachischisis without considering that specific genes may regulate just one aspect of neural tube closure. For instance, targeted disruption of *Msx2* has been shown to cause exencephaly in mouse (Liu *et al.*, 1995) and this prompted an investigation to determine whether mutations in *MSX2* in humans could also cause NTDs (Stegmann *et al.*, 2001). The study concluded that, despite identifying one deletion in one patient from 204 NTD cases, there was no statistical significance for the implication of *MSX2* in human NTDs. However from the 204 patients with NTD analysed, only 13 displayed cranial NTDs (also including craniorachischisis). Hence, this study included only a very small cranial NTD sample (Stegmann *et al.*, 2001), despite this phenotype being most likely *Msx2*-related based on the mouse studies.

Mutations in the *PAX3* gene have been found in patients with NTDs (Hol *et al.*, 1995). However, a second population study using 194 people among 50 NTD cases failed to find an association between the *PAX3* and NTD (Chatkupt *et al.*, 1995). A mutation in *SLUG*, a zinc finger transcription factor involved in neural crest development, was found in a human patient with NTD. Moreover, the mutation was not present in unaffected individuals raising the possibility that *SLUG* could be causative of the NTD observed in this patient (Stegmann *et al.*, 1999). A mutation in *PAX1* was

detected in a single patient with spina bifida, suggesting that this gene can also act as susceptibility factor (Joosten *et al.*, 1998).

Further genetic studies have centred on identifying mutations in enzymes that act in the folic acid pathway. The importance of folic acid in NTDs comes from studies indicating a protective effect of folic acid administration during the periconceptional period (Wald *et al.*, 1991). This prompted studies to identify mutations in genes that participate in the biochemical pathways involving folic acid, which may confer susceptibility to NTDs. A polymorphism in the 5,10-methylene-tetrahydrofolate reductase gene (*MTHFR*) has been found to confer a two-fold increased risk of NTDs in some populations (Van der Put *et al.*, 1995; Botto and Mastroiacovo, 1998), although there is no association with NTDs in other populations. *MTHFR* encodes an enzyme that catalyses the conversion of 5,10-methyl-tetrahydrofolate to 5-methylene-tetrahydrofolate. Homozygous individuals for the C677T polymorphism are predisposed to mild hyperhomocysteinemia when their folate status is low. The precise mechanism that confers susceptibility to NTDs in individuals homozygous for the C677T is unknown.

1.4 THE EMBRYONIC PROCESS OF SPINAL NEURULATION

After Closure 1 has occurred at the cervical-hindbrain region, closure of the spinal neural tube continues caudally forming the posterior neuropore. Failure of the posterior neuropore to complete closure leads to spina bifida. The embryonic mechanism that control closure of the posterior neuropore can be autonomous to the neural plate (intrinsic forces) or non-autonomous to the neural plate (extrinsic forces) (Colas *et al.*, 2001;Smith and Schoenwolf, 1997;Copp *et al.*, 2003b).

1.4.1 Intrinsic forces control morphogenesis of the neural plate

As spinal neurulation progresses along the body axis the neural plate bends in specific dorsoventral locations (Fig. 1.3). The MHP forms in contact with the notochord and the DLHPs form bilaterally in contact with the surface ectoderm (Shum *et al.*, 1996;Ybot-Gonzalez *et al.*, 2002). Bending in these regions has been suggested to be mediated by intrinsic forces so that the behaviour of neuroepithelial cells changes compared to those in the non-bending regions. Indeed, morphological studies in chick revealed that in the neuroepithelial cells can adopt one of three types of morphology: spindle-shape, wedge-shape and inverted wedge-shape cells (Smith *et al.*, 1994). In the MHP and DLHP the majority of the cells acquire a wedge-shape morphology which results from an expansion of the basal surface of the cell compared to its apical surface. In contrast, in the non bending regions, spindle-shape cells and inverse-wedge cells are in the majority (Smith *et al.*, 1994). Two different mechanisms have been proposed that result in cell wedging: constriction of apical microfilaments and changes in the cell cycle.

1.4.1.1 Constriction of apical microfilaments

A pseudostratified epithelium bends if its apical surface area is reduced with respect to its basal surface area. The reduction in apical surface area has been proposed to be mediated through the constriction of apical containing microfilaments in a purse-string fashion (see Fig. 1.4)(Karfunkel, 1974;Nagele and Lee, 1980;Sadler *et al.*, 1982). Indeed, microfilaments and cytoskeleton-associated proteins, such as actin, MARCKS, vinculin, spectrin and Shroom are localised apically during neural plate morphogenesis (Hildebrand and Soriano, 1999;Nagele *et al.*, 1980;Sadler *et al.*, 1982;Stumpo *et al.*, 1995;Xu *et al.*, 1998;Ybot-Gonzalez and Copp, 1999;Haigo *et al.*, 2003).

To test the function of the cytoskeleton in neurulation experimentally, actin microfilaments polymerisation has been disrupted in embryo culture using cytochalasins

and calcium chelating agents (Morriss-Kay and Tuckett, 1985;Ybot-Gonzalez *et al.*, 1999). In these experiments cranial neural tube closure was inhibited, whilst spinal neural tube closure occurred normally, indicating that cytoskeleton integrity is required for cranial neurulation whilst its loss is not detrimental for spinal neural tube closure (Ybot-Gonzalez *et al.*, 1999). However treatment of embryos with cytochalasin D prior to Closure 1 inhibited this closure site, resulting in a craniorachischisis-like phenotype (Ybot-Gonzalez *et al.*, 1999). It appears then that initiation of closure is dependent on the actin cytoskeleton but once Closure 1 has occurred, disruption of the actin cytoskeleton does not affect the continuation and completion of spinal neural tube closure.

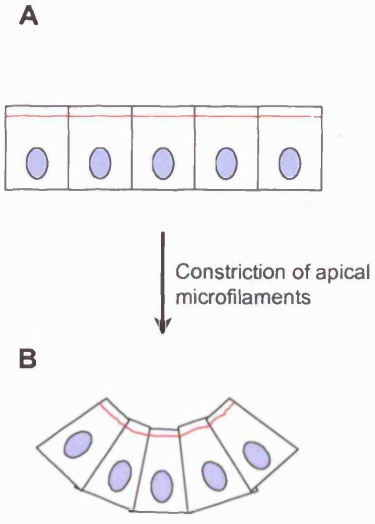

Figure 1.4 Constriction of apical filaments and bending of neural plate

Diagram to illustrate how constriction of apical microfilaments could generate bending of the neuroepithelium by reducing the apical surface area respective to the basal surface area.

This observation is partially supported by the findings that mouse mutants for cystokeletal or putative cytoskeletal dynamics proteins exhibit exencephaly but

generally not spina bifida (Copp *et al.*, 2003b). For instance, null embryos for MARCKS, the actin-binding protein vinculin, compound mutants for the Abl and Arg tyrosine kinases or for the protein kinase a subunits Cα/Cβ1 all display exencephaly but not spina bifida (Stumpo *et al.*, 1995;Koleske *et al.*, 1998;Xu *et al.*, 1998;Huang *et al.*, 2002). This supports the idea that cytoskeleton integrity is more important for cranial neurulation than spinal neurulation. However, it could also indicate that these genes are not expressed in the lower spinal regions, which would explain the lack of spina bifida in these mutants. Indeed, two mutants for cytoskeleton-related proteins, Shroom and MARKS-related (also called MacMARCKS) protein, develop spina bifida at low frequency (Hildebrand *et al.*, 1999;Wu *et al.*, 1996). Interestingly, Shroom has been shown to be required for apical microfilament constriction in polarised epithelial cells and to regulate hinge point formation in *Xenopus* (Haigo *et al.*, 2003). More studies are required to rule out a critical role for the actin cytoskeleton during mouse spinal neurulation and to establish whether the cytoskeleton functions simply to stabilise the neural plate once the bending has occurred.

1.4.1.2 Cell wedging mediated through changes in the cell cycle

The neuroepithelium is formed by a single pseudostratified cell layer in which the nucleus of each cell migrates from the basal surface to the apical surface and back to the basal surface, a phenomenon known as interkinetic nuclear cell migration (Langman *et al.*, 1967). Studies in chick embryos have shown that the positioning of the nucleus from basal to apical position is linked to the cell cycle (Smith and Schoenwolf, 1987) such that, during mitosis, nuclei are localised at the apical surface generating inverse wedge-shape cells, during G1 and G2 phases nuclei are located between apical and basal surfaces, creating a spindle-shape, and in S phase, nuclei are located basally, generating wedge-shape cells. If a subset of cells have their nuclei in a basal position, this can potentially generate wedge-shape cells by increasing the basal surface area

(Sauer, 1935)

respective to the apical surface area. Indeed, cells that form the MHP are mostly wedge-shaped and have longer S phase of the cell cycle and shorter M phase (Smith *et al.*, 1987;Smith and Schoenwolf, 1988). Hence, localised changes in the neuroepithelial cell cycle can generate specific sites of bending of the neural plate (see Fig. 1.6). These observations have been shown for the MHP in chick and mouse embryos. A similar mechanism could account for bending at the DLHP, although this has not been proven yet.

1.4.2 Extrinsic forces drive spinal neurulation

During neurulation the neuroepithelium is in contact with the surface ectoderm, the endoderm and the mesoderm. Changes in cell shape and/or cell number in these tissues can provide extrinsic forces that could assist neural plate folding (Schoenwolf, 1985). To test this hypothesis tissue isolation experiments in chick and mouse embryos, where the lateral mesoderm and endoderm tissues are removed, have been performed and result in normal folding of the spinal neural plate (Alvarez and Schoenwolf, 1992;Van Straaten *et al.*, 1993;Ybot-Gonzalez *et al.*, 2002). However, if the surface ectoderm is removed, the neural plate fails to bend dorsolaterally in both chick and mouse resulting in an open neural tube (Alvarez *et al.*, 1992;Ybot-Gonzalez *et al.*, 2002). This indicates that, of all the lateral tissues, only the surface ectoderm is sufficient and necessary for formation of DLHPs. One hypothesis to explain the extrinsic role of the surface ectoderm has been formulated from experiments in chick embryos, suggesting that medial expansion of the surface ectoderm through convergent extension movements could potentially provide the force that brings the paired neural folds together (Alvarez *et al.*, 1992).

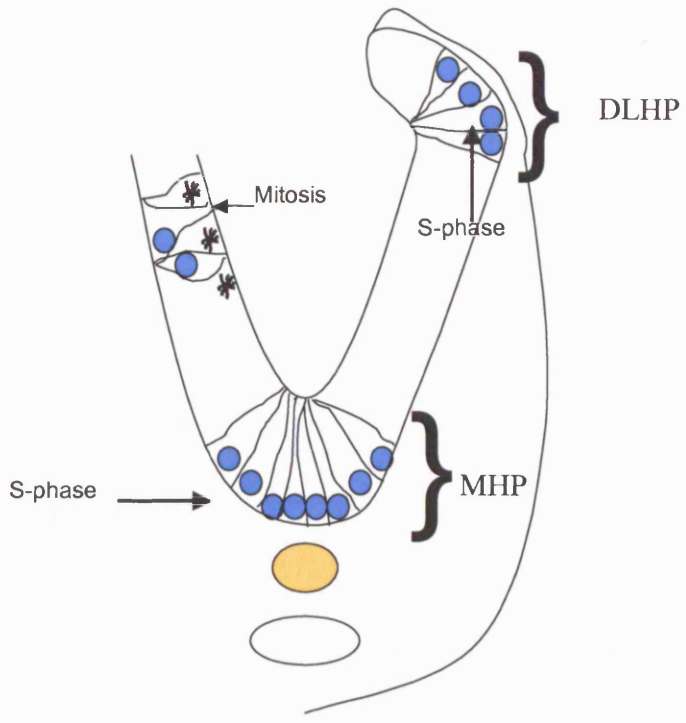

Figure 1.5. Diagram to illustrate the cell cycle-dependent position of the nucleus in formation of bending regions in a transverse section through the PNP

In the neural plate, cells undergo interkinetic nuclear migration, such that the nucleus is located apically during mitosis and basally during S-phase. When the nucleus is in a basal or apical position the cell acquires a wedge or inverted wedge shape respectively. In the median hinge point (MHP), an increased proportion of cells is in S-phase with basally located nuclei. The increase in number of wedge shaped cells in the ventral midline of the neural plate creates the MHP. Cell cycle variations resulting in cell wedging could also regulate DLHPs, although this has not studied in detail.

However, if the neural folds are dissected from the mesoderm and endoderm and only a small fragment of the surface ectoderm in contact with the neural fold is left intact, closure of the neural tube still occurs with the presence of DLHPs (Ybot-Gonzalez *et al.*, 2002). Therefore, whilst surface ectoderm could mediate a pushing force at early stages, it seems unlikely that this process functions during Mode 2 and Mode 3 of

neurulation, and rather the surface ectoderm may be required to signal to the underlying neural folds to form the DLHPs.

Whilst the mesoderm and endoderm are not required for DLHP formation, these tissues are nevertheless important for neurulation, since an imbalance of cell proliferation within these tissues can affect spinal neural tube closure. For example, an increase in axial curvature is seen in affected *curly tail* mutant embryos due to an imbalance in cell proliferation in the hindgut endoderm and notochord, which results in increased axial curvature and delay or failure of posterior neuropore closure (Brook *et al.*, 1991;Van Straaten *et al.*, 1993). In *curly tail,* bending at the DLHPs and MHP occurs normally, whereas the increase in axial curvature results in strain on the neural folds that impedes meeting at the dorsal midline. This has also been observed in chick, where delay in closure occurs by culturing embryos on a convex surface due to an increase in axial curvature (Van Straaten *et al.*, 1993).

1.4.3 Fusion of the neural folds

After apposition, the neural folds fuse in the dorsal midline to form the neural tube and surface ectoderm from each neural fold loses its continuity with the neuroepithelium to form the epidermis. Fusion of the neural folds has been proposed to be mediated by cell protrusions, lamelipodia, extending from the apposing cells (Geelen and Langman, 1979). Lamelipodia structures have been observed by scanning electron microscopy on the luminal surface of the neural plate and at the edges of the surface ectoderm (Geelen *et al.*, 1979). However, the molecules involved in cell to cell recognition have not been studied during closure of the spinal neural tube. Carbohydrate-rich material localised in the tips of the neural folds has been suggested to assist fusion by increasing the adhesiveness of the neural folds (Moran and Rice, 1975) (Sadler, 1978). Indeed, embryos cultured with phospholipase C to remove carbohydrate material exhibit delayed neural tube closure (O'Shea and Kaufman, 1980). However, the

observed phenotype could be due to enzymatic removal of glycosylphophatidylinositol-anchored (GPI) proteins, including cell adhesion molecules such as ephrins. GPI-anchored ephrinA1 and ephrinA3 have been recently shown to be expressed in the posterior neuropore (Abdul-Aziz and Copp, preliminary data). More studies are needed to understand the role of adhesion molecules in spinal neurulation.

1.5 MOUSE GENETIC MODELS OF NEURAL TUBE DEFECTS

To date more than 80 genes that cause NTDs in mouse have been identified by positional cloning, gene targeting or gene trap screens (Juriloff *et al.*, 2000;Copp *et al.*, 2003b). Despite the identification of a large number of genes required for neurulation, in most cases the embryonic mechanisms leading to NTDs in each individual mutant are not well characterised. The number of mouse mutants that display exencephaly is greater than the number with spina bifida, perhaps indicating greater complexity of genetic regulation of cranial tube closure. The identification of these "NTDs genes" provides a tool to determine the molecular pathways that regulate neurulation. Thus, some pathways are starting to emerge. For instance, the planar cell polarity pathway is now known to regulate Closure 1. In this section I will explain the importance of using mouse models for the study of NTDs and I will concentrate on some pathways for which information is available from mouse mutants that display spina bifida.

1.5.1 Use of mouse models to investigate NTDs

Mouse models offer an alternative to direct study of human NTDs, which is hampered by several factors. Human NTDs appear to have a multigenic complex aetiology, with strong influence of environmental factors, such as lifestyle and diet (Campbell *et al.*, 1986;Copp *et al.*, 1994). Moreover, the identification of causative genes for NTDs by linkage analysis requires large families, and this represents a

difficulty since families with large number of NTDs are rare. In addition to this, embryological studies using human embryos can raise serious ethical issues.

The use of the mouse represents an excellent model to elucidate the genetic programmes controlling NTDs. With the sequence of the mouse genome completed and the availability of microsatellite markers for genetic mapping, the identification of the mutated genes responsible for NTD phenotypes has become quicker. Moreover, several mutagenesis strategies, particularly using chemical mutagenesis, gene trap strategies or gene targeting, have begun to make a major contribution to the list of known NTDs genes. Phenotype-driven mutagenesis programmes using chemical mutagens such as ethylnitrosourea (ENU) or chlorambucil are available to the scientific community (Nolan *et al.*, 2000;Justice *et al.*, 1999;Justice, 2000). This approach, allows the identification of new mouse mutations that have a particular phenotype, for instance NTDs. The mutated gene must then be identified by positional cloning.

Another type of mutagenesis is the "gene-trap" strategy, where genes are disrupted by vector insertion in ES cells, generating ES-cell clones containing a disrupted gene. This strategy has the advantages that large numbers of genes can be disrupted and then identified by a forward-genetic strategy, prior to implantation of ES cells to generate the mouse mutant (Mitchell *et al.*, 2001;Skarnes *et al.*, 1992). The disadvantages of this technique include the unpredictable nature of the phenotype caused by the gene trap and the necessity for germ-line transmission of the mutated gene in order to generate a mouse mutant line.

A further mutagenesis approach is gene targeting that allows precision design of the type of mutation. Hence, deletions, point mutations or insertions can all be achieved. The advantage of gene targeting is that mapping of the mutated gene is not required. However the resulting phenotype is unpredictable and knowledge of the gene structure is required to generate the targeted mutant mouse.

The mouse also represents a good experimental tool to investigate the cellular and embryological bases of neurulation. Mouse embryos are easily accessible and can be cultured for up to 48 hours *in vitro* (Copp *et al.*, 1999). Neurulation in mouse takes place from the 5-somite stage to the 29 somite stage during a 48 hour period. Therefore, mouse embryos can be cultured throughout the entire neurulation process, allowing experimental manipulation. This is important in the study of the effects of teratogenic substances on closure of the neural tube as well as the analysis of vitamin supplementation to prevent NTDs.

1.5.2 Genes in the planar cell polarity pathway regulate Closure 1

Recently, mutations in the planar cell polarity (PCP) pathway genes have been found to be responsible for the craniorachischisis phenotype observed in three different mouse mutants, *loop tail*, *circletail* and *crash* (Kibar *et al.*, 2001;Murdoch *et al.*, 2001;Curtin *et al.*, 2003;Murdoch *et al.*, 2003). Embryos that are homozygous for mutation in *Vangl2* (*loop-tail*), *Scribble* (*circletail*) and *Celsr1* (*crash*) display failure of Closure 1 leading to craniorachischisis. The other mouse mutant known to display craniorachischisis is the *Dishevelled 1/2* double knockout (*Dsh1/2*) (Hamblet *et al.*, 2002). Embryonic examination shows that at least three of these mutants, *loop-tail, circletail* and *Dsh1/2* have a similar phenotype to that of *Xenopus* embryos where convergent-extension has been disrupted (Wallingford *et al.*, 2000;Wallingford and Harland, 2002). Embryos display shorter body axis, with a broad floor plate and failure of the neural tube to close.

Convergent extension movements occur during gastrulation and consist of the migration of cells from a lateral position towards the midline, where they intercalate, resulting in lengthening of the anterior-posterior axis and extension of midline cells anteriorly (Davidson and Keller, 1999;Keller *et al.*, 1992). Disruption of convergent-extension movements has not yet been reported in mouse mutants with

craniorachischisis but initial studies using DiI labelling suggest that convergent extension is disrupted in homozygous *loop-tail* (*Lp)* embryos (Savery, D. and Copp, unpublished results). The embryonic mechanism of convergent-extension has been studied in *Xenopus,* where disruption in the PCP pathway in the midline results in a broader floor plate or MHP, with formation of the neural folds far apart that prevent fusion (Wallingford *et al.*, 2002).

Genes that control the PCP pathway, also referred to as the non canonical-Wnt pathway, have been identified in *Drosophila* to control the polarisation of cells in the plane of the epithelium. This is required for example, for unidirectional array of bristles on the wing and for the arrangement of ommatidia in the compound eye (Kühl *et al.*, 2000;Mlodzik, 2002). The PCP pathway shares components of the Wnt pathway, such as the transmembrane receptor Frizzled and the downstream effector Dishevelled. However, unlike the Wnt pathway, the PCP pathway does not result in stabilisation and nuclear translocation of β-catenin by Dishevelled to control cell proliferation and cell fate decisions. Rather, Dishevelled is thought to signal through small GTPases such as RhoA and Rac to regulate cytoskeleton assembly and cell motility (Mlodzik, 2002; Keller, 2002). In support of this idea are the experiments in which mouse embryos treated with cytochalasin D before the onset of Closure 1 resulted in failure of this closure site, indicating that cell rearrangements that control Closure 1 are cytoskeleton-dependent. It is unknown how *Vangl2*, *Scribble* and *Celsr1* are related to each other within the PCP pathway.

1.5.3 Sonic hedgehog (Shh) pathway and neural tube closure

The Shh pathway has been implicated in neural tube closure, specifically in regulating the formation of DLHPs (Ybot-Gonzalez *et al.*, 2002). Shh is an extracellular signalling protein that regulates a number of embryological processes, such as patterning of the neural tube and limbs, cell proliferation and cell-fate determination.

Postnatally, aberrant Shh signalling pathway has been linked to basal cell carcinomas and medulloblastoma tumours (Chiang *et al.*, 1996;Goodrich *et al.*, 1997;Fan *et al.*, 1997;Wechsler-Reya and Scott, 1999). The molecular mechanisms underlying the Shh signalling pathway have been principally determined by studies in *Drosophila* (Ruiz i Altaba, 1999). The preliminary pathway involves binding of HH to its transmembrane receptor Patched (Ptc), which prevents the inhibition of Smoothened (Smo), a transmembrane protein that forms part of the HH receptor complex. De-inhibtion of Smo allows signalling to a cytoplasmatic protein complex formed by Fused, Costal-2 and Cubitus Interruptus (CI) (Tabin and McMahon, 1997). When Shh is not present, proteolytic processing of CI results in the generation of the shorter CI N-terminal form that functions as a transcriptional repressor of HH downstream genes. Binding of HH to its receptor inhibits the CI proteolysis resulting in the stable full length CI that functions as a transcriptional activator of HH downstream genes. In mouse, Shh, Patched and Gli are the vertebrate homologues of *Drosophila* HH, Patched and CI. In mouse three Gli proteins have been identified, Gli1, Gli2 and Gli3 that code for zinc finger domain (ZFD) transcription factors closely related to the Zic family of transcription factors. In mouse Gli1 and Gli2 displays a similar function to the full length CI, and acts as a transcriptional activator of Shh downstream genes. However, Gli3 has a repressive function similar to that of the N-terminal CI (Marigo *et al.*, 1996).

During neurulation, Shh emanating from the notochord functions as a morphogen, to pattern the neural tube so that progenitor cells in the ventral region acquire ventral fates and become ventral neural types including motor neurons. Mice that are null for Shh display a dorsalised neural tube, and dorsal markers such as *Pax3* become expressed in ventral regions* (Chiang *et al.*, 1996). In contrast over-expression of Shh results in loss of dorsal fates and a ventralised neural tube.

* Moreover, *Shh*$^{-/-}$ embryos exhibit holoprosencephaly, an embryonic malformation in which the telencephalic vesicles fail to divide resulting, in the most severe cases, in a unique hemisphere and cyclopia, suggesting a role for Shh and notochord in bilateralisation.

Several mice that carry mutations in Shh pathway genes display NTDs. Two mutant alleles of *Open brain* (*opb*), one spontaneous and the second ENU-induced, display NTDs. Embryos homozygous for either mutant allele display exencephaly, spina bifida, polydactyly and poorly developed eyes (Sporle *et al.*, 1996). Analysis of $opb^{-/-}$ mutant embryos shows a lack of dorsal neuronal cell types, a phenotype that resembles mice with partial loss of function of Patched or over-expression of Shh (Milenkovic *et al.*, 1999). The gene mutated in *opb* was identified as *Rab23,* encoding a member of the Rab family of GTPases, which controls vesicle transport. How this protein participates in Shh signalling remains unknown but, since *opb* phenocopies *Gli3* and *Patched1* mutant embryos, Rab23 may antagonistically regulate the Shh pathway.

Interestingly, null embryos for Patched1 (*Ptch1*) and double homozygotes for protein kinase a subunit Cα/Cβ1 (*Prkaca,Prkacb*), display cranial NTDs that may be caused by excessive Shh signalling. In *Drosophila,* protein kinase A phosphorylates CI, a process that is required for protein cleavage to yield the N-terminal transcriptional repressor form of CI (Chen *et al.*, 1999). In vertebrates, a similar mechanism has been proposed (Ruiz i Altaba, 1999). Double homozygote embryos for *Prkaca* and *Prkacb* have excess Shh signalling, possibly because pKA cannot phosphorylate Gli proteins (Huang *et al.*, 2002).

Further evidence for the importance of regulation of the Shh pathway in neurulation comes from the *Extra-toes*^{J} mouse (Xt^{J}), that carries a deletion in *Gli3*, and also displays cranial NTDs (Hui and Joyner, 1993). Lack of Gli3, which acts as a repressor of Shh downstream targets, results in excessive Shh signalling and exencephaly.

The information obtained from mouse mutants indicates that the Shh pathway is necessary for cranial and spinal neurulation. However, the embryonic mechanisms leading to NTDs in these mutants have not been characterised. One hypothesis to

explain the exencephalic phenotype could be the loss of dorsal structures due to excessive Shh signalling resulting in a ventralised neural tube. In the spinal neural tube, the role of Shh has been studied in more detail (Ybot-Gonzalez *et al.*, 2002). Shh signalling was found to inhibit DLHP formation. Indeed, homozygous null embryos for Shh develop DLHPs at an earlier stage of neurulation, during Mode 1, compared to the wild type embryos. DLHP formation can also be inhibited by local release of Shh peptide using implanted beads next to the neural folds, resulting in straight neural folds. In normal development, the inhibitory action of Shh on DLHPs formation declines at more caudal levels. Shh is expressed in the notochord at progressively lower intensity as spinal neurulation progresses, allowing DLHPs to appear and so enabling the transition to Mode 2 and Mode 3. Therefore, Shh controls the timing of DLHP development by inhibiting its formation.

A hypothetical model of DLHP regulation has been postulated (see Fig. 1.6)(Ybot-Gonzalez *et al.*, 2002). In this model, the balance between positive (inducing) and negative (inhibiting) signals regulates DLHP formation. An unknown inducing signal from the surface ectoderm stimulates bending of the neural plate, perhaps through regulation of the cell cycle of the adjacent tissue. Early in neurulation, at Mode 1, Shh is expressed at high levels in the notochord and antagonises the positive signal from the surface ectoderm resulting in straight neural folds. However, as neurulation progresses (Mode 2 and Mode 3 of neurulation) the expression of Shh decreases, reducing the inhibitory effect and resulting in bending of the neural folds that are under the influence of the inducing signal.

This model is supported by experimental observations and the analysis of mouse mutants. Once Closure 1 has occurred, the MHP is not required for closure of the neural tube. Thus, mouse mutants for *HNF3β*, *Gli2*, *Shh* and *Gli1/Gli2* double mutants do not form a floor plate (MHP) and yet close their neural tube successfully in a Mode 3

morphology (Park *et al.*, 2000;Ang and Rossant, 1994;Chiang *et al.*, 1996;Motoyama *et al.*, 1998;Matise *et al.*, 1998).

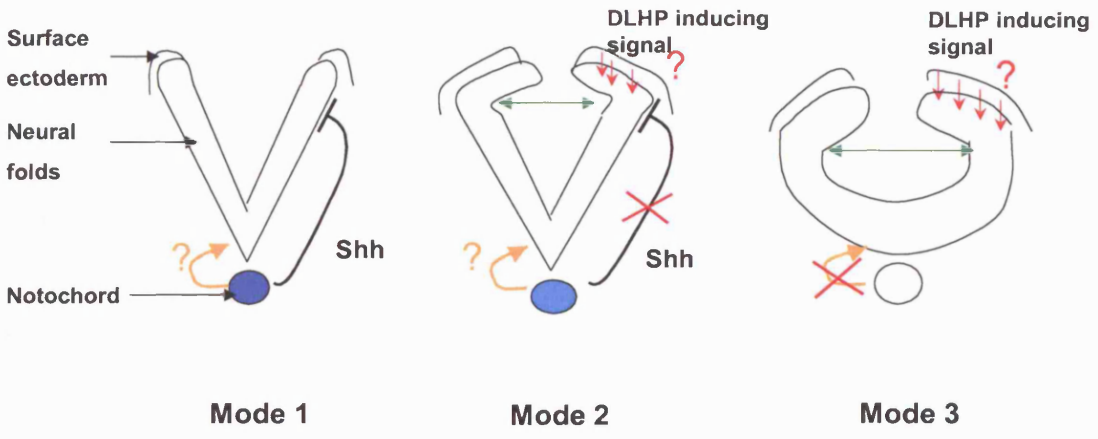

Figure 1.6 Diagram to illustrate the proposed regulation of DLHPs in three progressive stages of mouse neurulation

Strong expression of Shh from the notochord in Mode 1 of neurulation inhibits DLHPs, whilst an unknown signal from the notochord induces the MHP (orange arrow). In Mode 2, Shh expression declines and its inhibitory action is lost. An unknown inducing signal from the surface ectoderm (red arrows) induces bending of the underlying neural fold (green arrows). In Mode 3, the MHP inducing signal is lost and closure of the neural tube depends only on DLHPs. Diagram modified from Ybot-Gonzales (2002).

Removal of the surface ectoderm abolishes DLHPs formation (Ybot-Gonzalez *et al.*, 2002) showing that the surface ectoderm must signal to the underlying neural folds to induce the formation of DHLPs. Initially, *BMP2* expressed from the surface ectoderm, was thought to be a good candidate molecule to induce DLHP. However recent examination of embryos that lack BMP2 revealed that DLHP are formed normally in these embryos (Ybot-Gonzalez and Copp A, unpublished results). Hence the nature of the DLHP-inducing signal remains unknown.

Bending of the neural plate at the DLHPs regions ensures apposition of the neural folds prior to their fusion in the dorsal midline. However, determining how DLHPs are regulated has been hampered by the lack of mouse mutants that fail to develop DLHPs. A mouse mutant that lacked DLHPs would provide an opportunity to understand the molecular mechanisms required for DLPHs formation and neural tube closure in the low spinal region.

1.5.4 Wnt signalling pathway

Wnt are a family of secreted glycoproteins that control cell-fate determination, cell proliferation and morphogenesis during development (Cadigan and Nusse, 1997). The canonical Wnt signalling pathway has been extensively studied in different organisms and its components have emerged mostly from genetics in *Drosophila*. Extracellular secreted Wnts bind to the extracellular domain of Frizzled receptors, generating signals downstream to the cytoplasmatic protein Dishevelled. Dishevelled in turn stabilises β-catenin, which prevents its degradation and results in its cytoplasmatic accumulation. β-catenin binds to TCF/LEF transcription factors and translocates to the nucleus where it regulates Wnt signalling downstream targets (Nusse, 1999).

Arrow (LRP6 in mouse) is a low-density lipoprotein (LDL)-receptor related protein that acts as a single pass transmembrane receptor. *Drospophila* null embryos for arrow (arr^{null}) phenocopies the wingless (*wg*) null mutations, which display defects in parasegment identity, indicating that arrow could be involved in Wnt signalling (Wehrli *et al.*, 2000). Indeed, the extracellular domain of LRP6 binds to Wnt1 and forms a complex in *Drosophila* with the receptor Frizzled (Fz), demonstrating that LRP6 is required for Wnt signalling, by acting as a co-receptor for Fz (Tamai *et al.*, 2000). The LRP6 mutant mouse was generated in a screen for lethal gene trap insertions in cell surface proteins (Skarnes *et al.*, 1992). A proportion of $LRP6^{-/-}$ embryos display spinal NTDs with a phenotype that resembles the vestigal tail homozygous mutant ($vt^{-/-}$).

Vestigial tail results from a mutation in the *Wnt3a* gene, exhibiting excess neural tissue and loss of paraxial mesoderm resulting in caudal truncation with in some cases spina bifida (Pinson *et al.*, 2000).

1.6 Members of the *Zic* gene family are implicated in neurulation

Zic (zinc finger protein of the cerebellum) genes were firstly identified in the mouse for their specific restricted expression in the granule cell neurons of the cerebellum (Aruga *et al.*, 1994). To date, four members of the *Zic* gene family have been identified in mouse, named *Zic1-4* (Aruga *et al.*, 1994;Aruga *et al.*, 1996a;Aruga *et al.*, 1996b), with a fifth gene in amphibian, *Xzic5* (Nakata *et al.*, 2000). *Zic* genes have recently been implicated in the production of NTDs through positional cloning and gene targeting studies. *Zic2* is downregulated in the gene-targeted *Zic2* knock down mouse ($Zic2^{Kd}$) (Nagai *et al.*, 2000), while a second ENU-induced allele, *Kumba* ($Zic2^{Ku}$), carries a point mutation in the zinc finger DNA binding domain (Elms *et al.*, 2003). Homozygous embryos for either mutant allele develop spina bifida as a result of failure of PNP closure. A second member of the *Zic* gene family, *Zic3*, has also been shown to be essential for neurulation. Positional cloning of the *Bent tail* mutant mouse identified a deletion that comprises the entire *Zic3* locus as well as neighbouring genes (Klootwijk *et al.*, 2000;Carrel *et al.*, 2000). Direct targeting of *Zic3* generated a *Zic3* null mutant, allowing confirmation that the *Bent tail* phenotype results from the deletion of *Zic3* gene (Purandare *et al.*, 2002) and not from loss of an unknown neighbouring gene. Both *Bent tail* and *Zic3*, null embryos exhibit cranial NTDs together with a low frequency of lumbosacral NTDs with sacral agenesis and tail defects. Therefore, the phenotypes of mouse mutants for *Zic2* and *Zic3* indicate that these genes are required for neural tube closure.

1.6.1 *Zic* genes encode Zinc Finger Domain (ZFD) transcription factors

Mapping studies have located *Zic1* and *Zic4* to mouse chromosome 9, *Zic2* to chromosome 14 and *Zic3* to the X chromosome (Aruga *et al.*, 1994;Aruga *et al.*, 1996a). The genomic structure of *Zic1-3* comprises three exons and two introns whilst *Zic4* has two exons and a single intron (Fig. 1.7 A).

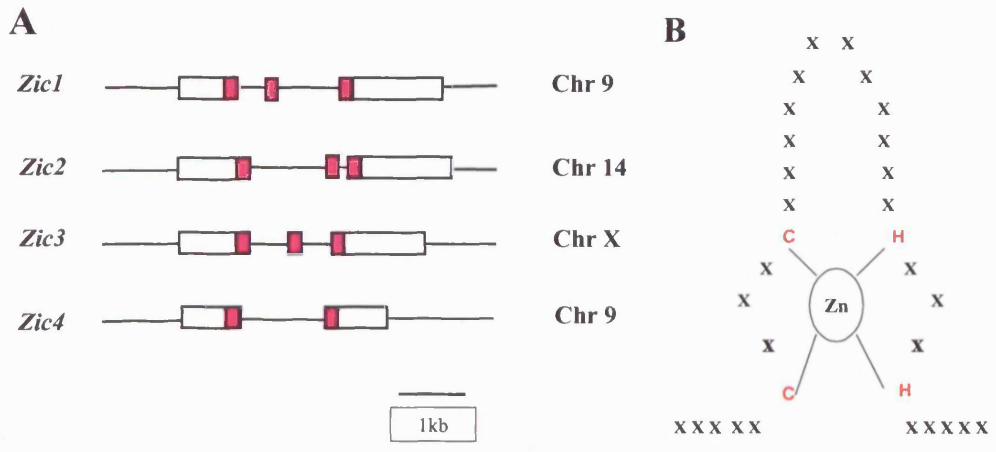

Figure 1.7 Genomic organisation of members of the *Zic* gene family, chromosomal localization and structure of the ZFD region

(A) Boxes represent exons and filled boxes represent the coding regions of the zinc finger DNA binding domain. B) Zinc finger domain structure showing the consensus sequences Cys-$X_{2,4}$-Cys-$X_{12,15}$-His-$X_{3,4}$-His characteristic of this domain. Each *Zic* gene contains five zinc finger domains. Modified from Aruga (1996a)

The *Zic* genes form a subfamily of one of the largest gene families: the Kruppel-like transcription factors, which are characterised by the presence of zinc finger domains (ZFD) (Dang *et al.*, 2000). The Kruppel-like family is divided into subfamilies depending on the structure and the number of ZFD present in the protein. Thus, the ZFD of the *Zic* subfamily typically contains two cysteines and two histidines (C2-H2) that fold in a tetrahedral configuration around the central zinc ion (Fig. 1.4B) (Pavletich and

Pabo, 1993;Wolfe *et al.*, 2000). *Zic1-4* contain five tandem repeats of each ZFD unit, which have high degree of homology to the *Gli* and *Glis* genes subfamilies (Aruga *et al.*, 1994; Aruga *et al.*, 1996a;Zhang *et al.*, 2002)

Until recently the ZFD region was considered to function as a sequence-specific DNA binding domain only (Pavletich *et al.*, 1993). However, several studies have indicated that ZFDs participate in both DNA-protein and protein-protein interactions (Weatherall, 1991;Mackay and Crossley, 1998). An example of a protein-protein interaction mediated through ZFD is the interaction between FOG-1 and the erythroid transcription factor GATA-1 (Tsang *et al.*, 1998). FOG-1 cooperates with GATA-1 to drive erythroid and megakaryocytic differentiation. Similarly, the C2-H2 zinc finger domain of the Ikaros transcription factor mediates homodimerisation involved in haematopoietic development (McCarty *et al.*, 2003). Yeast two-hybrid screens and co-immunoprecipitation assays have shown that Ikaros interacts with Ikaros family members through the ZFD (Hahm *et al.*, 1998; Perdomo *et al.*, 2000). Similarly, Zic proteins interact with Gli proteins through the 3rd, 4th and 5th ZF of each protein (Koyabu *et al.*, 2001b). The Zic-Gli interaction suggests that there may be a functional role for Zic proteins in the Shh signalling pathway (see section 1.5.3). However, *Zic* mutants display different specific phenotypes from *Shh* and *Gli* mutants, suggesting that Zic proteins do not solely function in the Shh downstream pathway.

The *Kumba* (*Zic2^{Ku}*) mutation affects the 4th ZFD of Zic2 and has been proposed to disrupt the function of this domain (Elms *et al.*, 2003). This raises two questions, first, whether transcriptional activity is disrupted due to abnormal DNA binding, and/or whether the binding of co-factors is hampered by the *Zic2^{Ku}* mutation. The identification of Zic-interacting proteins will help to elucidate in which signalling pathways *Zic* proteins participate and will provide new proteins to establish whether protein-protein interactions are affected by the *Kumba* mutation.

1.6.2 Role of *Zic* genes during embryonic development

The role of *Zic* genes during development has been studied in a variety of animal systems, including *Drosophila*, *Xenopus*, chick and mouse. The *Drosophila* homologue of *Zic* genes is the pair-rule gene *odd-paired* (*Opa*). *Opa* functions in the segmentation of the *Drosophila* embryo by conferring parasegment identity through the timely activation of *wingless* (*wg*) and *engrailed* (*en*) (Benedyk *et al.*, 1994). In the *Drosophila* embryo the anterior-posterior axis is divided into segmented units, the parasegments that are further subdivided into an anterior and posterior part (Martinez-Arias and Lawrence, 1985). *Wg* is expressed in a single row of cells at the posterior end of the parasegments, whilst *en* is expressed in the anterior end of the parasegments conferring boundary identity. *Opa* null embryos show anterior-posterior segmented pattern abnormalities with delayed expression of *wg* and *en*. However, unlike other pair-rule genes, such as *fushi tarazu* (*ftz*), which regulate segmental identity and are expressed in a restricted manner (Carroll and Scott, 1985), *opa* was found expressed ubiquitously in the segmented region of the embryo. This study hypothesises that *opa* may interact with co-factors of restricted expression to regulate the expression of *wg* and *en* in order to maintain parasegment identity.

Studies in lower vertebrates such as *Xenopus* and zebrafish have provided additional insights into the function of *Zic* genes during development. In *Xenopus*, *Zic2* has been shown to mediate a strong anti-neurogenic effect, whilst promoting neural crest formation (Brewster *et al.*, 1998). Unilateral over-expression of *Zic2* results in loss of cells expressing the neuronal markers *n-tubulin* and *neurogenin* on the injected side. Moreover, ectopic expression of *Zic2* results in the induction of neural crest markers such as *Xslug* and *Xsnail*, indicating a neural crest-inducing function for *Zic2*. The neural crest inducing activity could be mediated through repression of pro-neurogenic genes, since injection of a fusion protein in which Zic2 is bound to the strong activation

domain VP16, resulted in ectopic neurogenesis. Similar experiments using ectopic expression of *Xzic1, 3* and *5* have also been shown to promote neural crest formation leading to ectopic expression of neural crest markers *Xslug*, *Xsnail* and *Xtwi* (Kitaguchi *et al.*, 2000;Nakata *et al.*, 1997;Nakata *et al.*, 1998). In addition, *XZic3* regulates right-left asymmetry and looping of the heart (Kitaguchi *et al.*, 2000;Kitaguchi *et al.*, 2002).

In zebrafish, the *Zic1* domain of expression appears to be inhibited by bone morphogenetic proteins (BMPs) as indicated by a study in which the expression domain of *Zic1* was found to be extended in *swirl* homozygous embryos, which carry mutation in the *BMP2* gene (Grinblat and Sive, 2001). Similarly blocking *BMP4* in *Xenopus*, by over expression of either a dominant negative form of *BMP* receptor or *noggin*, results in induction of *Zic3.* In summary, in lower vertebrates, *Zic* genes have a role in promoting neural crest formation by antagonising neurogenesis and appear to be inhibited by *BMP* signalling.

The role of *Zic* in higher vertebrates has been revealed by over-expression studies in chick and through phenotypic study of mutant mice. Targeted disruption of *Zic1* in the mouse has revealed a requirement for this gene in formation of the cerebellum (Aruga *et al.*, 1998b). Mice homozygous for a null *Zic1* allele show a hypoplastic and abnormal foliation of the cerebellum, together with skeletal malformations (Aruga *et al.*, 1999;Aruga *et al.*, 1998b). As in *Xenopus,* overexpression studies in chick revealed an antineurogenic effect of *Zic1*. The mechanism appears to involve *Notch*-mediated inhibition, since *Zic1* over-expression results in upregulation of *Notch1* and *Hes1* (Aruga *et al.*, 2002). Similarly, transgenic mice that overexpress *Zic1* exhibit decreased number of cells expressing neuronal markers and upregulation of *Notch1* and *Hes1* expression. However, contrary to *Xenopus* and zebrafish, *Zic1* expression in the mouse neural tube has been suggested to be positively regulated by *BMP4/7* and negatively regulated by Shh signalling (Aruga *et al.*, 2002). Ectopic

expression of *BMP4/7* results in activation of *Zic1*, whilst notochord transplantation and *Shh* overexpression inhibits *Zic1* expression in the underlying tissue.

Zic2 knock down ($Zic2^{Kd}$) and Kumba ($Zic2^{Ku}$) mice display spina bifida and exencephaly, indicating that *Zic2* is required for neurulation (Nagai *et al.*, 2000;Elms *et al.*, 2003). Further phenotypic analysis has shown that *Zic2* also regulates other developmental processes. $Zic2^{Ku/Ku}$ embryos display delayed production and reduced numbers of neural crest cells, in accordance with the *Xenopus* overexpression studies which showed that Zic proteins promote neural crest formation. Interestingly, $Zic2^{Ku/Ku}$ embryos have aberrant hindbrain segmentation with smaller rhombomeres 3 and 5 (r3/5). Indeed, expression of *follistatin*, which is normally seen only in r2/4/6, expands into r3/5 in $Zic2^{Ku/Ku}$ embryos. Another study has shown that *Zic2* is important for patterning binocular vision by specifying a subtype of retinal ganglion cells that have uncrossed axon projections in the midline (Herrera *et al.*, 2003). $Zic2^{Kd/Kd}$ mice had fewer ipsilateral projections compared to the wild type and *Zic2* was found to be expressed only in the uncrossed retinal ganglion cells. This prompted an investigation of the role of *Zic2* in regulating retinal ganglion projection in the midline. Indeed, ectopic expression of *Zic2* in dorso-temporal cells, which normally do not express *Zic2*, changes the behaviours of these cells so that they are repelled by midline chiasm cells that express cues responsible for regulating the crossing in the midline. Therefore, *Zic2* appears to control the behaviour of retinal ganglion cells to encourage ipsilateral (uncrossed) projections of their fibres. In summary, *Zic2* is a key regulator of several different developmental processes: neurulation, neural crest production, hindbrain segmentation and innervation of the retina.

Zic3 has been implicated in several developmental processes. Embryos homozygous for either of the mutant alleles, the *Bent tail* and targeted *Zic3* mutations, develop left-right asymmetry defects, vertebral and rib abnormalities, tail defects and

NTDs (Klootwijk *et al.*, 2000;Carrel *et al.*, 2000;Purandare *et al.*, 2002). The left-right asymmetry defects include aberrant positioning of the organs with respect to each other (*situs ambiguous*), or mirror-image reversal of the structures (*situs inversus*). Homozygous null embryos for *Zic3* display abnormal *Nodal* and *Pitx2* expression, which could account for the observed laterality defects. Null embryos also show severe heart defects comprising transposition of the great arteries, interrupted aortic arch and atrio-ventricular septal defects (Klootwijk *et al.*, 2000;Carrel *et al.*, 2000;Purandare *et al.*, 2002). In addition to heart defects, some null embryos show hypoplastic spleen and reversed position of the lungs. The central nervous system (CNS) is also affected in *Zic3* null embryos, which display excencephaly, together with low frequency of lumbosacral spina bifida. Hence, Zic3 is required for the establishment of the embryonic right-left axes and for normal neurulation.

The function of *Zic4* during development remains unknown, as it has not been studied in any animal system to date.

1.6.3 Clinical relevance of *Zic* genes

The importance of *Zic* genes in humans has become evident with the identification of mutations in *ZIC2* and *ZIC3*. Mutations in human *ZIC2* have been linked to holoprosencephaly (HPE) in several human genetic studies (Brown *et al.*, 2001;Brown *et al.*, 1998;Nanni *et al.*, 2000). HPE is a common birth defect with a prevalence of 1:10,000 live births but at a higher frequency among embryos and foetuses dying *in utero* (Roach *et al.*, 1975;Croen *et al.*, 1996). During brain development the prosencephalon forms a single fluid-filled chamber that divides to form the two telencephalic vesicles, which will later become the cerebral hemispheres. HPE results from partial or complete failure of the bifurcation of the telencephalic vesicles, resulting in the fusion of the two cerebral hemispheres (Hayhurst and McConnell, 2003). Mutations in three other human genes have been reported to cause

HPE: *SHH*, *SIX3* and *TIGF* (Gripp *et al.*, 2000;Hayhurst *et al.*, 2003). This argues that *ZIC2* and *SHH* function in the same pathway, which is in accordance with the Zic-Gli interaction identified by Aruga (2001b). However, patients with mutations in *ZIC2* do not display facial abnormalities, whilst patients with mutations in *SHH* display facial abnormalities and in severe cases cyclopia. Hence the two genes must regulate distinct as well as overlapping functions.

Zic2 was initially considered as a good candidate for human NTDs because it mapped in the critical region of the 13q32 deletion syndrome, which results in HPE and exencephaly (Brown *et al.*, 1998). This, together with the neurulation phenotype observed in $Zic2^{Ku}$, prompted an investigation of a possible association of *ZIC2* with NTDs including exencephaly and spina bifida (Brown *et al.*, 2002). Among 192 NTDs patients screened, only one mutation was found consisting of an insertion in the first intron. However this mutation was also present in unaffected individuals in the same family. Single stranded conformation polymorphisms (SSCP) failed to show any mutation in *ZIC2* in NTD patients, indicating that the NTDs observed in the 13q32 deletion syndrome could be caused by another gene within the deletion rather than by the loss of function of *ZIC2* (Brown *et al.*, 2002). However, this report identified a polyhistidine tract polymorphism in *ZIC2* in non-Caucasian–Hispanic population that could confer susceptibility to NTDs. A second study, in a Dutch population, has also failed to identify mutations in *ZIC2* in NTD patients (Klootwijk *et al.*, 2004).

Lack of identification of mutations in *ZIC1* and *ZIC4* has not been informative on the role of these genes in humans. However, mutations in *ZIC3* have been shown to be responsible for X-linked heterotaxy (HTX1) (Gebbia *et al.*, 1997). The affected males exhibit *situs inversus*, heart malformations, abnormal lung lobulation and gastrointestinal malformations. These phenotypes correlate with those of embryos homozygous for the *Bent tail* and *Zic3 Knockout*alleles (see section 1.6.2). Other

malformations observed in humans carrying mutations in the *ZIC3* gene, include lumbosacral NTDs with anal abnormalities and sacral agenesis. The phenotypic resemblance between the mouse mutants and the human abnormalities makes *Bent tail* and the *Zic3* knockout a good model for the study of right-left asymmetry defects and heart defects. Other studies have found no association between human NTDs and *ZIC3* (Carrel *et al.*, 2001;Klootwijk *et al.*, 2004).

Despite the importance of *Zic2* and *Zic3* during development, little is known about the function of these genes during neurulation. Several fundamental questions remain to be answered: where are *Zic* genes expressed at the time of neural tube closure? How does *Zic2* affect the morphogenesis of the neural tube leading to spina bifida? Which aspects of neurulation does *Zic2* regulate? These questions will be addressed in this thesis.

1.7 OVERVIEW OF THE THESIS

This thesis describes a number of studies that aim to elucidate the function of *Zic* genes during neurulation. Chapter 3 includes a detailed expression analysis of the *Zic* genes at the time of neural tube closure in the mouse. Expression of *Zic2* and *Zic3*, genes implicated previously in the causation of spina bifida, are reported during normal neurulation and in the mouse mutants *curly tail* (*ct*), *loop tail* (*Lp*) and *Splotch* (Sp^{2H}) which develop NTDs. Chapter 4 presents a morphological analysis of the neurulation defect observed in the Kumba mouse, $Zic2^{Ku}$, and provides the first evidence for a gene directly involved in DLHP formation. The final two chapters are concerned with the identification of Zic2 interacting proteins in the neurulation stage embryo. The aim is to identify proteins that regulate Zic2 transcriptional activity and thereby discover pathways by which Zic2 regulates neurulation. Chapter 5 reports the identification of Zic2 interacting proteins using the yeast two-hybrid assay, while Chapter 6 contains

further analysis of the Zic2 interacting proteins identified in the previous chapter, using co-expression studies, co-immunolocalisation and biochemical assays. It is hoped that the work in this thesis significantly improves our understanding of the role of *Zic* genes in mouse neurulation.

CHAPTER 2: GENERAL METHODS

2.1 INTRODUCTION

In this chapter I describe the common experimental procedures used throughout the thesis. I have divided this chapter into 6 areas: 1) Mouse embryology and histology methods, 2) DNA methods, 3) RNA methods, 4) Yeast methods, 5) Protein methods, and 6) Tissue culture methods. Those methods that are specific to one particular chapter, such as primer sequences, cloning of constructs or optimisation of the standard conditions explained in this chapter, will be reported under the methods section of each corresponding chapter. All reagents were obtained from Sigma unless otherwise stated.

2.2 MOUSE EMBRYOLOGY AND HISTOLOGY METHODS

2.2.1 Embryo collection and dissection

Mice were maintained under light/dark conditions consisting of a 24 hour cycle consisting of 12 hours light, from 7 a.m. to 7 p.m, and 12 hours darkness. Adults were paired overnight and females were checked for the presence of a copulation plug in the morning. At midday, females with a copulation plug were considered to be 0.5-days post coitum or embryonic day 0.5 (E0.5). Pregnant females of the appropriate gestational age were culled by cervical dislocation and the uterus was placed for further dissection in pre-warmed Dulbecco's Modified Eagle's Medium (DMEM) containing 10% fetal calf serum.

Dissection was carried out using a dissecting microscope (ZEISS, Stemi SV6) and using flame-sterilised Number 5 watchmaker's forceps following the method described by Copp (1990). A hole was made in the uterine wall and enlarged until the decidual swelling could be removed from the uterus. This process was started at one end of the uterine horn and repeated along the uterus until all the decidual swellings had been removed. The conceptus was removed from each decidua and the embryo and extra embryonic membranes were dissected apart. Embryos were rinsed in cold

phosphate buffered saline (PBS) and fixed overnight (E8.5-9) or for 48 hours (older embryos) in 4% paraformaldehyde (PFA) in PBS. If embryos were needed for whole mount *in situ* hybridisation, all the solutions were treated with diethyl pyrocarbonate, DEPC (see section 2.4.4). After fixation, embryos for whole mount *in situ* hybridisation were dehydrated through a series of 25%, 50%, 75%, 90% and 100% methanol in DEPC-treated PBS and stored at -20°C until further use. Embryos used for histological analysis requiring wax embedding were dehydrated to 100% ethanol following the same series as above and kept at 4°C.

2.2.2 Embedding of embryos and sectioning

Embryos requiring wax embedding were cleared by two 30 minute incubations in HistoClear (National Diagnostics). After treatment with HistoClear, samples were placed in a pre-warmed HistoClear:paraffin (1:1) mixture at 60°C for 20 minutes and the mixture was changed to pre-warmed paraffin wax for another 20 minutes at 60°C. Embryos were then placed in warm glass moulds filled with warm paraffin wax and orientated using heated needles. Wax was left to set overnight at room temperature until sectioning. Sectioning was carried out on a rotary microtome (microtome, MICROM HM 325) and 7-10 μm sections were floated on distilled water on slides and heated to 40°C until the creases disappeared. The excess water was removed by suction and samples were left to dry at 37°C overnight. Tissue samples were kept at 4°C until used.

Vibratome sectioning was used to obtain thick sections (30-50 μm) of embryos after whole mount *in situ* hybridisation. Due to the thickness of the section, staining appears stronger allowing better visualisation of the signal compared to the 5-7 μm sections of the wax embedded embryos. Moreover, this technique allows differential interference contrast (DIC) in transmitted light microscopy, thereby avoiding the need for counterstaining.

After whole mount *in situ* hybridisation, embryos requiring vibratome sectioning were equilibrated in a gelatin-albumin solution (27 g of chicken egg albumin grade II, 18 g of sucrose and 0.45 g of gelatin 300 Bloom) for a minimum of one hour for E8.5 embryos, increasing to overnight for E10.5. Embryos were orientated and embedded by addition of glutaraldehyde to 2.5% (v/v). Once orientated, the gelatin-albumin-glutaraldehyde mixture was left to set for a maximum of one hour, after which cubes were stored in PBS at 4°C prior to sectioning. Three microlitres of thimerosal (10% w/v) were added to prevent growth of bacteria and yeast. Embedded embryos were sectioned at 50 μm thickness with a Series 1000 vibratome (Agar Scientific). Sections were mounted on slides in a 50% glycerol-PBS solution.

2.2.3 Haematoxylin and eosin staining

This is a histological method in which haematoxylin, a basic dye, stains nuclei a dark blue colour, while eosin, an acidic dye, stains the cytoplasm pink.

Before staining, paraffin sections were de-waxed by dipping the slides in two changes of HistoClear for 10 minutes each. Sections were re-hydrated by placing slides in an ethanol series of 100%, 90%, 75%, 50%, 25%, followed by PBS for 5 minutes each. Slides were then immersed in haematoxylin (BDH) for 1-2 minutes, rinsed in distilled water to clear the excess dye and briefly dipped in acid-alcohol (1% HCl in 70% ethanol). Slides were then left for 5 minutes in 250 mM sodium bicarbonate solution and rinsed with water before staining with 1% aqueous eosin (Raymond Lamb) for 2 minutes. The slides were then dehydrated using an ethanol series and treated with two changes of HistoClear for 5 minutes each. Sections were mounted with DPX mounting medium (Fisher Chemicals).

2.2.4 Microscopy and image analysis

Images from whole embryos were obtained using a microscope fitted with digital camera (LEICA MZFL III) and the Image Manager (IM LEICA1000 V1.20) software. Subsequent image processing was carried out using the Adobe Photoshop 6.0 software. Images from sections were generated with a ZEISS Axiophot 2 microscope, fitted with a digital camera (Kontron Electronik) using the Openlab 3.11 software (Improvision LTD) for immuno-fluorescence. For other purposes, photographs were taken manually using Ektachrome 160T film (Kodak). After processing, films were scanned using a Microtex Film Scan 1800 scanner and images imported into Adobe Photoshop.

2.3 DNA METHODS

2.3.1 Genomic DNA extraction from adult tissue

This method was used for extraction of genomic DNA from tail tips to be used for genotyping of the mutant mouse colonies by PCR amplification. Small lengths of mouse tail, about 0.5 cm, were digested with 1 mg/ml of proteinase K (PK) in 200 μl of lysis buffer (5 mM ethylenediaminetetraacetic acid [EDTA] pH 8.2; 50 mM Tris(hydroxymethyl)aminomethane [Tris]-HCl pH 8.5; 1% sodium dodecyl sulphate [SDS], 100 mM NaCl) at 55°C overnight. After incubation, PK enzymatic activity was stopped by heat inactivation at 95°C for 5 minutes and cell debris pelleted by centrifugation at 13,000 rpm. The supernatant was collected and placed in a clean eppendorf tube, 100 μl of saturated NaCl were added and samples were incubated on ice for 20 minutes to precipitate the proteins. Samples were centrifuged at high speed (13,000 rpm) to pellet the protein and the supernatant was transferred to a new eppendorf tube. To precipitate the DNA, 750 μl of ethanol were added to the samples followed by thorough mixing and centrifugation for 10 minutes at 13,000 rpm. The

pelleted DNA was then washed with 75% ethanol, air dried for 5 minutes, dissolved in 100 μl of distilled deionised H_20 (dd H_20) and 1 μl was used as a template for PCR.

2.3.2 DNA extraction from yolk sacs for genotyping of embryos

The yolk sac was carefully dissected from the embryo taking care to avoid contamination with maternal tissue, such as the decidua or maternal blood cells on the ectoplacental cone, which could contaminate the DNA giving an incorrect genotype. Yolk sacs were kept at -20°C until further use. The method to extract the DNA was as described above, but with a shorter digestion with PK, 3-5 hours. The DNA pellet was resuspended in 20 μl ddH_20 and 1 μl of DNA was used in the genotyping PCR reaction.

2.3.3 Polymerase chain reaction for DNA amplification

2.3.3.1 Standard PCR method

A reaction mix was prepared containing 1x NH_4 buffer (Bioline), 1.0 to 4.0 mM Mg^{2+} (optimised depending on the primers used in the PCR, see section 2.5.1), 0.16 mM of each deoxynucleoside triphosphate (dNTP), 0.48 μM reverse and forward primer and 0.17 Units of Taq or Biopro polymerase (Bioline). The reaction mix was kept on ice and 24 μl of the reaction mix was carefully added to 1 μl of sample containing 20-100 ng of DNA template, trying not to contaminate the mix. In all reactions a negative control reaction was included without template DNA, in order to check for the presence of contaminating DNA. If possible, a positive control was used with a known good quality template DNA to check the quality of new samples and the components of the reaction mix. The cycling reaction involved an initial step of denaturation at 94°C for 1 minute; followed by 30-35 amplification cycles each consisting of a denaturation step for 1 minute at 94°C, primer annealing for 1 minute at 50-68°C, and primer elongation for 1 minute at 72°C. To ensure that all the PCR amplified products were full length, a final

elongation step at 72°C for 10 minutes was included. PCR products were resolved by agarose gel electrophoresis (see section 2.3.6) and visualised under UV light (MultiImage Light Cabinet).

2.3.3.2 PCR optimisation

The primer annealing temperature and concentration of Mg^{2+} were modified empirically for each set of primers, in order to achieve specificity in the amplification process. For each new reaction, a 1.5 mM final concentration of Mg^{2+} and 55°C annealing temperature was assayed. If the PCR yielded non-specific products, the annealing temperature was increased by 2°C and the Mg^{2+} was decreased until only the expected PCR product was amplified. Alternatively, if the initial PCR did not yield the expected product, the concentration of Mg^{2+} was increased by 0.5 mM and the temperature decreased by 2°C, to decrease specificity until the product of the expected size was obtained.

To amplify cDNA fragments for cloning in the generation of constructs, ACCUZYME DNA polymerase (Bioline) was used, which has a proof reading activity that yields fewer mutations in the amplification cycles. The reaction mix was prepared as described above and the number of cycles was decreased to 25 in order to reduce possible PCR generated mutations.

2.3.3.3 Primer design

To design primers, three basic considerations were taken into account: avoidance of palindromic regions within each primer sequence, complementarity at the 3' end between a pair of primers and runs of Gs or Cs at the 3' end of the primer (Kawasaki, 1990). Palindromic regions within the primer can lead to hairpin formation, making the primer unable to anneal to the DNA template. Complementarity between the 3' end of a primer pair can result in dimerisation of a primer and long runs of Gs and Cs

in the 3' end of the primer can result in misspriming to G/C rich regions. Primers were designed to be 18 to 23 bases long and to contain 50-60% G/C within its sequence, in order to have the same melting temperature for each primer pair. Primers were ordered from Qiagen and rendered salt free by HPLC purification.

2.3.4 Restriction enzyme digestion of DNA

Restriction digestion of DNA samples was carried out according to the manufacturer's recommended conditions (Promega, Gibco BRL or New England Biolabs). Normally, restriction digestions were carried out in a 50 μl total volume containing 5 μl of the enzyme-specific 10x buffer, 5 μl of 10x BSA acetylated bovine serum albumin (Promega), 2 μg of template DNA and 1 μl (12 Units) of the appropriate enzyme. The solution was mixed well and left to incubate for 2 hours. The optimal temperature for the digestion was modified according to the manufacturer's recommendations for that enzyme.

Restriction enzyme digestion varied depending on the purpose of the experiment. Those digestions to linearise plasmid for *in vitro* transcription of RNA probes were scaled up in order to obtain large amounts of linearised plasmid. Those restriction digestions to check the orientation of a particular cloned insert, or to check for the presence of insert in a recombinant plasmid, were carried out with small amounts of DNA, 500 ng, and shorter incubation times, 1 hour. This was sufficient as complete digestion of the plasmid was not required. For other purposes such as cloning of PCR generated fragments the conditions were also modified (see section 2.3.6.1).

2.3.5 Agarose gel electrophoresis

The size of the DNA sample was checked by horizontal gel electrophoresis in a Horizon gel tank (Gibco BRL) using agarose gels prepared with TAE buffer (40 mM Tris, pH 7.2; 0.114% v/v glacial acetic acid; 1 mM EDTA). The percentage of each

agarose gel depended upon the size of the DNA samples and the resolution required to visualise DNA products. For high resolution of small DNA fragments in order to distinguish alleles of 10-30 bases difference, used in the genotyping of *Kumba* mice (*Zic2*^{Ku}) or *loop tail* (*Lp*), 4% (w/v) agarose gel were used. For larger fragments, 100-300 base pairs (bp), used in *splotch* (*Sp*^{2H}) or Shh genotyping, a 2% gel was sufficient to resolve the bands. Agarose gels (4-2%) were prepared using a 1:1 mixture of normal and low melting points (LMP) agarose in TAE. A 1% agarose gel was used for high molecular weight DNA samples such as linearised plasmids or to check the quality of the purified plasmid DNA. The agarose mixture was heated in a microwave oven with intermittent agitation until the agarose was melted. The mixture was then left to cool down at room temperature or on ice. At this point 2.5 μl of ethidium bromide (10 mg/ml stock solution) were added and the agarose was left to solidify at room temperature in a casting tray with combs. Ethidium bromide intercalates into the DNA and fluoresces in long wave UV light. Product sizes were determined by running DNA markers alongside the DNA samples, normally 1 kb ladder or Hyperladder1 (Bioline). After electrophoresis at 80-120 V for 1-3 hours DNA gels were photographed under UV light using a video-documentation system (MultiImage™ Light Cabinet).

2.3.5.1 Purification of DNA fragments from agarose gels

The DNA bands were excised from 1% LMP agarose gels, after staining with ethidium bromide. Three volumes of 6 M NaI were added, and incubation was performed at 55°C until the agarose had melted. Then, 5 μl of 10% silica were added for each μg of DNA. Samples were left on ice for 10 minutes with consecutive inversions to allow the DNA to bind to the silica. Silica was pelleted by centrifugation at 13,000 rpm for 30 seconds and washed three times with 500 μl of wash solution (50 mM NaCl; 10 mM Tris.HCl, pH 7.5; 2.5 mM EDTA; 50% v/v ethanol). DNA was recovered by addition of 1 volume of ddH_2O to the volume of silica and the slurry was heated at 55°C

in a heated block for 5 minutes. The slurry was cleaned of silica by centrifugation and the supernatant containing the purified DNA was kept at -20°C until further use.

2.3.5.2 Purification of DNA fragments using spin columns

QIAquicK Spin columns (QIAGEN) were used for direct purification of double or single-stranded PCR products of size, 100 bp to 10 kilo bases (kb). This method has the advantage that a large number of PCR products can be purified quickly and simultaneously, yielding good quality DNA fragments that can be used for sequencing and cloning into vectors. For the purification, 50-100 μl of QIAGEN PB buffer was added to 10-20 μl of PCR reaction and mixed thoroughly by vortexing. The sample was then loaded onto the column, which contains a silica-membrane to which the DNA can bind in the presence of high concentrations of salt. Impurities were eluted from the column by centrifugation at 13,000 rpm for 30 seconds. The membrane was further washed by addition of 750 μl of QIAGEN washing solution PE and by centrifugation at high speed for 1 minute. The column was left to air dry and the DNA was eluted with 30 μl of ddH_20 or TE buffer.

2.3.6 Procedures for cloning of DNA fragments

Unless otherwise specified, constructs used throughout this thesis were generated using the following protocols.

2.3.6.1 Ligation

When cloning cDNA into vectors, if possible, gel purification was avoided in order to prevent contamination of the DNA. Moreover, whenever possible, directional cloning was designed to insert the cDNA into two different restriction sites so that the insert could be ligated in the vector in the required orientation. Directional cloning saves time when screening recombinant clones after ligation and transformation into bacteria,

compared with cloning into a single restriction site where the insert can be ligated in either a 5'-3' or 3'-5' direction with a 50% chance of a particular clone having the insert in the correct orientation. Finally, restriction enzyme digestions were performed for no more than 2 hours and if the incubation temperature and buffer for two different enzymes were the same, simultaneous digestions using both enzymes were performed.

To generate complementary overhanging ("sticky") ends, 2 μg of midiprep purified DNA (see section 2.3.12) vector was digested with the appropriate enzyme (see section 2.3.4) for 2 hours in a total volume of 50 μl. After digestion, 3 μl were electrophoresed to check that digestion had been successful and enzyme activity was stopped by heat inactivation. The vector was then treated with 1 μl (20 units) of calf intestine phosphatase (CIP) (Roche), by scaling up the reaction to 100 μl total volume and including 10 μl of 10x CIP buffer. The reaction mix was incubated at 37°C for 1 hour. CIP catalyses the hydrolysis of 5' phosphate residues, which are needed to covalently join the DNA. Hence, CIP prevents self re-ligation of the vector. Enzyme and buffer were then removed from the linearised DNA sample using the QIAquick columns (see section 2.3.5.2) and the vector was used immediately or stored at -20°C.

Insert cDNA was prepared in two different ways depending on whether it had been generated by PCR amplification (see section 2.3.3) or was already cloned into a plasmid. Inserts cloned into plasmids were released by restriction digestion and, following electrophoresis in a 1% low melting point agarose gel (see section 2.3.5), the insert was gel purified (see section 2.3.5.1). For inserts generated by PCR, 25% of the product (5 μl of the total reaction) was digested with the appropriate restriction enzyme but the digestion time was increased to 4 hours. The PCR product was then purified using QIAquick columns (see section 2.3.5.2).

Once the insert and vector had been prepared, 2 μl of linearised vector and insert were electrophoresed and quantified by comparison with a DNA marker. The ligation

reaction was prepared in a 15 μl volume containing 50 ng of vector and with the appropriate mass of insert DNA to give a 3:1 molar ratio of insert: space vector. Three units of T4 DNA ligase (1 μl) and 1.5 μl of 10x T4 DNA ligase buffer (Gibco BRL) were added and the reaction was left at 16°C for 4 to 5 hours. A reaction control containing only vector, ligase enzyme and ligase buffer, but without insert was performed in parallel to determine whether the colonies obtained after transformation were products of self re-ligation of plasmid due to unsuccessful CIP treatment or partial restriction enzyme digestion. At this point 5 μl of the ligation reaction was used to chemically transform *E. coli* DH5α cells (see section 2.3.10). Cells were plated on agar culture plates containing 50 μg/ml of ampicillin and placed in a bacterial incubator at 37°C overnight.

2.3.7 Identification of recombinant plasmids

After transformation, recombinant plasmids were identified in different ways depending on the size of the insert cloned, the type of vector used in the cloning and number of colonies to be screened.

2.3.7.1 DNA shift assay

Vectors containing inserts bigger than 600 bp can be distinguished by gel electrophoresis due to a size shift compared to the empty vector. This method was used when large numbers of colonies had to be screened. Typically, clones were picked and grown for 5 hours in 1 ml of LB with antibiotic selection. After growth, 150 μl of each culture was pelleted by centrifugation at 13,000 rpm to harvest cells and the supernatants were discarded. Cells were then lysed in 150 μl of lysis buffer (0.5 mM of EDTA, 10% sucrose, 0.25% w/v SDS, 100 mM NaOH, 60 mM KCl and 0.025% Briliant Blue dye), at 65°C for 5 minutes, followed by 5 minutes incubation on ice. Samples were centrifuged at high speed for 5 minutes and 10 μl of supernatant was

carefully removed and loaded onto an agarose gel for electrophoresis. Recombinant clones appeared as higher molecular weight compared to the empty vectors.

2.3.7.2 Restriction enzyme digest

Restriction digest was the most frequently used method for identification of recombinant plasmids. Colonies were grown overnight with the appropriate antibiotic selection and the plasmid purified using the small-scale plasmids isolation method (see section 2.3.11). Purified plasmid was digested with the same restriction enzymes used to insert the cDNA into the vector, then 10 μl of the reaction was electrophoresed, visualised under UV light and photographed. Recombinant plasmids were identified by the presence of two bands, one corresponding to the plasmid DNA and the other to the insert. Non-recombinant plasmids were identified as a single band.

2.3.7.3 White and blue selection

When the pGEM-T vector (Promega) was used in the cloning of cDNA, for example to generate probes for whole mount *in situ* hybridisation, recombinants were selected by white and blue colony selection. The pGEM-T vector contains a functional β-galactosidase gene within the multi-cloning site. In the presence of isopropyl-1-thio-β-D-galactosidase (IPTG), β-galactosidase acts on the chromogenic substrate 5-bromo-4-chloro-3-indolyl-β-D-galactosidase (X-gal) to produce a blue product resulting in blue colonies. When a cDNA is inserted into the multi-cloning site of the vector, the β-galactosidase gene is disrupted and colonies appear white in the presence of IPTG and X-gal. This method provides a useful and quick way to screen for recombinants.

2.3.7.4 Colony PCR

In cases where a large number of colonies needed to be screened for the presence of recombinant plasmids with inserts smaller than 600 bp the colony PCR

method was used. Colonies were streaked onto an agar culture plate, carefully numbered and left to grow overnight. After overnight culture each colony was picked gently with a plastic tip and immersed in PCR mix-containing primers designed to flank the multicloning site. The PCR product was electrophoresed and photographed under UV light. Clones with an insert were visualised due to the presence of a PCR-generated band with molecular weight corresponding to the size of the insert.

2.3.8 Preparation of competent *Escherichia coli* DH5α cells

The calcium chloride method (Sambrook *et al.*, 1989) was used to make *E. coli* DH5α cells competent for transformation. This method yielded large amounts of competent cells with poor efficiency of transformation. However, their competence was sufficient to carry out routine transformation of plasmids. All the procedures involving bacteria were carried out while observing standard sterile practice.

A colony was picked from a non-selective agar plate (containing no antibiotic) and grown overnight at 37°C in 5-10 ml of non-selective L-broth (LB) medium. A 1-2 ml aliquot of the overnight culture was then used to inoculate 50 ml of LB without antibiotic selection at 37°C for 2 hours. Optical density (OD) was measured using an UVmini1240 spectrophotometer (Shimadzu) and when an OD of 0.5-0.7 was reached, indicating exponential growth, cells were then pelleted by centrifugation at 1,300 rpm at 4°C. The pellet was then resuspended in 20 ml sterile ice-cold 50 mM $CaCl_2$ by carefully pipetting the solution. This centrifugation/resuspension step was repeated twice, after which the pellet was resuspended in 4 ml of sterile ice-cold 50 mM $CaCl_2$ and left overnight at 4°C. Cells were then ready to be used for transformation. For long-term storage, 140 μl of dimethyl sulfoxide (DMSO) was added to the 4 ml cell suspension and left on ice for 15 minutes. After the incubation, another 140 μl of DMSO was added to the cells and mixed gently. Aliquots of 50 μl were snap-frozen by immersion in liquid nitrogen and stored at –80°C until further use.

For expression of recombinant proteins, as used in the glutathione-S-transferase (GST) pull-down experiments, BL21 *E. coli* cells (Promega) were used (see section 2.6.1.1). The BL21 strain has been genetically modified to eliminate proteases so that the expression of large foreign proteins can be achieved with minimal degradation. The calcium chloride method described above was used to make BL21 cells competent.

For those cases in which high efficiency transformation was needed, such as transformation of low amounts of plasmid DNA or unfavourable ligations, commercially available ultra competent XL1 Blue or Ultracompetent XL2 Blue cells (Stratagene) were used.

2.3.9 Preparation of electro-competent cells

In cases where plasmid recovery was very low, such as in the recovery of "bait" or "prey" plasmids from the host yeast strain PJ69-4A (see section 2.5.3), or following ligations that yielded low amounts of DNA, electroporation was used as a means of introducing plasmid DNA into bacterial cells.

The XL-10 *E. coli* (Stratagene) strain was used to make stocks of electro-competent cells. A 50 ml overnight culture, grown at 37°C without antibiotic selection, was used to inoculate 1 L of LB and grown for 1-2 hours monitoring the optical density (OD) reading at 550 nm until it reached an OD of 0.5-0.6. The bacteria were placed on ice for 15 minutes before harvesting by centrifugation at 4,000 rpm for 15 minutes at 4°C. The pelleted cells were then washed free of salts by re-suspension in 1 L of ice-cold water and re-centrifugation at 4,000 rpm for 15 minutes at 4°C. Cells were then washed twice with 500 ml of sterile ice-cold water each time harvesting the cells by centrifugation. The pellet was re-suspended in 40 ml of sterile ice-cold 10% v/v sterile glycerol and then centrifuged again. The pellet was resuspended in 2 ml of ice-cold 10% v/v sterile glycerol and the cell suspension was snap-frozen in 50 μl aliquots by immersion in liquid nitrogen and the aliquots were stored at -80°C.

2.3.10 Transformation of foreign DNA into bacterial cells

Transformation of plasmid DNA into bacteria was achieved by heat-shock or electroporation. The recombinant *E. coli* strains used throughout this thesis were selected on the basis of acquired antibiotic resistance to ampicillin. All plasmids used in the present study had ampicillin as the antibiotic-resistance gene.

2.3.10.1 Chemical transformation by heat-shock

A 50 μl aliquot of competent DH5α *E. coli* cells was thawed on ice for 10 minutes and placed into a pre-chilled falcon polypropylene tube and 50 ng of plasmid DNA was added and gently pipetted up and down. Cells were left on ice for 30 minutes before heat-shocking at 42°C for 45 seconds in a water bath. The duration of heat-shock was according to the manufacturers instructions for commercially available cells. After the heat-shock, cells were placed back on ice for 1-2 minutes. At this point, 1 ml of LB containing 20 mM glucose, 2.5 mM KCl and 10 mM $MgCl_2$ was added and the bacteria were placed at 37°C with vigorous shaking for 1 hour to allow the expression of antibiotic resistance proteins. For routine plasmid transformation, 100 μl were plated onto an agar culture plate containing 50 μg/ml of ampicillin. Plates were inverted and incubated overnight at 37°C.

2.3.10.2 Transformation by electroporation

A 50 μl aliquot of electrocompetent cells was thawed on ice for 10 minutes, and 1 μl of ligation or 5 μl of yeast miniprep was added to the bacteria and gently mixed by pipetting. The mixture was then transferred to a pre-chilled 1 mm gap electroporation cuvette (Invitrogen) and placed in an electroporation machine (Invitrogen Electroporator II) set to 1,800 V and 150 Ω and connected to a power supply of 1,500 V, 25 mA and 25W. A pulse current was applied and the cuvette was then placed on ice for 1 to 2 minutes. Cells were allowed to recover by adding 1 ml of LB containing 20

mM glucose, 2.5 mM KCl and 10 mM $MgCl_2$ and incubating at 37°C for 1 hour to allow the expression of antibiotic resistance proteins. Since this method was used for difficult transformations, all the bacterial cells were harvested by centrifugation at 3,000 rpm and pellet was resupended in 100 μl of LB. The entire volume was then plated out onto agar cultures plates containing 50 μg/ml ampicillin and incubated at 37°C overnight.

2.3.10.3 Small-scale isolation of plasmid DNA: miniprep

Small-scale isolation of plasmid DNA yielded up to 5-6 μg of template DNA. This technique was used for the identification of recombinant plasmids after ligation, for sequencing to verify identity of the insert after cloning, or as a quick method to prepare plasmid stocks. The small-scale isolation of plasmid DNA is a quick protocol but yields poor quality DNA, with the possibility of endonucleases being co-purified with the plasmid. For those experiments that required high quality DNA such as transfection of the plasmid DNA into yeast or mammalian cells (see chapter 5/6), or for *in vitro* translation/transcription methods, where purity of the template DNA was critical, a large scale isolation of plasmid DNA was performed.

The GFX MicroPlasmid Kit was used (Amersham Pharmacia Biotech) according to the manufacturer's protocol. One colony was picked and grown overnight at 37°C in 5 ml of LB with the appropriate selective antibiotic, after which 1.5 ml of culture was centrifuged at 13,000 rpm for 2 minutes. The supernatant was discarded and the cells were resuspended in 150 μl of solution 1 (100 mM Tris.HCl, pH 7.5; 10 mM EDTA; 400 μg/ml RNase I). Cells were ruptured by alkaline lysis using 150 μl of solution II (190 mM NaOH; 1% w/v SDS) and gently inverting the tube 10 times. A viscous solution was formed containing cell debris, protein, genomic and plasmid DNA. In order to precipitate cellular debris and protein, solution III (acetate-buffered solution containing chaotropic salt) was added to the mixture and the tube was gently inverted 10 times. The precipitate was then pelleted twice by centrifugation at 13,000 rpm for 5

minutes. The supernatant containing the plasmid DNA was loaded onto a GFX glass fibre matrix column, incubated at room temperature for 1 minute, and centrifuged for 30 seconds at 13,000 rpm. Genomic DNA and protein were removed by addition of 750 µl of wash solution (10 mM Tris.HCl, pH 8.0; 1 mM EDTA; 80% v/v of ethanol) followed by centrifugation. To elute the DNA, the column was placed in a fresh eppendorf tube and 100 µl of TE buffer or ddH_2O was added to the column, and incubated at room temperature for 3 minutes. The DNA was recovered by centrifugation at 13,000 rpm for 1 minute. The plasmid DNA sample was stored at -20°C

2.3.11 Large-scale isolation of plasmid DNA: midi/maxiprep

Large-scale isolation of plasmid DNA was carried out according to the QIAGEN manufacturer's instructions. This method typically yielded 100 to 500 µg of good quality DNA that could be used for transfection or for *in vitro* transcription-translation. Midi and maxi-prep followed the same basic protocol with changes in volumes and times as indicated by midi/maxi.

A colony was picked and grown overnight in 5 ml of LB with the appropriate selection antibiotic. The overnight culture was used to inoculate 50/500 ml by diluting the culture 1:1000. Bacteria cells were then harvested by centrifugation at 6,000 g for 15 minutes at 4°C and the supernatant was discarded. The pellet was resuspended in 4/10 ml of solution P1 (50 mM Tris.HCL, pH 8.0; 10 mM EDTA; 100 µg/ml of Rnase A). Bacteria were lysed by addition of 4/10 ml of P2 (200 mM NaOH, 1% w/v SDS), followed by inversion 4 times and left at room temperature for 5 minutes. Cell debris was precipitated by addition of 4/10 ml of ice-cold P3 solution (3 M potassium acetate, pH 5.5) followed by gentle inversion of the solution 5 times, incubation on ice for 15/20 minutes and centrifugation at 20,000 g for 30 minutes at 4°C. Meanwhile, an anion-exchange resin column (QIAGEN-tip 100/500), equilibrated by addition of 4/10 ml of buffer QBT (750 mM NaCl; 50 mM MOPS, pH 7.0; 15% v/v isopropanol; 0.15% v/v

Triton X-100), was allowed to empty by gravity. The supernatant was loaded and the column was allowed to empty by gravity. The column was then washed twice by addition of 10/30 ml of buffer QC (1 M NaCl; 50 mM MOPS, pH 7.0; 15% v/v isopropanol) and allowed to drain by gravity. The DNA was eluted from the column with 5/10 ml of Buffer QF (1.25 M NaCl; 50 mM Tris.HCl, pH 8.5; 15% v/v isopropanol) and precipitated by addition of 0.7 volumes of isopropanol followed by centrifugation at 15,000 g for 30 minutes at 4°C. The DNA pellet was washed with 70% ethanol, and air-dried at room temperature for 5 minutes, before being redissolved in TE (10 mM Tri.HCl, pH 8.0; 1 mM EDTA). The quantity of DNA recovered was estimated by gel electrophoresis (see section 2.3.5), compared with known concentration of a DNA marker run alongside. Further quantification was achieved spectrophotometrically by measuring absorption at 260 nm (A_{260}). The purity of the DNA was assessed by measuring the absorption at 280 nm (A_{280}), the ratio A_{260} : A_{280} should be 1.8-2.0 for good quality DNA.

2.3.12 Automated DNA sequencing

DNA sequences were obtained using a MegaBACE 1000 capillary sequencing machine (Amersham Bioscience). Each sequencing reaction (20 μl) typically contained 0.5 μg of plasmid DNA or 0.1-0.2 μg of cleaned PCR product, 8 μl of fluorescent dye ET terminator mix (Amersham Bioscience) and 1 μl of sequencing primer at 5 μM final concentration. The PCR sequencing reaction included three steps: denaturation at 94°C for 30 seconds, annealing of the sequencing primer at 50°C for 20 seconds and extension at 60°C for 1 minute. These series were repeated for 20 to 25 cycles.

The sequencing PCR products were cleaned of unincorporated ET terminators by addition of 55 μl of 100% ethanol and 2 μl of 7.5M sodium acetate, mixed by vortexing . Samples were then centrifuged at 13,000 rpm for 15 minutes, the pellet was washed with 100 μl of 75 % ethanol, left to air dry for 5 minutes and stored at –20°C.

Before loading in the MegaBACE capillary sequencing machine, reactions were dissolved in 10 μl of loading buffer (Amersham Biosciences).

2.3.13 Sequence analysis

Sequence analysis was performed using BioEdit software, which allowed reading of the electropherogram, as well as giving the sequence in FASTA format. To verify the identity or correct sequence of a cDNA, sequences were analysed for homology to other cDNAs using the Basic Local Alignment Search Tool (BLAST) on the National Centre for Biotechnology Information (NCBI) web site (http://www.ncbi.nlm.nih.gov/blast), using the Mouse Genome Database.

Sequences that display no homology to any known cDNA, were analysed for homology to an expressed sequence tag (EST) database. The sequence of the EST was then analysed using the Sanger Centre Mouse Genome Database to identify the chromosomal location, genomic organisation and related sequences (http://www.ensembl.org/Multi/blastview).

2.4 RNA METHODS

2.4.1 General considerations when working with RNA

Solutions were treated with diethyl pyrocarbonate (DEPC), a potent inhibitor of ribonucleases (Ehrenberg *et al.*, 1976) in order to avoid degradation of cellular or newly synthesised RNA. Only solutions containing Tris and EDTA or those solutions that could not be autoclaved, such as SDS, were not DEPC-treated. However, in these cases, DEPC-treated H_2O was used to make up these solutions. DEPC was added to 0.05% v/v and shaken vigorously before being left overnight at room temperature and then autoclaved. The bench and pipettes were wiped with 70% ethanol to make sure that the area of work was dust free and gloves were worn at all times. Filtered RNAse-free

pipette tips were used throughout. Glassware and metal racks were rinsed with MilliQ water and cleaned with acetic acid before being baked at 280°C for 5 hours. All reagents were freshly prepared and were used only for RNAse-free work.

2.4.2 Extraction of total RNA from mouse embryos

The guanidine isothiocyanate/phenol method developed by Chomezynski and Sacchi (1987) was used to extract total RNA from mouse embryos. This method uses the TRIzol Reagent (Gibco BRL), which induces formation of RNA complexes with guanidine and water molecules, excluding proteins and DNA from the aqueous phase by inhibiting hydrophilic interactions.

After dissection (see section 2.2.1) embryos were homogenised in TRIzol by sucking the embryos through syringe needles, of successively smaller gauge (12G-19G). For a single E8.5 embryo, 200 μl TRIzol was used, whereas for E9.5-10.5 embryos 0.5 to 1 ml were used respectively. After homogenisation, samples were incubated at room temperature for 5 minutes to allow complete dissociation of nucleoprotein complexes. Cellular debris was then pelleted by centrifugation at 13,000 rpm for 5 minutes at 4°C. The supernatant was collected and a one-fifth volume of chloroform was added followed by vigorous shaking and incubation at room temperature for 2 minutes. In order to separate the solution into two phases, samples were centrifuged at 13,000 rpm for 15 minutes at 4°C. The upper colourless phase was removed and the RNA precipitated by addition of one volume of isopropanol followed by incubation at room temperature for 10 minutes. The sample was centrifuged at 13,000 rpm for 15 minutes at 4°C to pellet the RNA, which was washed with 75% ethanol, re-centrifuged for 5 minutes at 13,000 rpm and the pellet left to air dry. The RNA was then resuspended in 10-300 μl of DEPC-ddH_2O depending on the number of embryos used in the sample and the size of the pellet. The RNA was stored at -20°C.

2.4.3 Reverse transcription to generate cDNA

First strand cDNA was generated by reverse transcription using RNA purified from embryos. The first cDNA strand was used as template to amplify cDNA fragments for cloning of probes and constructs.

In preparation for the reverse transcription reaction, 300-500 ng of total RNA was mixed with 0.2 μg of hexanucleotides (Gibco BRL) in a volume of 9.5 μl. The mixture was denatured at 70°C for 7 minutes followed by annealing at 37°C for 10 minutes. This step allowed the hexanucleotides to anneal to the RNA. After the incubation, 9.5 μl of the annealed RNA/hexanucleotide mixture was used for the reverse transcription reaction that contained 1 x first strand RT reaction buffer, 0.25 mM each dNTP, 10 mM DTT, 0.5 μl RNase inhibitor (Pharmacia) and 1 μl (200 units) Moloney murine leukaemia virus (MMLV) reverse transcriptase (Gibco BRL). A control, NO-RT, was also prepared following the above procedure but without adding the reverse transcriptase. The RT and the NO-RT samples were incubated at 37°C for 1 hour. To stop the reaction samples were heated to 95°C for 5 minutes and the samples diluted with 40 μl of ddH_20 and stored at -20°C.

2.4.3.1 PCR to amplify first cDNA strand

To amplify cDNA for production of constructs, 1 μl of first strand cDNA was used as template in a standard PCR reaction (section 2.3.3). Simultaneously, a second PCR was performed with the NO-RT control sample to verify that the PCR amplified only cDNA and not contaminating genomic DNA. To verify the quality of the cDNA, PCR was carried out with primers specific for hypoxanthine-guanine phosphoribosyltransferase (HPRT), which is a ubiquitously expressed house keeping gene (Melton *et al.*, 1984).

2.4.4 Whole mount *in situ* hybridisation

Whole mount *in situ* hybridisation was performed using the methodology of (1992).

2.4.4.1 Preparation of template DNA

In order to obtain single stranded RNA probes, *in vitro* transcription was performed using cDNA cloned into the pGEM-T vector (Promega, UK) (see appendix 1). To obtain DNA template, plasmids were purified using the midiprep method (see section 2.3.9). Then, 10 μg of the template was digested in a 50 μl volume with appropriate restriction enzyme (see section 2.3.4), after which the linearised plasmid was treated with 10 μl of PK (10 mg/ml) and 40μl of H_20. The linearised template DNA was further purified by adding 1 volume of phenol-chloroform (100 μl), followed by vigorous shaking until a white homogenous solution was formed. Centrifugation at 13,000 rpm for 20 minutes produced two layers with the top aqueous phase containing the DNA and the bottom, non-aqueous layer containing proteins. The aqueous layer was collected and DNA was precipitated by addition of 2.5 volumes of 100% ethanol and 1/10 initial volume of sodium acetate, followed by incubation at –20°C for 2 hours, or –80°C for 30 minutes, and centrifugation at 13,000 rpm for 20 minutes. Pelleted DNA was cleaned free of salts by resuspension in 75% ice-cold ethanol and pelleted by centrifugation at 13,000 rpm. The DNA pellet was then dissolved in 10 μl DEPC-treated ddH_2O. For *in vitro* transcription, 1 μl of the linearised plasmid containing 1 μg of template DNA was used.

2.4.4.2 Synthesis of digoxigenin-labelled probes

In vitro transcription using Sp6 or T7 RNA polymerases (Roche), produced an antisense or sense probe depending on the orientation of the cDNA with respect to the location of the flanking promoters in the vector. The following reagents were added in

sequence to a total volume of 20 μl: 2 μl of 100 mM DTT, 1 μl of RNAse inhibitor, 2 μl of digoxigenin-labelling mix (10 mM each of ATP, CTP, and GTP; 6.5 mM UTP; 3.5 mM digoxigenin-labelled-UTP), 1 μl of RNA polymerase (Sp6 or T7) and 1 μl of linearised plasmid DNA. The reaction was vortexed and centrifuged for 3 seconds to ensure that all reagents were well mixed. The reaction was incubated at 37 °C for 2 hours.

An optimal *in vitro* transcription reaction yielded 10 μg of single stranded RNA that could be visualised by electrophoresis on an agarose gel (see section 2.3.5) by the presence of two bands, one of high molecular weight corresponding to the linearised template DNA, and a second of low molecular weight (which was normally ten times brighter) corresponding to the newly synthesised RNA. Newly *in vitro* transcribed probe was precipitated, and purified from unincorporated nucleotides that could lead to a high background in the detection of the signal. Precipitation was performed by addition of 70 μl of DEPC-treated H_2O, 300 μl of 100% ice-cold ethanol and 10 μl of 3 M lithium chloride, followed by vortexing and incubation at –20°C for 2 hours. The probe was pelleted by centrifugation at 13,000 rpm at 4°C for 30 minutes, then washed free of salts with 100 μl of 70% ethanol and air-dried, before being dissolved in 75 μl of DEPC-treated H_2O and 25 μl of formamide. The labelled probe was visualised on an agarose electrophoresis gel to check that no degradation had occurred during the precipitation step. Probes were stored at –20°C.

2.4.4.3 Pre-treatment of embryos and hybridisation

Embryos stored in 100% methanol at –20°C were hydrated through a series of 90, 75, 50 and 25% methanol in PBT (DEPC-treated PBS containing 1% Tween) for 15 to 20 minutes and then washed twice in PBT for ten minutes. Embryos were then incubated for 1 hour in 6% hydrogen peroxide in PBT in order to inhibit endogenous peroxidase. The reaction was stopped by three washes in PBT for 10 minutes each.

Embryos were permeabilised by treatment with 5 μg/ml of PK to allow penetration of the labelled probe into the tissue. The PK treatment varied depending upon the size and age of the embryos; E8.5 were treated for 1 minute, E9.5 for 2 minutes and E10.5 embryos for 5 minutes. The PK enzymatic activity was inhibited by incubating the embryos in 2 mg/ml glycine in PBT for 10 minutes followed by three consecutive washes of PBT. At this stage, embryos were re-fixed in 4% PFA/0.2% glutaraldehyde in PBS for 20 minutes followed by three PBT washes of 5 minutes each. Embryos were prehybridised for at least 2 hours at 70°C using freshly prepared pre-hybridisation mixture containing: 50% formamide, 5x sodium chloride/sodium citrate buffer (SSC) pH 4.5, 50 μg/ml heparin, 50 μg/ml yeast transfer RNA and 1% sodium dodecyl sulphate (SDS). After pre-hybridisation, embryos were stored at –20°C in some cases. Embryos were then transferred to a 1 ml tube containing fresh pre-hybridisation solution and 1 μg/ml of digoxigenin-labelled probe was added followed by an overnight incubation at 70°C. The hybridisation temperature varied depending on the probe, and this was optimised empirically. For probes designed in conserved regions of a gene family, the starting hybridisation temperature was 70°C to avoid cross-hybridisation. If no specific signal was observed, or the signal was of low intensity the hybridisation temperature was decreased to 67-65°C.

2.4.4.4 Washes and detection of digoxigenin-labelled probes

After overnight hybridisation, embryos were washed free of unbound probe by high stringency washes. Solution 1 (50% formamide, 5x SSC pH 4.5, 1% SDS) and solution 2 (50% formamide, 2x SSC) were heated to the same temperature as the hybridisation mixture. Embryos were transferred to 15 ml falcon tubes and washed twice for 45 minutes each with 5-10 ml of solution 1 and 2. At this stage the embryos were very delicate and damage was avoided by letting the embryos settle to the bottom of the tube and leaving liquid above them in each of the washing steps. All washes were

carried out in a water bath with regular but gentle agitation of the tubes. Embryos were washed with TBST (137 mM NaCl, 2.7 mM KCl, 25 Tris HCl pH 7.5, 1% Tween-20, 0.48 mg/ml levamisol) and then blocked for 1 hour at 4°C with 10% sheep serum in TBST to prevent non-specific binding of the antibody. During blocking of the embryos, the anti-digoxigenin antibody conjugated to alkaline phosphatase (Boehringer Manheim) was diluted 1 in 1000 in TBTS and preabsorbed by incubating for 90 minutes in the presence of embryo powder (homogenised E9.5-12.5 mouse embryos, washed with acetone and dried at room temperature to form a powder). Preabsorbed antibody was separated from the embryo powder by centrifugation and the supernatant was filtered through a 0.45 μm Millipore filter. Embryos were incubated with the preabsorbed antibody at 4°C overnight in a 2 ml volume. Excess of unbound antibody was removed by ten TBST washes of 30 minutes each at room temperature and left overnight rocking at 4°C. The following day, embryos were washed three times for 20 minutes in NTMT (100 mM sodium chloride; 50 mM magnesium chloride; 1 mM levamisol; 0.1% Tween-20; 100 mM Tris, pH9.5). Colour development was achieved by incubating the embryos in NBT/BCIP (4.5 μl of 100 mg/ml nitroblue tetrazolium; 3.5 μl of 50 mg/ml of 5-bromo-4-chloro-3-indolylphosphate; 1 ml NTMT), within a dark box. The length of time that development was continued varied with the probe. Once signal was present, at the required intensity, the reaction was stopped, in order to avoid background staining, by washing the embryos with PBT three times. Embryos were kept in PBT with 0.05 % thimerazol until photographed. Some embryos were embedded in albumin gelatin and sectioned using a vibratome (see section 2.2.2).

2.5 YEAST METHODS

2.5.1 Growth and maintenance of the host yeast strain

In the yeast two-hybrid analysis for the identification of Zic2 protein partners (chapter 5), the PJ69-4A host yeast strain (James *et al.*, 1996) was used. When working with yeast, extra care was taken, to avoid contamination with bacteria, by working in a sterile hood used only for yeast.

2.5.1.1 Preparation of the non-selective rich medium YPAD

For routine growth, the host yeast strain was grown on a non-selective rich medium either in liquid or on the surface of a solid agar plate. Rich medium contained yeast extract, peptone, adenine and dextrose (YPAD), which provides the yeast with amino acids, nucleotide precursors, vitamins and essential metabolites needed for optimal cell growth. The rich medium YPAD was prepared following the concentrations given in Table 2.1 and sterilised by autoclaving. A 40% w/v stock solution of glucose was prepared separately, filter sterilized and 50 ml added to1 L of YPAD.

2.5.1.2 Preparation of selective SD minimal medium

To provide selective conditions, the host yeast strain was grown on a minimal medium known as synthetic defined (SD) medium, which contained yeast nitrogen base, ammonium sulphate and dextrose. SD medium was used as a basal medium to which amino acids and nucleoside precursors were added to produce the SD-drop out medium, which lacked one or several amino acids allowing the selection or maintenance of a particular plasmid, or selection based on transcriptional activation of a reporter gene.

Table 2.1 Components of YPAD medium for growth of PJ69-4A yeast without selection

Constituent	Concentration	Supplier
Bacto yeast extract	1 %	Difco
Bacto peptone	2 %	Difco
Glucose	2 %	Sigma
Bacto- agar	2 %	Difco
Adenine sulfate	0.004 %	Sigma
Distilled water	1000 ml	

Minimal SD medium was prepared following the concentrations given in Table 2.2, while SD-drop out medium was prepared as described in Table 2.3. Solutions were filter-sterilised using a 0.2 μm Millipore filter and kept at 4°C until required. Stock solutions were kept for 4-5 months.

Table 2.2 Components of SD minimal medium for growth of PJ69-4A yeast

Constituent	Concentration	Supplier
Bacto yeast nitrogen without amino acids	0.67 %	Difco
Glucose	2 %	Sigma
Bacto agar	2 %	Difco
Distilled water	1000 ml	

Table 2.3 Components of the drop out medium for PJ69-4A used for genotyping the host yeast strain, selection of the recombinants and interactions from the library screen.

Constituent	Stock concentration (g/100 ml)	Volume of stock for 500 ml of SD medium (ml)	Final concentration in medium (mg/l)	Supplier
Adenine sulfate	0.2	5	20	Sigma
Uracil	0.2	5	20	Sigma
L-Tryptophan	1	1	20	Sigma
L-Histidine	1	1	20	Fluka
L-Methionine	1	1	20	Sigma
L-Leucine	1	3	60	Fluka
L-Lysine	1	1.5	30	Fluka

2.5.1.3 Preparation of PJ69-4A glycerol stocks

To make glycerol stocks from the PJ69-4A strain, yeast were plated out on YPAD-agar plates and grown for 48-72 hours at 30°C until colonies were visible. One colony was then picked and grown overnight in 5 ml YPAD liquid medium (without adding bacto-agar to the solution) in a shaking incubator at 30°C. Growth was assessed by measuring the optical density (OD) at 600 nm using an Uvmini1240 spectrophotometer (Shimadzu). 1-3 ml of the overnight culture was used to inoculate 25 ml of pre-warmed YPAD medium, and once the OD_{600} reached 0.5-0.7, the yeast culture was considered to be in exponential growth. Glycerol stocks were made by adding 30% v/v of glycerol to 1 ml of culture and stored at -80°C. The same procedure was used to produce glycerol stocks of recombinant PJ69-4A containing either *Gal4-Zic2* bait plasmid or VP16 library plasmid but in these cases the recombinant PJ69-4A was grown in SD medium lacking the selective amino acid.

2.5.2 High efficiency transformation of PJ69-4A with foreign DNA

Transformation of the host yeast strain, PJ69-4A, was performed to generate a recombinant strain that expressed the bait protein of interest and to allow potential interactions between the bait protein and the library plasmid. Co-transformation was avoided as it yielded very few double recombinants compared with serial transformation. Transformation was accomplished by the high-efficiency lithium acetate/ single-stranded carrier DNA/polyethylene glycol (LiAc/ssDNA/PEG) protocol (Gietz and Schiestl, 1991).

2.5.2.1 Quick yeast transformation

The transformation procedure typically involved the growth of JP69-4A overnight in 5 ml pre-warmed YPAD at 30°C with vigorous shaking. An appropriate volume of the overnight culture was used to inoculate 60 ml of YPAD to produce an

OD_{600} of 0.1. At this OD, PJ69-4A required 4-5 hours of further growth to reach the cell density needed for transformation (i.e. an OD_{600} of 0.5-0.7). The optical density was checked in all transformations since a culture at incorrect OD led to poor efficiency of transformation. Cells in the 60 ml culture were pelleted by centrifugation at 2,500 rpm for 5 minutes, the pellet was resuspended in 20 ml of sterile distilled H_20 and spun again at 2,500 rpm to make sure that no traces of YPAD medium were left. The cleaned pellet containing only PJ69-4A cells was resuspended in 0.3 ml of 1XTE/LiOAC (0.5 ml of 10xTE, 0.5 ml of 10xLiOAc, 4 ml of ddH_2O).

Carrier DNA was denatured by boiling 150 µl of salmon testis DNA at 105°C for 5 minutes. Then, 100 ng of purified plasmid DNA from a midiprep (see section 2.3.11) was added to 100 µl PJ69-A4 in 1XTE/LiOAc along with 50 µl of the denatured carrier DNA and mixed by inversion. After thorough mixing, 300 µl of 1xTE/LiOAc/polyethylene glycol (Fluka) (0.5 ml of 10xTE, 0.5 ml of 10xLiOAc, 4 ml of PEG) was added to each tube and the mixtures were incubated at 30°C with shaking for 30 minutes.

To carry out the transformations, 70 µl of DMSO was added to each tube and the PJ69-4A cells were heat shocked at 45°C for 5-6 minutes. The PJ69-4A cells were then pelleted, washed with ddH_20, to make sure that no traces of DMSO were left. The transformed PJ69-4A cells were then plated on SD-uracil. Only recombinant colonies were able to grow on the selection medium 48-72 hours after being plated.

2.5.2.2 High efficiency transformation of VP16 mouse E9.5-10.5 library

Recombinant PJ69-4A was plated out on SD-uracil to select for the bait plasmid. After 72 hours growth at 30°C a whole colony was inoculated into 20 ml of SD-uracil medium and grown for 24 hours at 30°C. This step was important to get high efficiency transformation and use of old yeast cells was avoided. An aliquot of this overnight culture was inoculated into 1000 ml of SD-uracil to produce an OD_{600} 0.1-0.2. After 5

hours, the OD_{600} of the culture reached 0.7. Yeast cells were pelleted by centrifugation using 250 ml bottles at 2,500 rpm for 5 minutes. Pellets were washed with TE several times by resuspending the pellet and centrifugation, and the pelleted cells were then resuspended in 1.2 ml of denatured carrier DNA, plus 20 ml of 1xTE/LiOAC. After shaking, 140 ml of 1xTE/LiOAC/PEG was added together with 250 μg VP16 E9.5-10.5 mouse library provided by Professor Peter Scambler, Molecular Medicine Unit, Institute of Child Health, UCL.

The mixture was incubated for 30 minutes at 30°C with vigorous shaking. Cells were then heat-shocked at 45°C in the presence of DMSO for 5-7 minutes and rinsed to get rid of the DMSO by pelleting the yeast cells, resuspending in distilled water and re-centrifuging. After transformation, pellets were resuspended in 2 L of pre-warmed YPAD media and left to recover for one hour. Cells were then pelleted by centrifugation and washed with SD-uracil-leucine several times to make sure no traces of YPAD remained. Pellets were then resuspended in 2 ml SD -uracil-leucine and recovery was allowed for no more than 9 hours. Cells were then pelleted by centrifugation and resuspended in 30 aliquots of 0.5 ml each. Each aliquot was then plated onto SD-uracil-leucine-histidine-adenine plates.

After 72 hours, clones were re-streaked onto SD -uracil-leucine-histidine-adenine containing 2 mg/ml final concentration of X-α-Gal (BD Biosciences). Only colonies that grew on the selection medium (SD -uracil-leucine-histidine-adenine), and turned blue in the presence of X-α-gal, were considered as possible interactors. For the low scale transformation the same procedure was followed but using ten times lower volumes of each reagent.

2.5.3 Identification of interacting clones and rescue of plasmid

This method was used in the identification of interacting clones that were able to grown on the appropriate SD selection medium. Clones were grown for 48 hours in SD

-leucine medium, which selects only for the VP16 library plasmids, in order to eliminate the bait plasmid from the double PJ69-4A recombinants. Cultures were centrifuged at 2,500 rpm for 5 minutes to harvest the yeast cells containing the plasmid of interest and the supernatant was discarded. Pellets were kept at -20°C until further use.

To purify the plasmid of interest, pellets were rapidly thawed, resuspended in lysis buffer (50 mM Tris-HCl, pH 7.5; 1.2 M sorbitol, 10 mM EDTA, 10 mM mercaptoethanol) and treated with Lyticase enzyme (30 units/ µl) overnight at 37°C in order to digest the yeast cell walls. After digestion, cells were harvested by centrifugation and the supernatant was discarded. The GFX microplasmid Kit was then used to purify plasmid DNA (see section 2.3.11). After purification, 1 µl of the final miniprep was used in a PCR reaction (see section 2.3.3.1) to amplify the insert of the VP16 library plasmid. The PCR product was cleaned using QIAGEN spin columns (see section 2.3.5.2) and then sequenced.

To verify the identity of each interacting clone, the resulting sequence was analysed for homology to other cDNAs using the BLAST search on the NCBI mouse genome database (http://www.ncbi.nlm.nih.gov/blast). Only in-frame inserts that did not appear on the list of false positives (http://www.fccc.edu/research/labs/golemis) were considered as possible interactors.

Interacting clones from the VP16 library considered to be potential true physiological interactors were transformed by electroporation (see section 2.3.10.2) and recombinant clones were identified by colony-PCR (see section 2.3.7.4) using primers flanking the VP16 plasmid (see methods in chapter 5 for primer sequences). Only clones containing the VP16 library plasmids were grown and the plasmids were purified using the GFX microplasmid kit (see section 2.3.11).

2.6 PROTEIN METHODS

2.6.1 *In vitro* glutathione-S-transferase (GST) pulldown assay

The glutathione-S-transferase pull-down assay (GST pull-down) is the most widely used method for evaluation of protein interactions found in a yeast two-hybrid experiment. In this assay, either the protein of interest (prey) or bait protein used in the library screen, is expressed as a fusion protein with GST. The GST-fusion protein is immobilised on sepharose beads and incubated with *in vitro* transcribed and translated candidate interacting protein labelled with [^{35}S]-methionine. After several washes protein-protein complexes are separated by sodium dodecyl sulfate polyacrylamide gel electrophoresis (SDS-PAGE) and bands visualised by autoradiography.

2.6.1.1 Expression and purification of GST fusion protein

Fusion proteins were generated using *pGEX* constructs (see methods chapter 6 and section 2.8), which allowed high-level bacterial protein expression. Constructs were transformed into BL21 cells (see section 2.3.10.1) and plated on agar plates with ampicillin selection. One colony was picked and grown overnight in 50 ml of LB at 37°C with vigorous shaking. The culture was then diluted 10 times by addition of 450 ml of LB and grown with antibiotic selection for 1 hour at 37°C. One aliquot was kept to serve as an uninduced fraction. Induction of protein expression was then achieved by addition of IPTG to a final concentration of 0.1 mM and incubation at 30°C for 3-5 hours. The pGEX vector contains the *lac* repressor gene, which binds to the *tac* promoter and suppresses the expression of the GST fusion protein. In presence of IPTG, which acts as a *lac* analog, derepression of the *tac* promoter occurs, leading to expression of the GST fusion protein.

Cultures were chilled on ice and phenylmethane sulphonyl fluoride (PMSF) was added to a final concentration of 0.1 mM. Bacterial cells were harvested by

centrifugation at 5,000 g for 5 minutes at 4°C. The cell pellet was snap-frozen by dipping in liquid nitrogen, followed by storage at -70°C. Snap-freezing helped improve subsequent lysis of the cells.

To purify the GST fusion protein, cell pellets were quickly thawed at 37°C in a water bath and resuspended in 10 ml of ice-cold sterilised NETN buffer (20 mM Tris-HCl, pH8; 100 mM NaCl; 1 mM EDTA; 0.5% NP-40). Protease inhibitor Complete (Roche Diagnostics GmbH: 1 tablet in 50 ml) was prepared and DTT was added at 1 mM. Lysozyme (2 mg/ml) was added to the cell suspension in order to lyse the cells and the reaction was incubated on ice for 10 minutes with occasional shaking. To ensure disruption of cells and to shear DNA, samples were sonicated three times for 15 seconds at 4°C. Cell debris was pelleted by centrifugation at 12,000 rpm for 15 minutes at 4°C and an aliquot was kept for further analysis. The supernatant was placed in a chilled eppendorf tube and centrifuged at 12,000 rpm for 15 minutes at 4°C and the pellet was kept for further analysis to check for the presence of GST fusion protein in the insoluble fraction by SDS-PAGE electrophoresis. The supernatant was carefully removed, KCl was added to a final concentration of 200 mM to improve the binding capacity of the affinity resin and placed at 4°C.

Meanwhile, 250 μl of glutathione-sepharose beads were washed 4 times with 10 volumes of NETN buffer by centrifugation at 13,000 rpm, resuspended as a 50% slurry in NETN, and stored at 4°C. To improve blocking of non-specific binding, the beads were incubated at room temperature with 100 μg/ml of BSA for 15 minutes. Unbound BSA was removed by washing 3 times in NETN prior to storage as a 50 % slurry.

To immobilise the GST fusion protein on the beads, the supernatant kept at 4 °C was mixed with beads and left incubating for 2-3 hours on an a rotating wheel at 4 °C. Beads were then collected by pulse spinning for 30 seconds at 4,000 rpm, and the supernatant was discarded. The beads with GST fusion protein bound, were further

washed with three changes of 10 ml NETN at 4°C by pulse spinning at 4,000 rpm, and then stored as 50% slurry at -70°C.

2.6.1.2 *In vitro* transcription and translation of candidate proteins

In vitro translation/transcription (IVT) was used to produce [^{35}S]-methionine labelled proteins that were candidates for interaction with Zic2. This method was performed using the TNT-coupled reticulocyte lysate system (Promega), following the manufacturer's protocol. The success of the IVT reaction depends on the purity of the DNA (template DNA was purified by midiprep; see section 2.3.12). The IVT requires an uninterrupted cDNA sequence that must contain the initiation methionine codon (AUG) in the correct frame relative to the T7 promoter.

The TNT-coupled transcription/translation system includes a reaction mix that contains RNA polymerase, salts, nucleotides and ribonuclease inhibitor. An *in vitro* transcription/ translation IVT reaction was prepared by mixing 20 μl of TNT reaction mix, 3 μl of [^{35}S]-methionine (Amersham Biosciences), 1 μg of template plasmid DNA, and dd$H_2$0 to 25 μl total volume. The reaction was mixed thoroughly and left incubating at 30°C for 90 minutes. Then, 2 μl of the reaction was run on an SDS-PAGE gel to check that the IVT had been successful. Samples were stored at –70°C.

2.6.1.3 In vitro protein interaction assay

GST-fusion protein bound to glutathione-sepharose beads (section 2.6.1.1) was thawed and 500 ng of beads were washed twice with 1 ml of ice cold NETN, without DTT, by centrifugation at 4,000 rpm. DTT was not added to the NETN since it can inhibit weak interactions. Then, 2-10 μl of IVT was added together with 1 ml of fresh NETN and the reaction was incubated at 4°C between 6 hours and overnight on a rotating wheel to allow protein complexes to form. After incubation, protein complexes bound to the beads were pelleted by pulse spinning at 4,000 rpm for 1 minute followed

by four consecutive washes with NETN. Supernatant containing unbound protein was discarded and pellets were kept at -70°C prior to electrophoresis.

2.6.1.4 SDS-PAGE electrophoresis

Pellets containing the complex between the GST-fusion protein (bound to beads) and the *in vitro* translated/transcribed protein were thawed on ice. Two volumes of Laemmli gel loading buffer (192 mM glycine; 25 mM Tris; 0.1% w/v SDS) was added to the beads and boiled at 95°C for 3 minutes to release the protein complex from the beads. Samples were then incubated on ice for 5 minutes and centrifuged at high speed for 1 minute. A 10 μl volume of each sample was loaded onto a 12% sodium dodecyl sulfate polyacrylamide (SDS-PAGE) gel. The gel mix (12% acrylamide; 375 mM Tris, pH 8; 0.1% w/v SDS; 0.1% w/v ammonium persulphate; 0.1% v/v TEMED) was poured into the cassette until the meniscus reached 2.5 cm from the top of the glass plates. An overlay of water-saturated butanol was added in order to avoid oxygen contact with the solution to speed the polymerisation of the acrylamide. Once the acrylamide had set, the overlay was poured off and the acrylamide solution for the stacking gel (5.1% acrylamide; 130 mM Tris, pH 6.8; 0.1% w/v SDS; 0.1% w/v ammonium persulphate; 0.1% v/v TEMED) was added and the comb placed into the gel solution. Once the stacking gel had set, the comb was removed, the wells were washed with ddH_2O and the gel was placed in a running tank containing running buffer (43 mM Tris, 192 mM glycine, 0.1% (w/v) SDS). Electrophoresis was carried out at 25 mA until the dye front had reached the bottom of the gel. The gel was stained by immersion in Coomassie Blue stain for 15 minutes, destained with 25% v/v methanol, 7.5% v/v acetic acid, then dried for 30 minutes and exposed to Biomax-MR autoradiography film overnight to determine the presence or absence of the *in vitro* translated protein.

2.7 TISSUE CULTURE

2.7.1 Transient transfection of 293T cells

The 293T fibroblast cell line was used in co-immunolocalisation experiments. 293T cells were seeded onto glass cover slips in 2 ml of medium (DMEM, 100 units/ml of penicillin, 100 μg /ml streptomycin, 10% v/v FCS) and cultured at 37°C in 5% CO_2. Approximately 10^4 cells were used in each experiment and left to grow for 16-24 hours until the culture reached 60-70% confluency.

The $CaCl_2$ method was used for transformation. A 5-7 μg aliquot of DNA construct was diluted in 450 μl of ddH_2O with 50 μl of 2.5 M $CaCl_2$. After mixing, 500 μl of 2x Hepes buffer (20 g HEPES, 0.54 g $Na_2HPO_4.2H_2O$, 32 g NaCl, 1.48 g KCl diluted in 2 L of ddH20, pH 7.05 and filter sterilised using 0.22 μm Millipore filter) was placed in a sterile 1.5 ml eppendorf tube and the mixture containing the construct DNA was added dropwise followed by vortexing. Gradual addition of DNA was crucial to avoid the DNA coming out of solution. The mixture was incubated at room temperature for 10 minutes. Meanwhile, cells were washed with PBS once and new pre-warmed medium was added. The DNA construct solution was added to the culture cells dropwise, making sure to cover the entire surface by gently swirling the culture dish. Cells were incubated at 37°C in 5% CO_2 for 4 to 5 hours, washed with pre-warm sterile PBS and fresh medium was added. Cells were left to grow for 24 to 48 hours.

2.7.2 Immunohistochemistry

Immunohistochemistry was used to detect expression of epitope tagged proteins in 293T fibroblast cells. This method allowed coimmuno-localisation using fluorescence microscopy of candidate proteins identified in the yeast two-hybrid screen.

After transformation with the appropriate construct, 293T cells were washed with PBS twice and the cells were fixed with 1-2 ml of 3% PFA for 15 minutes. After

fixation, PFA was washed off with two changes of PBS. Cells were permeabilised, by addition of 1 ml 0.5% Triton detergent in PBS at room temperature for 15 minutes. The cells were blocked with DMEM containing 10% FCS (v/v) for at least one hour, at room temperature, or overnight at 4°C in cases of high background. Cells were then washed thoroughly with PBS. The first antibody, either mouse anti-Flag (Santa Cruz) or rabbit anti-Myc (Jackson Research) were diluted 1:200 and 1:500 in DMEM respectively and 50 μl was used to flood each cover slip. After incubation at room temperature, unbound antibody was washed off with 4 changes of PBS. The secondary antibodies, Cy2-conjugated goat anti-mouse and Cy3-conjugated goat anti-rabbit, were prepared by diluting 1:100 in DMEM and 50 μl were placed on each cover slip for 1 hour at room temperature. Samples were washed with PBS and the cell nuclei were stained using 4'-6-Diamidino-2-phenylindole (DAPI) and left to incubate for 2 minutes. Excess of DAPI was washed off with 4 changes of PBS and cover slips mounted with Mowiol and left at 4°C in a dark box. Fluorescence microscopy was performed as described in section 2.2.4.

CHAPTER 3: EXPRESSION OF *ZIC* GENES DURING NEURULATION

3.1 INTRODUCTION

Despite strong evidence for a role of the *Zic* genes during embryonic neurulation in humans and mice (Klootwijk *et al.*, 2000;Brown *et al.*, 2001;Carrel *et al.*, 2000;Nagai *et al.*, 2000;Brown *et al.*, 1998;Copp *et al.*, 2003a), the expression pattern of the *Zic* genes at the time of neurulation is poorly characterised. The mRNA expression patterns of *Zic1-3* have been described in the recently closed neural tube (Nagai *et al.*, 1997), but there is no information on their expression in the posterior neuropore region at the stage of closure of the spinal neural tube (E9.5). Moreover, no expression data have been reported for *Zic4*. This prompted an investigation of the distribution of *Zic1-4* mRNA at the stage of neurulation by whole mount *in situ* hybridisation, in order to understand how these genes can affect neurulation. The non-mutant mouse strain CD1 was used for the expression analysis of *Zic* genes during neurulation.

3.1.1 The *curly tail* (*ct*), *loop tail* (*Lp*) and *splotch* (Sp^{2H}) mouse models of NTD

Genes that produce NTDs in the mouse mutants have been identified by positional cloning, gene trap or gene targeting strategies (Copp *et al.*, 1990;Juriloff *et al.*, 2000) (Copp *et al.*, 2003b). The function of these genes varies from transcription factors such as *Gli3* or *Pax3* (Hui *et al.*, 1993), transmembrane receptors such as Fgfr1 (Xu *et al.*, 1999) and actin binding proteins such as *Shroom* (Hildebrand *et al.*, 1999). A speculative idea would be that the genes that produce NTDs in the mouse and in humans interact genetically by sharing a common or a few genetic pathways, all leading to NTDs. To test the hypothesis that mutant genes that produce NTD in the mouse share the same genetic pathway as *Zic2* and *Zic3*, the expression patterns of *Zic2* and *Zic3* have been studied by whole mount in situ hybridisation at the time of neurulation in three unrelated mouse mutants that exhibit NTDs: *curly tail* (*ct*), *loop tail* (*Lp*) and *splotch* (Sp^{2H}).

Homozygous *ct* embryos exhibit a delay of posterior neuropore closure, which can lead to spina bifida and/or tail flexion defects. The embryonic mechanism leading to NTDs in *ct/ct* embryos has been reported in several studies (Brook *et al.*, 1991;Peeters *et al.*, 1996;Van Straaten and Copp, 2001). A subset of *ct/ct* embryos has an imbalance in cell proliferation, such that the ventral tissues in the caudal region, the hindgut endoderm and the notochord, proliferate more slowly than dorsal tissues (especially the neuroepithelium), creating an increase in the axial curvature of the posterior neuropore region. The increase in axial curvature creates strain in the apposing neural folds that, when severe, causes the neural tube to remain open. The gene responsible for the *ct* phenotype has recently been proposed to be *grainyhead-like-3* (*Grhl3*), since *Grhl3* null mice exhibit a similar phenotype to *ct/ct* embryos and the gene maps in the critical region of the *ct* locus on chromosome 4 (Ting *et al.*, 2003). However, no mutations in the *Grhl3* coding sequence have been identified in *ct/ct* mouse, although *Grhl3* expression levels were found to be reduced in affected embryos. This study indicated that *ct* might be a hypomorphic allele of *Grhl3*, an idea that is supported by the observation of genetic non-complementation between the *Grhl3* null and *ct* mutation. NTDs in the curly tail mouse are insensitive to folate treatment, whereas the frequency and severity of NTDs can be significantly reduced by maternal inositol supplementation (Greene and Copp, 1997). Surprisingly, *Grhl3* null mice where found to be insensitive to inositol, calling into question the candidacy of *Grhl3* as the *ct* gene.

The *loop tail* mouse (*Lp*) develops the severe form of NTD, craniorachischisis. Positional cloning identified the *Lp* gene as *Strabismus/Vangl2* (Kibar *et al.*, 2001;Murdoch *et al.*, 2001). In amphibia (Goto and Keller, 2002) and zebrafish (Park and Moon, 2001;Goto *et al.*, 2002) *Strabismus* has been functionally linked to the planar cell polarity (PCP) pathway that regulates convergent extension cell movements during gastrulation, while studies in *Drosophila* have linked this pathway to

specification of the unidirectional array of bristles in the wing. In the mouse, *Strabismus/Vangl2* has been shown to affect the orientation of hair cells of the inner ear, indicating that *Strabismus/Vangl2* is involved in the PCP pathway (Montcouquioi *et al.*, 2003). However, it is unknown whether convergent extension movements are disrupted in *Lp/Lp* embryos.

The Sp^{2H} allele of splotch results from a 32 bp deletion in the homoedomain region of the gene encoding the *Pax3* transcription factor (Epstein *et al.*, 1991). Homozygous mutant embryos (Sp^{2H}/Sp^{2H}) exhibit exencephaly and/or spina bifida. The Sp^{2H} mouse is a model of folate-responsive NTDs since the incidence of NTDs is reduced by treatment with folic acid (Fleming *et al.*, 2000). Excessive incorporation of [3H] thymidine in Sp^{2H}/Sp^{2H} embryos suggests that there is a deficiency in folate-cycle intermediates for the biosynthesis of pyrimidines. The embryonic basis of neural tube defects in *splotch* mice has not been determined. However excess apoptosis has been suggested to play a role in the pathogenesis of NTDs (Pani *et al.*, 2002) based on the finding that double mutants of p53 and Sp^{2H} have diminished apoptosis and reduced NTD frequency.

The aim of this chapter is to provide a description of the expression of *Zic* genes during normal neurulation and during failure of the neural tube closure in the *ct*, Sp^{2H} and *Lp* mutants.

3.2 METHODS

3.2.1 Mouse strains and embryos

Four different mouse strains were used: one non-mutant, CD1, and three mutants *loop tail* (*Lp*), *splotch* (Sp^{2H}) and *curly tail* (*ct*) (see Table 3.1). Embryo collection and dissection were performed as described in section 2.2.1.

Table 3.1. Mouse strains used in the present study

Mouse mutant	Gene and chromosome localisation	Source	Protein function	Homozygous phenotype	Reference
Loop tail (Lp)	*Vangl2*, Chr 1	Spontaneous	Transmembrane protein	crn	(Murdoch *et al.*, 2001)
Splotch (Sp^{2H})	*Pax3, Chr 1*	X-ray generated	Transcription factor	sb+ex	(Epstein *et al.*, 1991)
Curly tail (ct)	*Grhl3?*, Chr 4	Spontaneous	Transcription factor	sb+(ex occasionally)	(Gruneberg, 1954)

Only the neural tube phenotype is described in this table. Abbreviations: crn, craniorachischisis; ex, exencephaly; sb, spina bifida.

DNA extraction from yolk sacs was performed as described in section 2.3.2. The PCR conditions used to genotype Sp^{2H} and *Lp* mice (the Crp microsatellite polymorphism) are summarised in Table 3.2.

Table 3.2 PCR conditions for genotyping Sp^{2H} and *Lp* mice

PCR conditions	Sp^{2H}	*Lp*
$MgCl_2$	1.5 mM	1.5 mM
Primer sequence	F 5'CCTCGGTAAGCTTCGCCCTCTG 3' R 5'CAGCGCAGGAGCAGAACCACCTTC 3'	F 5'AGAATCTGACTTACCCATGGT 3' R 5'GAGGGAGAAGAATTATGTCT G3'
Annealing temperature	58 °C 30 cycles	58 °C 30 cycles
PCR product size	Wild type allele 122 bp Mutant allele 90 bp	Wild type allele 150 bp Mutant allele 140 bp

All mice in the *curly tail* colony are homozygous (*ct/ct*). Those destined to develop spinal NTDs (approximately 20%) were identified by measuring the PNP at the 30 somite stage. Embryos with large PNPs (0.5 mm or more in length) were considered to be affected, while embryos with small PNPs (0.1-0.2 mm) were considered unaffected. Embryos with intermediate length PNPs (0.2-0.5 mm) were not studied further.

3.2.2 Generation of mRNA riboprobes and whole mount in situ hybridisation

To generate probes for *Zic1-4*, the 3' untranslated region of *Zic1-3* and the 5' untranslated region of *Zic4* were chosen, as no significant homology to other cDNAs was found by BLAST searching. Primers were designed to specifically amplify these regions (Table 3.3). In each case, the PCR product was gel purified and subcloned into a pGEM-T vector (see Fig. 3.1 for map). The identity of each probe was verified by DNA sequencing. Labelling of *Zic1-4* probes and *in situ* hybridisation were performed as described in section 2.4.4.

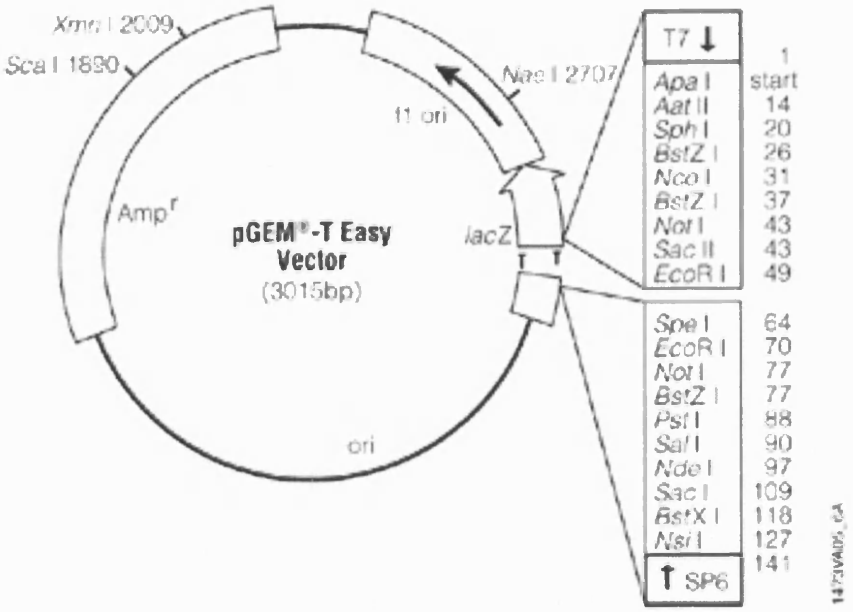

Figure 3.1 pGEM-T Easy vector map used to generate *Zic1-4* probes for whole mount *in situ* hybridisation.

pGEM-T Easy has 3'T overhangs that allow insertion of PCR products without the need for restriction enzyme digestion. Cloning of the cDNA disrupts the *lacZ* gene allowing identification of recombinants by white and blue selection. The cDNA is flanked by a T7 and a SP6 promoter allowing transcription of the sense or antisense probes by the T7 or SP6 polymerase, depending on the orientation of the inserted cDNA (diagram obtained from PROMEGA)

Table 3.3 Primers to generate *Zic1-4 probes*, together with the Genbank accession numbers, the amplified region and the enzymes to generate antisense probes

Gene	Primer sequence	NCBI accession number	Amplified region	Labelling
Zic1	F 5' CACCCCTTGGTGTTGGTGGA 3' R 5' GTCATCCCCTAGCCACTTGCA 3'	NM_009573	642 bp from 2244 to 2886*	Antisense ApaI Sp6
Zic2	F 5' GGCCAGGCCTTTCTCCCATT 3' R 5' GTGGAAAAGGAAGGCGTCCG 3'	D70848	354 bp From 1838-2192*	Antisense SalI T7
Zic3	F 5'TCTAGATTCCTTACAATGTCAG 3' R 5' AAGAAGCACTTTAACCATGAG 3'	D70849	471 bp From 2825-3296*	Antisense NotI T7
Zic4	F 5' CACCCCTTGGTGTTGGTGGA 3' R 5' GTCATCCCCTAGCCACTTGCA 3'	D78174	706 bp From 225-931*	Antisense SacII Sp6

*Note that the base number corresponds only to the Genbank accession numbers given.

3.3 RESULTS

3.3.1 Expression patterns of *Zic1-4* immediately following neurulation

Zic1-4 belong to the same family of transcription factors genes, with closely related nucleotide sequences. However, by designing RNA probes specific for each mRNA transcript, expression of each of the *Zic* genes was detected in distinct but partially overlapping locations at the time of neurulation (Fig. 3.2).

3.3.1.1 Expression of *Zic* genes in the neural tube

Zic1, *Zic2* and *Zic4* mRNA transcripts were detected in the prospective central nervous system at the dorsal midline of the cranial neural tube and spinal neural tube (Fig. 3.2 A-D). Examination of transverse sections through the already closed neural tube at the level of the heart (Fig. 3.2 E, G, I and K) illustrates the differential domains of expression of the *Zic* genes. *Zic1* mRNA is localised to the dorsal one third of the neural tube including the roof plate (arrows in Fig. 3.2 E). Similarly, *Zic2* and *Zic4* are expressed in the dorsal neural tube (arrows in Fig. 3.2 G and K), but *Zic2* expression is restricted to the roof plate and dorsal quarter of the neural tube, whereas *Zic4* is absent from the roof plate and is expressed in a domain restricted to a dorsal stripe (arrows in Fig. 3.2 K). These different domains of expression of the *Zic* genes in the neural tube at the level of the heart persist in the more caudal spinal neural tube (Fig. 3.2 F, H and L). Low levels of expression of *Zic3* have been reported at E12.5 in the neural tube (Nagai *et al.*, 1997), but unlike *Zic1*, *2* and *4*, *Zic3* transcripts were undetectable in the neural tube at E9.5 (Fig. 3.2 I and J).

Figure 3.2 Localisation of *Zic1-4* mRNA at E9.5 by whole mount in situ hybridisation

(E-L) show 50 μm vibratome sections taken at the level of the dotted lines in A-D. *Zic1* mRNA transcripts are localised at the dorsal midline of the cranial neural tube (asterisks (and in sections, data not shown) in A), dorsal part of the spinal neural tube along the majority of the body axis (white arrowheads in A), and dorsal part of the somites (black arrowheads in A). Sections through the neural tube at the level of the heart (E) or mid-trunk spinal neural tube (F) reveal that *Zic1* mRNA transcripts are localised in the dorsal 1/3 of the neural tube (arrows in E and F), the dorsal part of the somite (arrowheads in E and F) and dorsal sclerotome (asterisks in E and F).

(B) *Zic2* mRNA transcripts are expressed in the midbrain and hindbrain (white arrows in B), the telencephalon (white asterisk in B), spinal neural tube (black arrows in B) and at the posterior neuropore (black arrowheads in B). Sections through the embryo (G and H) show that *Zic2* transcripts are localised to the dorsal quarter of neural tube (arrows in G and in the myotome (arrowhead in H) and H) and to the sclerotome lateral to the neural tube (asterisks in G).

(C) *Zic3* mRNA transcripts are detected in the rostral telencephalon (white arrowhead in and rostral mesencephalon C), dorsal somites (white arrows in C) and the PNP region (black arrowheads in C). Sections (I and J) show that *Zic3* transcripts are localised to the dorsal part of the somite and more caudally to the dorsal lip of the dermomyotome (arrowheads in I and J).

(D) *Zic4* mRNA transcripts are localised in the dorsal midline of the cranial neural tube (black arrows) and the dorsal sclerotome (arrowheads). Sections (K and L) reveal that the expression domain of *Zic4* is restricted to a dorsal stripe in the neural tube with the roof plate being negative (arrows in K and L). The sclerotome adjacent to the ventral neural tube (asterisks in K and L) and the dorsal lip of the dermomyotome (arrowheads in L) are positive for *Zic4*. Abbreviations: nt, neural tube; pnp, posterior neuropore; rp, roof plate. Scale bar in A represents 1 mm (A-D); scale bar in E represents 200 μm.

Figure 3.2

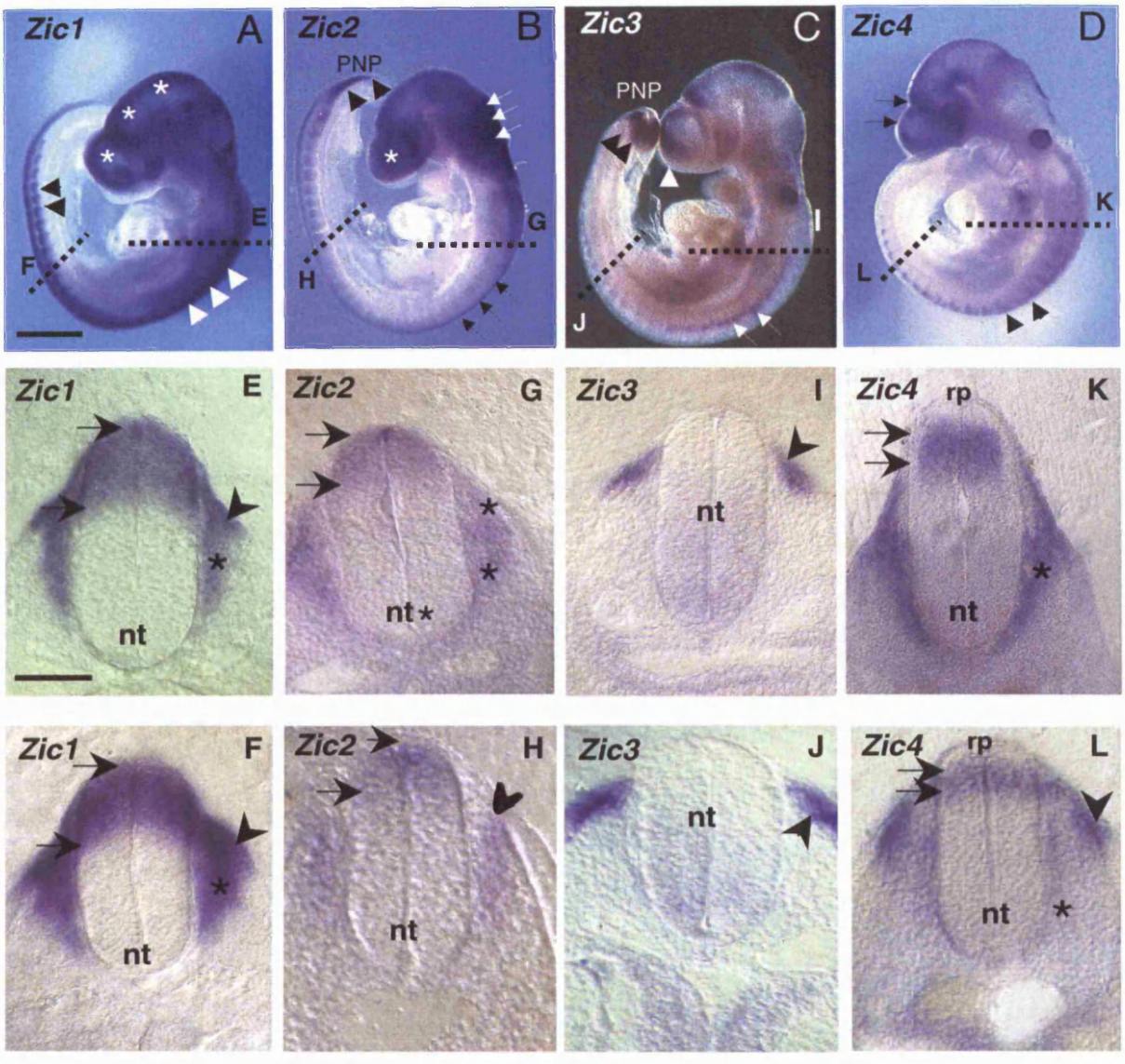
Zic1
A
Zic2
B
PNP
Zic3
C
PNP
Zic4
D
E
F
G
H
I
J
K
L
Zic1
E
Zic2
G
Zic3
I
Zic4
rp
K
nt
nt
nt
nt
Zic1
F
Zic2
H
Zic3
J
Zic4
rp
L
nt
nt
nt
nt

3.3.1.2 Expression of *Zic* genes in the somites

At E9.5, the developing somites can be subdivided into sclerotome and dermomyotome. Cells that are located in the lateral and dorsal parts of the newly formed somite develop into the dermomyotome, which gives rise to the future muscle and dermal derivatives. The medial part of the somite forms the sclerotome, which will develop into the future vertebrae (Cossu *et al.*, 1996). *Zic1, Zic2* and *Zic4* mRNA transcripts can be detected in a population of sclerotomal cells adjacent to the neural tube (Fig. 3.2 asterisks in E-L), although the precise domain of sclerotomal expression differs between the three genes. *Zic1* is expressed in the dorsal sclerotome (Fig. 3.2 asterisk in E) whereas *Zic2* and *Zic4* are not expressed in this dorsal zone, but transcripts are present only in the ventral domain adjacent to the ventral part of the neural tube. The perinotochordal region is negative for all *Zic* genes. *Zic3* is not expressed in the sclerotome whereas the dermomyotome shows strong *Zic3* expression (Fig. 3.2 I and J). At more caudal levels *Zic2* and *Zic4* are also expressed in the dermamyotome (arrowheads in Fig 3.2 H and L respectively).

3.3.2 *Zic2* and *Zic3* show a dynamic pattern of expression at the PNP

Only *Zic2* and *Zic3* are expressed in the posterior neuropore region at E9.5 (Fig. 3.2 B and C, black arrowheads). Given the relationship between loss of function mutations of *Zic2* and *Zic3* and spinal NTDs, the expression of these genes at the posterior neuropore was examined in greater detail at both E9 and E9.5.

Zic2 mRNA transcripts localise strongly to the posterior neuropore region at E9 and E9.5 (Fig. 3.3 A and E). Sections through the posterior neuropore reveal that *Zic2* transcripts are present throughout almost the entire neural plate before the neural folds converge in the dorsal midline (Fig. 3.3 B and F). The surface ectoderm does not express *Zic2* (arrows in Fig. 3.3 B and F). Immediately after the neural folds have fused dorsally forming the neural tube, the expression of *Zic2* continues throughout the neural

tube (Fig. 3.3 C and G). However, in the more mature neural tube, *Zic2* becomes dorsalised, so that expression is seen only in the roof plate. The dorsalisation of the neural tube expression is first noticeable at the level of the rostral presomitic mesoderm, corresponding to the incipient somite, which is also *Zic2*-positive (Fig. 3.3 D and H). Hence, during closure of the neural tube at the posterior neuropore region, *Zic2* is expressed throughout the entire neural plate but not in adjacent tissues including the surface ectoderm, notochord and paraxial mesoderm.

Next, the expression pattern of *Zic3* was determined in the posterior neuropore region at E9 and E9.5. The domain of expression of *Zic3* differs radically from that of *Zic2* (compare Fig. 3.3 with Fig. 3.4). *Zic3* is absent from the neural tube at E9 and E9.5, although transcripts are present in the notochord and, at lower intensity, in the mesenchyme surrounding the ventral hindgut (Fig. 3.4 B and C). At more rostral levels, where the neural tube is closed, *Zic3* is expressed in the presomitic mesoderm in the same fashion as *Zic2* although *Zic3* expression is also detected in the notochord at this level (Fig. 3.4 D). At later stages (E9.5), strong expression becomes apparent in the tail bud, in the mesenchyme surrounding the secondary neural tube, in the notochord, and in the presomitic mesoderm (Fig. 3.4 F, G and H).

3.3.3 Expression of *Zic2* and *Zic3* in *ct*, *Lp* and Sp^{2H} mutant embryos

The expression of *Zic2* and *Zic3* was studied in embryos with delayed (*ct*, Sp^{2H}) or absent (*Lp,* craniorachischisis) neural tube closure (between the arrowheads in A, E, I, M in Fig. 3.5 and Fig. 3.6). Embryos of the non-mutant strain, CD1 served as normal controls. *Zic2* and *Zic3* mRNA expression in *ct/ct* embryos (Fig. 3.5 E-H and Fig. 3.6 E-H) does not show any major difference in distribution compared with the pattern seen in CD1 embryos (Fig. 3.5 and 3.6 A-D). In *ct/ct* embryos *Zic2* expression is detected throughout the neural plate before closure of the neural tube (Fig. 3.5 B and F). At the level where the rostral presomitic mesoderm first becomes positive for *Zic2*, transcripts

Figure 3.3 Localisation of Zic2 mRNA in the posterior neuropore by whole mount in situ hybridisation at E9-9.5

A and E show *Zic2* mRNA expression in the posterior neuropore at E9 and 9.5 respectively.B-D and F-H show 50 μm vibratome sections through the posterior neuropore at the level of the dotted lines in A and E respectively. *Zic2* mRNA is expressed in the posterior neuropore region with a dynamic pattern at early E9 (B-D) and E9.5 (F-H). *Zic2* is expressed throughout the neural plate during neural fold elevation and fusion (arrowheads in B and F), until just after the neural tube closure is complete (arrowhead in C and G). More rostrally, *Zic2* transcripts become confined to the roof plate of the more mature neural tube (arrowheads in D and H). At the axial levels where this dorsalisation first becomes apparent, transcripts can also be detected in the rostral presomitic mesoderm marking the incipient somite (arrows in D and H). Abbreviations: nc, notochord; nf: neural fold, pm, presomitic mesoderm; rp, roof plate. Scale bars in A represents 500 μm. Scale bar in E represents 1 mm and in B represents 200 μm

Figure 3.4 Localisation of *Zic3* mRNA in the posterior neuropore by whole mount *in situ* hybridisation at E9-E9.5

A and E show *Zic3* mRNA expression in the posterior neurore at E9 and 9.5 respectively. B-D and F-H show 50 μm vibratome sections at the level of the dotted lines in A and E respectively. *Zic3* mRNA transcripts show a quite different distribution from *Zic2* (Fig. 3.3). Sections through the posterior neuropore at early E9 and E9.5 confirm that *Zic3* is absent from the neural plate and neural tube (B-D and F-H), whereas it is expressed in the notochord underlying the neural tube (arrowheads in C and D). Transcripts are also detected at low intensity in the mesenchyme surrounding the ventral hindgut (asterisks in C). Like *Zic2*, *Zic3* mRNA transcripts are present in the rostral presomitic mesoderm (arrow in D). Unlike *Zic2*, *Zic3* transcripts are also present in the notochord at this level (arrowhead in D). At E9.5, *Zic3* transcripts are present in the tail bud region (arrow in F) as well as, more rostrally, in the mesenchyme surrounding the neural tube, which is emerging through the process of secondary neurulation (nt in G). *Zic3* transcripts are also present in the presomitic mesoderm (arrow in H) and in the notochord (arrowheads in G and H). Abbreviations: hg, hindgut; nc, notochord; nf, neural fold; nt, neural tube; pm, presomitic mesoderm. Scale bars represent: A, 500 μm; B, 300 μm; E, 1 mm.

Figure 3.3

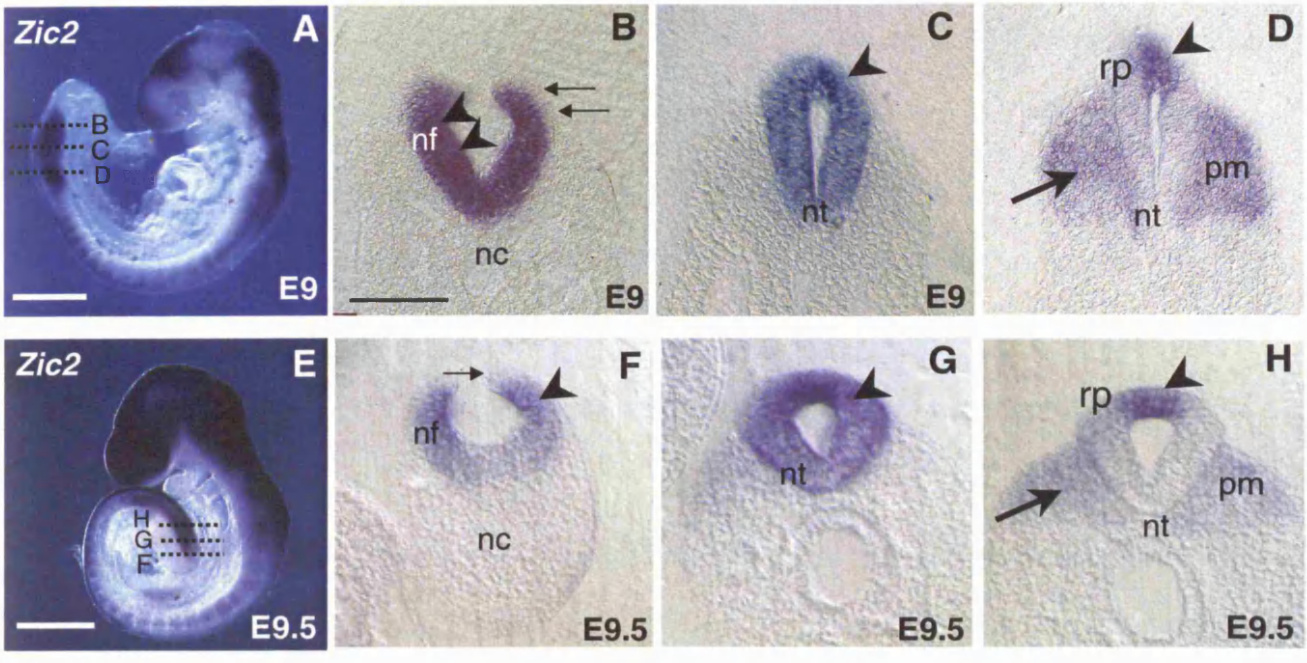

Figure 3.4

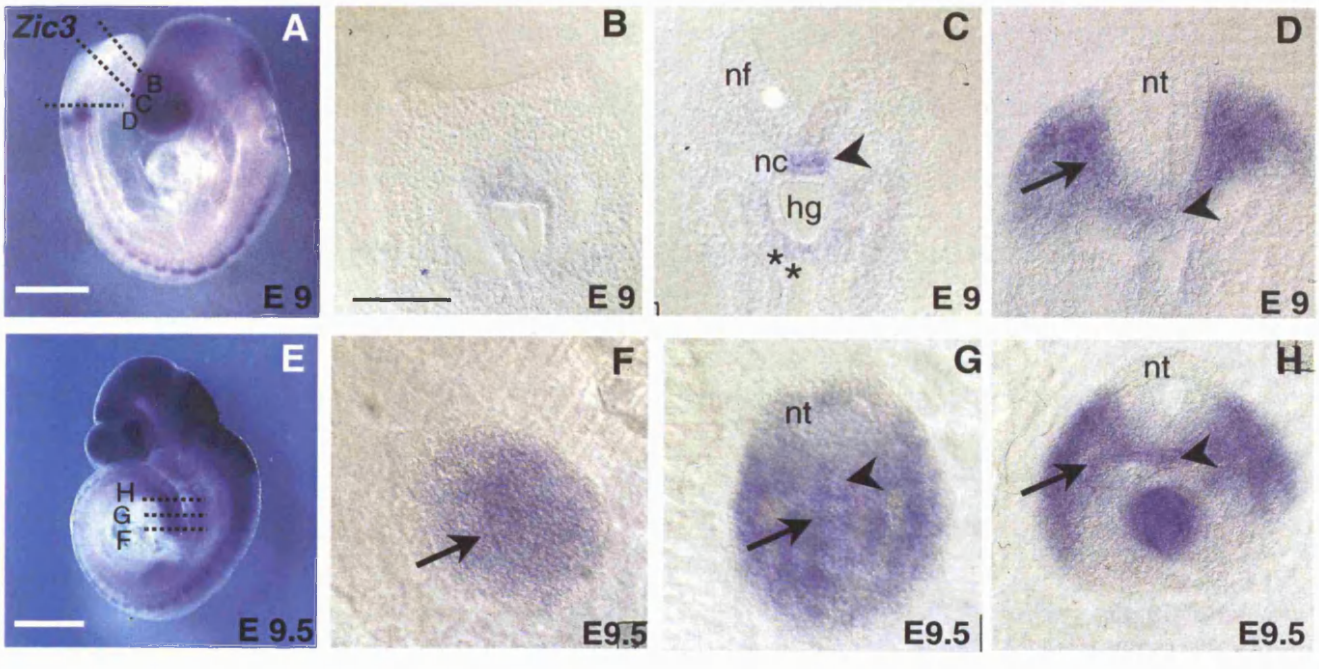

start to become dorsalised in the neural plate even though the neural tube is still open (Fig. 3.5 G). At the axial level where the "closed" neural tube is first visible, *Zic2* shows two loci of expression in the roof plate, separated by a gap (Fig. 3.5 arrowheads), which appears to result from the neural tube having failed to fuse. The surface ectoderm, negative for *Zic2*, appears to be growing across the gap between the open neural folds.

The expression of *Zic3* is strong in the tail bud region *ct/ct* embryos (Fig. 3.6 B and F). Further rostrally, *Zic3* expression is strong in the mesenchyme surrounding the neural tube with the notochord being positive (arrow and arrowhead in Fig. 3.6 G respectively).

In *Lp/Lp* homozygous embryos, *Zic2* mRNA is localised in the same fashion as in CD1 embryos (compare Fig. 3.5 I-L to A-D). The caudal end of E9.5 *Lp/Lp* embryos shows expression of *Zic2* throughout the neural plate, with expression becoming dorsalised to the tips of the neural folds at the level where the presomitic mesoderm becomes positive for *Zic2* (Fig. 3.5 J and K). Rostrally, *Zic2* is expressed solely in the lateral edges of the *Lp/Lp* neural plate, which, although wide open, appear to have undergone the same specification as the roof plate of normal embryos. Interestingly, unlike *Zic2, Zic3* expression is absent from both the caudal end and the cranial neural tube of the *Lp/Lp* embryos (Fig. 3.6 I-L). Expression of *Zic3* is observed only in the somites of the upper trunk of *Lp/Lp* embryos. *Zic3* is absent from the notochord and the tail bud regions compared to the CD1 and the other mouse mutant strains.

Zic2 expression in Sp^{2H}/Sp^{2H} embryos does not show any obvious differences in distribution (Fig. 3.5 M-P) compared with CD1 (Fig. 3.5 A-D) embryos. *Zic2* is expressed throughout the neural plate at caudal levels and becomes dorsalised to the roof plate more rostrally. Similarly, *Zic3* is expressed in the same fashion as in CD1, Sp^{2H}/Sp^{2H} and *ct/ct* embryos

Figure 3.5 Expression of *Zic2* is not altered in the posterior neuropore region of the mouse NTD mutants *ct*, *Lp* and Sp^{2H}

Localisation of *Zic2* mRNA in the posterior neuropore region of CD1 (A), *ct/ct* (E), *Lp/Lp* (I) and Sp^{2H}/Sp^{2H} (M) embryos at E9.5. Vibratome sections through the posterior neuropore of CD1 (B-D), *ct/ct* (F-H), *Lp/Lp* (J-L) and Sp^{2H}/Sp^{2H} (N-Q) embryos are also shown. Note that *ct/ct* (E) and Sp^{2H}/Sp^{2H} (M) embryos exhibit an enlarged posterior neuropore (arrowheads in E and M) that will develop into spina bifida. In *Lp/Lp* embryos closure fails from the hindbrain down the entire length of the spinal cord (arrowheads in E). Sections through these embryos reveal that *Zic2* mRNA transcripts are localised throughout the caudal neural plate in each mutant (arrows in B, F, J and N). More rostrally where the presomitic mesoderm becomes positive for *Zic2* (arrows in G, K and O), *Zic2* transcripts can be seen dorsalised to the tips of the persistently open neural folds (arrowheads in G, K and O). Thus, dorsalisation of *Zic2* is independent of closure of the neural tube. Further rostrally, *Zic2* becomes restricted to the roof plate of the closed neural tube in *ct/ct* and Sp^{2H}/Sp^{2H} embryos (arrowheads in H and P) as in CD1 embryos (D). *Lp/Lp* embryos, in which the entire spinal neural tube is open, nevertheless show dorsalised *Zic2* expression in the neuroepithelium (L). Sections are representative of four embryos for each of the genotypes. Abbreviations: nf, neural folds; np, neural plate; nt, neural tube; pm, presomitic mesoderm; rf, roof plate. Scale bar in M represents 500 μm (A, E, I and M) and in P represents 200 μm (B-D, F-H, J-L, N-P).

Figure 3.5

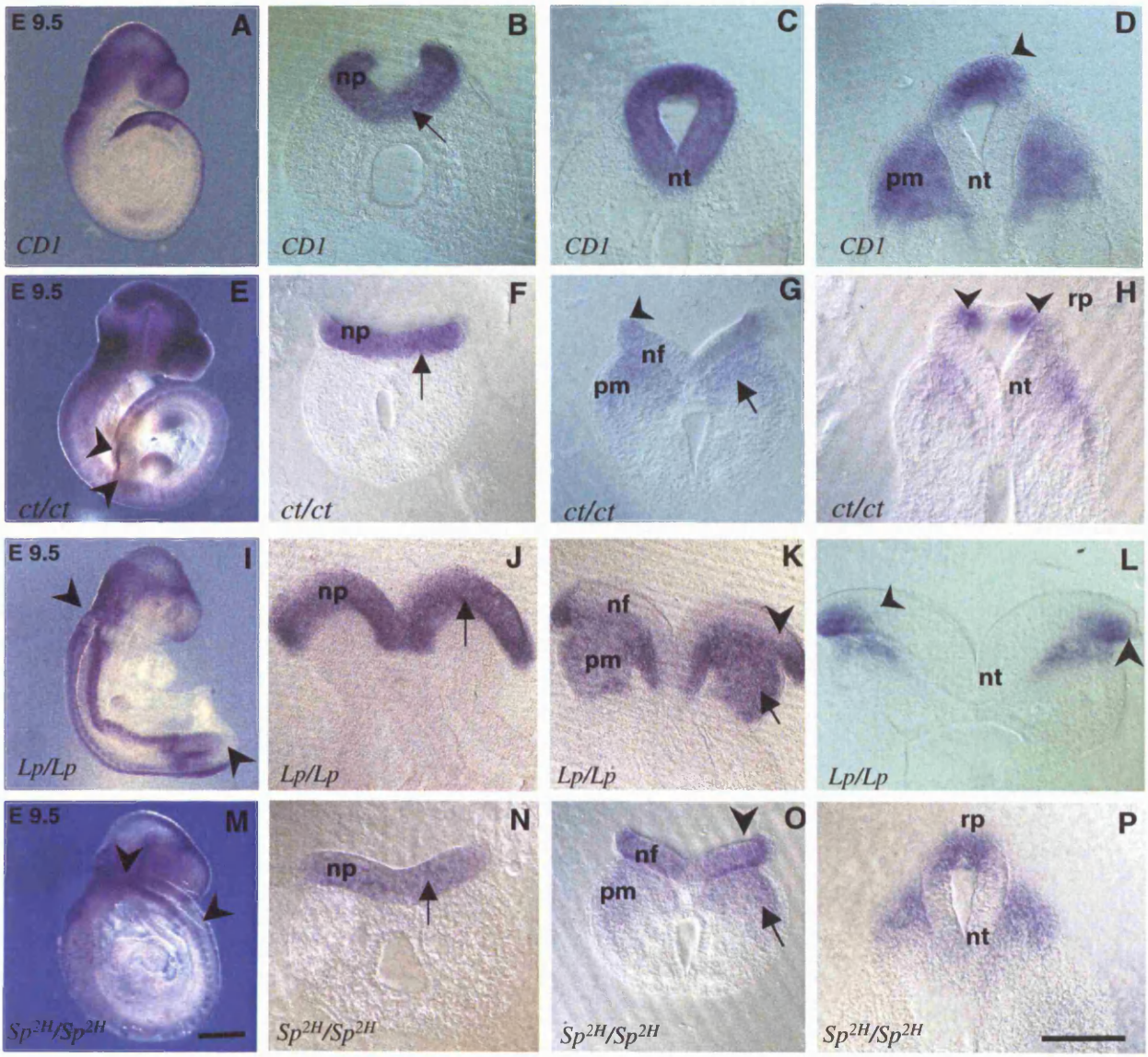
E 9.5
A
CD1
B
np
CD1
C
nt
CD1
D
pm
nt
CD1
E 9.5
E
ct/ct
F
np
ct/ct
G
nf
pm
ct/ct
rp
H
nt
ct/ct
E 9.5
I
Lp/Lp
J
np
Lp/Lp
K
nf
pm
Lp/Lp
L
nt
Lp/Lp
E 9.5
M
Sp2H/Sp2H
N
np
Sp2H/Sp2H
O
nf
pm
Sp2H/Sp2H
rp
P
nt
Sp2H/Sp2H

Figure 3.6 Localisation of *Zic3* mRNA in the posterior neuropore region of CD1, *ct/ct*, *Lp/Lp* and Sp^{2H}/Sp^{2H} embryos at E9.5 by whole mount *in situ* hybridisation

Localisation of *Zic3* mRNA in CD1 (A), *ct/ct* (E), *Lp/Lp* (I) and Sp^{2H}/Sp^{2H} (M) embryos Vibratome sections through the posterior neuropore of CD1 (B-D), *ct/ct* (F-H), *Lp/Lp* (I-L) and Sp^{2H}/Sp^{2H} (M-P). Note that *ct/ct* (E) and Sp^{2H}/Sp^{2H} (M) embryos exhibit an enlarged posterior neuropore (between arrowheads in E and M) that will develop into spina bifida. In *Lp/Lp* embryos, closure fails from the hindbrain throughout the entire length of the spinal cord (between arrowheads in I), termed craniorachischisis. *Zic3* is similarly expressed in CD1 embryos (A) and in the *ct/ct* (E) and Sp^{2H}/Sp^{2H} (M) mutants. Sections through the embryos reveal that *Zic3* mRNA transcripts are present in the tail bud region (arrows in B, F and N), and more rostrally become localised to the mesenchyme surrounding the neural tube. The notochord is also positive (arrowheads in C, G and O respectively). In CD1 embryos, once the neural tube has closed, transcripts persist in the presomitic mesoderm (arrowhead in D). In the *ct/ct* and Sp^{2H}/Sp^{2H} mutants with large posterior neuropores, *Zic3* transcripts are apparent in the presomitic mesoderm lateral to the persistently open neural tube (arrows G and O). *Zic3* is also expressed in the dermomyotome (arrows in H and P). In contrast to the *ct* and Sp^{2H} mutants, *Zic3* expression is absent from *Lp/Lp* embryos in both cranial and caudal regions of the neural tube although the somites are positive in the upper trunk region (I). Sections through *Lp/Lp* embryos reveal a lack of expression of *Zic3* including a notable absence of tail bud expression (J-L). Sections are representative of three embryos for each of the genotypes. Abbreviations: np, neural plate; nt, neural tube; pm, presomitic mesoderm. Scale bar in M represent 500 μm and in P represents 200 μm.

Figure 3.6

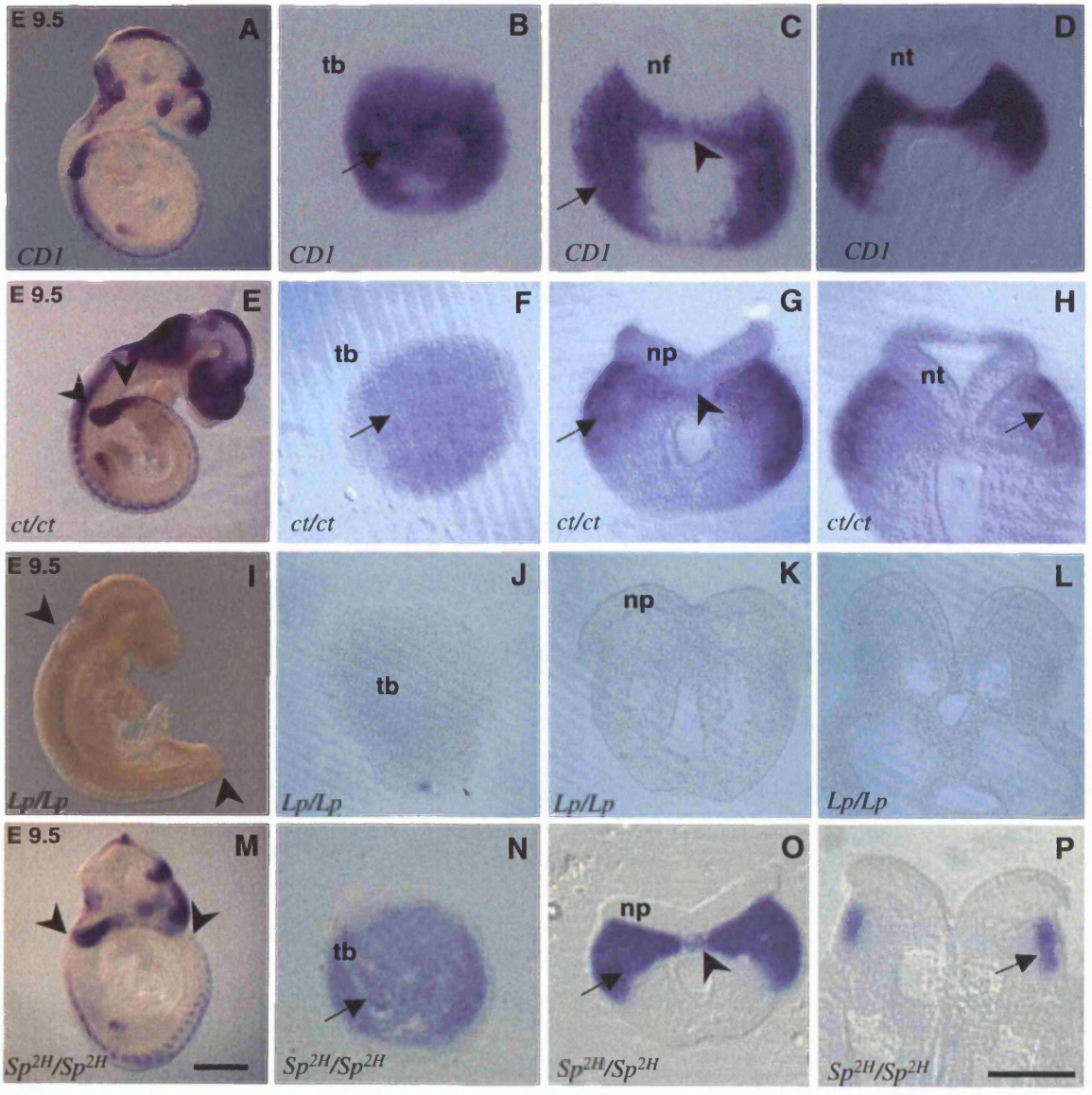
E 9.5
A
CD1
B
tb
CD1
C
nf
CD1
D
nt
CD1
E 9.5
E
ct/ct
F
tb
ct/ct
G
np
ct/ct
H
nt
ct/ct
E 9.5
I
Lp/Lp
J
tb
Lp/Lp
K
np
Lp/Lp
L
Lp/Lp
E 9.5
M
Sp2H/Sp2H
N
tb
Sp2H/Sp2H
O
np
Sp2H/Sp2H
P
Sp2H/Sp2H

* For instance, in contrast to the distinct specific functions mentioned above, *Zic2*$^{Ku/Ku}$, *Zic2*$^{Kd/Kd}$ and *Zic3*$^{-/-}$ embryos exhibit excencephaly (Nagai *et al.*, 2000; Elms *et al.*, 2000; Klootwijk *et al.*, 2000; Carrel *et al*, 2000) suggesting that *Zic2* and *Zic3* both act during cranial neurulation. As will be shown in Chapter4 the excencephlay phenotype in *Zic2*$^{Kd/Kd}$ is not completely penetrant suggesting that *Zic3* could compensate. In addition, *Zic1* and *Zic2* have been shown to have redundant functions in the formation of the cerebellum, such that compound heterozygous *Zic1*$^{-/+}$; *Zic2*$^{Kd/+}$ exhibit cerebellar abnormalities consisting of reduced proliferation of the external granule cell layer similar to the homozygous *Zic1* mutant (*Zic1*$^{-/-}$) (Aruga *et al.*, 2002).

3.4 DISCUSSION

3.4.1 Distinct patterns of *Zic* gene expression at the time of neural tube closure

The expression pattern of *Zic1-4* overlap in the neural tube and somites, although each gene has a distinct pattern of expression. Moreover, *Zic1*$^{-/-}$, *Zic2* $^{Ku/Ku}$, *Zic2* $^{Kd/Kd}$ and *Zic3*$^{-/-}$ each exhibit specific phenotypes. *Zic1*$^{-/-}$ mice exhibit hypoplastic cerebellum but survive to birth and are viable (Aruga *et al.*, 1998a). *Zic2* $^{Ku/Ku}$ mice die at E13.5 exhibiting NTD and forebrain malformations (Elms *et al.*, 2003). *Zic3*$^{-/-}$ embryos develops right-left asymmetry defects with a low frequency of NTD (Purandare *et al.*, 2002). The existence of these phenotypes demonstrates a specific individual function for each member of the *Zic* gene family. Nevertheless, a degree of functional redundancy or compensation for loss of function of one of the *Zic* genes by other family members may also be possible in tissues where *Zic* genes are co-expressed. As an example, *Gli2* and *Gli3* have been shown to have specific as well as redundant functions. *Gli2* and *Gli3* show functional redundancy in the formation of the skeleton since *Gli2*$^{zfd/zfd}$; *Gli3*$^{XtJ/+}$ compound mutants show an exacerbated phenotype with regard to various skeletal elements (Mo *et al.*, 1997). In contrast, *Gli2* mediates the induction of motor neurons, whilst *Gli3* inhibits motor neuron differentiation (Altaba, 1998). Hence, closely related genes can mediate different specific functions, as well as exhibiting functional redundancy, and this may well be true for *Zic1-4*. *

3.4.2 The expression of *Zic1-3* parallels the skeletal defects seen in mouse mutants for these genes

The differential domains of expression of *Zic1, 2* and *3* also extend to the somites. *Zic1* and *Zic2* are expressed in the sclerotome whereas *Zic3* is expressed in the dermomyotome. The medial part of the newly formed somite forms the sclerotome,

from which the vertebral bodies arise (Cossu *et al.*, 1996). Skeletal malformations, in which the vertebrae are severely affected, occur in *Zic1*$^{-/-}$ mice, *Zic1*$^{-/-}$; *Gli3*$^{XtJ/XtJ}$ compound mutants (Aruga *et al.*, 1999) and *Zic2*$^{Kd/Kd}$(Nagai *et al.*, 2000). These observations fit well with the finding of expression of *Zic1* and *Zic2* in the sclerotome.

Some studies have suggested that the dermomyotome can give rise to the ribs (Kato and Aoyama, 1998). In support of this idea, *Zic3* null mice show rib malformations in keeping with the dermomyotome expression of *Zic3*. Compared to *Zic1* and *Zic2, Zic3* is not expressed in the sclerotome, which explains the milder phenotype seen in the vertebrae of *Zic3*$^{-/-}$ mutant.

3.4.3 NTDs caused by mutations in *Zic2* and *Zic3* parallel the gene expression pattern

The main abnormality seen in *Zic2*$^{Ku/Ku}$ and *Zic2*$^{Kd/Kd}$ embryos is spina bifida, an abnormality that can be traced back to E9, when primary neurulation is underway. Since *Zic2* is expressed solely in the neural plate, the cause of the neurulation phenotype observed in *Zic2* mutant mice is most probably intrinsic to the neural plate.*

The expression pattern of *Zic3* at the posterior neuropore region parallels the defects reported in studies of the *Bent tail* and *Zic3* knockout mice (Gruneberg, 1955) (Klootwijk *et al.*, 2000;Purandare *et al.*, 2002). Mice that carry a null mutation in *Zic3* do not show spina bifida as the main malformation. Rather, primary neurulation in the prospective spinal cord region occurs normally in most cases, in agreement with the absence of *Zic3* expression from the neural tube, as observed in the present study. However, delay in the posterior neuropore closure has been observed at low frequency in these mutants and this can lead to mild spina bifida at very caudal levels. Since *Zic3* is expressed in the notochord, this delay in neuropore closure could be explained by an extrinsic mechanism rather than an intrinsic abnormality within the neural tube. An example of such an extrinsic mechanism is provided by the *curly tail* mutant in which

decreased proliferation in the notochord and hindgut causes an increased angle of curvature of the caudal region, creating strain on the neural folds that inhibits closure in the dorsal midline (Copp *et al.*, 1988;Brook *et al.*, 1991).

Other defects reported in *Zic3* mutants, at more caudal levels of the spinal cord, include as asymmetric growth of caudal vertebrae leading to kinked tails and sacral agenesis. These defects probably result from abnormal secondary neurulation, as *Zic3* is strongly expressed in the tail bud region, perhaps regulating the proliferation, survival or differentiation of cells required for secondary body development. Mutations in human *Zic3* can cause sacral agenesis (Gebbia *et al.*, 1997). This defects likely also reflects the expression of *Zic3* in the tail bud, notochord and mesenchyme surrounding the gut, as seen in the present expression studies.

The mechanism by which *Zic3* regulates right-left asymmetry is unknown. *Zic3* is expressed symmetrically unlike other genes involved in right-left specification, such as *Nodal* (Lowe *et al.*, 2001)or *Pitx2* (Kitamura *et al.*, 1999), whose mRNAs are localised asymmetrically at the 2-somite stage. *Nodal* and *Pitx2* appear to be expressed normally in 2-somite stage *Zic3* null embryos, although after the 2 somite stage, homozygous $Zic3^{-/-}$ embryos fail to express *Nodal*, while *Pitx2* expression is randomised with regards to left and right sides. This places *Zic3* upstream of *Nodal* and *Pitx2* expression (Purandare *et al.*, 2002). It has been hypothesised from experiments in *Xenopus* that the *Zic3* protein may bind to an unknown asymmetrically expressed protein to activate downstream targets in the right/left asymmetry pathway (Kitaguchi *et al.*, 2002). It is probable that *Zic3* function in right/left asymmetry occurs early during gastrulation when the initial right/left axes are specified.

3.4.4 Expression of *Zic2* and *Zic3* in *ct, Lp and* Sp^{2H} mutants

Expression of *Zic2* is normal in *ct*, *Lp* and Sp^{2H} homozygous embryos, with no marked differences from non-mutant embryos. It seems very unlikely, therefore that

* Although the present results suggest that *Zic3* is downstream of *Vangl2* at the neurulation stage embryo, the right and left asymmetry defects observed in the *Bent tail* or *Zic3*$^{-/-}$ are not present in *Lp/Lp* homozygous embryos. This difference could be explained by the non-overlapping expression of *Zic3* and *Vangl2* in tissues in which the initial right and left asymmetry is specified during early gastrulation. *Zic3* is expressed in the primitive streak during head fold formation and in the node at later stages of gastrulation, structures that have been shown to be important in the establishment of the initial right and left asymmetry (Elms, P et al, 2004). The expression of *Vangl2* during early gastrulation has not been reported and it is therefore difficult to conclude whether these two genes are co-expressed at this stage. However, the absence of asymmetry defects in *Lp/Lp* embryos suggests that the *Vangl2* is not required for initial establishment of right and left axis. Therefore *Zic3* may function independently of *Vangl2* in left-right determination.

Zic2 is downstream of these mutated genes. An alternative possibility is that *Zic2* could lie upstream of the *Lp, ct, or* Sp^{2H} genes. Since *Zic2* is a transcription factor, it could directly regulate the expression of the genes mutated in the *Lp*, *ct*, or Sp^{2H} mice (i.e. the *Vangl2*, *Grhl3* or *Pax3* genes). Alternatively these genes may mediate independent functions such that when mutated, completely unrelated pathways lead to development of NTDs.

Another observation from the present study is that *Zic2* expression in the roof plate is independent of neural tube closure, as *Zic2* mRNA was seen to become dorsally restricted even when the neural tube was wide open, as seen particularly in the *Lp/Lp* embryos.

Zic3 expression is localised apparently normally in *ct/ct* and Sp^{2H}/Sp^{2H} embryos, whereas the expression of *Zic3* is absent from *Lp/Lp* embryos. *Vangl2* the gene mutated in *Lp*, has been implicated in the planar cell polarity pathway (Montcouquioi *et al.*, 2003). There have been no suggestions, to date, of abnormalities in the PCP pathway in *Bent tail* or *Zic3* mutants. On the other hand, down-regulation of *Zic3* in homozygous *Lp/Lp* embryos suggests that *Zic3* may be regulated downstream of *Vangl2* signalling. Heterozygous *Lp/+* mice display tail defects, which could be linked to downregulation of *Zic3*. Moreover, the absence of *Zic3* expression from the caudal end of *Lp/Lp* embryos may suggest that the tail bud is not correclty formed. However, *Lp/Lp* embryos undergo secondary neurulation and develop looped tails (Strong and Hollander, 1949) ruling out this hypothesis. It is tempting to speculate that the origin of the tail defects in the *Lp/+* and *Lp/Lp* is related to reduced or absent *Zic3* expression downstream of *Vangl2* gene mutation. *

The present study represents a qualitative analysis of the expression of *Zic2* and *Zic3* in several mutant strains with NTDs. Further work could involve a quantitative assay, perhaps using RT-PCR or real time RT-PCR, which could give an accurate

quantitative measurement of the levels of *Zic2* and *Zic3* mRNA in the mutants *ct, Lp* and Sp^{2H}.

CHAPTER 4: ANALYSIS OF KUMBA, A NEW MUTANT ALLELE OF *ZIC2*

4.1 INTRODUCTION

In Chapter 3, I have shown that the expression of *Zic2* is restricted to the neural plate at the time of closure of the neural tube in the posterior neuropore region. This expression pattern suggests that the function of *Zic2* in neural tube closure is probably intrinsic to the neural plate, and therefore *Zic2* activity could affect the morphogenesis of the neural tube. Although homozygous embryos for the hypomorphic alleles $Zic2^{Kd/Kd}$ and the $Zic2^{Ku/Ku}$ have been shown to exhibit spina bifida and exencephaly, a study of the morphology and timing of the NTDs in these embryos has not been reported. The aim of this chapter was to perform a morphological analysis of the spina bifida observed in $Zic2^{Ku}$, in order to understand the embryonic mechanism by which disruption of *Zic2* leads to spina bifida.

4.1.1 *Kumba* carries a mutation in the fourth zinc finger domain of *Zic2*

The *Kumba* mouse was recovered from a phenotype-driven ENU screen for dominant mutations. Its heterozygous phenotype consists of a curly tail, belly spot and low frequency of spina bifida (Nolan *et al.*, 2000). The mutation arose in a male of the BALB/c genetic background, and the mutation was maintained by successive backcrosses to C3H/He inbred mice. Initial mapping located the mutation on chromosome 14 between D14Mit137 (6.5 cM)-D14Mit239 (42.5 cM) (Nolan *et al.*, 2000). Further refinement of the critical region containing the mutation was performed using simple sequence length polymorphisms (SSLP), and the mutation was identified by sequencing of candidate genes within the critical region. A base pair transversion, A to T, was identified in the *Zic2* gene that results in a missense mutation changing a cysteine to a serine, C370S, in the fourth ZFD (Elms *et al.*, 2003). The mutation changes the cysteine that chelates the central zinc ion of the ZFD and is thought to disrupt the function of this domain (see Fig.1).

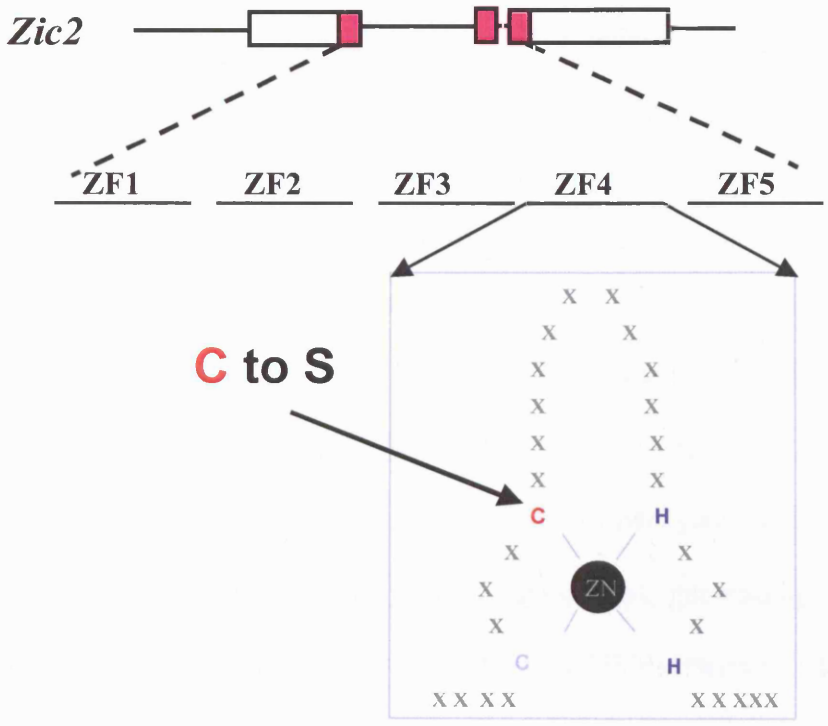

Figure 4.1 Schematic representation of the mutation identified in *Kumba* mice

Zic2 consists of three exons; the ZFD region is shown in red and involves all three exon. The ZFD region encodes five tandem repeats of the zinc finger unit: ZF1-5. The base pair transversion, A to T, results in a missense mutation that changes the second cysteine of the fourth ZF to a serine.

4.2 METHODS

4.2.1 Maintenance of the colony and generation of experimental litters

The *Zic2*^{Ku} allele was provided originally by Dr. Ruth Arkell, MRC Mammalian Genetics Unit, Harwell, Oxon and is maintained by successive backcrosses of heterozygous *Zic2*$^{Ku/+}$ males with inbred C3H/He strain females. To obtain experimental litters, *Zic2*$^{Ku/+}$ male and female offsprings were mated. Mice used in this study have been backcrossed to C3H/He for at least 11 generations.

4.2.2 Genotyping of adults and experimental litters

Genotyping of adult mice and experimental litters was performed by SSLP using the microsatellite marker D14Mit107. The *Zic2*^{Ku} mutation arose on the BALB/c genetic background and has been backcrossed onto a C3H/He background. D14Mit107 was found to be informative on this hybrid genetic background, generating different sized PCR products for the BALB/c (mutant-linked) and C3H/He (wildtype-linked) alleles (see Fig. 4.2). PCR conditions and primer sequences are provided in Table 4.1.

Table 4.1 PCR conditions for genotyping *Zic2*^{Ku} mice using D14Mit107

PCR conditions	*Zic2*^{Ku}
$MgCl_2$	1.5 mM
Primer sequence	F5' AAATGGTCATCCCTGAAAAGA 3' R5' CAGGCCTCTCCAAAGTACCA 3"
Annealing temperature Number of cycles	58 °C 35 cycles
PCR product size	Wild type C3H/He allele 150 bp Mutant BALBc allele 176 bp

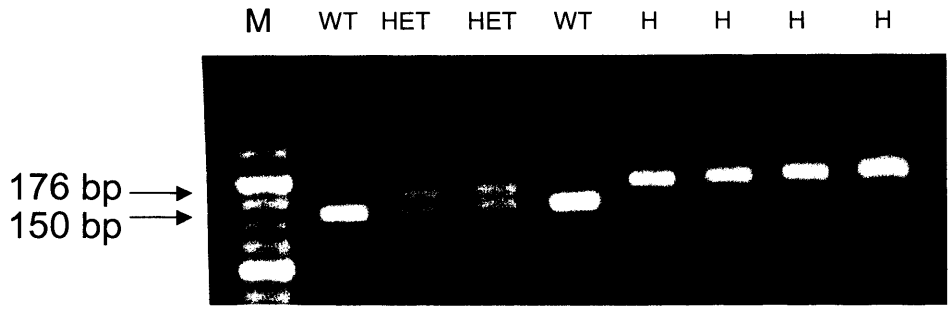

Figure 4.2 Agarose gel illustrating the polymorphism for the microsatellite marker D14Mit107

PCR for D14Mit107 was found to generate two different sized products: a band of 150 bp, linked to the wild type allele (*Zic2*$^{+}$; C3H/He) (WT) and a 176 bp band linked to the mutant (*Zic2*^{Ku}; BALB/c) allele (H). Note that heterozygotes (HET) have both 150 and 176 bp alleles whilst homozygotes (H) have only the 176 bp band, corresponding to the BALB/c allele.

4.3 RESULTS

4.3.1 The *Kumba* phenotype is partially penetrant in heterozygotes

On a predominantly C3H/He genetic background, the $Zic2^{Ku}$ allele shows incomplete penetrance in heterozygotes. In this study, 30% of the $Zic2^{Ku/+}$ mice displayed a phenotype, with 16% exhibiting a curled tail, 10% a white belly spot and 6% displaying both phenotypes (Fig. 4.3 and Table 4.2). A low frequency of spina bifida was observed in $Zic2^{Ku/+}$ newborn pups but the precise frequency was difficult to establish due to cannibalization of affected pups by their mothers.

Table 4.2 Phenotypes observed in $Zic2^{Ku/+}$ mice

Phenotype	No of mice (% total)
Normal	115 (70%)
Tail curled only	24 (16%)
Belly spot only	15 (10%)
Tail curled and belly spot	6 (4%)
Total	150

To determine whether the $Zic2^{Ku}$ allele is transmitted in a Mendelian fashion, embryos from crosses between $Zic2^{Ku/+}$ males and females were genotyped and the proportion of embryos with each genotype ($Zic2^{+/+}$, $Zic2^{Ku/+}$ and $Zic2^{Ku/Ku}$) was compared with the expected Mendelian ratio of 1:2:1 using the X^2 statistical test. The finding of $p = 0.96$ shows that there was no statistically significant difference from a 1:2:1 ratio, and therefore the observed genotype ratios were as expected from Mendelian inheritance. Hence, there appears to be no early embryonic lethality in $Zic2^{Ku/Ku}$ or $Zic2^{Ku/+}$ embryos.

Table 4.3 *Zic2*^{Ku} allele shows Mendelian inheritance in heterozygote matings

Genotype	*Zic2*$^{+/+}$	*Zic2*$^{Ku/+}$	*Zic2*$^{Ku/Ku}$
Number of embryos (observed)	29	57	28
Percentage (observed)	25.4%	50.9%	24.5%
Expected Mendelian ratios	25%	50%	25%

4.3.2 Neurulation phenotype of *Zic2*$^{Ku/Ku}$ embryos

To assess the effect of the *Zic2*^{Ku} allele on neurulation, homozygous embryos were collected at different gestational ages between E9.5 and E12. The main abnormalities observed in *Zic2*$^{Ku/Ku}$ are an open neural tube in the cranial and caudal regions of the embryo, resulting in exencephaly and spina bifida respectively (Fig. 4.4). In order to determine the penetrance of the phenotype, embryos that had reached the 20 somite stage or beyond were analysed for the presence of spina bifida and/or exencephaly. Cranial neural tube closure is completed at 17 somites and, therefore, normal embryos with 20 or more somites are expected to have a closed neural tube in the cranial region. Exencephaly of the midbrain and hindbrain was observed in 76.9% of *Zic2*$^{Ku/Ku}$ embryos whilst spina bifida was observed in all homozygous embryos (i.e. 100% penetrant). Therefore exencephaly was always accompanied by spina bifida (see Table 4.4). In *Zic2*$^{Ku/Ku}$ embryos that completed cranial neural tube closure, a reduction in forebrain size was observed, compared to the appearance of wild type littermates (white arrow in Fig. 4.4 C). This phenotype suggests that *Zic2* is required for forebrain development subsequent to neural tube closure as well as for neural tube closure itself.

Figure 4.3 *Zic2*^{Ku} phenotype is not fully penetrant in heterozygotes

On the C3H/He background, a proportion of *Zic2*$^{Ku/+}$ mice display a curled tail (A) and or a white belly spot (B)

Figure 4.4 *Zic2* $^{Ku/Ku}$ embryos display NTDs

Comparison between *Zic2*$^{+/+}$, (A and D) and *Zic2*$^{Ku/Ku}$ embryos (B, C and E) at E9.5 (A-C) and E12 (D-E). In homozygous embryos the neural tube fails to close in the spinal region (between the black and red arrowheads in B and C). A proportion of homozygous embryos also exhibit an open cranial neural tube, exencephaly (between the white arrowheads in B and E). *Zic2*$^{Ku/Ku}$ embryos that undergo successful cranial neural tube closure display a reduced forebrain size (white arrow in C: compare with wild type littermate in A). Scale bars represent 500 μm (A to C) and 1 mm (D, E).

Figure 4.3

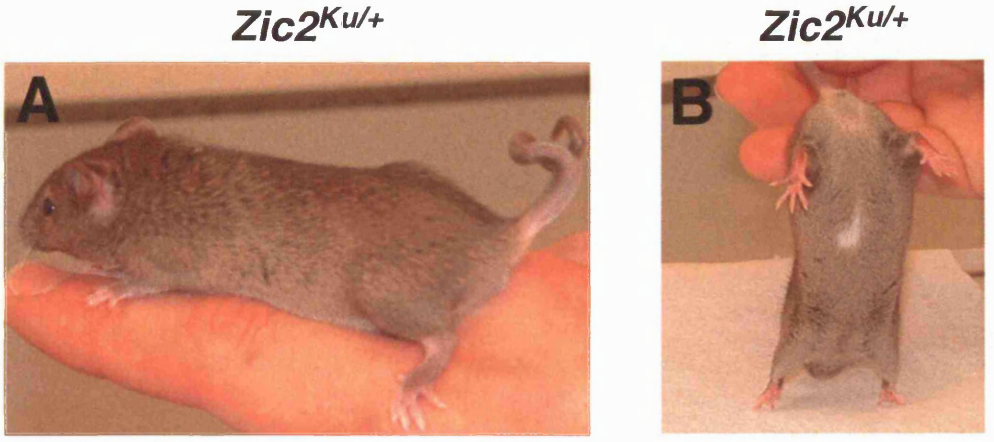

Figure 4.4

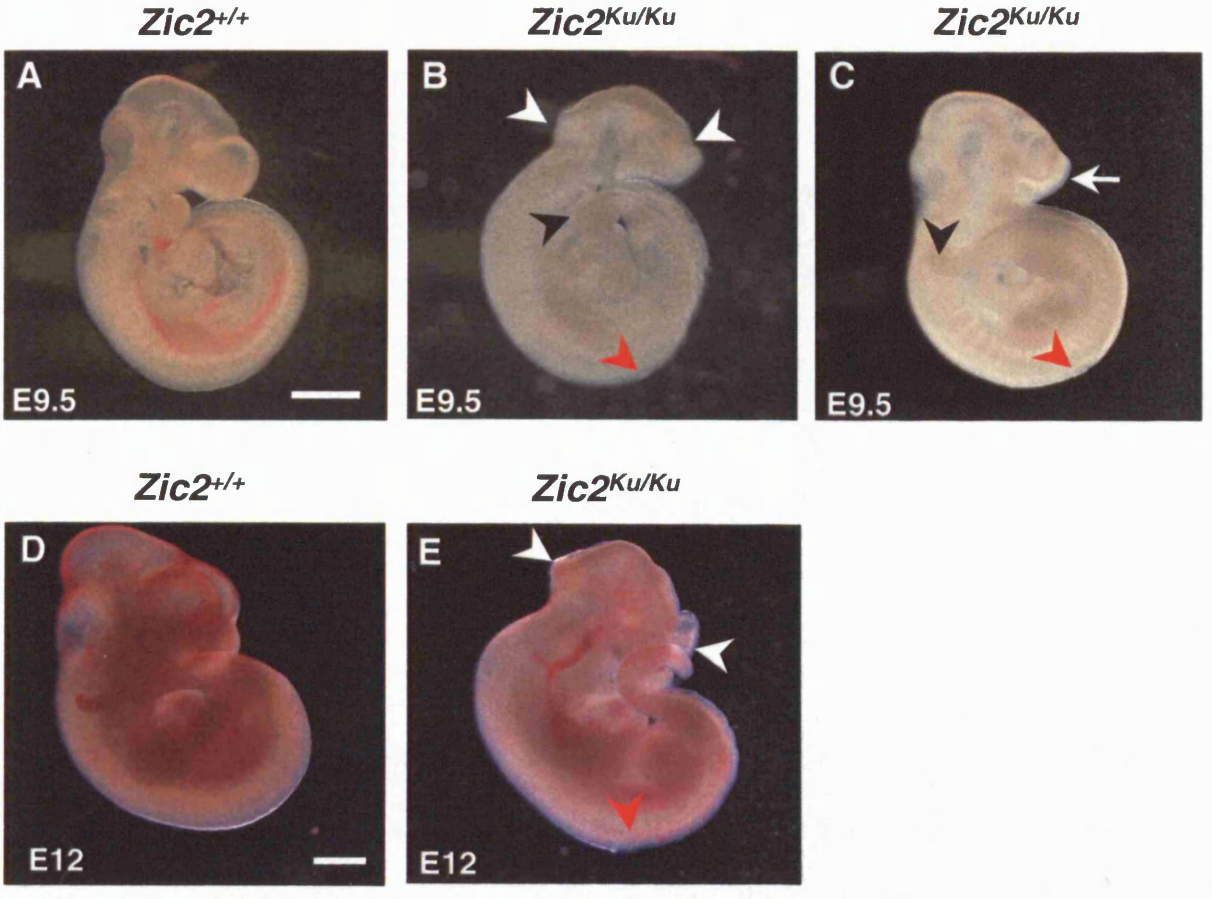

Table 4.4 Penetrance of the NTD phenotype observed in *Zic2*$^{Ku/Ku}$ embryos

Phenotype	Sb alone	Ex alone	Sb + Ex	Total
Number of *Zic2*$^{Ku/Ku}$ embryos	4	0	9	13
Percentage	30.7%	0%	69.2%	100%

Abbreviations: Ex, exencephaly; sb, spina bifida.

To establish the embryonic stage at which the spinal neural tube failed to close in homozygotes, the somite level of the most rostral point at which the neural tube was open was determined (shown in Fig. 4.5 B, C and E by red arrowheads). This somite level varied from 12 to 14 with most embryos failing to close their neural tube beyond the 13th or14th somite (see Figure 4.5).

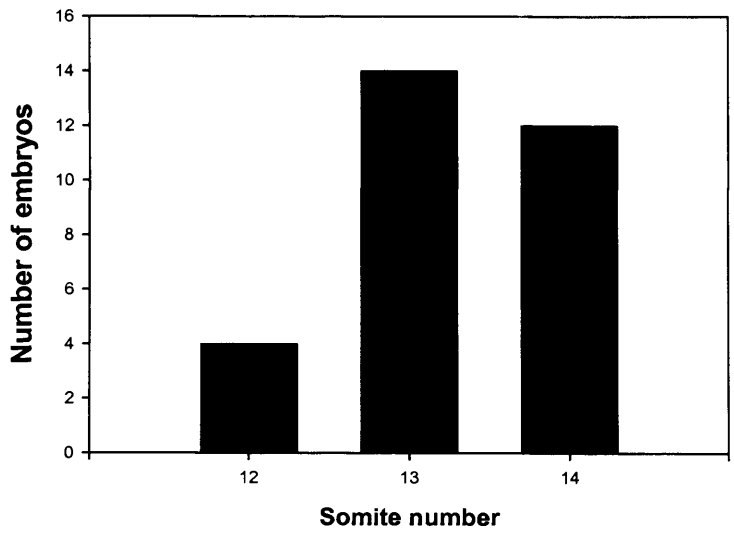

Figure 4.5 Somite number at neural tube closure in *Zic*$^{Ku/Ku}$ embryos

Graphic representation of the somite number at which the neural tube fails to close in *Zic2*$^{Ku/Ku}$ embryos. Most homozygous embryos fail to close the neural tube caudal to the 13th-14th somites.

4.3.3 *Zic2*$^{Ku/Ku}$ embryos lack dorsolateral hinge points (DLHPs)

The finding of an open neural tube in *Zic2*$^{Ku/Ku}$ embryos caudal to somites 13-14 suggested that the transition of spinal neurulation from Mode 1 to Mode 2 could be compromised in *Zic2*$^{Ku/Ku}$ embryos (see section 4.4.1). To investigate this further, histological sections through the PNP of *Zic2*$^{Ku/Ku}$ embryos were compared with sections through the PNP of wild type littermates. Care was taken to ensure that similar levels of the body axis were compared. For this reason, embryos with 15 somites were studied (Fig. 4.6) in which the PNP of the *Zic2*$^{Ku/Ku}$ embryos was only slightly enlarged compared with wild type littermates. *Zic2*$^{Ku/Ku}$ embryos were found to exhibit abnormal spinal neural tube morphogenesis with a striking lack of DLHP formation (arrowheads Fig. 4.6 B-E) compared with wild type controls (arrowheads Fig. 4.6 G-J). The neural plate of *Zic2*$^{Ku/Ku}$ embryos also appeared thicker compared to wild type littermates (arrows in Fig. 4.6 D-E, compared with J). DLHPs are proposed to facilitate apposition of the neural folds at the dorsal midline prior to fusion of the neural folds (Fig. 4.6 F-I). One possibility to be considered was that the lack of DLHPs in 15 somite *Zic2*$^{Ku/Ku}$ embryos reflected a delay in their appearance rather than complete absence. To test this idea, more advanced *Zic2*$^{Ku/Ku}$ embryos, at the 20 and 21 somite stage, were studied (Figure 4.7). The mutant PNP in this case was much longer than the wild-type littermates, reflecting the cessation of neural tube closure at an earlier stage. Sections of the enlarged PNP revealed a thickened neural plate with lack of DLHPs, as at the 15 somite stage, confirming that *Zic2*$^{Ku/Ku}$ embryos totally lack DLHPs.

Figure 4.6 DLHPs are absent in *Zic2*$^{Ku/Ku}$ embryos

A-J show 8 μm consecutive sections through the posterior neuropore of a *Zic2*$^{Ku/Ku}$ embryo (A-E) and a *Zic2*$^{+/+}$ embryo (F-J) stained with haematoxylin and eosin. In each sequence (A to E, and F to J) the top section is the most rostral, passing through the recently closed neural tube of the *Zic2*$^{Ku/Ku}$ (A) or wild type (F) embryos respectively. Successive sections then progress caudally through the open PNP. Sections through the PNP of the wild type embryos reveal the presence of DLHPs that are bringing the tips of the neural folds in apposition in the dorsal midline (i.e. Mode 2 morphology; arrowheads in G-J). In contrast, DLHPs are not formed in any sections through the *Zic2*$^{Ku/Ku}$ embryo (arrowheads in B-E) and the neural folds appear straight (i.e. Mode 1 morphology). The tips of the neural folds do not converge towards the midline (B-E) in *Zic2*$^{Ku/Ku}$, indicative of an incipient spina bifida. Moreover the neural folds of *Zic2*$^{Ku/Ku}$ embryos appear thicker than in the wild type littermate (arrows in D-E and J respectively). Note that the open PNP of the *Zic2*$^{Ku/Ku}$ embryos (sections B-D) are flanked by epithelial somites (s) in contrast to those of the wild type embryo which are flanked by presomitic mesoderm. This reflects the longer PNP in the mutant embryo, which extends as far rostrally as the somites. Abbreviations: DLHP, dorsolateral hinge point; nc, notochord; nf, neural folds; nt, neural tube. Sections are representative of 4 embryos per genotype. Scale bar in A represents 400 μm for all sections.

Figure 4.6

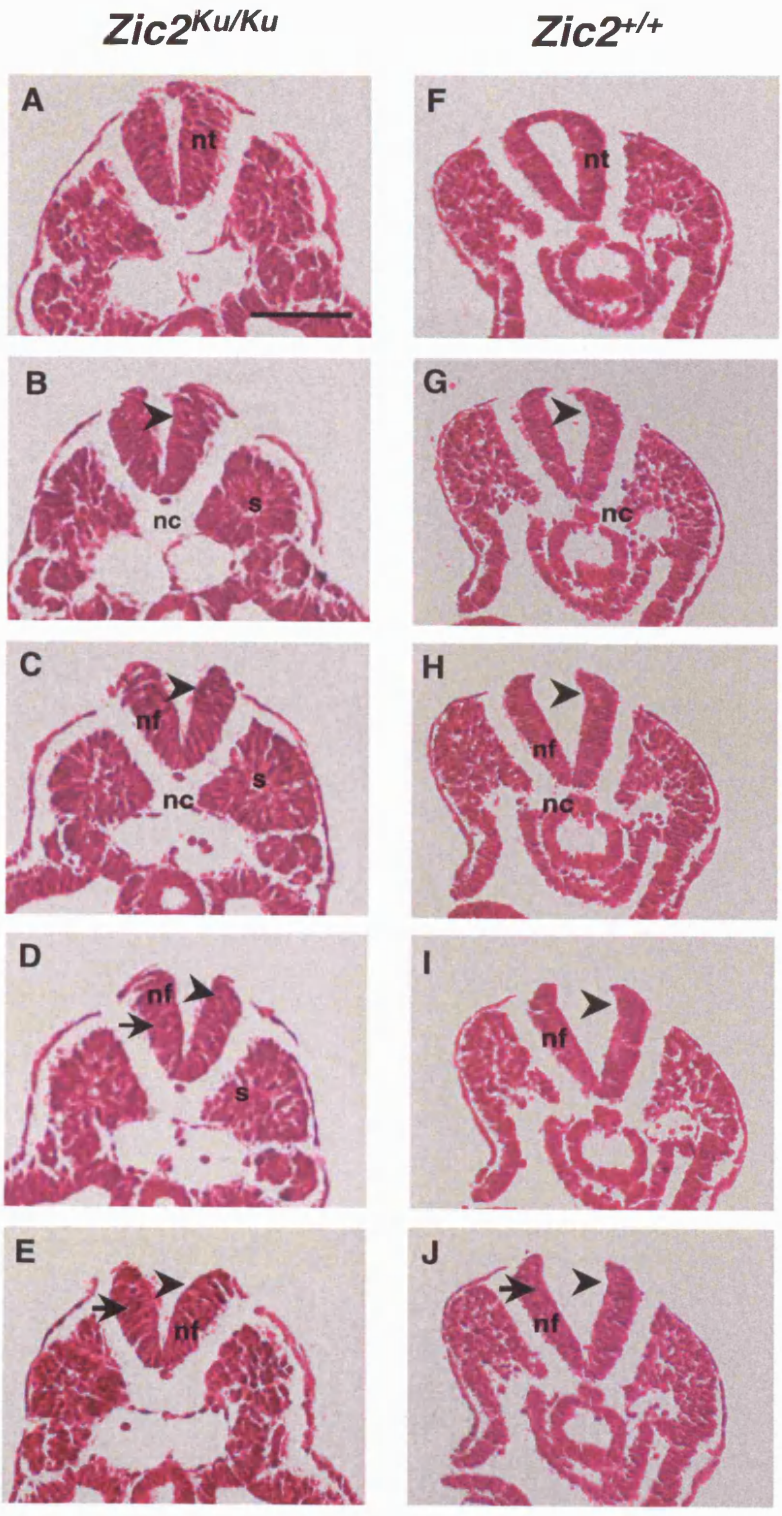
Zic2Ku/Ku
Zic2+/+
A
nt
F
nt
B
nc
s
G
nc
C
nf
nc
s
H
nf
nc
D
nf
s
I
nf
E
nf
J
nf
15 somites
15 somites

Figure 4.7 The *Kumba* mutation results in failure of neural tube closure with abnormal bending of the neural plate

Haematoxylin/eosin stained sections through the rostral end of the posterior neuropore of E9 (20-21 somites) wild type (A: $Zic2^{+/+}$) and homozygous (B: $Zic2^{Ku/Ku}$) embryos. (A) Sections through the $Zic2^{+/+}$ littermate show neural folds approaching each other dorsally to form a lumen with a diamond like shape. The median hinge point (MHP) and paired dorsolateral hinge points (DLHPs arrowheads) are both visible. (B) In the $Zic2^{Ku/Ku}$ embryos the neural plate is thicker than in wild type and fails to bend dorsally so that DLHPs are absent (arrowheads in B). Absence of DLHPs may result in the failure of the neural plate to bend dorsally, leading to an open neural tube phenotype, as observed in $Zic2^{Ku/Ku}$. Note that a MHP is present in the $Zic2^{Ku/Ku}$ embryos. Contact between the surface ectoderm and dorsal neural tube, essential for DLHPs formation, is present in $Zic2^{Ku/Ku}$ and wild type embryos (red arrowheads in A and B). Sections are representative of 2 embryos per genotype. Abbreviations: DLHP, dorsolateral hinge point; nc, notochord; nf, neural fold; MHP, median hinge point.

Figure 4.7

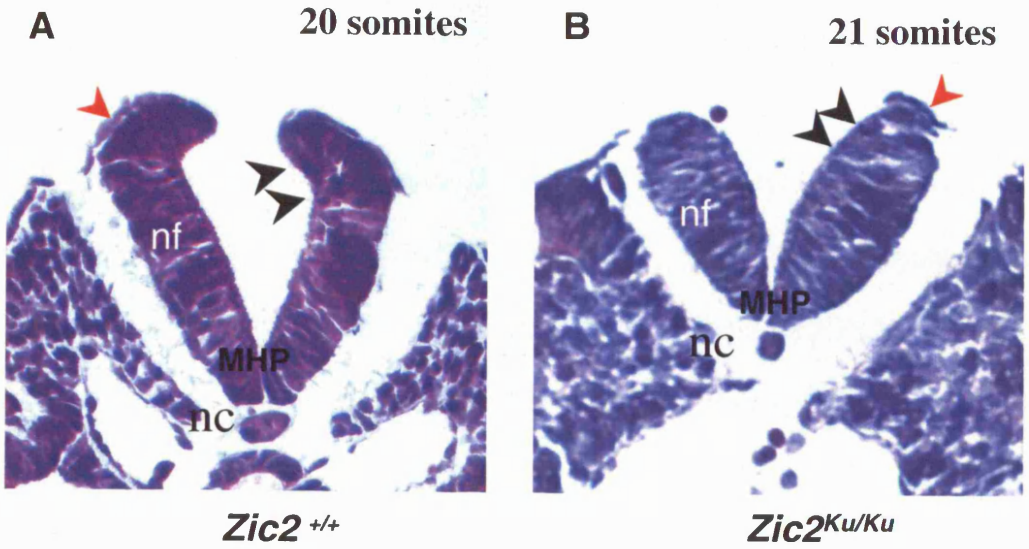

* Although the presence of DLHP in *ct/ct* can be explained because the neural tube stopped closing when Mode2 was initiated.

4.4 DISCUSSION

In the present chapter, the frequency of neural tube defects and the precise morphology of spinal neurulation were studied in the *Zic2*^{Ku} embryos. This analysis provided possible insights into the specific requirement for *Zic2* during neural tube closure.

4.4.1 *Zic2* is required for formation of DLHPs

Closure of the spinal neural tube in the mouse follows a pattern that is characterised by changes in morphology of the neural plate from midline bending (Mode 1) to DLHP-mediated bending (Mode 3), via an intermediate stage of combined midline and dorsolateral bending (Mode 2). Although the timing of the transition between modes varies between strains, the three modes of spinal neurulation have been observed in all normal strains studied (Shum *et al.*, 1996). Several mutants develop spina bifida, but in no case (prior to the present study) have DLHPs been found to be absent in such mutants. For example, in the *curly tail* mouse DLHPs are delayed in appearance but are clearly formed during low spinal neurulation (Shum *et al.*, 1996)*. Moreover, in the *splotch* (*Sp*^{2H}) mutant where a large spina bifida occurs, DHLPs are also seen during spinal neurulation (AJ Copp, unpublished).

The data presented in this chapter demonstrate that the *Zic2* transcription factor is required for formation of DLHPs in spinal neurulation. DLHPs are proposed to facilitate apposition of the neural folds at the midline prior to fusion of the neural folds. In Mode 1 of neurulation, DLHPs are absent in normal embryos, demonstrating that dorsolateral bending is not essential for the closure at high spinal levels. However, in the mouse, Mode 1 of neurulation occurs in the pre-turning embryo when the dorsal surface is concave. It seems likely that neural tube closure is mechanically facilitated by the concave morphology, as has been demonstrated in chick embryos cultured on

substrates with different curvatures (Van Straaten *et al.*, 1993). Once axial rotation (turning) occurs in the mouse, around the 12 somite stage, there is a transition from Mode 1 to Mode 2 in normal embryos. This suggests that dorsolateral bending is necessary to ensure closure of the neural folds in the more mechanically unfavourable convex morphology of the turned embryo. Homozygous *Zic2*^{Ku} embryos undergo axial rotation normally but do not exhibit DLHPs, and fail in all subsequent stages of spinal neurulation. The extremely consistent somite level at which neural tube closes (level of 13th-14th somites) is strongly suggestive of a failure of *Zic2*$^{Ku/Ku}$ embryos to make the transition from Mode 1 to Mode 2 of neurulation. Moreover the neural plate is thickened and remains in the V-shape characteristic of Mode 1, with no apposition of the neural folds in the dorsal midline. Thus, *Zic2*^{Ku} represents the first mouse mutant identified in which DLHPs fail to form. *Zic2*^{Ku} offers an opportunity to gain insight into the molecular mechanisms of DLHPs formation in mouse neurulation.

4.4.2 Possible mechanisms underlying failure of DLHP formation in *Zic2*^{Ku}

At least two distinct mechanisms should be considered as possibly underlying the failure of *Zic2*$^{Ku/Ku}$ embryos to undergo normal low spinal neurulation. First, the thickened neural plate may suggest a change in *Zic2*$^{Ku/Ku}$ embryos in the strength of intracellular adhesion between neighbouring neuroepithelial cells. The neural plate is a single-layered pseudostratified epithelium in which cell morphology varies with phase of the cell cycle (see Introduction). An increase in cell-cell adhesion would be expected to lead to adjacent cells maximising their area of contact, leading to an apparent thickening of the neural plate. Whatever the mechanism, the thickened neural plate is likely to be resistant to bending and this could underlie the lack of DLHPs in the *Zic2*$^{Ku/Ku}$ embryos. It is noticeable, however, that midline (MHP) bending of the neural plate (in Mode 1) does not appear to be compromised in *Zic2*$^{Ku/Ku}$, perhaps arguing against a model based on mechanical resistance to bending.

The second potential mechanism views the Zic2 transcription factor as an essential participant in the DLHP formation process. According to this idea, the lack of DLHPs in *Zic2*$^{Ku/Ku}$ reflects an abnormality in the specific regulatory mechanism governing DLHP regulation. It is known that different mechanisms underlie MHP and DLHP regulation (Ybot-Gonzalez *et al.*, 2002) consistent with a lack of DLHPs but normal formation of MHP in *Zic2*$^{Ku/Ku}$ embryos. Shh is both necessary and sufficient for negative regulation of DLHPs suggesting that Shh and Zic2 may participate in a mutually antagonistic interaction in regulating DLHP formation. This speculative topic is considered further in Chapter 7.

4.4.3 *Zic2* is required for cranial neurulation and forebrain development

Homozygous *Zic2*^{Ku} embryos display exencephaly as result of failure of the midbrain and hindbrain neural tube to close. Unlike spina bifida, exencephaly is not fully penetrant with only around three quarters of *Zic2*$^{Ku/Ku}$ embryos displaying this phenotype. Closure 1, at the hindbrain-cervical boundary, and Closure 3, at the rostral extremity of the prosencephalon, both occur normally in *Zic2*$^{Ku/Ku}$ embryos, whereas Closure 2 at the forebrain/midbrain boundary does not occur, resulting in a persistently open midbrain and hindbrain.

Interestingly, *Zic2*$^{Ku/Ku}$ embryos also exhibit a reduction in size of the forebrain. This phenotype was easiest to detect in embryos that complete cranial neurulation, where exencephaly is not a complicating factor. Hence, *Zic2* is required for forebrain development. In support of this idea, *ZIC2* mutations in humans have been shown to cause holoprosencephaly (HPE) (Brown *et al.*, 1998), a forebrain malformation that arises due to failure of forebrain development and formation of the distinct telencephalic vesicles. More studies are needed to determine whether the abnormal forebrain observed in homozygous *Zic2*^{Ku} embryos may be related to the human HPE phenotype.

4.4.4 The *Zic2*^{Ku} mutation

It is not known whether *Zic2*^{Ku} is a hypomorphic or a null allele of *Zic2*. The *Zic2* knockdown mouse, *Zic2*^{Kd}, generated by gene targeting, is a hypomorphic allele of *Zic2* such that western blot detects only 21% of the normal level of Zic2 protein in homozygous embryos (Nagai *et al.*, 2000). *Zic2*$^{Kd/Kd}$ have a milder phenotype than *Zic2*$^{Ku/Ku}$ embryos and survive to birth. Since *Zic2*$^{Ku/Ku}$ die between E12 and E13, this suggests that *Zic2*^{Ku} is a more severe allele than *Zic2*^{Kd}. Indeed, homozygous *Zic2*^{Ku} embryos exhibit abnormal heart looping and outflow tract defects, a phenotype that has not been described in *Zic2*^{Kd} allele, but which could account for the embryonic death of *Zic2*$^{Ku/Ku}$ embryos (Elms, P. and Gaston-Massuet, C. preliminary data). This argues that *Zic2*^{Ku} could be a null allele of *Zic2* or that *Zic2* function is more severely compromised in *Zic2*^{Ku} than in *Zic2*^{Kd}.

The change of a cysteine to a serine in the fourth finger domain of Zic2 is likely to adversely affect chelation of the zinc ion in the zinc finger domain. The nature of the mutation in *Zic2*^{Ku} raises the possibility that the function of the 4th ZFD is disrupted such that the DNA-binding of Zic2 is hampered, which a consequent disruption of transcriptional activity. A second possibility is that the mutation affects the binding of Zic2 to protein partners that could affect transcriptional regulatory activity. Indeed, the 4th ZF of Zic2 has been shown to mediate protein-protein interactions (Koyabu *et al.*, 2001b) suggesting that this second possibility is quite likely. Without biochemical information on the identity of Zic2 protein partners, or how the *Zic2*^{Ku} mutation affects protein-protein interactions, it is impossible to determine the likely mechanism of the *Zic2*^{Ku} mutation in causing NTDs. Moreover, identification of Zic2 protein partners will indicate which proteins are likely to regulate Zic2 transcriptional activity and, thereby, provide information on the signalling pathways by which Zic2 mediates its function.

The next two chapters describe yeast two-hybrid and related studies aimed at identification of Zic2 interacting proteins.

CHAPTER 5: IDENTIFICATION OF ZIC2 PROTEIN PARTNERS USING THE YEAST TWO-HYBRID SYSTEM

5.1 INTRODUCTION

Protein-protein interactions form the basis of most biological processes, including signal transduction and transcriptional regulation of developmental genetic programmes. Therefore, the identification of protein binding partners for a protein of interest is crucial to elucidate the molecular basis of a biological system.

As has been shown in the previous chapter, *Zic2* is a key regulator of neurulation. Disruption of *Zic2* produces exencephaly and spina bifida as observed in $Zic2^{Ku/Ku}$ embryos, which show an open cranial and spinal neural tube with the absence of DLHPs. Moreover, the clinical relevance of *Zic2* has been shown by the identification of mutations in humans that display HPE (Brown *et al.*, 2001;Brown *et al.*, 1998). Despite its importance, little is known about the proteins that interact with Zic2. One study has shown that Zic2 can be immunoprecipitated with all three Gli proteins (Gli1-3) suggesting that Zic2 is involved in the Shh signalling pathway (Koyabu *et al.*, 2001a). However the identification of other additional co-factors remains to be achieved. Therefore, it was the aim of this chapter to identify possible Zic2 protein partners, and thereby reveal aspects of the transcriptional regulation of Zic2 and the pathways by which Zic2 could mediate its function.

5.1.1 The yeast two-hybrid system to identify protein-protein interactions

In the 1980s, two major discoveries on the nature of transcriptional regulation provided the basis for the development of the two-hybrid system as a genetic tool for identification of protein-protein interactions. Brent and Ptashne, discovered that a hybrid transcription factor could be generated by combining two domains from two different proteins, while preserving the transcriptional activation function (Brent and Ptashne, 1985). In this experiment, the *E. coli* LexA repressor DNA binding domain was fused to the yeast Gal4 transcriptional activation domain creating a chimeric protein

that, when expressed in yeast containing LexA operator sites, was able to activate transcription. This experiment identified the presence of two separable modules in a transcription factor: the DNA binding and the activator domains. Moreover, this study showed that these modules could fold independently into two functional units that are not influenced by the rest of the protein (see Fig. 5.1).

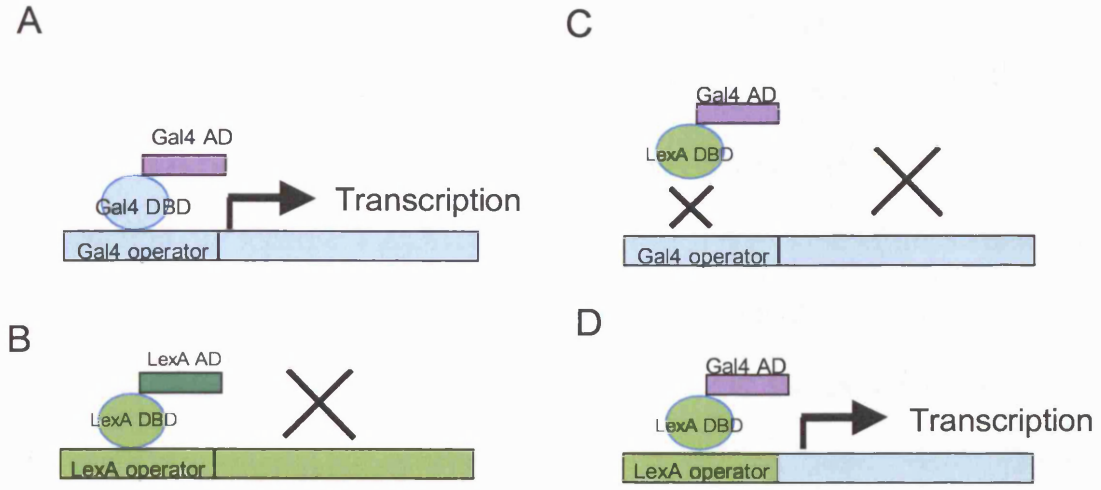

Figure 5.1 Diagram representation of the Brent and Ptashne experiment

A and B show the yeast transcription factor Gal4 and the bacterial repressor LexA activating and inhibiting transcription respectively in the presence of the appropriate operator. (C) A chimeric protein containing the LexA DNA binding and the Gal4 activation domain will not activate transcription of genes under the Gal4 operator, but can function as a transcriptional activator if the LexA operator is present (D). Therefore the ability of Gal4 to activate transcription is independent of the DNA binding domain.

The second important discovery came from experiments showing that transcriptional activators, such as VP16 from herpes simplex virus, do not need to bind directly to DNA; rather they are able to activate transcription through specific binding to DNA-binding proteins (Triezenberg *et al.*, 1988). Based on these studies, the two-hybrid system was developed by Fields and Song (Fields and Song, 1989). In this

system, two hybrid proteins are generated that can reconstitute the function of a transcriptional activator. The first hybrid protein is generated as a fusion protein between a DNA binding domain (DBD) protein and the protein of interest whose partners are to be identified. This hybrid protein is commonly referred to as the "bait" protein. The second hybrid protein contains polypeptides encoded by a cDNA library fused to an activator domain (AD) and is referred to as the "prey" (see Fig. 5.2). When these proteins are transformed into yeast separately, neither is able to activate transcription of a reporter. However, if the proteins interact, when co-transformed, the interaction brings together the DBD with the AD and activation of transcription occurs for those genes that contain the binding site for the DBD in their promoter. In the initial two-hybrid approach, the yeast strain was modified by transformation with the colorimetric reporter *LacZ*, encoding a β-galactosidase gene, which cleaves the substrate X-Gal to produce a blue colour that allows identification of the interacting clones.

5.1.2 Two-hybrid components used to identify Zic2 protein interactions

Since the first description of the yeast two-hybrid system by Fields and Song (Fields *et al.*, 1989), and with the advances in yeast genetics and molecular biology, the components of the yeast two-hybrid method have been optimised to generate a plethora of host yeast strains, plasmids and libraries (Mendelsohn and Brent, 1999;Vidal and Legrain, 1999). Nevertheless, with all these options, one has to be careful in choosing which yeast strain, type of DBD and library to use, since this choice is important for the outcome of the experiment. It is important to know that the three components are not always exchangeable and one should plan which library and yeast strain are compatible with the AD and DBD, before designing constructs.

Two main systems have been designed for use in yeast two-hybrid. The first system uses the yeast transcription factor Gal4 (Chien *et al.*, 1991) and the second uses

the bacterial operator binding protein LexA (Golemis and Khazak, 1997). While Gal4 plasmids contain a nuclear localisation signal (NLS), directing the expressed hybrid protein to the nucleus, LexA plasmids do not contain the NLS and the baits enter the nucleus provided they are below the size exclusion limit of the nuclear pore (Brent and Finley, Jr., 1997). It is not recommended, therefore, to use the LexA DBD with large full-length constructs unless the NLS signal is also introduced. A second difference between the systems is that the Gal4 DBD can utilise multiple reporter genes that contain different promoter sequences, such as *Gal1*, *Gal2* and *Gal7* (James *et al.*, 1996) (Corrick *et al.*, 1996). The LexA DBD, on the other hand, has only the LexA operator driving the expression of the reporter gene making this system prone to false positives. Recently, two new DBDs have been introduced: the bacteriophage λ repressor protein (Serebriiskii *et al.*, 1999) and the DBD of the estrogen receptor (ER) protein (Le Douarin *et al.*, 1995). Neither has been used widely so far.

The Gal4 yeast DBD was chosen in the present study to generate the chimaeric protein Zic2-DBD for two main reasons. Firstly, the Gal4 DBD is compatible with the host yeast strain PJ69-4A which contains Gal4 specific promoters that drive the expression of the selectable genes. Moreover, the plasmid (see section 5.2.3) contains the *URA3* gene, which can complement the minus uracil (*ura*$^-$) genotype of the host yeast strain allowing selection and maintenance of the recombinant clones.

5.1.2.1 PJ69-4A host yeast strain

When screening for protein interactions, the host yeast strain is the most important component in order to avoid false positives. The yeast must have selectable reporter/s, such as histidine, driven by a promoter that is compatible with the DBD used to generate the bait fusion protein. For instance, if the Gal4 DBD is used, the selectable reporter needs to be under control of a promoter specific to Gal4, such as the *Gal1* promoter, so that reporter transcription-based selection of an interaction can be

achieved. Moreover, if the Gal4 system is used, the yeast strain must contain mutations in the endogenous Gal4 and its repressor Gal80 to avoid interference with the fusion proteins (Brent *et al.*, 1997). In addition, the host yeast strain must have auxotropic mutations, which allow selection and maintenance of the bait/prey plasmids by complementation of the yeast strain genotype.

Figure 5.2 Diagrammatic representation of the two-hybrid components

(A) The first hybrid protein contains the protein of interest (X) fused to the DNA binding domain (DBD). This bait can bind to the promoter (P) but needs the activation domain to activate transcription. (B) The second hybrid, prey, consists of the library-encoded proteins (Y) fused to the activation domain (AD). When prey and bait are co-transformed into yeast cells, an interaction can occur between the protein of interest (X) and the library-encoding protein (Y). This interaction brings the activator domain into close proximity with the DNA binding domain, leading to the activation of the selectable reporter. The selectable reporter complements the auxotrophic mutation in the yeast strain, allowing growth of the yeast on a selection medium.

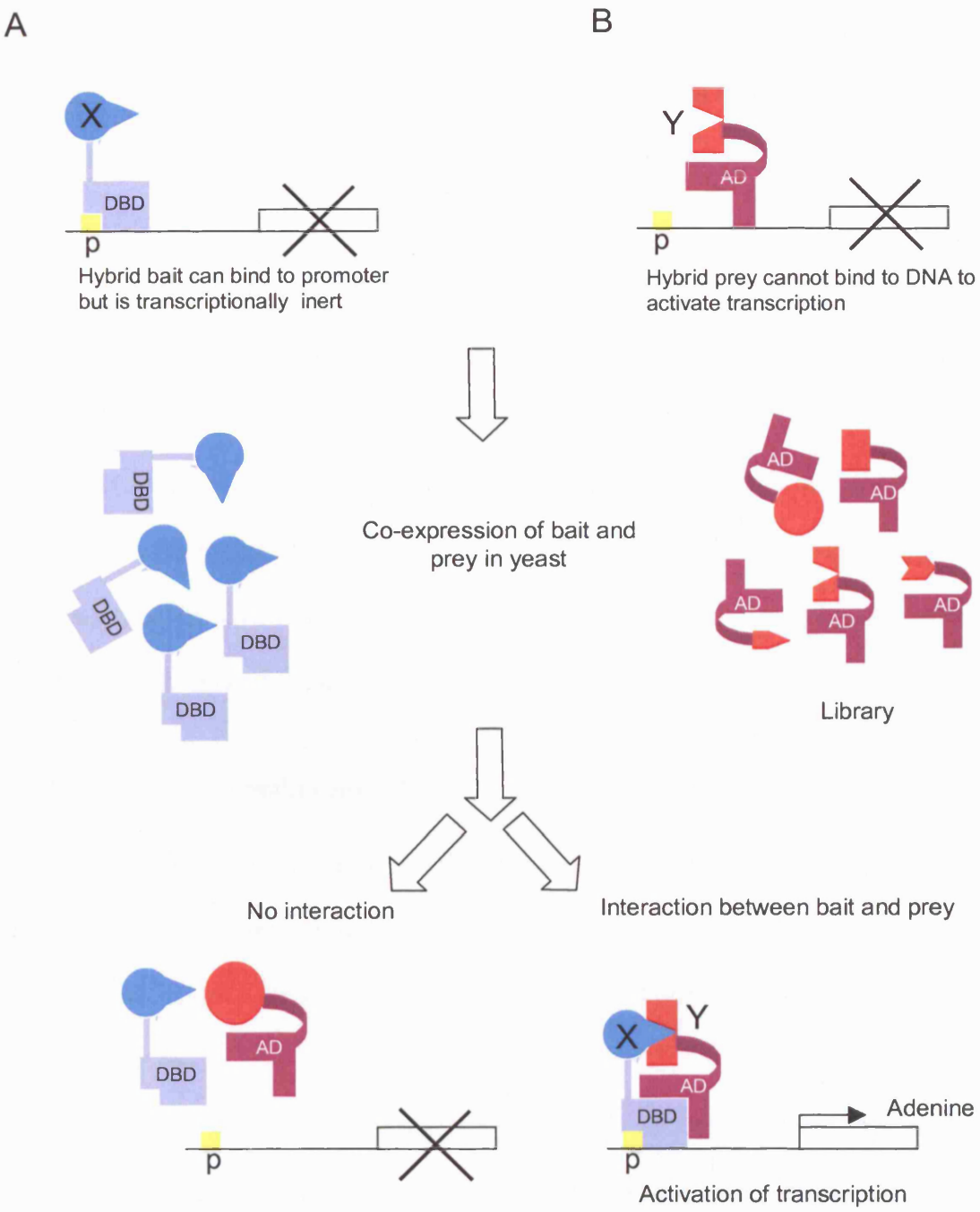
A
B
X
DBD
p
Hybrid bait can bind to promoter
but is transcriptionally inert
Y
AD
p
Hybrid prey cannot bind to DNA to
activate transcription
Co-expression of bait and
prey in yeast
Library
No interaction
Interaction between bait and prey
Adenine
Activation of transcription

To identify Zic2 protein-binding partners the PJ69-4A host yeast strain was used (James *et al.*, 1996). PJ69-4A has been genetically modified to contain the *histidine* (*his*), *adenine* (*ade*) and *LacZ* reporter genes driven by three Gal4-specific promoters. These promoters, *Gal1*, *Gal2* and *Gal7* respond to the same Gal4 DBD and can be activated to induce high levels of expression (Bram *et al.*, 1986). In this chapter, I will refer to the histidine reporter as *GAL1-HIS3*, the adenine reporter as *GAL2-ADE2* and the LacZ reporter as *GAL7-lacZ.*

The PJ69-4A yeast strain has auxotropic mutations for histidine and adenine allowing, in the case of an interaction, complementation of the *his*$^-$ and *ade*$^-$ genotype by the transcriptional activation of the selectable reporters *GAL1-HIS3* and *GAL2-ADE2* (James *et al.*, 1996). Two more auxotropic mutations are found in PJ69-4A, *URA3* and *LEU2*, that can be complemented by the presence of the bait and prey plasmids which express uracil and leucine respectively, allowing the selection of recombinants after transformation (see Figure 5.3 for constructs).

5.1.2.2 Mouse E9.5-10.5 embryonic library

To identify protein partners for Zic2 that have a potential role in the regulation of neurulation, a mouse embryonic library prepared from neurulation stage cDNA was required. For this reason a VP16-mouse E9.5-10.5 cDNA library was used to screen for Zic2 protein partners.

Unlike the DBD and host yeast strain, the AD is exchangeable. The only requirement is that the selectable amino acid for maintenance of the plasmid has to be different from that of both the bait plasmid and the selectable reporters of the host yeast strain. Three different ADs are commonly used, the difference between them being the strength of activation provided: B42 is a weak activator, Gal4 is moderate whereas VP16 is a very strong activator (Brent *et al.*, 1997).

The VP16 E9.5-10.5 mouse library was originally designed to be used for identification of novel bHLH proteins that are capable of interacting with E proteins (Hollenberg *et al.*, 1995). The library was prepared using the random priming approach, which allows amplification of the primary cDNA pool with primers containing one restriction enzyme site (Wang and Brown, 1991). After amplification, the cDNA can be digested with the appropriate restriction enzyme and cloned into the AD vector, creating prey clones representing the expressed genes at this particular gestational stage. The initial library contained 5 x 10^6 clones with cDNA fragments of 350 to 700 nucleotides in length.

The VP16 mouse embryonic library was kindly provided by Professor Peter Scambler, Molecular Medicine Unit at the Institute of Child Health, UCL, whose laboratory had used it successfully in yeast two-hybrid analysis in the past (Hollenberg *et al.*, 1995;Magnaghi *et al.*, 1998)

5.2 METHODS

5.2.1 Cloning of *Zic2* constructs for yeast two-hybrid analysis

Constructs were designed to contain either the entire open reading frame, or only the zinc finger DNA binding domain of Zic2. Both coding sequences were cloned in frame with the cassette encoding the Gal4 DNA binding domain (see Fig. 5.3 for vector map) in order to generate Zic2-Gal4 fusion proteins.

Full-length Zic2 was amplified from a PEBOS-Zic2 plasmid kindly donated by Jun Aruga (Mizugishi *et al.*, 2001b). However, after checking the identity of the fragment by sequencing, the last coding codon and the stop codon were found to be missing from the plasmid. Moreover, the restriction sites where Zic2 was cloned into PEBOS-Zic2 were not compatible for cloning full length Zic2 in frame with the Gal4 pGBDU-C plasmid. Therefore, primers (see Table 5.1 for primer sequence) containing the SalI and BamHI sites were designed to amplify the entire open reading frame of the Zic2 gene using Accuzyme DNA polymerase (see section 2.3.3.2). The PCR conditions used to amplify Zic2 were as follows: denaturation at 94°C for 1 minute, followed by 25 cycles consisting of: denaturation step at 94°C for 1 minute, primer annealing at 58°C for 1 minute, elongation at 72°C for 2 minutes; and a final elongation step at 72°C for 10 minutes. The PCR product was gel-purified (see section 2.3.5.1) and ligated into the Gal4 pGBDU-C plasmid (see section 2.3.6.1).

Of several recombinant clones identified by blue and white selection, only one clone failed to show PCR-induced mutations after sequencing (see Table 5.2 for primer sequence). This clone, pGEMt-Zic2FL was grown overnight and plasmid DNA was purified using a midiprep Kit (see section 2.3.12). The plasmid was then double digested with SalI and BamHI, and following gel purification, the digested fragment was cloned into the pGBDU-C plasmid (Genbank accession number U70020).

Recombinants were identified using the DNA shift assay technique. The recombinant plasmid was sequenced to check that Zic2 was in frame with the Gal4 activation domain and that no mutations were present. This construct was named Gal4-Zic2FL.

To clone the zinc-finger DNA-binding domain into the Gal4 pGBDU-C plasmid, primers were designed with EcoRI and SalI sites (see Table 5.1 for primer sequence) using the Gal4-Zic2FL as a template for the PCR amplification. The PCR cycling reaction was performed as described above, but the elongation step was reduced to 30 seconds because the DNA fragment to be amplified was shorter. The DNA fragment was digested with EcoRI and SalI, purified and ligated. Identification of recombinants was performed by colony PCR using PGBD-F and PGBD-R primers flanking the muticloning site (see Table 5.3 for primer sequence). Recombinants were sequenced to verify identity. The construct was named Gal4-Zic2FD.

5.2.2 Identification of VP16 library interacting clones

Interacting clones that grew on the selection medium were purified as described in section 2.5.3. A map of the pVP16 plasmid is provided in Figure 5.3. To obtain the inserts for sequencing, PCR amplification was performed using pVP16-F and pVP16-R primers flanking the multicloning site of the pVP16 plasmid (see Table 5.3). The PCR reaction was performed as follows: denaturation at 94°C for 1 minutes, followed by 35 cycles consisting of: denaturation at 94°C for 1 minute, primer annealing at 68°C for 1 minute, elongation at 72°C for 1 minute and a final elongation step at 72°C for 10 minutes. PCR products were purified using Qiagen spin columns and the pVP16R primer was used for sequencing the inserts.

Figure 5.3 Plasmid maps and restriction enzyme sites of the bait, pGBDU-C and prey pVP16

(A) pGBDU-C contains a Gal4 DNA binding cassette followed by a multicloning site for cloning cDNAs under the control of the alcohol dehydrogenase1 (*ADH1*) promoter. The Gal4 cassette encodes amino acids 1-147 of the GAL4 DBD. For selection in yeast the plasmid contains the *URA3* gene that complements the *ura*$^-$ genotype of the PJ69-4A yeast host strain. (B) pVP16 contains the VP16 activation domain of the herpes simplex virus, followed by a multicloning site to insert library cDNAs under control of the *ADH1* promoter. To allow selection of yeast containing the plasmid, pVP16 contains the *LEU2* gene that complements the *leu*$^-$ genotype of PJ69-4A. Both plasmids have the yeast 2μ origin of replication and ß-lactamase that confers resistance to ampicillin, to select for recombinant colonies in bacteria. Maps obtained from (Hollenberg *et al.*, 1995) and (James *et al.*, 1996).

Figure 5.3

A

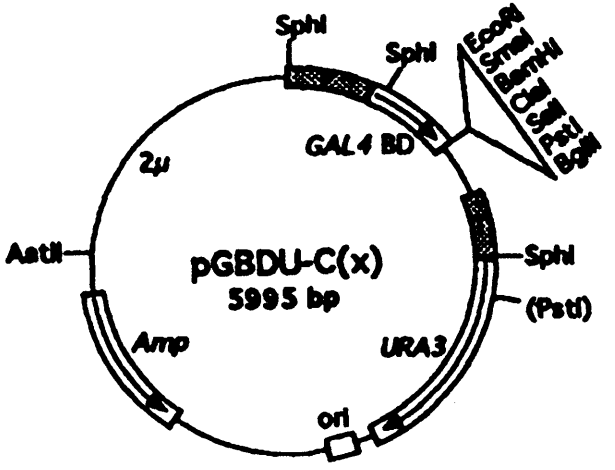
SphI
SphI
EcoRI
SmaI
BamHI
ClaI
SalI
PstI
BglII
GAL4 BD
2μ
AatII
pGBDU-C(x)
5995 bp
SphI
(PstI)
Amp
URA3
ori

B

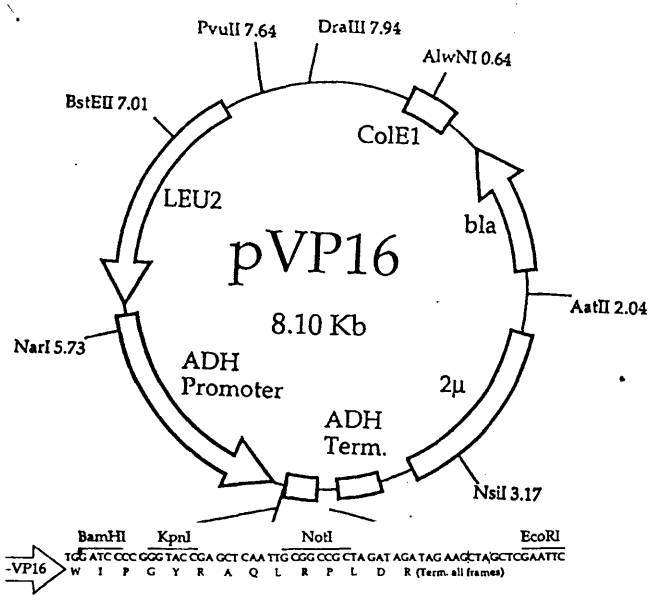
PvuII 7.64
DraIII 7.94
AlwNI 0.64
BstEII 7.01
ColE1
LEU2
bla
pVP16
8.10 Kb
AatII 2.04
NarI 5.73
ADH
Promoter
2μ
ADH
Term.
NsiI 3.17
BamHI
KpnI
NotI
EcoRI
TGG ATC CCC GGG TAC CGA GCT CAA TTG GGG CCG CTA GAT AGA TAG AAG CTA GCT CGA ATTC
-VP16
W I P G Y R A Q L R P L D R (Term. all frames)

Table 5.1 Primers designed to generate Gal4-Zic2FL and Gal4-Zic2FD. Genbank accession number and the region amplified

Construct	Primer sequence	Genbank accession number	Amplified region (bp)
Zic2FL	F 5' TCAGGATCCCATGCTTCTGGACGCGGGGCGA3' R 5' ATCGTCGAGTCACACACGTACCATTCATTGA3'	D70848	1592
Zic2FD	F5'GTAGAATTCAAGCAAGAGCTCATCTGCAAGTG3' R5'CTAGTCGACTCAATGGACCTTCATGTGCTTCCG3'	D70848	490

Table 5.2. Primers used in the sequencing of the Gal4-Zic2FL and Gal4-Zic2FD constructs.

Primer name	Primer sequence
2SF1	5'-GGATCCTGGCCATGCTTCTGGA-3'
2SF2	5'-TCAGAACGGCTTCGTGGACT-3'
2SF3	5'-GCGTGTGCAACCGAGGATAA-3'
2SF4	5'-CACCTTCTTTTCCCTGGCCTT-3'
2SF5	5'-TACATGCGGCAGCAGTGCAT-3'
2SF6	5'-TGGTCAACCACATCCGCGTGCA-3'
2SF7	5'-GCAAGATGTGTGACAAGTCC-3'
2SF8	5'-ACAAAGCAGCTCCAACCTGT-3'
2SF9	5'-CCTCCAACTTCAATGAATGG-3'
2SR1	5'-AATAGGAGCCAACGTGTGCG-3'
2SR2	5'-CCCTAGGCGCATTTGCCCATT-3'
2SR3	5'-TTCATAGGGCCGTACTGGTT-3'
2SR4	5'-AGCTCGTGCATGGTGCTGAAA-3'
2SR5	5'-GGTTTCTCCCCTGTATGAGTTC-3'
2SR6	5'-TGTGGACGACTCGTAGCCAGA-3'
2SR7	5'-TATGGCCTCCGGTTGTCCCT-3'
2SR8	5'-TGCCCTCGATGGGTTTTGGGA-3'
2SR9	5'-GTTTCAGACATACAGAGAG-3'

Table 5.3. Primers flanking the multicloning site of pVP16 and pGBDU-C

Primer name	Primer sequence
pVP16-F	5'-GAGTTTGAGCAGATGTTT -3'
pVP16-R	5'- GTTGTAAAACGACGGCCAGT -3'
PGBD-F	5'-TGCCTCTAACATTGAGACAG -3'
PGBD-R	5'-CACAGTTGAAGTGAACTTGC -3'

5.3 RESULTS

5.3.1 Genotyping of the host yeast strain

Before starting the screening of the VP16 mouse embryonic library using Zic2 constructs, the host yeast strain was genotyped by assessing its growth restriction. PJ69-4A has been genetically modified such that growth will occur only in the presence of specific amino acids. Three reporter genes *Gal1-HIS3*, *Gal2-ADE* and *Gal7-LacZ* allow transcriptional activation in the presence of protein interactions that lead to reporter gene expression which complement the *his*$^-$ and *ade*$^-$ genotype. To select for the presence of bait and prey plasmids, the host yeast strain also has the *ura*$^-$ and *leu*$^-$ genotypes, which are rescued by expression of the *URA3* and *LEU2* from the bait and prey plasmids respectively.

It was crucial at the start of the study to check that the host yeast strain had not mutated and reversed its phenotype enabling it to grow on any of the selectable markers. The yeast genotype was assessed by determining the capacity of the PJ69-4A to grow on SD "drop out medium", in which one of the amino acids had been excluded (Fig. 5.4). PJ69-4A yeast was streaked onto a SD plate containing all the amino acids. After 72 hours in culture colonies became apparent. Four individual colonies were then streaked onto each SD-drop out medium and left to grow for 72 hours. PJ69-4A was not able to grow on SD-adenine, SD-uracil, SD-methionine, SD-histidine, SD-tryptophan and SD-leucine plates, but grew normally on SD-lysine medium, which was used as a control (Fig. 5.4). Some growth was detected on the SD-histidine plates due to the leaky expression of the *Gal1-HIS3* reporter gene. This was overcome by addition of 3 mM 3-amino-1,2,4-triazole (3AT) to the SD-histidine medium (data not shown). Hence, PJ69-4A had the expected genotype (*ade*$^-$, *ura*$^-$, *met*$^-$, *his*$^-$, *trp*$^-$, *leu*$^-$) and therefore was suitable for screening the cDNA library.

5.3.2 Auto-activation of the selectable reporter

Successful two-hybrid selection requires a library that contains clones representing a high level of coverage of the genome, a host yeast strain that yields low levels of background false positives and, importantly, a bait protein suitable for screening (Fields and Sternglanz, 1994). Two problems can arise from using a fusion protein as bait. First, the bait protein may not be expressed at sufficient levels, and second, the bait protein may have the capacity to activate the selectable reporter on its own without the presence of the library plasmid, a phenomenon known as auto-activation.

To verify that the Gal4-Zic2FL and Gal4-Zic2FD bait constructs did not auto-activate the *Gal1-HIS3* and the *Gal2-ADE2* reporters in the absence of VP16-prey constructs, bait constructs were transformed into the PJ69-4A host strain and grown on SD-uracil to select recombinants. Four colonies were picked and re-streaked onto SD-uracil-histidine containing 3 mM 3AT, or onto SD-uracil-adenine. Growth was detectable for both bait proteins, Gal4-Zic2FL and Gal4-Zic2FD, on the SD-uracil-histidine with 3 mM 3AT (Fig. 5.5 A), whereas no growth was detected on the SD-uracil-adenine for either of the bait constructs (Fig. 5.5 B). Therefore, Gal4-Zic2FL and Gal4-Zic2FD baits have the capacity to auto-activate the *Gal1-HIS3* reporter but not the *Gal2-ADE2* reporter. Hence, in subsequent screens to identify interacting proteins, only the *Gal2-ADE2* reporter was used, and positive interactions were detected by growth on SD-uracil-leucine-adenine and by activation of *Gal7-LacZ*, as detected by colour change.

5.3.3 Interacting clones from the small-scale transformation of the VP16 library

In order to identify potential Zic2 interacting proteins, the Gal4-Zic2FL was used to screen the E9.5-E10.5 mouse VP16 cDNA library. Gal4-Zic2FL was used for the initial screening for two reasons. Firstly, use of the zinc finger DNA binding domain

Figure 5.4 Genotyping of the host yeast strain PJ69-4A to verify auxotrophic mutations

PJ69-4A grows on a SD minimal medium that contains adenine, uracil, histidine, methionine, tryptophan, leucine and lysine. (B-H). SD medium plates where one of the constituents has been excluded ("dropped out"). Growth of PJ69-4A requires supplementation with adenine (B), uracil (C), histidine (D), methionine (E), tryptophan (F) and leucine (G) to grow, but not lysine (arrows in H). Some growth can be seen on the SD-HIS plates (arrowheads in D) due to leaky expression of the histidine reporter.

Figure 5.5 Gal4-Zic2FL and Gal4-Zic2FD auto-activate the *GAL1-HIS3* selectable reporter but not the *GAL2-ADE2* reporter

Bait constructs Gal4-Zic2FL (A) and Gal4-Zic2FD (B) were transformed into PJ69-4A and recombinants were grown on either SD minus uracil-histidine containing 3 mM 3AT, or on SD minus uracil-adenine. Note that both constructs are able to complement the *his*$^-$ phenotype of PJ69-4A (as shown by growth on SD-ura-his + 3 mM 3AT) indicating that the histidine reporter has been activated (arrows in A and B). In contrast, the PJ69-4A *ade*$^-$ phenotype is not rescued after transformation with either bait construct.

Fig. 5.4

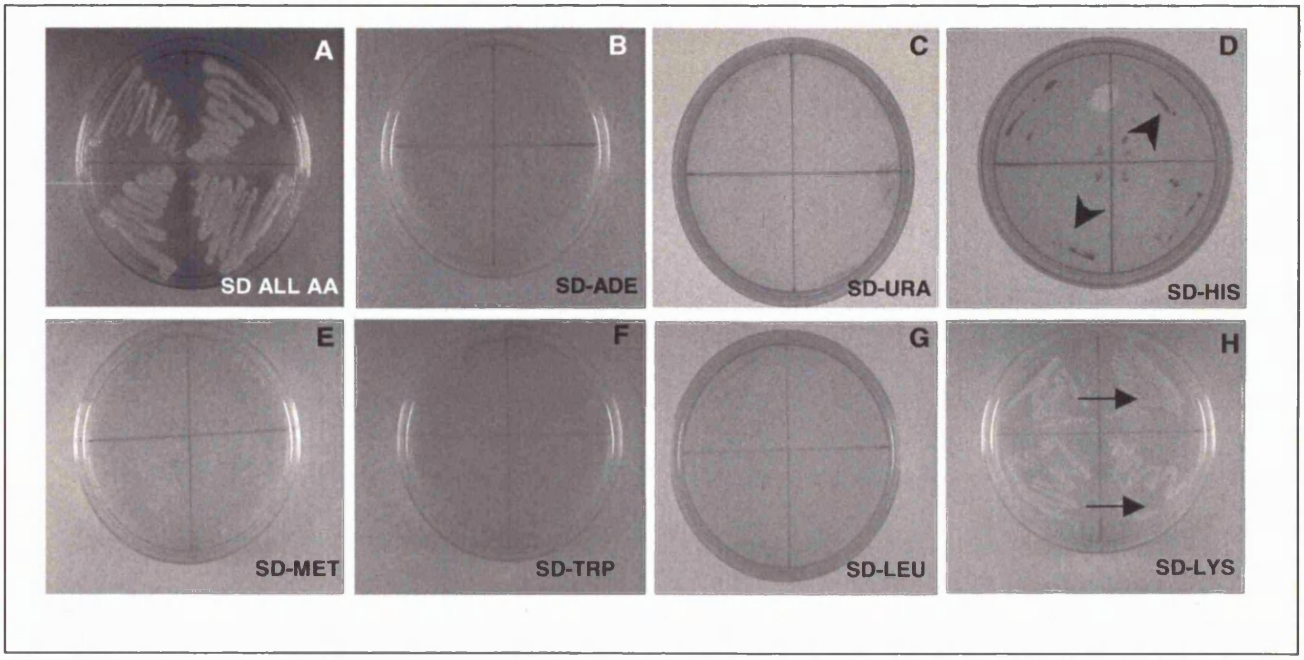
A
SD ALL AA
B
SD-ADE
C
SD-URA
D
SD-HIS
E
SD-MET
F
SD-TRP
G
SD-LEU
H
SD-LYS

Fig. 5.5

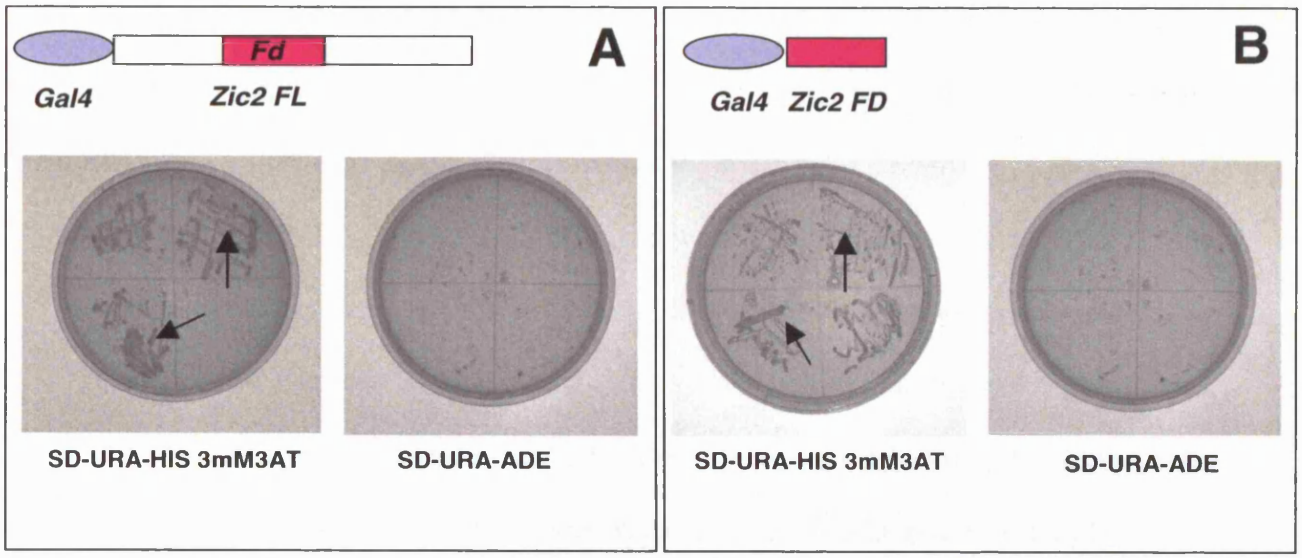
A
Fd
Gal4
Zic2 FL
SD-URA-HIS 3mM3AT
SD-URA-ADE
B
Gal4
Zic2 FD
SD-URA-HIS 3mM3AT
SD-URA-ADE

alone could have caused important interacting partners to be missed, if they interacted with Zic2 through a domain other than the zinc finger. Secondly, small baits that represent only one domain of a protein can exhibit large numbers of interactions that do not necessarily represent true physiological interactions involving the full length protein. Use of the full length Zic2 as bait was more likely to yield a normally folded protein similar to the wild type protein, thereby reducing the chance of possible false positive interactions.

To initiate the screen a tenth of the volume of the library was transformed to assess the number of interacting clones that could be identified. Some baits function as strong activators resulting in a large number of positive clones, many of which are shown to be false positives on further analysis. If small-scale transformation experiments reveal a large number of interacting clones, for example more than 150 clones, it is advisable not to continue the screening with that particular bait, as ten times more clones are likely to require analysis when transforming the whole library.

After co-transformation of the VP16 mouse embryonic library with Gal4-Zic2FL, 45 clones were rescued from growth on SD-uracil-leucine-histidine-adenine from 7 x 10^4 double recombinants. These clones were re-streaked onto SD-uracil-leucine-histidine-adenine containing X-α-gal. From the 45 initials clones only 39 were Ade^+ β-$galactosidase^+$ (grew on an adenine deficient medium and exhibited β-galactosidase activity). VP16 library plasmids were purified and sequenced to determine their identity. Only in-frame plasmids were considered as possible interactors (Table 5.4). Of the 10 clones that were out of frame, 8 were cloned in the wrong orientation. The presence of a cDNA cloned in a 3'-5' direction can be attributed to the nature of the amplification/cloning procedure to generate the VP16 library (see section 5.1.2.1.2).

5.3.4 Identification of interacting clones from the large-scale transformation

Since a relatively small number of clones resulted from the small-scale transformation, the Gal4-Zic2FL construct was next used to screen the whole VP16 library (see section 2.5.2.2). After transformation, 800 *ade*$^+$ *β-galactosidase*$^+$ clones were recovered that were able to grow on SD-uracil-leucine-histidine-adenine from a total of 1 x 10^6 double recombinants. Plasmids from 250 these clones were recovered and purified. Inserts were amplified by PCR and sequenced. Only in frame clones are represented in Table 5.5.

5.3.5 Analysis of the VP16 interacting clones

The small and large-scale transformations yielded several candidate genes whose protein products appear to interact with Zic2. On the other hand, some of the identified clones are predicted to be "false positives". Because the two-hybrid screen identifies interacting clones by transcriptional activation of reporter genes, this makes the system prone to identification of artefacts that are not true interactions. The term false positive refers to prey proteins that interact with bait protein in the yeast two-hybrid system but this interaction fails to be reproduced when clones are further analysed biochemically. Genes identified in the screen were compared to a database of known false positives (http://www.fccc.edu/research/labs/golemis). RNA binding proteins, mitochondrial proteins, cytoskeletal proteins, and heat shock proteins are known to commonly give false positive results. From the screening clones, *Poly (rC)*, *ZFR*, *Glutaminyl-tRNA*, *Lysyl-tRNA*, all of which encode RNA binding proteins, and *Hsp70*, that encodes a heat shock protein (shown in blue in Tables 5.4 and 5.5), were considered as false positives.

A second approach to focus on the likely proteins of interest was to discard those proteins that are not co-expressed or co-localised with Zic2 and are therefore unlikely to represent biologically relevant interactions. This type of false positive arises from the nature of the two-hybrid system, in which both bait and prey proteins, are directed to the yeast nucleus by nuclear localisation signals within the plasmid construct.

Table 5.4. Interacting clones from the small scale transformation of the VP16 E9.5-10.5 mouse library using Gal4-Zic2FL

Interacting clones	β-gal activity[a]	Number of clones	Nature of the encoded protein
Capicua (Cic)	***	3	HMG box transcription factor
LOC210444	**	3	EST
Acetylcholinesterase	**	3	Enzyme
Poly(rC)	*	3	RNA binding protein
ZFR	***	1	Zinc finger protein
WSB-1	***	1	SOCS box containing protein
CCR4	**	1	Transcription factor
NDAP7	***	3	Neural development associated protein
Glutaminyl-tRNA	*	2	RNA binding protein
Lysyl-tRNA	**	1	RNA binding protein
LEK1	**	2	Transcription factor/mitosis
Foxp4	***	2	Similar to forkhead protein Foxp1
Nidogen1	***	2	Transmembrane protein
TCF20	**	1	Transcription factor
Heat shock cognate	***	1	Heat shock protein

Genes in blue: listed on a database of known false positives
(http://www.fccc.edu/research/labs/golemis)
Genes in green: ESTs representing unknown genes
a β-gal activity: *** = strong; **= moderate; * = weak

Table 5.5. Interacting clones from the large scale transformation of the VP16 E9.5-10.5 mouse library using Gal4-Zic2FL

Interacting clones	β-gal activity[a]	Number of clones	Nature of the encoded protein
TIF9	*	3	Translation initiation factor
Ubiquilin 1	**	6	Cytoplasmic protein
Hnrpa3	**	3	Nuclear heteroprotein 3
P53bp1	***	6	P53 binding protein 1
Midkine	***	5	Growth factor
Similar to P130	*	3	Unknown
Ncor2	**	1	Transcription factor
BC023767.1	***	4	Unknown
Twisted gastrulation	*	4	Signalling molecule
Itgb5	*	1	Transmembrane protein
Fibulin1	***	6	Extracellular matrix protein
Matrin	*	4	Extracellular matrix protein
Loc218747	***	5	Unknown
FLJ13855	**	3	Unknown
HSP70	***	2	Heat shock protein
Kielin	**	5	Signalling molecule
Glis2	***	4	Zinc finger transcription factor
TIF4	**	2	Translation initiation factor
Glutaminyl-tRNA	*	5	RNA binding protein
Laminin	*	3	Extracellular matrix protein
Suppressorof Variegation	**	3	Transcription factor
Notch3	**	4	Transmembrane protein/ transcription factor
Krox20	***	5	Transcription factor

Genes in blue: listed on a database of known false positives
(http://www.fccc.edu/research/labs/golemis)
Genes in green: ESTs rpresenting unknown genes
a β-gal activity: *** = strong; **= moderate; * = weak

Table 5.5 (continued) Interacting clones from the large scale transformation of the VP16 E9.5-10.5 mouse library using Gal4-Zic2FL

Interacting clones	β-gal activity[a]	Number of clones	Nature of the encoded protein
Notch1	**	6	HMG box transcription factor
Acetylcholinesterase	**	2	Enzyme
Poly(rC)	*	3	RNA binding protein
Jumonji	***	3	Zinc finger protein
Usp5	***	5	Ubiquitin specific protease
AK030766.1	***	4	Unknown
BC003244.1	**	6	Similar to nuclear phosphoprotein
Fibrillin2	*	3	Extracellular matrix protein
Plu1	***	6	Transcription factor
BC03882.1	*	2	Zn-finger, C-x8-C-x5-C-x3-H type protein
XM_133779	**	2	Similar to ATP-binding cassette
XM_013509.1	***	5	Unknown
AK017880.1	***	3	Unknown
BC004063.1	***	4	Unknown
Lysyl-tRNA	***	3	RNA binding protein
Foxp4	***	4	Transcription factor
AT-hook1	***	5	Transcription factor

Genes in blue: listed on a database of known false positives

(http://www.fccc.edu/research/labs/golemis)

Genes in green: ESTs representing unknown genes

a β-gal activity: *** = strong; **= moderate; * = weak

Therefore, even though a particular interaction may occur between the protein domain identified and the bait under experimental conditions, this may not reflect the physiological situation. To avoid analysis of such clones, proteins of known function such as extracellular matrix proteins, signalling molecules, growth factors or extracellular domains of receptors were not further characterised, as they were considered unlikely to interact physiologically with the Zic2 transcription factor. Genes identified in the library screen that code for extracellular matrix proteins were *nidogen1, fibulin1*, *matrin*, *laminin*, and *fibrillin2* and these were not further analysed. Similarly, the extracellular-EGF-like domains of the transmembrane receptors *Notch3* and *Notch1* that were identified in the screen (see Table 5.5) as well as the extracellular domain of *integrin beta 5* were considered unlikely to have a physiological interaction with the transcription factor Zic2. Finally, two genes that code for the secreted signalling molecules, *twisted gastrulation* and *kielin*, and a third gene *midkine* that codes for a growth factor that promotes neurite outgrowth, were not analysed, for similar reasons.

The translation imitation factors, TIF9 and TIF4, that bind to RNA polymerase to initiate translation, were considered to be likely false positives, since Zic2 functions in regulation of transcription, not translation.

Several ESTs that code for unknown genes were identified in the library screen (represented in green colour in Tables 5.4 and 5.5). These include *LOC210444*, *1200010k03*, *BC023767.1*, *LOC218747*, *FLJ13855*, *AK030766.1*, *BC003244.1*, *BC03882.1*, *XM_ 133779*, *NM_013509.1*, *AK017880.1*, *BC004063.1*. As the encoded proteins have not been characterised, they could fall into any of the false positive categories described above. Hence, these clones were not analysed in this thesis although functional interactions with Zic2 cannot be ruled out.

From the list of remaining interacting clones, *VP16-p53bp1*, *VP16-Foxp4*, *Vp16-Glis2*, *VP16-Krox20*, *VP16-Jmj*, *VP16-Athook1*, *VP16-Capicua* and *VP16-Plu1*

were chosen for further analysis. These genes encode transcription factors that could have a physiological role as co-activators or co-repressors of Zic2 function. Several clones representing each of the proteins were identified and the ß-galactosidase activity was strong in each case (see Tables 5.4 and 5.5), suggesting that these proteins may represent genuine Zic2 interacting proteins.

5.3.6 Further analysis of candidate interacting proteins

5.3.6.1 Auto-activation of the selectable reporter by VP16 candidate clones

One type of false positive that can arise from the yeast two-hybrid screen is the situation where library proteins bind to the upstream promoter sequence and activate the transcription of the selectable reporter, in the absence of the bait. This phenomenon is known as auto-activation of the selectable reporter by the prey. Therefore, prior to biochemical characterisation of the interacting proteins, clones obtained in the screen were tested for their ability to activate the selectable reporter in the absence of Gal4-Zic2FL.

Clones VP16-Foxp4$_{(71\text{-}216AA)}$, VP16-Glis2$_{(175\text{-}318AA)}$, VP16-Krox20$_{(270\text{-}423AA)}$, VP16-Cic$_{(927\text{-}1100AA)}$, VP16-Jumonji$_{(1102\text{-}1300AA)}$, VP16-PLU1$_{(692\text{-}745AA)}$, VP16-Athook1$_{(6\text{-}107AA)}$ and VP16-p53bp1$_{(1535\text{-}1750AA)}$ were purified and transformed into the host yeast strain PJ69-4A. The amino acid numbers in brackets for each clone correspond to the region of the protein coded for the cDNA identified in the screen. Recombinants were grown on SD-leucine plates for 72 hours at 30°C to select for the presence of the pVP16 library plasmid. Once colonies were apparent, each clone was re-streaked onto a SD-leucine-histidine-adenine plate and incubated for 4 days (Fig. 5.6). If auto-activation of the selectable reporter occurred, the protein encoded by the library plasmid would activate *Gal1-HIS3* and *Gal2-ADE2* producing histidine and adenine, allowing growth of the *his*$^-$, *ade*$^-$ PJ69-4A yeast strain on the selective medium.

Figure 5.6 Auto-activation of the selectable reporter by VP16 library proteins

VP16-p53bp1 (A, B), VP16-Foxp4 (C, D), VP16-Glis2 (E, F), VP16-Krox20 (G, H), VP16-Cic (I, J), VP16-Athook1 (K, L), VP16-Jumonji (M, N), VP16-Plu1 (O, P), were transformed into the PJ69-4A and recombinants grown on SD minus leucine selective medium (A, C, E, G, I, K, M, O). Recombinant colonies containing VP16 library plasmids were re-streaked onto SD-leucine-histidine-adenine selection medium (B, D, F, H, J, L, N, P). VP16-p53bp1 (B), VP16-Glis2 (F), VP16-Krox20 (H), VP16-Cic (J), VP16-Athook1 (L), VP16-Jumonji (N), VP16-Plu1 (P) did not grow on the SD-leucine-histidine-adenine selection medium indicating that they are not able to auto-activate the selectable reporters. In contrast, VP16-Foxp4 (D) is able to auto-activate the *Gal1-HIS3* and *Gal2-ADE2* selectable reporters in the absence of the Gal4-Zic2FL plasmid, as shown by its ability to grow on the selection medium lacking histidine and adenine.

Fig. 5.6

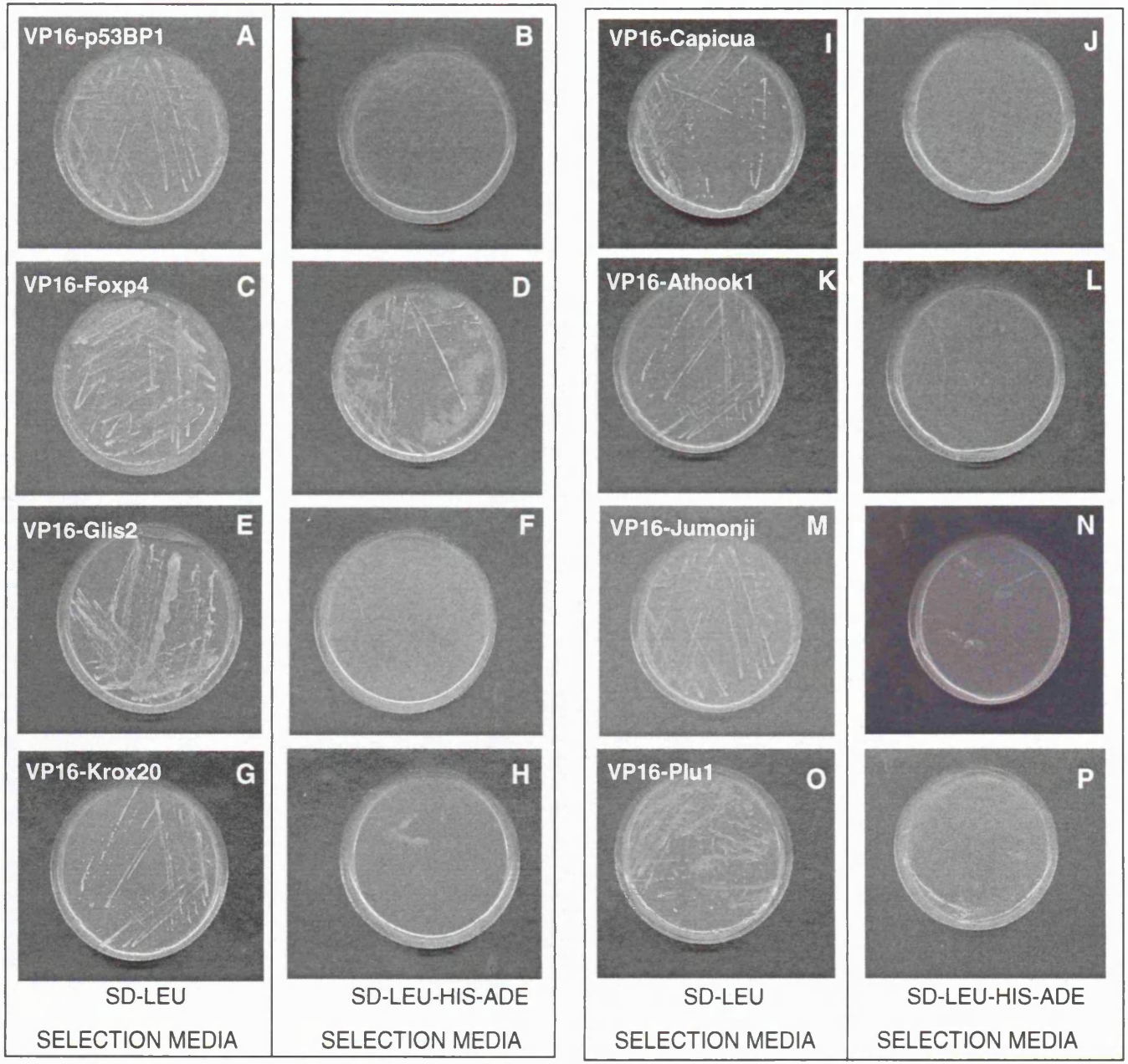
VP16-p53BP1
A
B
VP16-Foxp4
C
D
VP16-Glis2
E
F
VP16-Krox20
G
H
SD-LEU
SELECTION MEDIA
SD-LEU-HIS-ADE
SELECTION MEDIA
VP16-Capicua
I
J
VP16-Athook1
K
L
VP16-Jumonji
M
N
VP16-Plu1
O
P
SD-LEU
SELECTION MEDIA
SD-LEU-HIS-ADE
SELECTION MEDIA

VP16-Glis2, VP16-Krox20, VP16-Capicua, VP16-Jumonji, VP16-PLU1, VP16-Athook1 and VP16-p53bp1 were unable to auto-activate the selectable reporters in these assays (Fig. 5.6). Therefore, the interaction obtained in the library screen could not had been mediated by self-activation of the reporters, but rather by the interaction with *Gal4-Zic2FL.* One clone, *VP16-Foxp4*, did grow on SD-leucine-histidine-adenine (Fig. 5.6) indicating that VP16-Foxp4 can activate the selectable reporters without interacting with Gal4-Zic2FL. VP16-Foxp4 was considered to be a false positive and was not analysed further.

5.3.6.2 Reproduction of the interaction by re-co-transformation

For library-encoded proteins that did not auto-activate the selectable reporter, it was next important to test whether the interaction obtained in the two-hybrid screen was reproducible, by co-transformation of the bait and prey into the host yeast strain. Interactions could occur between the protein under study and the library-encoding protein, but might alternatively be mediated through the direct interaction of the Gal4 DBD and the prey, or the VP16 AD with the Zic2 protein. These possibilities can be checked by the co-transformation of an empty VP16-AD expressing vector with the bait, or the Gal4-DBD empty vector with the prey. If growth occurs on the SD-selection medium this clone can be considered as a false positive.

To check whether the interactions were reproducible, the PJ69-4A was co-transformed with Gal4-Zic2FL and with one of the interacting clones VP16-p53bp1, VP16-Cic, VP16-Krox20, VP16-Glis2, VP16-Plu1, VP16-Jmj or VP16-At-hook1. After transformation, double recombinants were selected by growth on SD-uracil-leucine to select for presence of the plasmid and colonies where then re-streaked onto SD-uracil-leucine-histidine-adenine to test for the interaction (see Fig. 5.7). The interaction between Gal4-Zic2FL and all of the VP16-fusion proteins was reproducible as seen by

growth of the double recombinants on the SD-uracil-leucine-histidine–adenine + X-Gal selection medium that yielded blue staining, indicating strong β-galactosidase activity.

To map the region of Zic2 required for the interaction with the library-encoding proteins, the Gal4-Zic2FD, which contained only the zinc finger DNA binding domain, was co-transformed with the VP16-interacting clones as above. After transformation, double recombinants were grown on SD-uracil-leucine-histidine-adenine medium. Co-transformation of the Gal4-Zic2FD with VP16-Krox20 or VP16-Glis2 allowed growth on the selection medium (Fig. 5.7 E-F and G-H) indicating that these proteins can interact with Zic2 through its zinc finger DNA binding domain alone. In contrast, the other library clones did not interact with the Gal4-Zic2FD indicating that these interactions occurred through other regions of Zic2 protein.

In order to check that the interaction was mediated by contact of Zic2 with the library-encoded protein, rather than with VP16-AD, a plasmid containing only the VP16-AD cassette was co-transformed with Gal4-Zic2FL. In this case, the co-transformed PJ69-4A was not able to grow on the selection medium indicating that Gal4-Zic2FL and VP16 do not interact with each other (Fig 5.7 upper left quadrants). However, interaction could also occur by physical contact between the VP16 library-encoded protein and Gal4-DBD, rather than with the Zic2 protein. To assess this possibility, VP16-p53bp1, VP16-Cic, VP16-Krox20, VP16-Glis2, VP16-Plu1, VP16-Jmj and VP16-At-hook1 were co-transformed with a plasmid encoding only the Gal4-DBD cassette. Double recombinants were selected by growth on SD-uracil-leucine (Fig 5.7, lower left quadrants) and then tested for the ability to grow on the SD-uracil-leucine-histidine-adenine selection medium. None of the double recombinants grew on the selection medium indicating that the reporter was not activated and that the VP16-fusion proteins do not interact directly with the Gal4-DBD. These experiments demonstrate that the interactions of Glis2, Krox20, Capicua, Jumonji, Plu1, VP16-At-

hook1 and p53bp1 with Zic2 are reproducible and do not occur through contact with VP16-AD or Gal4-DBD. Moreover, the region of interaction of Zic2 with Krox20 and Glis2 maps to the zinc finger DNA binding domain of Zic2.

Figure 5.7 Reproduction of interactions by co-transformation

VP16-p53bp1 (A, B), VP16-Cic (C, D), VP16-Krox20 (E, F), VP16-Glis2 (G, H), VP16-Plu1 (I, J), VP16-Jmj (K, L), VP16-Athook1 (M, N) were co-transformed with either Gal4-Zic2FL (upper right quadrant), Gal4-Zic2FD (lower right quadrant) or Gal4 (lower left quadrant) constructs into PJ69-4A, and double recombinants selected by growth on SD minus uracil-leucine (A, C, E, G, I, K, M). Gal4-Zic2FL was also co-transformed with empty VP16 vector (upper left quadrant). Colonies were re-streaked onto SD-uracil-leucine-histidine-adenine+XGal (B, D, F, H, J, L, N). Double recombinants containing Gal4-Zic2FL and VP16-p53bp1 (B), VP16-Cic (D), VP16-Krox20 (F), VP16-Glis2 (H), VP16-Plu1 (J), VP16-Jmj (L) and VP16-Athook1 were able to grow on the selective medium and turned blue in the presence of X-Gal (upper right quadrant) indicating that the interaction can be reproduced. Moreover, VP16-Krox20 and VP16-Glis2 interacted with Gal4-Zic2FD (F and H) as seen by growth and blue colour of the double recombinants (lower right quadrants). This indicates that the region of Zic2 required for the interaction with Krox20 and Glis2 is the zinc finger DNA binding domain. The Gal4 empty plasmid alone was unable to activate transcription of the selectable reporters in the presence of any of the prey plasmids (lower left quadrant in B, D, F, H, J, L, N) indicating that the interaction observed is not due to the Gal4 cassette, but rather to the library- encoded protein. Double recombinants Gal4-Zic2FL and VP16 were not able to grow on the selection medium (upper left quadrant in B, D, F, H, J, L, N) indicating that the observed interactions did not depend on the VP16 activation domain cassette.

Fig. 5.7

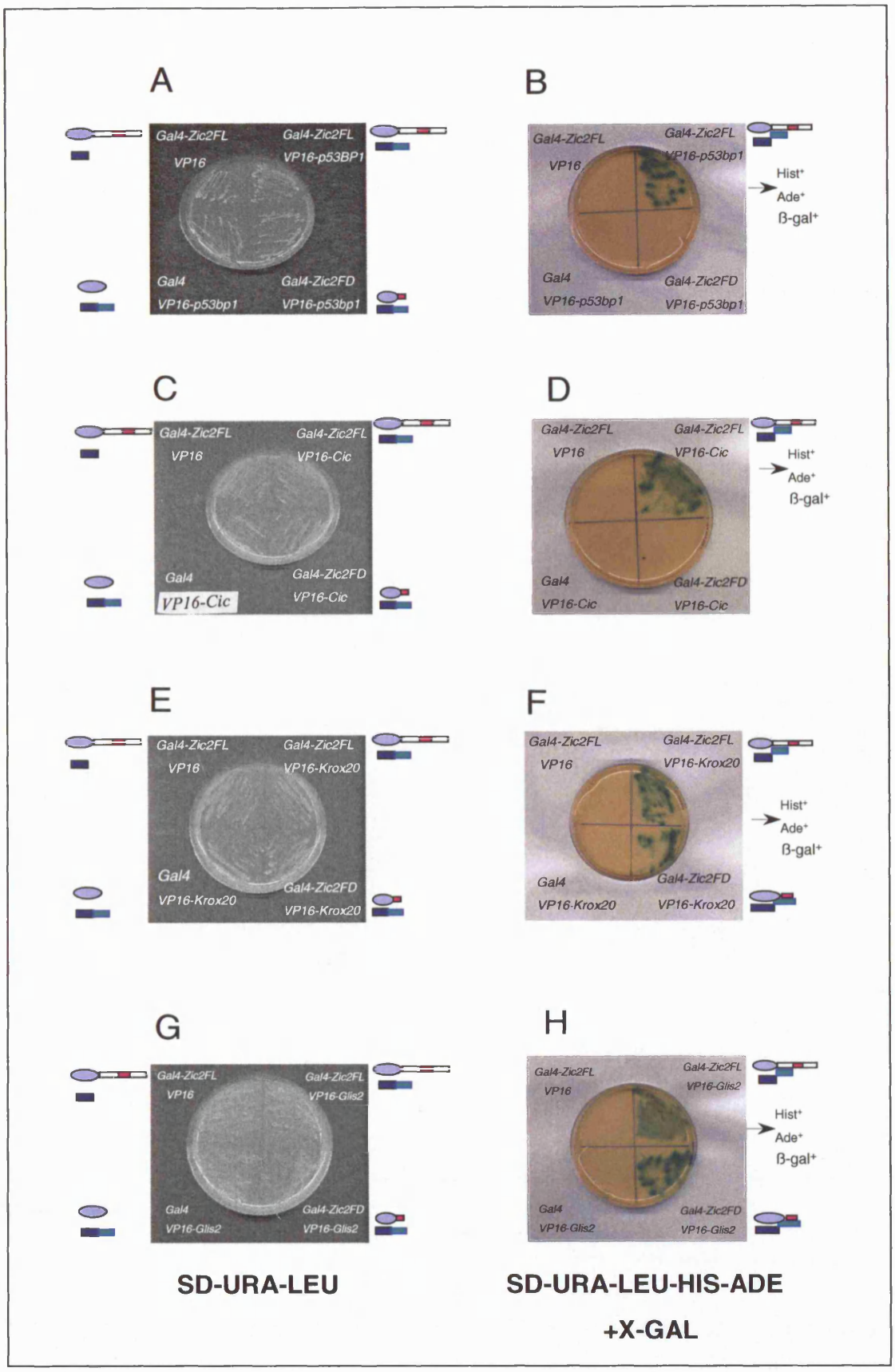
A
Gal4-Zic2FL
VP16
Gal4-Zic2FL
VP16-p53BP1
Gal4
VP16-p53bp1
Gal4-Zic2FD
VP16-p53bp1
B
Gal4-Zic2FL
VP16
Gal4-Zic2FL
VP16-p53bp1
Hist+
Ade+
ß-gal+
Gal4
VP16-p53bp1
Gal4-Zic2FD
VP16-p53bp1
C
Gal4-Zic2FL
VP16
Gal4-Zic2FL
VP16-Cic
Gal4
VP16-Cic
Gal4-Zic2FD
VP16-Cic
D
Gal4-Zic2FL
VP16
Gal4-Zic2FL
VP16-Cic
Hist+
Ade+
ß-gal+
Gal4
VP16-Cic
Gal4-Zic2FD
VP16-Cic
E
Gal4-Zic2FL
VP16
Gal4-Zic2FL
VP16-Krox20
Gal4
VP16-Krox20
Gal4-Zic2FD
VP16-Krox20
F
Gal4-Zic2FL
VP16
Gal4-Zic2FL
VP16-Krox20
Hist+
Ade+
ß-gal+
Gal4
VP16-Krox20
Gal4-Zic2FD
VP16-Krox20
G
Gal4-Zic2FL
VP16
Gal4-Zic2FL
VP16-Glis2
Gal4
VP16-Glis2
Gal4-Zic2FD
VP16-Glis2
H
Gal4-Zic2FL
VP16
Gal4-Zic2FL
VP16-Glis2
Hist+
Ade+
ß-gal+
Gal4
VP16-Glis2
Gal4-Zic2FD
VP16-Glis2
SD-URA-LEU
SD-URA-LEU-HIS-ADE
+X-GAL
Gal4-Zic2FD
Gal4-Zic2FD
VP16-cDNA library
VP16

Fig. 5.7 continued

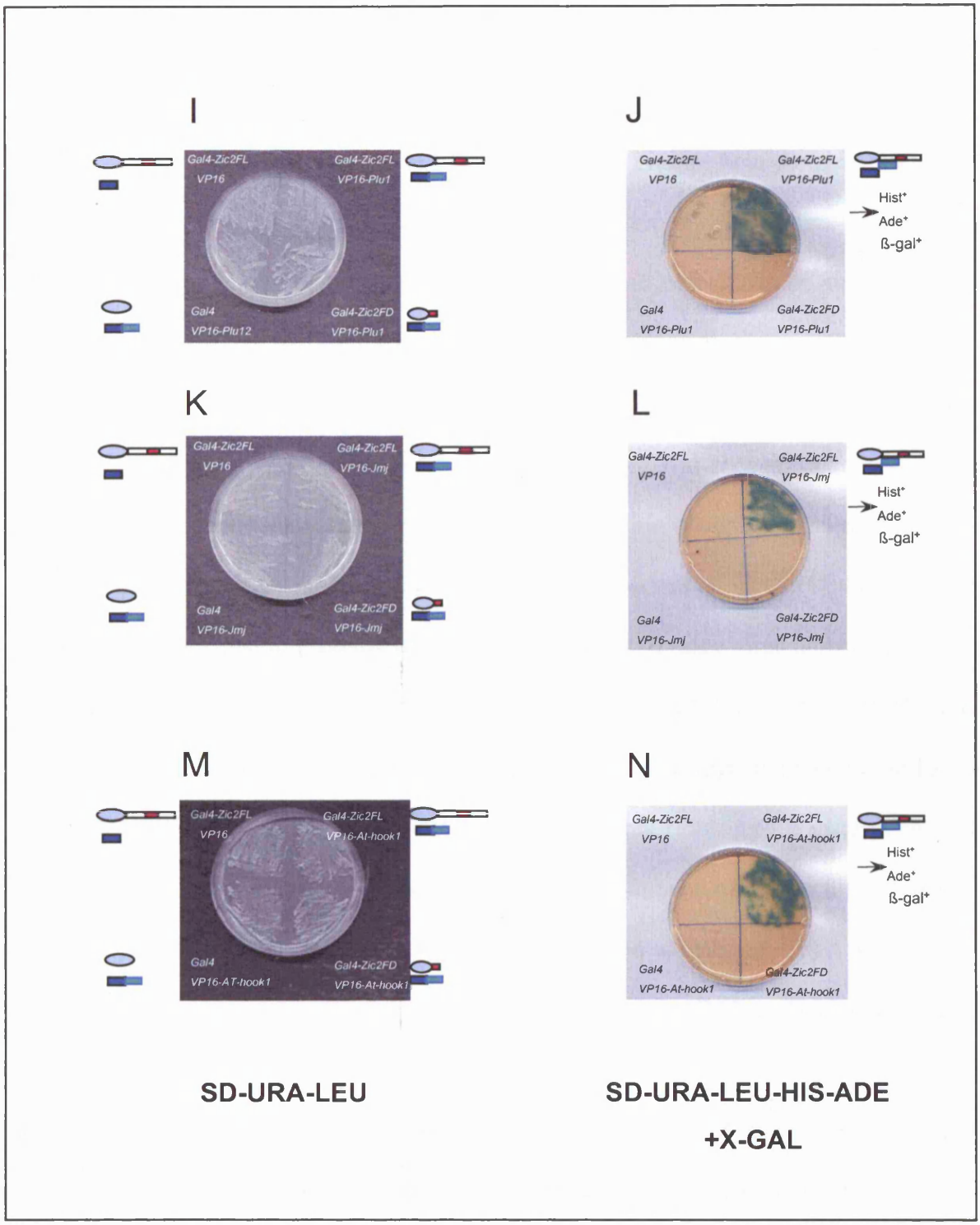

Gal4-Zic2FL

Gal4-Zic2FD

VP16-library cDNA

VP16

5.4 DISCUSSION

5.4.1 Yeast two-hybrid components used to identify Zic2 protein partners: why so many clones?

In the large scale screen to identify potential Zic2 protein partners, 800 clones were able to grow on the SD-adenine medium and were β-galactosidase positive. This represents a large number of positive interacting clones, which can be attributed to the components of the two-hybrids used in this chapter, such as the VP16 activation domain, the PJ69-4A yeast strain and the nature of the mouse embryonic cDNA library.

Firstly, the library used in the screening for Zic2 was chosen because it contains cDNAs from the neurulation stage mouse embryo, within which Zic2 interactions are of particular interest for the neurulation phenotype observed in $Zic2^{Ku/Ku}$. However, the library encodes fusion proteins with the VP16 herpes simplex virus activation domain, which is a very strong activator compared to the *E. coli* B42 (Gyuris *et al.*, 1993) and *S. cerevisiae* Gal4 (Brent *et al.*, 1997). This can lead to a large number of interacting clones since even a small affinity between bait and prey can trigger transcription of the selectable reporters. In those cases where large numbers of interacting clones are identified, one way to overcome the strong activation activity of VP16 is by using a library that contains a milder activation domain, such as B42 or Gal4 (Brent *et al.*, 1997).

Another possible explanation for the large number of interactions is that the VP16 mouse library contains 500 bp inserts that may encode domains that can interact with Zic2 even though the full length protein does not interact due to inaccessibility of that particular domain. This is probably true for clones identified in the screen such as the EGF-like extracellular domains of Notch1 and Notch3. One approach to address this issue is to screen two libraries in parallel, one containing the small fragments like the

VP16 mouse embryonic library and a second library containing large fragments of cDNA such as a Hela cell library (Gyuris *et al.*, 1993;Lorain *et al.*, 1998). In this case those clones identified in both screens are more likely to be true physiological interactors.

It is important to notice that each individual clone isolated from the large-scale screen appeared on average 3-4 times. Some clones had higher representation such as *p53bp1*, *fibulin1* or *Plu1* with 6 clones each. This could indicate a higher representation of that particular clone in the VP16 library, which can probably be attributed to the PCR amplification step used in the generation of the cDNA library. Those clones that are expressed at high levels will have more representation than those which are expressed at very low level or which expression is very restricted in the embryo.

5.4.2 Identification of false positives from the VP16 library screen

Clones obtained from the screen can be divided into potential Zic2 candidate partners or false positives. False positives are those interactions that, even though they can occur in a yeast two-hybrid system, would never occur in nature. This can arise from proteins that are not co-expressed, proteins that are not properly folded, "sticky" proteins and prey proteins that can auto-activate the selectable reporter.

The PJ69-4A yeast strain has three reporters that are integrated into the genome, *Gal1*, *Gal2* and *Gal7*. These reporters are different in sequence but all can be activated by Gal4. This reduces one type of false positive: preys that are able to auto-activate a selectable reporter without the presence of the bait protein. For instance, a prey protein could activate *Gal1* reporter alone, but it is less likely to have the potential to activate the *Gal2* and the *Gal7* reporters as the sequences vary from each other. Therefore, having 3 different reporters should reduce this type of prey auto-activation. However, it was found that the Gal4-Zic2FL and Gal4-Zic2FD fusion proteins had the ability to auto-activate the *Gal1-HIS3* selectable reporter, leaving only the *Gal2-ADE2* and the

Gal7-LacZ to be used as selectable reporters in the screen to identify Zic2 protein partners. Since it was not possible to use all three selectable reporters in the screening, an increased number of false positives were expected. One example of this type of false positive is VP16-Foxp4, which activated the selectable reporter in the absence of Gal4-Zic2, indicating that growth on the selective medium was not due to an interaction with Zic2.

5.4.3 Candidate Zic2 protein partners

In this chapter I have identified genes whose protein products are potential Zic2 interactors. In the yeast two-hybrid screen using a mouse embryonic VP16 cDNA-library, p53bp1, Glis2, Krox20, Capicua, Jumonji, Plu1 and At-hook1 were all able to interact with Zic2, and these interactions could be reproduced in co-transformation experiments.

In addition, I have shown that the region of Zic2 required for interaction with Glis2 and Krox20 maps to nucleotides 258-416 of Zic2. This region contains the five tandem repeats of the Cys_2-His_2 (C2H2) zinc finger domain (ZFD), indicating that Zic2 interacts with Krox2 and Glis2 through its finger domain region. The domain of Krox20 and Glis2 in the screen corresponded to the C2H2 ZFD motif (VP16-$Krox20_{(270\text{-}423AA)}$ and VP16-$Glis2_{(175\text{-}318AA)}$), which is similar in sequence to that of the Gli and Zic families of transcription factors. Therefore, the interaction of Zic2 with Krox20 and Glis2 appears to be mediated through the ZFD of both proteins, indicating that this domain is important not only for DNA binding but also for protein-protein interactions. It is notable, that a previous study has shown that Gli3 interacts with Zic1 through the 3^{rd}, 4^{th} and 5^{th} zinc fingers of the ZFD of Zic1 (Koyabu *et al.*, 2001a). Since Krox20 and Glis2 contain 3 and 5 tandem repeats of C2H2 zinc fingers respectively, closely related to the Gli and Zic family of transcription factors, one could hypothesise that the interaction could also be mediated through the 3^{rd}-5^{th} zinc fingers of Zic2. Interestingly,

the mutation responsible for the *Zic2*^{Ku} phenotype changes a cysteine to serine in the 4th zinc finger, presumably abolishing the function of this domain (Elms *et al.*, 2003). This mutation might affect the binding of Zic2 to Glis2 and Krox20. Indeed, Sun and co-workers have shown that mutations of the cysteines or histidines, that chelate the zinc ion in the transcription factor Ikaros ZFD, are sufficient to disrupt protein-protein interactions (Sun *et al.*, 1996).

5.4.3.1 Do interactions mediated through ZFD represent "true"-interactions?

Similarly to Glis2 and Krox20, the region of Plu1 and Jmj that interacted with Zic2 in the screen contains a ZFD. In these cases, however the ZFD of the Zic2 did not appear to be implicated in the interaction, as VP16-Plu1 and VP16-Jmj did not interact with the Gal4-Zic2FD. One could argue that the interactions observed between zinc finger domain-containing proteins and Zic2 are the result of non-specific interactions between such domains. However, in this case, Jmj and Plu1 would be expected to interact with the ZFD region of Zic2, but instead this interaction appears to occur through another domain of the Zic2 protein. Moreover, it has been shown that the interaction between ZFD of transcription factors is highly specific. For instance, the C2H2 ZFDs of Ikaros and Hunchback have been shown to form homodimers but fail to form heterodimers even though the C2H2 ZFD regions are highly similar (McCarty *et al.*, 2003). If interactions mediated through ZFD were non-specific, Ikaros would bind to Hunchback but in this particular case Ikaros interacts only with other Ikaros family members.

The ZFDs are among the commonest protein motifs in the mammalian proteome, with the C2H2 ZFD domain estimated to be present in around 5000 mammalian genes (Lander, 1996) (Venter *et al.*, 2001). If interactions between ZFDs were non-specific, a larger number of positive clones containing this domain would be expected. Although Zic2 was found to interact with the ZFD of several proteins,

interactions with different domains of other proteins were also detected. At-hook1 is a small transcription factor of only 107 amino acid residues. The clones obtained contained almost the full-length protein At-hook1 $_{(6\text{-}107)}$ including the HMG-box DNA binding domain that has been shown, in other proteins, to function in protein-protein interactions. For instance, this motif is required in the interaction between the HMG-box protein Sox10 and the Pax3 transcription factor (Lang and Epstein, 2003).

5.4.3.2 Two independent clones from Plu1 and Cic interact with Zic2

Proteins identified in the screen for which two independent clones were isolated were Plu1 and Cic (VP16-Plu1$_{(607\text{-}712)}$, VP16-Plu1$_{(692\text{-}745)}$, and VP16-Cic$_{(927\text{-}1100)}$ and VP16-Cic$_{(982\text{-}1100)}$). Therefore, the interaction of Plu1 and Cic with Zic2 is not only reproducible but can occur independently using partially overlapping sequences. This gives importance to the putative Cic-Zic2 and Plu1-Zic2 interaction as two different VP16-Cic and VP16-Plu1 fusion proteins show interaction with Zic2.

5.4.4 Other candidate proteins not analysed in this chapter

In this chapter other possible Zic2-interacting were identified proteins that do not fall into the category of false positives. These proteins, CCR4, LEK1, TCF20, Ncor2, and Suppressor of Variegation could be potential Zic2 interactors as they encode transcription factors. CCR4, LEK1, Ncor2 have been shown to have a role in transcriptional regulation (Liu *et al.*, 1998;Denis *et al.*, 2001; Goodwin *et al.*, 1999), whereas the functions of TCF20 and suppressor of Variegation are unknown (Rajadhyaksha *et al.*, 1998). All five clones showed only moderate β-galactosidase activity compared to p53bp1, Glis2, Krox20, Capicua, Jumonji, Plu1 and At-hook1, and therefore, were not considered for further analysis. However, their possible physiological importance as Zic2 interactors cannot be excluded. A moderate β-galactosidase activity could indicate a weak interaction that is still functionally

important. The next chapter aims to analyse biochemically some of the putative interactions identified in the yeast two-hybrid screen.

CHAPTER 6: ANALYSIS OF CANDIDATE ZIC2 INTERACTING PROTEINS

6.1 INTRODUCTION

The yeast two-hybrid system used in the previous chapter represents a genetic tool to identify protein interactions *in vivo*. However, the system does not represent a physiological situation. The yeast two-hybrid is a transcription-based system that requires localisation of both interacting proteins to the nucleus; this is accomplished by insertion of nuclear localisation signals into the expression plasmids. This could lead to localisation of two proteins in the nucleus, which would never be localised to the nucleus in a physiological situation. Therefore, if an observed interaction is physiologically relevant, bait and prey proteins should be found to be co-expressed in a tissue-specific and subcellular manner.

A further possibility is that protein interactions identified in the yeast two-hybrid system are mediated through an endogenous yeast protein that functions as a bridge, linking both prey and bait. Therefore, a direct protein interaction between Zic2 and potential candidate interacting proteins needs to be demonstrated.

In this chapter, these queries will be addressed by expression analysis of Zic2 interacting proteins in the neurulation stage mouse embryo, co-immunolocalisation of Zic2 and candidate interacting proteins in 293T cells and glutathione-S-transferase pull-down assays.

6.1.1 Candidate Zic2 interacting proteins analysed in this chapter

Plu1, Jumonji and At-hook1 represent putative Zic2 interacting proteins, and thereby, might regulate Zic2 function. However they were not further analysed in this thesis for time reasons. Capicua, Glis2, Krox20 and p53bp1 identified from the yeast two-hybrid screen were selected for expression and biochemical analysis. Schematic representation and putative regions of interaction with Zic2 are shown in Figure 6.1.

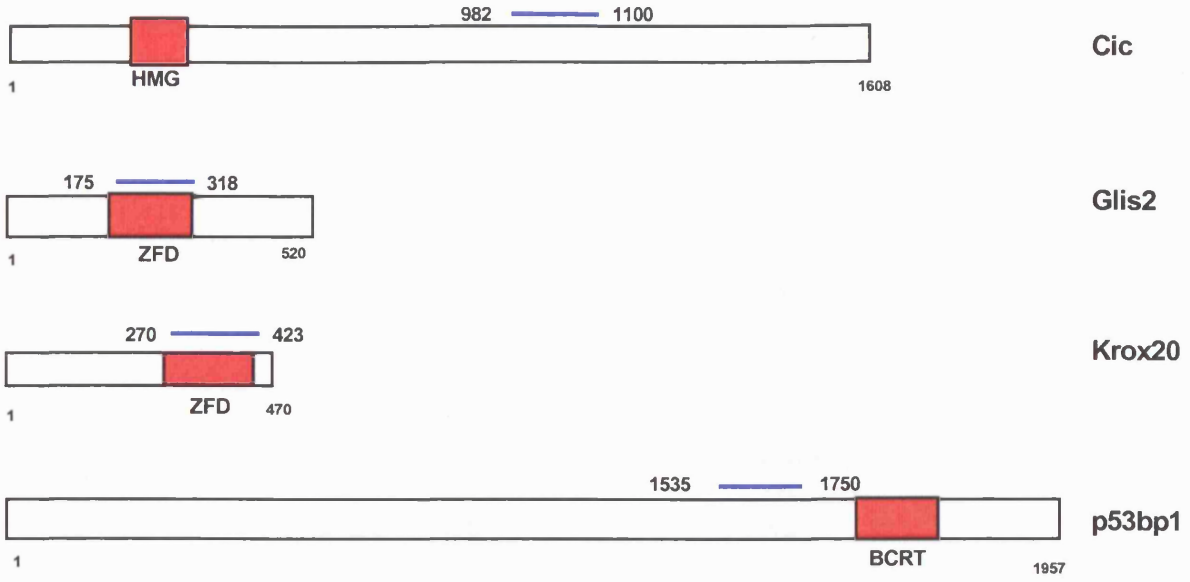

Figure 6.1 Schematic representation of $Cic_{(1-1608)}$, $Glis2_{(1-520)}$, $Krox20_{(1-470)}$ and $p53bp1_{(1-1957)}$ proteins

The blue line represents the region of interaction identified in the yeast two-hybrid screen (Chapter 5). Red boxes represent: in Cic the HMG box DNA binding domain; in Glis2 and Krox20, the ZFD which consists of five and three tandem repeats of C2H2 ZFD respectively; in p53bp1 the BRCT domain involved in the interaction with the p53 protein. Note that the region of interaction of Glis2 and Krox20 identified in the yeast two-hybrid screen corresponds to the zinc finger domain region.

6.1.1.1 Capicua, Cic

Capicua, Cic, encodes a protein of 164 kilo Daltons (kD), which is known to be an HMG-box (high mobility group box) transcription factor. Cic is located on mouse chromosome 7, spanning 4820 bp, and contains 20 exons. The region of putative interaction between Cic and Zic2 identified in the yeast two-hybrid screen was between amino acids 982-1100 of Cic. This region lies outside the HMG box DNA binding domain. Cic was first identified in Drosophila melanogaster in a transposon P-element

screen for mutations affecting anterior-posterior and dorso-ventral patterning of the embryo (Jimenez *et al.*, 2000). Embryos homozygous for the cic mutation failed to develop a segmented trunk whilst developing head and tail structures. In Drosophila Cic has been shown to function as a transcriptional repressor downstream of torso (Tor), a receptor tyrosine kinase (TRK). Cic interacts with the co-repressor Groucho (Gro) (Jimenez *et al.*, 2000).

The embryonic expression of mouse Cic has not been reported. At postnatal stages, Cic is expressed in the CNS, specifically in the granule cell neurons of the cerebellum, hippocampus and olfactory bulb (Lee *et al.*, 2002).

6.1.1.2 Glis2

Glis2 (Gli-similar 2), also named *NKL,* encodes a Kruppel-like zinc finger transcription factor that contains five tandem repeats of the C2H2 ZFD homologous to the Gli and Zic family of transcription factors (Zhang and Jetten, 2001;Zhang *et al.*, 2002). *Glis2* is composed of six exons and five introns, maps to mouse chromosome 16 and encodes a 55 kD protein. The region of Glis2 required for interaction with Zic2 encompassed the ZFD region from amino acids 175 to 318. *Glis2* has been shown to be expressed in the neural tube, caudal somites, forebrain and limbs (Lamar *et al.*, 2001;Zhang *et al.*, 2002). The role of *Glis2* during mouse development remains unknown and a null allele for *Glis2* has not yet been described.

Glis2 was identified in two independent studies in different animal systems. The first study identified Glis2 in a yeast two-hybrid system to identify proteins that can interact with Pax3, although subsequent studies failed to show a physiological interaction (Lamar *et al.*, 2001). In a second study *Glis2* was identified in a kidney cDNA library screen for genes that are homologous to *Glis1*. So far three members of the Glis family of transcription factors have been identified, *Glis1-Glis3*. The function of *Glis2* has been studied in chick and frog, where ectopic expression promotes

neurogenesis as shown by an increase in N-tubulin positive cells (Lamar *et al.*, 2001). Interestingly, Glis2 and the other two members, Glis1 and Glis3, have been shown to bind to the DNA Gli binding sequences (Gli-BS) in electro-mobility shift assay (EMSA) experiments (Kim *et al.*, 2003). Likewise, Zic family members have also been shown to be able to bind to Gli-BS (Mizugishi *et al.*, 2001a), indicating that these transcription factors can bind to similar promoter regions.

6.1.1.3 Krox20

Krox20/EGR2 encodes a zinc finger transcription factor that contains three tandem repeats of C2H2 ZFD. *Krox20* was initially isolated as an immediate serum response gene (Chavrier *et al.*, 1988), and was subsequently found to be expressed in a restricted fashion in rhombomeres 3 and 5 (r3/r5) during segmental patterning of the hindbrain (Wilkinson *et al.*, 1989). Targeted disruption revealed that Krox20 is required for specifying r3/r5 identity (Schneider-Maunoury *et al.*, 1993) (Swiatek and Gridley, 1993). Further molecular studies have shown that Krox20 directly regulates the expression of the *Hoxa-2*, *Hoxb2* and *Eph4* genes, highlighting its importance in the specification of r3/r5 identity (Sham *et al.*, 1993) (Theil *et al.*, 1998).

In addition to regulating hindbrain segmentation, *Krox20* has also been shown to have other roles during mammalian development. *Krox20* null mouse embryos display severely defective myelination of peripheral nerves (Topilko *et al.*, 1994). This phenotype also occurs in humans that harbour mutations in *Krox20*, resulting in peripheral neuropathies (Warner *et al.*, 1998;Bellone *et al.*, 1999). Further analysis of *Krox20* homozygous mutant embryos has revealed defects in endochondral ossification and bone formation suggesting that *Krox20* normally has a role in this process (Levi *et al.*, 1996). *Krox20* is a marker for boundary cap cells which are neural crest derived cells that cluster in the spinal nerve entry and exit points (Wilkinson *et al.*, 1989). However *Krox20* null mice do not show a boundary cap cell phenotype (Schneider-

Maunoury *et al.*, 1993;Topilko *et al.*, 1994). The Krox20 protein contains 470 amino acids and the region of interaction with Zic2 in this study corresponds to the ZFD between amino acids 270-423.

6.1.1.4 p53 binding protein 1

p53 binding protein 1 is a member of the BRCA1 carboxy terminal (BRCT) repeat family (Bork *et al.*, 1997). This family includes the BRCA1 and BARD1 proteins, mutations in which have been associated with breast and ovarian cancer respectively (Scully and Livingston, 2000). p53bp1 was identified in a yeast two-hybrid screen to find proteins that interact with the p53 tumour-suppressor protein (Franzén *et al.*, 1991) and was subsequently shown to function as a transcriptional activator of p53. The role of p53bp1 in DNA damage response after irradiation has been focus of several studies (Abraham, 2002). After DNA damage, p53bp1 is activated by phosphorylation and binds to p53 that in turn activates transcription of genes required for cell cycle arrest and p53-mediated apoptosis. The role of p53bp1 in tumorigenesis has been shown *in vivo* by targeted disruption of *p53bp1* in mouse. *p53bp1* null mice are viable, immune deficient and cancer prone but do not exhibit NTDs (Ward *et al.*, 2003). The putative region of interaction of p53bp1 with Zic2 encompasses amino acids 1535 to 1750, a region that lies next to the BCRT domain known to interact with p53.

6.2 METHODS

6.2.1 Generation of *Cic* and *p53bp1* mRNA riboprobes

Primers were designed to specifically amplify *Cic* and *p53bp1* cDNA regions by PCR. Table 6.1 shows the PCR conditions and Table 6.2 shows the primer sequences, cDNA region, and method for generating sense and antisense probes. PCR products were gel purified and cloned into a pGEM-T vector.

Table 6.1 The PCR conditions to amplify *Cic* and *p53bp1* cDNA

	Cic	*p53bp1*
$MgCl_2$	1.5 mM	1.0 mM
Annealing temp and number of cycles	58 C 25 cycles	61 C 25 cycles

Table 6.2 Primers designed to generate *Cic* and *p53bp1* probes

Probe	Primer sequence	NCBI accession number	Amplified region	Sense and antisense
p53bp1	F 5'AGAATGCCAGCTTCGAGCAGG 3' R 5'ATACCACAGGCAGTTGCAAGG 3'	MMU414734	500 bp From 5291-5791*	NotI (sense) T7polymerase; ApaI (antisense) Sp6 polymerase
Cic	F 5' TTCCAGTTCGGCGCGGAATGT 3' R 5' ATCTCGGTCATTGCGGCTTCTC 3'	AF363690	442 bp From 4988-5430*	NotI (sense) T7polymerase; ApaI (antisense) Sp6 polymerase

*Note that the base number corresponds only to the Genbank accession numbers given.

6.2.2 Plasmids used to generate constructs

Due to the lack of available antibodies to the native proteins, Zic2, Krox20, Glis2, Cic and p53bp1 were epitope-tagged using either pcDNA-flag or pcDNA-myc vectors (Invitrogen) in order to be able to co-immunolocalise Zic2 with the candidate interacting proteins. The vector was modified to contain the flag or myc epitope inserted into a KpnI-BamHI site.

6.2.3 Cloning and generation of flag and myc epitope tag proteins

To generate flag-Zic2, the Gal4-Zic2FL construct (section 5.2.1) was digested with EcoRI and SalI restriction enzymes to release Zic2 full-length cDNA and the fragment was gel purified. The Zic2 cDNA fragment was cloned into the EcoRI and XhoI sites of the pcDNA3.1-flag plasmid.

The full length myc-Cic, myc-$Cic_{598\text{-}1608}$ and the empty pcDNA3.1-myc vector were gifts from Dr. Paul Scotting, Children's Brain Tumour Research Centre, Institute of Genetics, University of Nottingham, Queen's Medical Centre. The pcDNA3.1 vector was modified by insertion of the myc cassette into a KpnI and BamHI site.

To generate myc-tagged Glis2, Krox20 and p53bp1, primers were designed to contain the restriction site required for cloning and amplify Glis2, Krox20 and P53bp1 cDNAs by PCR (see Table 6.3 for PCR conditions and Table 6.4 for primers and restriction sites used for cloning). The amplified cDNAs and pcDNA3.1 myc plasmid were restriction enzyme digested with the appropriate enzymes and ligated to generate the myc-tagged proteins.

A myc-$Calmin_{(1\text{-}455)}$ construct was used as a negative control in the GST pull-down assay and was provided by Dr. Annia Koziell, Molecular Medicine Unit, Institute of Child Health , UCL. The HA-$Gli1_{(241\text{-}781)}$ construct was used as a positive control in the GST pull-down assay and was provided by Dr. Fujita, Laboratory for Molecular Cell Biology , UCL.

6.2.4 Cloning and generation of constructs used in GST pull-down assays

To generate fusion proteins between Zic2 and glutathione S-transferase (GST), the Zic2FL cDNA was cloned into an EcoRI-SalI site of the pGEX-4T plasmid (Amershambiosciences). The GST-Krox20 construct was kindly donated by Dr. Patrick Charnay, Laboratoire de Biologie Moleculaire du Developpement, INSERM, Ecole Normale Superieure, Paris.

Table 6.3 PCR conditions to amplify *Glis2*, *Krox20* and *p53bp1* to generate myc epitope tagged proteins

	Glis2	Krox20	P53bp1
$MgCl_2$	1.5 mM	1.5 mM	1.0 mM
Annealing temp and number of cycles	58 °C 25 cycles	55 °C 25 cycles	61 °C 25 cycles

Table 6.4 Primers designed to generate myc-Glis2, myc-Krox20, myc-p53bp1

Construct	Primer sequence	Genbank accession number	Amplified region (bp)
Glis2	F 5'-GACGCGGCCGCTGCACTCCTTGGACGAGCCCCT-3' NotI R 5'-GCGCTCGAGTCAGTTTACCACAGCTGGTTTG-3' XhoI	AF325913	1565 bp (from 25-1590)
Krox20	F 5'-GGCGAATTCATGAACGGAGTGGCGGGAGATGG3' EcoRI R 5'GGCCTCGAGTCAGTGTTCCTGGTTCGAGAGGTG3' XhoI	D70848	1262 bp (from 393-1655)
p53bp1	F 5'-GGCGGATCCAGAATGCCAGCTTCGAGCAG-3' BamHI F 5'-GGCCTCGAGTCAATACCACAGGCAGTTGC-3' XhoI	MMU414734	500 bp (from 5291-5791)

Sequences in blue correspond to the restriction enzyme sites used for cloning.

Table 6.5 Primers used in the sequencing of the constructs

Primer name	Primer sequence
Glis2F1	5'-CCTTGGACGAGCCCCTCGACC- 3'
Glis2F2	5'-CTGAGAAGGTGGACGGACGC- 3'
Glis2F3	5'-CTCATTCACATCCGGACACACA- 3'
Glis2F4	5'- GACAGTGGCTCCTATGTCAG- 3'
Glis2R1	5'-GCCCAGCTCTCGATGCAAAGC- 3'
Glis2R2	5'-ATAGCGAAGTGGCTGGAAATCC- 3'
Glis2R3	5'-CTTCTCACCTGTGTGGGAGCG- 3'
Glis2R4	5'-GGCAGAACAGCCTGGCAGC- 3'
Glis2R5	5'-CACAGCTGGTTTGAGCAGCAC- 3'
Krox20F1	5'-GGAGAGAAGAGACCCTGGATCT- 3'
Krox20F2	5'-CGAAAGCCGTTTCCCTGTCCTCT- 3'
Krox20F3	5'-CCACACAAGCCCTTCCAGTGTC- 3'
Krox20R1	5'-AGGGGTGACCCCTTGCAAGA- 3'
Krox20R2	5'-GGCAGGTGGTGCGGATTATA- 3'
Krox20R3	5'-GTGTCCTGGTTCGAGAGGTGC- 3'
p53bp1F1	5'-TATCCTTGAAGACTTCAATG- 3'
p53bp1R1	5'-CTTGAATGGTGCTGCTTCAC- 3'

6.3 RESULTS

6.3.1 Co-expression of *Zic2* with *p53bp1* and *Cic*

To determine whether the candidate Zic2 interacting proteins identified in the yeast two-hybrid system were co-expressed with Zic2, whole mount *in situ* hybridisation was performed for those genes whose pattern of expression had not been reported previously. Expression of *Cic* and *p53bp1* was found to be widespread throughout the E8.5-9.5 neurulation-stage embryo. Both genes were expressed in the forebrain, hindbrain and spinal neural tube (Fig. 6.3 A, D and B, E respectively), with expression of *p53bp1* being more intense and widespread than *Cic*. Compared with the generalised expression patterns of *Cic* and *p53bp1, Zic2* is expressed in quite specific domains (Fig. 6.3 C, F) in the brain, dorsal spinal cord and somites. *Zic2* expression overlapped with *Cic* and *p53bp1* in the forebrain, hindbrain and upper spinal neural tube, at the level of the heart. In the PNP region, *Cic* was not expressed at E8.5 (Fig. 6.3 A), but expression became visible at E9.5 (Fig. 6.3 D). Towards the stage of PNP closure *p53bp1* was already expressed in the PNP at E8.5 (Fig. 6.3 B) and this expression continued at E 9.5 (Fig. 6.3 E). Therefore, *Cic* and *p53bp1* have overlapping expression patterns during neurulation and are co-expressed with *Zic2,* particularly in the PNP region.

Glis2 has been shown to be expressed in the forebrain, dorsal neural tube and limbs (Lamar *et al.*, 2001;Zhang *et al.*, 2001) which overlaps with the expression pattern of *Zic2* reported in Chapter 3 and Fig. 6.3 C and F. Similarly, *Krox20* has been shown to be expressed in the rhombomeres 3 and 5 of the hindbrain in the neurulation stage embryo (Wilkinson *et al.*, 1989), pattern that overlaps with *Zic2.* Hence, *Zic2* is co-expressed with *Glis2* and *Krox20* during neurulation.

Figure 6.3

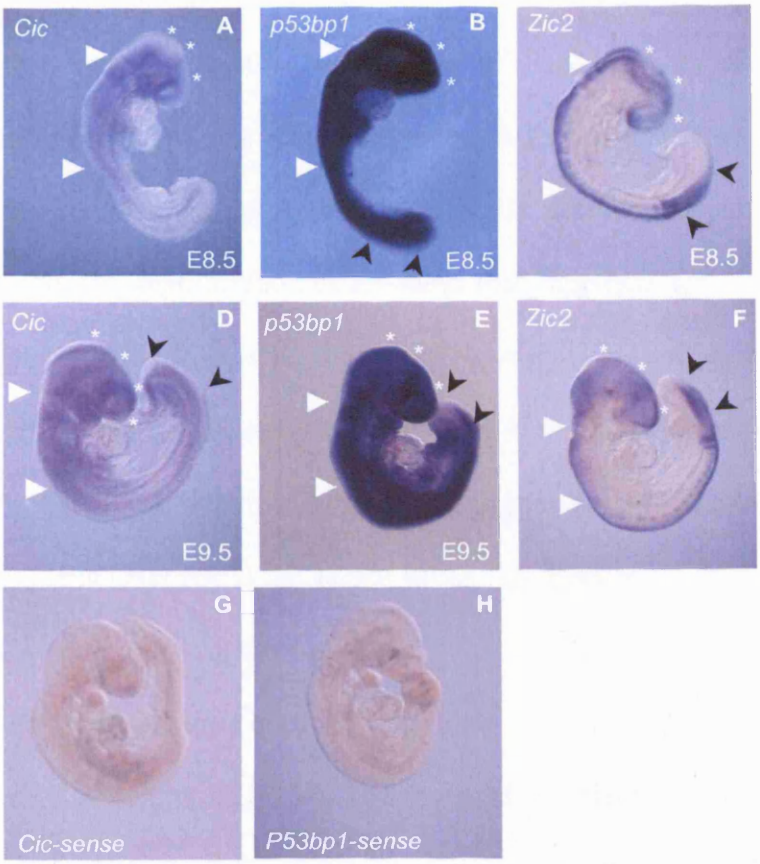

Figure 6.3 Localisation of *Cic* (A, D), *p53bp1* (B, E) and *Zic2* (C, F) mRNA by whole mount *in situ* hybridisation during neurulation stages (E8.5-9.5) in CD1 mouse embryos

Cic is expressed in the forebrain and midbrain (asterisks in A and B), hindbrain and upper spinal neural tube (white arrowheads in A and D). Expression also becomes apparent in the PNP at E9.5 (black arrowheads in D). *p53bp1* expression is stronger and more widespread than *Cic*, with all tissues except the heart showing mRNA transcripts. As described in Chapter 3, *Zic2* (C, F) is expressed in the forebrain and midbrain (white asterisks in C-F), in the hindbrain and spinal neural tube at the level of the heart (white arrowheads) and in the PNP region (black arrowheads). Therefore *Zic2* co-localises with *Cic* and *p51bp1*, although *Cic* and *p53bp1* are also expressed in *Zic2* negative areas . Sense probes for *Cic* and *p53bp1* (G and H respectively) did not give any specific signal.

6.3.2 Zic2 co-localises with p53bp1, Cic, Glis2 and Krox20 in 293T cells

To analyse the subcellular localisation of Zic2 and candidate interacting proteins, immunolocalisation was performed using flag or myc epitope-tagged proteins which were transiently co-expressed into 293T cells. Immunohistochemical analysis using anti-flag and anti-myc antibodies revealed that flag-Zic2 (green) and the myc-tagged interacting proteins (myc-Cic, myc-Krox20, myc-Glis2 and myc-p53bp1 (red)), all localise to the nucleus as confirmed by 4'-6-diamidino-2-phenylindole (DAPI) staining (see Fig. 6.4). DAPI forms fluorescent complexes with double stranded DNA and stains the nucleus (Fig. 6.4 D, H, L, P). When flag-Zic2 is co-expressed with myc-Cic, myc-Krox20, myc-Glis2 or myc-p53bp1 in the same cell (Fig. 6.4 A-D, E-H, I-L, M-P respectively), both proteins are localised to the nucleus, which can be seen in the merged image (Fig. 6.3 C, G, K, O white arrowheads). Therefore, Zic2 co-localises to the nucleus with Cic, Krox20, Glis2 and p53bp1 when expressed in 293T cells.

6.3.3 GSTpull-down assay to verify interactions found in the yeast two-hybrid screen

In order to examine whether the interaction observed in the yeast two-hybrid screen represented a direct interaction between Zic2 and Glis2, Krox20, Cic or p53bp1, the glutathione-s-transferase pull-down assay was performed. In this assay, candidate proteins generated by *in vitro* transcription/translation, are tested for the ability to bind directly to the GST-fusion protein, which is immobilised on glutathione sepharose beads.

6.3.3.1 Purification of GST-Zic2 fusion protein and GST

To obtain the GST and GST-Zic2 fusion proteins, pGEX and pGEX-Zic2 plasmids were transformed into BL21 cells. Protein induction was achieved by addition of IPTG to a final concentration of 0.1 mM to the BL21 cell culture.

Figure 6.4

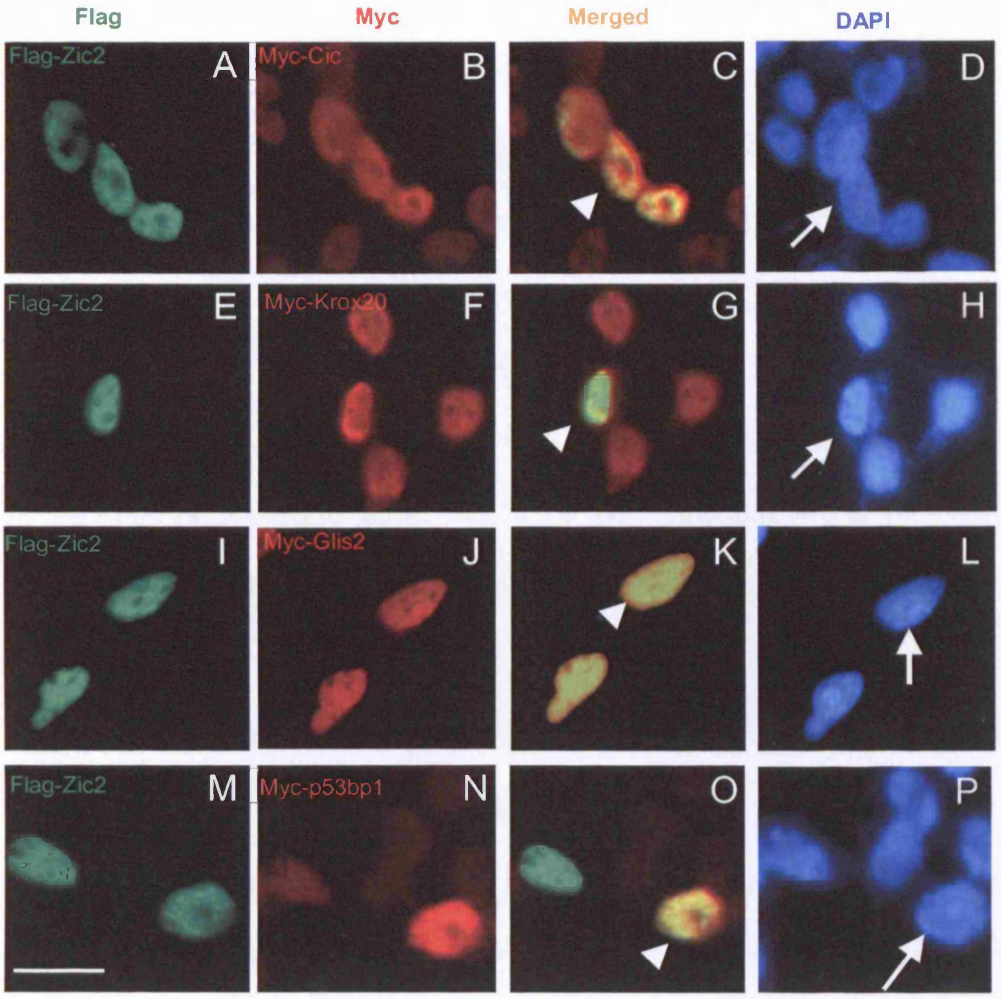

Figure 6.4 Co-immunolocalisation of Zic2 with Cic, Krox20, Glis2 and p53bp1

293T cells were co-transfected with flag-Zic2 (green; A, E, I, M) and either myc-Cic (B), myc-Krox20 (F), myc-Glis2 (J) or myc-p53bp1 (N) (red). White arrow-heads in merged images indicate that Zic2 co-localises to the nucleus with Cic (C), Krox20 (G), Glis2 (K) and p53bp1 (O) as compared to the DAPI staining of the same field (white arrows in D, H, L, P). Scale bar in M represents 20 μm.

Two problems can arise when expressing proteins in bacteria. First, the induction of protein expression by addition of IPTG may not be successful. Second, the induced bacterial expressed protein may be insoluble and therefore cannot be bound to the glutathione sepharose beads. To verify that the induction of the protein was successful, an aliquot of the BL21-pGEX-Zic2 culture prior to (uninduced fraction) and following IPTG induction (induced fraction) were subject to SDS-PAGE and the proteins were stained with Coomassie Blue (see Fig. 6.5 A lane U for uninduced and I for induced fractions). A band of 80 kD corresponding to the GST-Zic2 fusion protein was seen in the induced fraction but was absent from the uninduced fraction. To check if GST-Zic2 was insoluble, pellets from the purification step (see section 2.6.1) were electrophoresed to visualise the presence of the GST-Zic2 protein (see Fig. 6.5 lanes P1 and P2 insoluble fractions). The GST-Zic2 fusion protein was present in both the insoluble and the soluble fractions (supernatant, S, in Fig. 6.5). The supernatant was incubated with glutathinone sepharose beads in order to immobilise GST-Zic2 on the beads and, after incubation, a sample was electrophoresed (see Fig. 6.5. 7^{th} lane, bead capture GST-Zic2). The GST-Zic2 fusion protein could be seen as a band of 80 kD confirming that GST-Zic2 had bound to the sepharose beads.

To obtain GST bound to sepharose beads the same procedure was followed and an aliquot was electrophoresed to check for the presence of the GST protein, which has a molecular weight of 25 kD (Fig. 6.5, 8^{th} lane, bead capture GST). This experiment showed that GST could be immobilised on the glutathione sepharose beads after incubation.

Figure 6.5 Purification of GST and GST-Zic2 fusion protein and *in vitro* translation of proteins used in GST pull-down assays

(A) SDS-PAGE gel stained with Coomassie Blue to show relative amounts of the IPTG-induced GST-Zic2 fusion protein and capture of the GST-Zic2 fusion protein by glutathione-sepharose beads. Lane M corresponds to the protein marker; U: uninduced BL21 cell culture; I: IPTG-inducted BL21 cell culture; P1: first pellet corresponding to the first insoluble fraction; P2: second pellet corresponding to the second insoluble fraction, S: supernatant corresponding to the soluble fraction. Gutathione sepharose bead capture of the GST-Zic2 fusion protein can be seen as a band of 80 kD (arrow). Right hand lane corresponds to the glutathione sepharose bead capture of the GST protein that yields a band of 25 kD, the expected size of GST. (B) Auto-radiographic exposure of [^{35}S]-methionine labeled Gli1 (61 kD), Zic2 (55 kD), Glis2 (54 kD), Krox20 (50 kD), Cic (163 kD), Calmin (41 kD), and p53bp1 (30 kD), generated by in *vitro* translation.

Figure 6.5

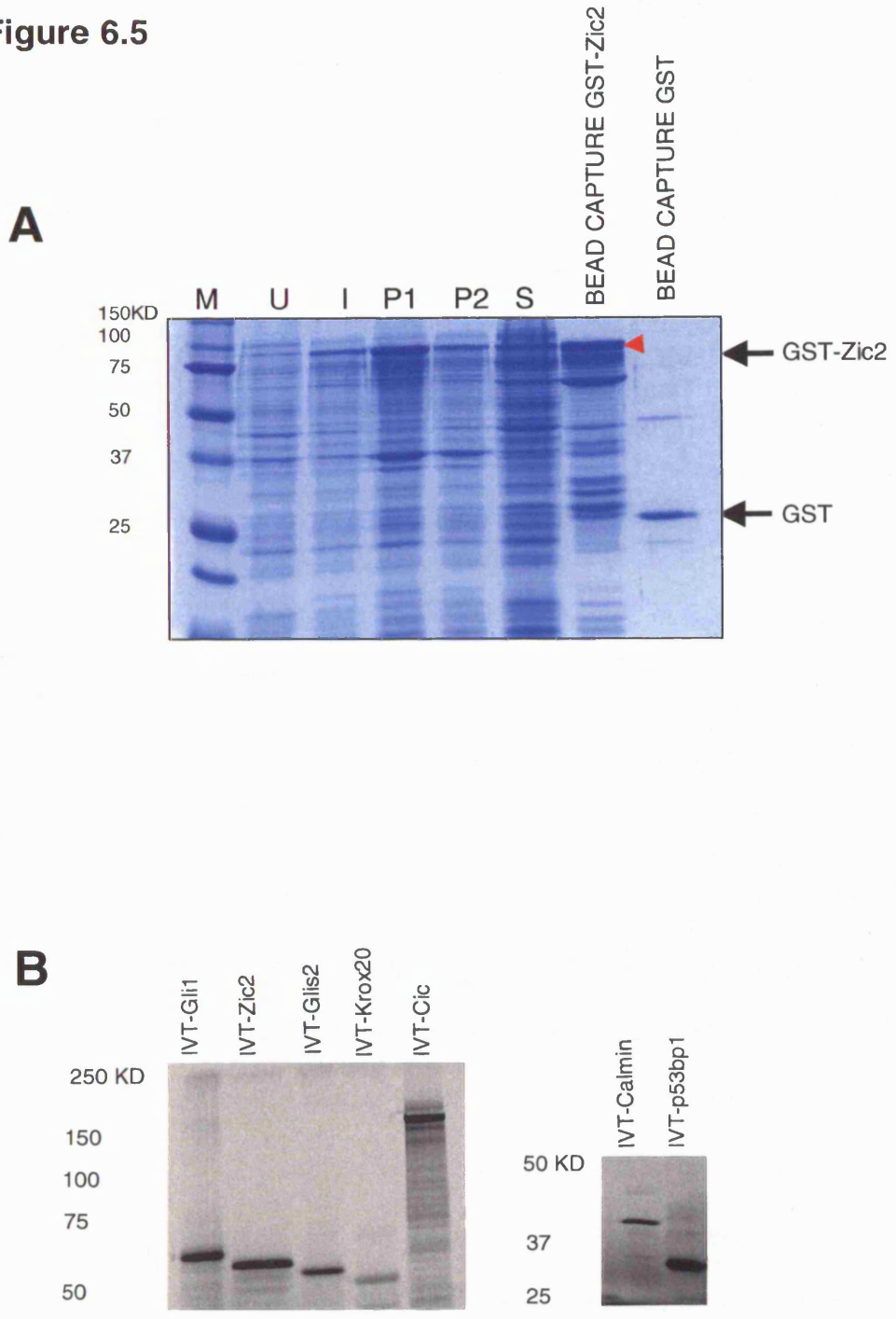
A
M
U
I
P1
P2
S
BEAD CAPTURE GST-Zic2
BEAD CAPTURE GST
150KD
100
75
50
37
25
GST-Zic2
GST
B
IVT-Gli1
IVT-Zic2
IVT-Glis2
IVT-Krox20
IVT-Cic
250 KD
150
100
75
50
IVT-Calmin
IVT-p53bp1
50 KD
37
25

6.3.3.2 *In vitro* transcription/translation of candidate interacting proteins

To generate [^{35}S]-methionine labelled candidate interacting proteins, flag-Zic2, myc-Cic$_{(598\text{-}1608)}$, myc-p53bp1$_{(1535\text{-}1750)}$, myc-Krox20, myc-Glis2, myc-Calmin$_{(1\text{-}361)}$ and HA-Gli1$_{(241\text{-}781)}$ were used in the *in vitro* transcription/translation (IVT) reactions. After IVT, the candidate proteins were resolved on 10% SDS-PAGE gels and the [^{35}S]-methionine labelled proteins were visualised by overnight exposure to autoradiography film. Gli1$_{(241\text{-}781)}$, Zic2, Glis2, Krox20, Cic$_{(598\text{-}1608)}$, Calmin$_{(1\text{-}361)}$ and p53bp1$_{(1535\text{-}1750)}$ proteins were successfully *in vitro* translated and radioactively labelled, migrating to the expected position on SDS-PAGE gels (Fig. 6.5 B).

6.3.3.3 GST-Zic2 co-precipitates with Gli1, Glis2, Krox20, Cic and p53bp1

IVT-Glis2, IVT-Krox20, IVT-Cic and IVT-p53bp1 were tested for their ability to co-precipitate with either the GST or GST-Zic2FL fusion proteins bound to sepharose beads (Fig 6.6 A and B). A known Zic2 interacting protein, Gli1, was used as a positive control in the pull-down assay. *In vitro* translated Gli1 interacted directly with GST-Zic2 as shown by its ability to co-precipitate with GST-Zic2 bound to beads but not with GST alone. *In vitro* translated Glis2, Krox20, Cic and p53bp1 were also able to precipitate with GST-Zic2 bound to beads but not with the GST alone, indicating that these proteins directly interact with Zic2 like Gli1. To test whether the co-precipitation of proteins with Zic2 was non-specific, or might have occurred through an interaction between the myc tag and Zic2, myc-Calmin$_{(1\text{-}361)}$ was used as a negative control in the pull-down assays. Calmin is a novel transmembrane protein that is expressed in testis and kidney during mouse development. Calmin has two calponin homology (CH) intracellular domain, shared with proteins such as α-actinin, β-spectrin and dystrophin and is thought to bind to cytoskeleton components (Ishisaki *et al.*, 2001). Therefore, calmin was predicted to be highly unlikely to interact with Zic2. *In vitro* translated myc-

Calmin$_{(1-361)}$ was incubated with GST-Zic2 or GST bound to beads and no interactions were detected. These data suggest that the myc tag is not responsible for the observed interactions of Zic2 with myc-Glis2, myc-Krox20, myc-Cic and myc-p53bp1. In all the pull-down experiments a tenth of the volume of the IVT generated protein was loaded on the SDS-PAGE gel to be able to compare with the amount pulled down by the GST-Zic2 (see Fig. 6.6 INPUT 10 % lane in A and B). The intensity of the bands generated by binding to GST-Zic2 were approximately the same as the 10% input, suggesting that around one tenth of the total [^{35}S]-methionine labelled protein had been immobilised on the GST-Zic2-sepharose beads.

Figure 6.6 Interaction between Zic2 and *in vitro* radioactively labelled Gli1, Glis2, Krox20, Cic and p53bp1 proteins

(A) [^{35}S]-methionine labelled Gli1, Glis2, Krox20, and (B) [^{35}S]-methionine labeled Cic, Calmin and p53bp1 were tested for interaction with GST or GST-Zic2 immobilised on glutathione-agarose beads. The top gel image in A and B represents the autoradiographic detection of the [^{35}S]-methionine labeled proteins after SDS-PAGE and the lower image is the same gel stained with Coomassie Blue. A tenth of the amount of the labelled proteins used in the experiment was loaded as a control (input 10%) for each protein. Glis2, Krox20, Cic and p53bp1 were bound by the GST-Zic2 fusion protein (band in lanes 6 and 9 in A and lanes 3 and 9 in B) but not by GST alone (lanes 2, 5 and 8 in both A and B). Gli1 was used as a positive control since it has been shown to interact with Zic2 and it bound to GST-Zic2 (lane 3 in A). Calmin was used as a negative control since this protein has not been functionally associated nor is it co-expressed with Zic2. Calmin did not bind to either GST or GST-Zic2 (lanes 5 and 6 in B).

Figure 6.6

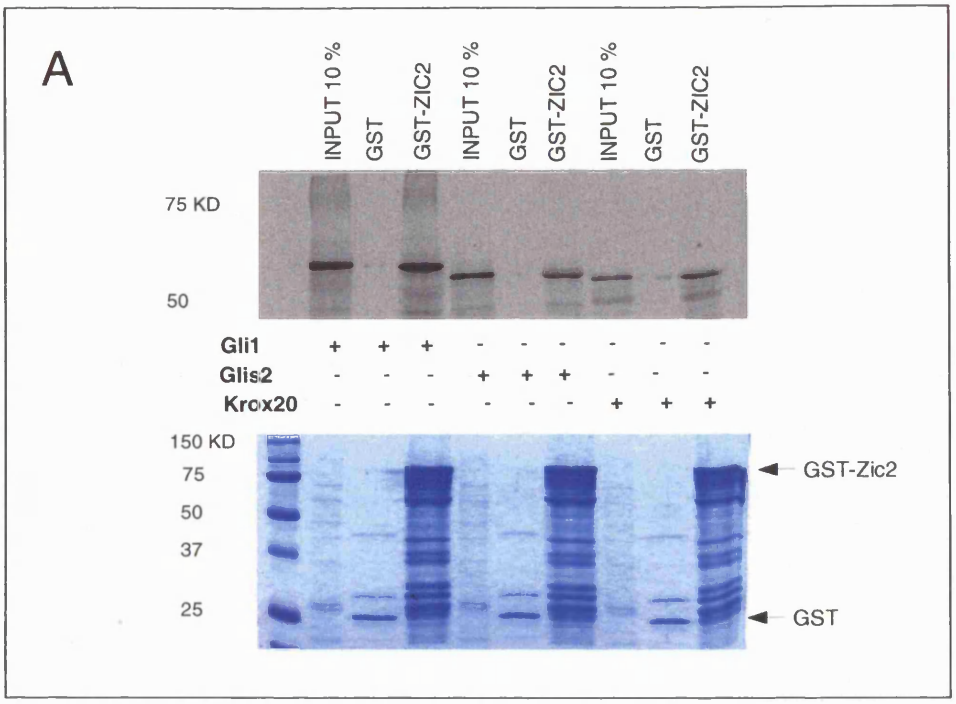
A
INPUT 10 %
GST
GST-ZIC2
INPUT 10 %
GST
GST-ZIC2
INPUT 10 %
GST
GST-ZIC2
75 KD
50
Gli1 + + + - - - - - -
Glis2 - - - + + + - - -
Krox20 - - - - - - + + +
150 KD
75
50
37
25
GST-Zic2
GST

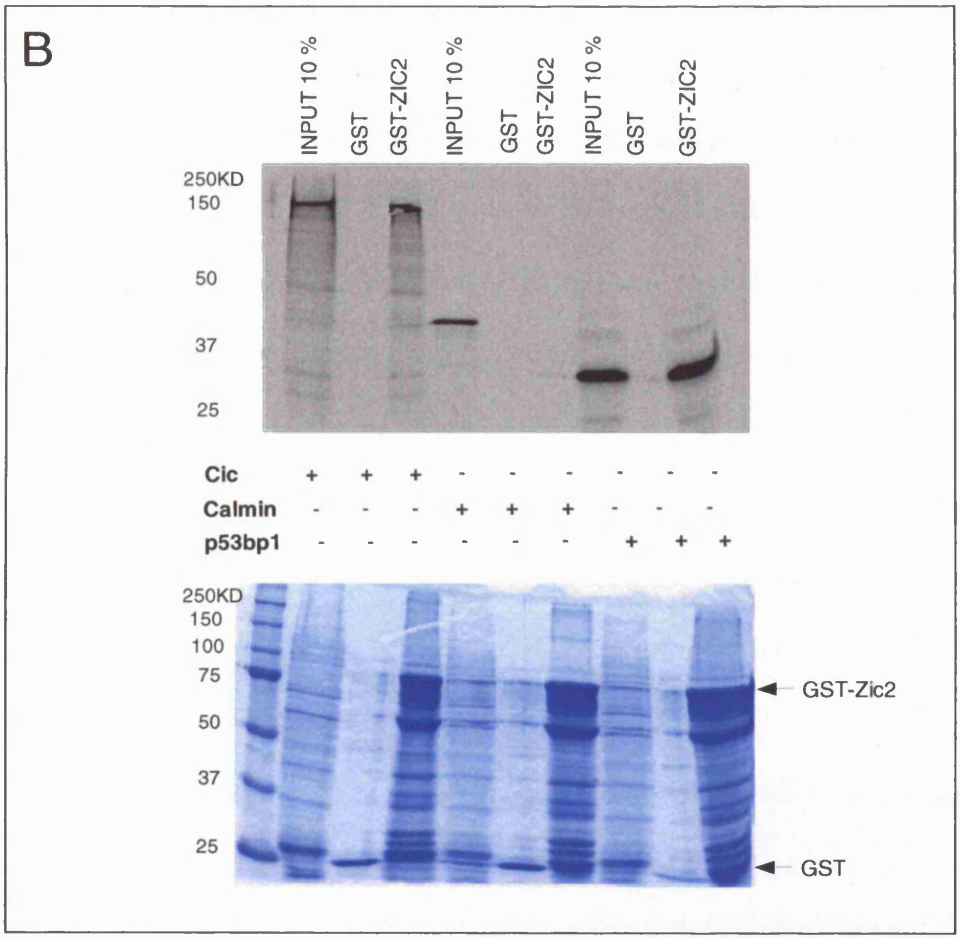
B
INPUT 10 %
GST
GST-ZIC2
INPUT 10 %
GST
GST-ZIC2
INPUT 10 %
GST
GST-ZIC2
250KD
150
50
37
25
Cic + + + - - - - - -
Calmin - - - + + + - - -
p53bp1 - - - - - - + + +
250KD
150
100
75
50
37
25
GST-Zic2
GST

6.4 DISCUSSION

6.4.1 Zic2 interacts directly with Glis2, Krox20, Cic and p53bp1 *in vitro*

In this chapter I have shown that the interactions identified in the yeast two-hybrid screen between Zic2 and Glis2, Krox20, Cic and p53bp1 can also be detected by biochemical methods *in vitro.* The detection of interactions between proteins using the GST pull-down assay indicates that there is direct physical interaction, rather than an interaction mediated by a third protein that functions as a bridge. As a positive control, the Gli1 protein containing the ZFD was used in the experiment as it has been shown previously to interact with Zic2 (Koyabu *et al.*, 2001a). The interaction observed in the GST pull-down assay is unlikely to be due to the myc epitope binding to the GST-Zic2 fusion protein, since a negative control protein, myc-calmin failed to interact with GST-Zic2.

Further evidence that the observed binding represents a true physiological interaction is provided by the observation that *Zic2* is expressed in overlapping domains with *p53bp1*, *Cic*, *Glis2* and *Krox20* during embryogenesis. The expression of *Krox20* in the neurulation stage mouse embryos is segment-specific (Wilkinson *et al.*, 1989), with expression in rhombomeres 3 and 5 of the developing hindbrain. Glis2 on the other hand, has been shown to be expressed in the limb bud, caudal somites, neural tube and telencephalon (Zhang *et al.*, 2002). These sites of expression correlate with the embryonic expression of *Zic2* in the telencephalon, dorsal somites, dorsal neural tube and limb buds. I also found that the expression of *Cic* and *p53bp1* is expressed in overlapping domains with *Zic2.*

At the cellular level, Zic2 co-localises with the candidate interacting proteins in the nucleus, when they are co-expressed in 293T cells. Taken together, the GST-pull down, *in situ* hybridisation and co-transfection experiments suggest strongly that Zic2

interacts physiologically with Cic, Glis2, Krox20 and p53bp1, as shown by the yeast two-hybrid study.

6.4.2 Does Zic2 interact with Cic, Glis2, Krox20 and p53bp1 *in vivo*?

The results presented in this chapter, and in Chapter 5, do not allow a definitive conclusion that the proteins interact *in vivo*. GST-pull down is an *in vitro* assay in which one of the proteins, in this case Zic2, is expressed and purified in large amounts as a GST-fusion protein in bacteria. It is theoretically possible that spurious binding can occur owing to abnormal folding of Zic2 *in vitro*. This could have resulted from conformational changes caused by the expression in bacteria, the presence of the GST fusion, and/or the process of *in vitro* transcription/translation which may not produce a native folding or correct post-translational modification of proteins. Hence, the binding properties of the GST-Zic2 protein in the present study could have been abnormal. On the other hand, the similar results obtained in the yeast two-hybrid study and the pull-down assay are strongly suggestive of a true interaction.

One possible additional approach to investigate the *in vivo* interaction of Zic2 with its putative binding proteins is co-immunoprecipitation of the epitope-tagged proteins. In this assay, the protein under study is co-expressed in mammalian cells with the candidate interacting protein. Cellular lysates are prepared and protein is immobilised on beads bearing covalently bound antibody against the protein or its tag. As in the GST pull-down assay, the candidate interacting protein is tested for its ability to co-precipitate with the complex bound to the beads. Detection of binding is carried out by SDS-PAGE and western blotting using an antibody against the second protein or its tag. This method has several advantages compared to the GST pull-down assay. Firstly, in the co-immunoprecipitation strategy, both proteins are produced in mammalian cells, which ensures correct protein folding. Secondly, the interaction occurs *in vivo* rather than *in vitro* where experimental conditions can affect the

interaction. The disadvantage of co-immunoprecipitation is that, unlike the *in vitro* GST pull-down assay it does not prove that an interaction is direct, since other binding proteins may participate, but will not be detected.

6.4.3 Do Cic, Glis2, Krox20 and p53bp1 play a role in the NTD phenotype of Zic2 mutants?

In Chapter 4, I showed that Zic2 is required for normal morphogenesis of the neural tube and when disrupted leads to NTDs. One hypothesis is that the Zic2 candidate interacting proteins analysed in this chapter could have a direct role in the production of the NTD phenotype.

6.4.3.1 Krox20

Knockout mice for *Krox20* have been generated by gene targeting (Schneider-Maunoury *et al.*, 1993). Homozygous null embryos do not show an NTD phenotype, demonstrating a lack of a direct role of Krox20 in the production of the NTDs observed in $Zic2^{Ku/Ku}$ embryos. This is not surprising, since the NTDs in $Zic2^{Ku}$ are mainly in the lower spine and *Krox20* is not expressed in this embryonic region. On the other hand, the Krox20-Zic2 interaction suggests a novel physiological role for Zic2 in hindbrain development. Indeed aberrant hindbrain patterning has been observed in $Zic2^{Ku/Ku}$ embryos (Elms *et al.*, 2003). This study showed that *follistatin*, which is normally expressed specifically in rhombomeres (r) 2, 4 and 6, extends its domain into r3 and r5 in $Zic2^{Ku/Ku}$ embryos. Moreover, r3 and r5 appear significantly smaller in $Zic2^{Ku/Ku}$ embryos compared with wild-type littermates, as shown by the smaller domains of Krox20-expressing cells. Therefore, the hindbrain patterning defect observed in $Zic2^{Ku/Ku}$ mutant embryos phenocopies embryos null for *Krox20,* strongly suggesting that Zic2 and Krox20 co-operate in embryonic hindbrain patterning and that the interaction identified by the yeast two-hybrid assay is indeed physiological. Further

experiments could be performed to elucidate the involvement of a Krox20-Zic2 interaction in the specification of r3/r5 identity. Zic2 could act as co-factor that represses or activates some of the Krox20 downstream targets. Therefore, it will be important to study the expression pattern and levels of mRNA of known Krox20 downstream targets, such as *Eph4* and *Hoxb2* in $Zic2^{Ku/Ku}$ embryos. The Krox20-Zic2 interaction could also be investigated by epistatic analysis, since it would be predicted that the hindbrain phenotype of $Krox20^{+/-}$, $Zic2^{Ku/+}$ compound heterozygotes should phenocopy the hindbrain patterning of $Zic2^{Ku/Ku}$.

The *Drosophila* homologue of *Zic* genes, *Opa,* has been shown to play a role in segmentation of the embryo, controlling parasegment identity by activating the expression of *wingless* (*wg*) and *engrailed* (*en*) (Benedyk *et al.*, 1994). *Opa*, in contrast to other pair-rule genes that specify segment identity, is expressed in a non-restricted fashion, and therefore a model has been proposed where *Opa* specifies boundary identity by interacting with spatially restricted transcription factors (Benedyk *et al.*, 1994). A parallel could be drawn between the segmentation patterning of the *Drosophila* embryos and mouse hindbrain rhombomeres, which are transient, segmented structures. *Zic2* could mediate rhombomere boundary identity by interacting with the transcription factor *Krox20*, which has a restricted expression domain.

6.4.3.2 p53bp1

Gene targeted mice that are null for *p53bp1* are viable, immune-deficient and cancer prone (Ward *et al.*, 2003). This study suggests that *p53bp1* is not essential for nervous system development. However, the phenotype of $p53bp1^{-/-}$ embryos *in utero* was not analysed in the knockout mouse and a proportion of embryos dying perinatally with NTDs could have been overlooked as in the first description of the p53 knockout mice (Donehower *et al.*, 1992;Jacks *et al.*, 1994). The original study of p53 null mice showed that mice deficient for p53 protein were developmentally normal and viable, but

were susceptible to spontaneous tumours. Therefore, it was suggested that p53 did not have a role in neural development (Donehower *et al.*, 1992). However, a second study showed that a small proportion of homozygous mutant offspring did not survive postnatally (Sah *et al.*, 1995). Analysis of $p53^{-/-}$ embryos at E13.5 revealed that a proportion of embryos developed exencephaly indicating a role for p53 in cranial neurulation. The strong effect of genetic background on the proportion of affected $p53^{-/-}$ embryos indicates an important role for genetic modifier (Sah *et al.*, 1995).

The data implicating p53 in the development of NTDs suggest that a p53bp1-Zic2 interaction could have an important role in the exencephaly phenotype of $Zic2^{Ku/Ku}$ embryos, as described in Chapter 4. By interacting with p53bp1, Zic2 could regulate its binding to p53 and in turn affect p53-mediated cell cycle arrest or apoptosis. Apoptosis was studied by TUNEL (terminal deoxynucleotidyltransferase-mediated UTP end labelling) staining in mice carrying the knockdown allele of Zic2 (Aruga *et al.*, 1996a). $Zic2^{Kd/Kd}$ embryos exhibited abnormally low levels of apoptosis in the telencephalic roof plate, which might account for the abnormal forebrain observed in $Zic2^{Kd/Kd}$ embryos. Knockout mice for genes involved in apoptosis such as caspase 9 (*Casp9*) and *Apaf1* display exencephaly attributed to reduced apoptotic cell death in the cranial neural folds (Kuida *et al.*, 1998;Cecconi *et al.*, 1998;Hakem *et al.*, 1998). However, increased apoptosis can also lead to exencephaly as seen in knockout mice for *ApoB*, *Bcl10* or *Mdm4*, which show increased apoptosis in the cranial neural folds (Farese, Jr. *et al.*, 1995;Migliorini *et al.*, 2002). Hence, the level of apoptosis must be precisely regulated to allow normal completion of cranial neurulation. Further analysis will be necessary to investigate the role of a Zic2-p53bp1 interaction in the regulation of neural plate morphogenesis.

6.4.3.3 Cic and Glis2

Cic and Glis2 could act as transcriptional repressors or co-activators with Zic2 and, therefore might be involved in the observed *Zic2*$^{Ku/Ku}$ NTD phenotype. However, because mouse mutants for *Cic* and *Glis2* have not yet been reported, it is difficult at present to determine whether these genes play a role in the production of NTDs. It will be interesting to determine the phenotype of mice in which these genes are disrupted. In *Drosophila, Cic* has been shown to repress downstream genes of receptor tyrosine kinases (RTKs) by interacting with the co-repressor *Groucho* (Gro)(Jimenez *et al.*, 2000). If such a repressive interaction was also reproduced in mammals, *Cic* could possibly function as a transcriptional repressor of *Zic2*. Whatever the mechanism of its interaction with Zic2, the co-expression of *Cic* and *Zic2* in the PNP region at E9.5 makes *Cic* the best candidate to emerge from the yeast two-hybrid study as a possible co-regulator of spinal neurulation, and potential contributor to the spinal NTD phenotype of *Zic2*$^{Ku/Ku}$. *Glis2*, on the other hand, is expressed in the cranial neural tube and dorsal spinal neural tube, which could indicate a role in regulating the exencephaly phenotype of *Zic2*$^{Ku/Ku}$.

CHAPTER 7: GENERAL DISCUSSION

The overall aim of this thesis was to further understand the role of Zic2 during mouse spinal neurulation. To achieve this goal the initial approach was to study the expression pattern of *Zic* genes at the time of neural tube closure (Chapter 3). The description of when and where *Zic* genes are expressed during neurulation was a prerequisite in understanding the role of *Zic* genes in neurulation.

Zic1-4 are expressed at the time of neural tube closure in distinct but partially overlapping domains. Among the four *Zic* genes examined, only *Zic2* and *Zic3* were found to be expressed in the posterior neuropore region at the time of neural tube closure. This observation is in accordance with the spina bifida phenotype reported in mouse mutants for these genes. Interestingly, at the time of neural tube closure, *Zic2* was found to be expressed solely in the neural plate, in the region where the neural folds are open. This expression pattern suggests that the function of *Zic2* during neurulation is probably intrinsic to the neural plate. Conversely, *Zic3* was found not to be expressed in the neural tube indicating an extrinsic mechanism in the production of the neural tube defects observed in the *Bent tail* and *Zic3 Knockoutl*mutant mice. *Zic1* and *Zic4* are not expressed in the PNP or caudal region of the embryos suggesting that these genes are not involved in regulating closure of the low spinal neural tube. Accordingly, *Zic1* null embryos do not exhibit NTDs. A null mouse for *Zic4* has not been reported yet, but based on the expression pattern described in Chapter 1 it is unlikely that *Zic4* plays a role in closure of the lower spinal neural tube.

The requirement for *Zic2* in neural tube closure has been reported previously in the hypomorphic allele, $Zic2^{Kd}$. However, similarly to other mouse mutants that exhibit neural tube defects, the embryonic basis of the neurulation phenotype is poorly described. The next question to be addressed was the direct role of *Zic2* in the causation of spinal neural tube closure defects. To answer this question the phenotype of a new allele, $Zic2^{Ku}$ was studied morphologically (Chapter 4). Interestingly, $Zic2^{Ku/Ku}$ embryos

were found to lack DLHPs, indicating that *Zic2* regulates the morphogenesis of the neural tube and could be required for the formation of bending points.

7.1 HYPOTHESIS TO EXPLAIN HOW ZIC2 COULD REGULATE DLHP FORMATION

Formation of DLHPs during mouse spinal neurulation is negatively regulated by Shh (Ybot-Gonzalez *et al.*, 2002). This has been shown in Shh null embryos where DLHPs form during Mode 1 of neurulation compared to the straight neural folds characteristic of Mode 1 in wild type embryos. Conversely, DLHPs are inhibited by local release of Shh peptide next to the site of bending. In fact, Shh emanating from the notochord appears to control the timing of DLHP formation. During Mode 1, Shh is strongly expressed and its inhibitory function on DLHP is strong, impeding formation of DLHP. As expression of Shh declines along the body axis during the progression of neurulation from Mode 2 to Mode 3, the inhibitory action of Shh weakens, allowing formation of DLHPs (see Chapter 1 section 1.5.3 and Fig. 1.6).

Interestingly, the surface ectoderm has been shown to be necessary for the formation of DLHPs, such that unilateral removal of this embryonic structure leads to absence of bending on the operated side (Ybot-Gonzalez *et al.*, 2002). This observation suggests that the surface ectoderm signals to the underlying tissue to form DLHPs. This led to the hypothesis that Shh emanating from the notochord inhibits DLHP-inducing signals during Mode 1 of neurulation. However as neurulation progresses to Mode 2 and Mode 3, Shh signalling weakens its inhibitory effect on the surface ectoderm-derived signals and formation of DLHPs can occur.

How could *Zic2* function as part of the molecular mechanism regulating DLHPs? Three hypothetical models arise from the morphological data that I have presented. In the first model (Fig. 7.1), Zic2 expressed in the neural plate, functions to

inhibit Shh signalling. During Mode 1 of neurulation Shh expression levels are high and Zic2 cannot fully inhibit Shh signalling, leading to inhibition of the DLHP-inducing

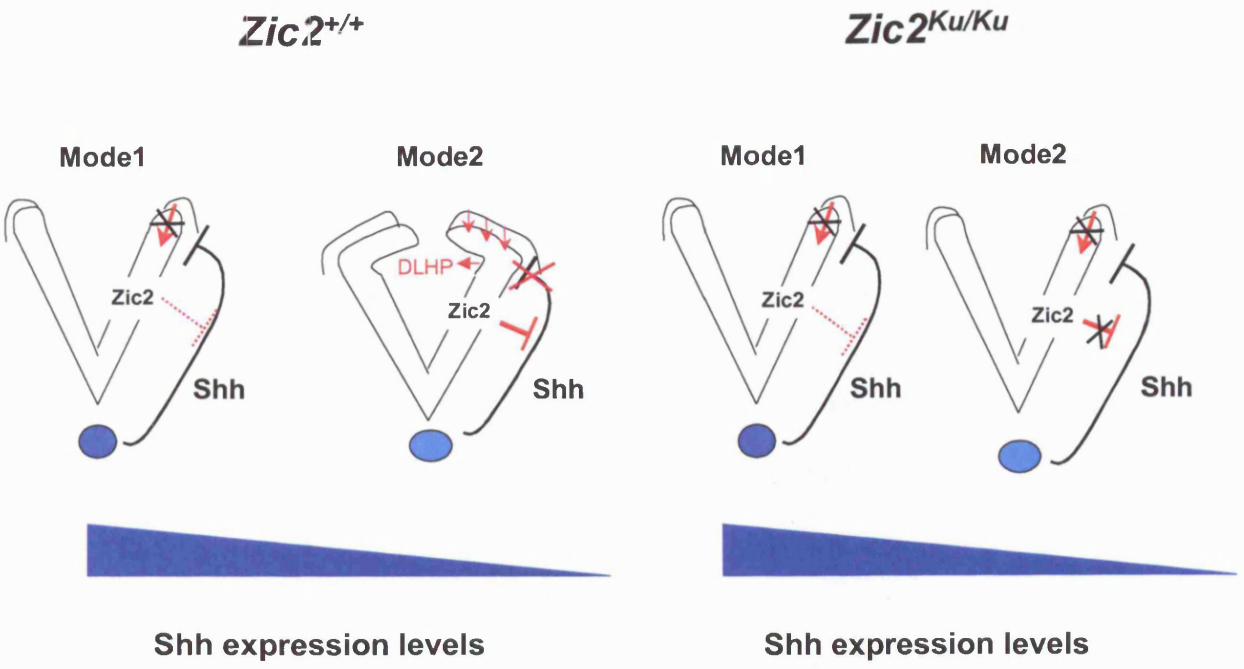

Figure 7.1 Diagram representing a hypothetical model 1 of the function of Zic2 in the formation of DLHPs

In this model Zic2 is required during Mode 2 of neurulation to block the Shh inhibition of the DLHPs-inducing signals from the surface ectoderm. During Mode 1 of neurulation, in *Zic2*$^{+/+}$ embryos, Shh influence is strong and can not be overcome by Zic2. Hence, Shh inhibits signals from the surface ectoderm that are required for DLHP formation. During Mode 2 of neurulation, Shh expression weakens, and Zic2 functions to block the inhibitory effect on the DLHPs-inducing signal from the surface ectoderm, leading to formation of DLHPs. This mechanism is impaired in *Zic2*$^{Ku/Ku}$ embryos where, during Mode 2 of neurulation, signals from the surface ectoderm are still inhibited by Shh signalling due to the failure of Zic2 to block its inhibitory effect.

signals from the surface ectoderm. During Mode 2 of neurulation Shh levels are lower and Zic2 is now able to block Shh signalling. In homozygous *Zic2*$^{Ku/Ku}$ embryos inhibition of Shh signalling does not occur because the mutation abolishes the ability of Zic2 to inhibit Shh signalling. Hence during Mode 2 of neurulation, in *Zic2*$^{Ku/Ku}$ embryos, Shh is still able to inhibit the surface ectoderm DLHP-inducing signal, leading to absence of DLHPs and the appearance of Mode 1 morphology. In this model, the blocking effect of Zic2 on Shh signalling could be direct, or else mediated by binding of Zic2 to a co-factor, which is not present during Mode 1 of neurulation. Although speculative, Cic has been shown to interact with Zic2, and interestingly is not expressed during Mode 1 of neurulation in the PNP region (Chapter 6). Cic expression in the PNP starts during Mode 2 of neurulation and could act as a co-factor required for the inhibition of Shh.

A second hypothetical (Figure 7.2) model places Zic2 as a transcription factor required to transduce the DLHP-inducing signals from the surface ectoderm to the neural plate. In this model, Shh signalling inhibits the action of DLHP-inducing signals from the surface ectoderm during Mode 1 of neurulation. This inhibition results in impairment of the ability of *Zic2* to activate DLHPs at this stage of neurulation. However, as the strength of Shh influence decreases in Mode 2, its inhibitory function is abolished, so that the signals from the surface ectoderm can act upon the underlying neural fold, via Zic2 function, resulting in a Mode 2 morphology with formation of DLHPs. In *Zic2*$^{Ku/Ku}$ embryos, where *Zic2* function is impaired, formation of DLHPs does not occur because the signals from the surface ectoderm cannot be transduced in the neural plate, so that the transition from Mode 1 to Mode 2 does not occur.

A third model (Figure 7.3) envisages that the function of Zic2 is to transduce the inhibitory effect of Shh signalling on DLHP-inducing signals from the surface ectoderm. During Mode 1 of neurulation, Shh expression is strong and its signalling, via

Zic2, inhibits the DLHP-inducing signals from the surface ectoderm. As neurulation progresses Shh expression decreases and the inhibitory effect on DLHP-inducing signals weakens, so that the surface ectoderm can signal to the underlying neural folds and induce DLHPs characteristic of Mode 2 of neurulation.

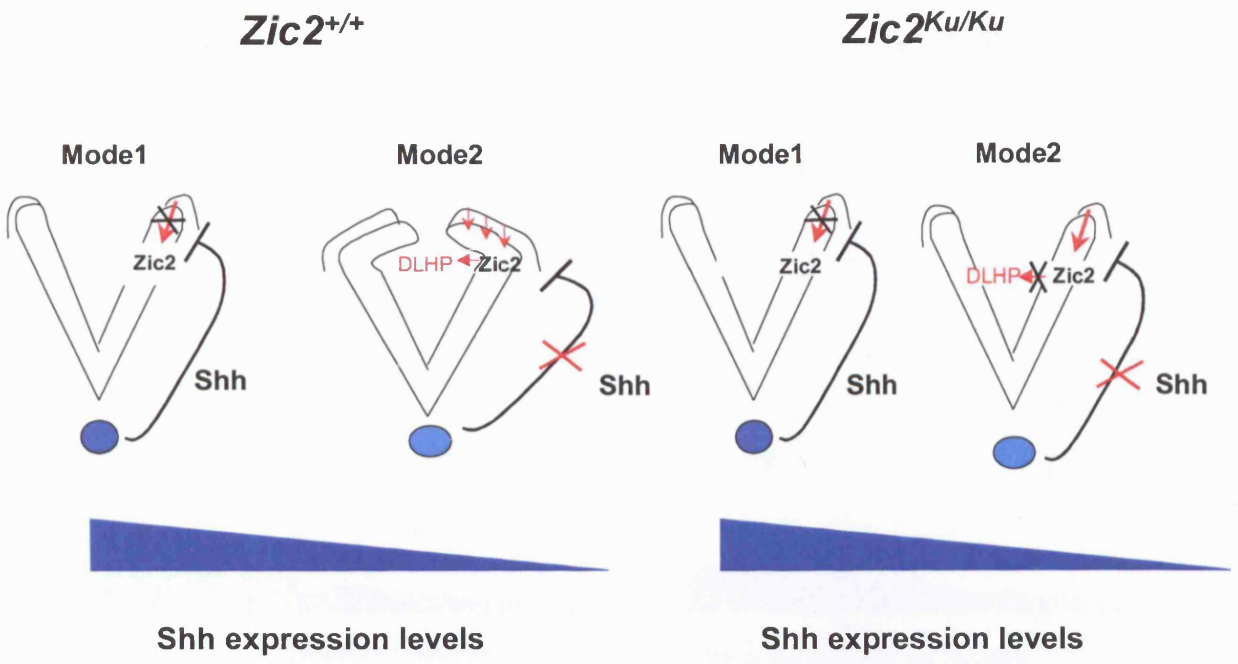

Figure 7.2 Diagram representing a hypothetical model 2 on the function of Zic2 in the formation of DLHPs

In this model Zic2 activates DLHPs by transducing the DLHP-inducing signals from the surface ectoderm. During Mode 1 of neurulation in *Zic2*$^{+/+}$ embryos, Shh inhibits signals from the surface ectoderm that are required for DLHPs formation. Zic2 cannot act to transduce the signal for formation of DLHPs. During Mode 2 of neurulation, Shh expression weakens so that DLHP-inducing signals from the surface ectoderm can be transduced by Zic2, leading to formation of DLHPs. This mechanism is impaired in *Zic2*$^{Ku/Ku}$ embryos, where DLHP-inducing signals from the surface ectoderm cannot be transduced within the neural folds by *Zic2*, so DLHPs are not formed.

However, in *Zic2*$^{Ku/Ku}$ embryos, where the *Zic2* mutation acts as a gain-of-function, the decrease of Shh signalling is not recognised and the inhibitory function of *Zic2* on DLHP-inducing signals from the surface ectoderm persists. Hence, DLHPs are absent and a Mode 1 morphology persists.

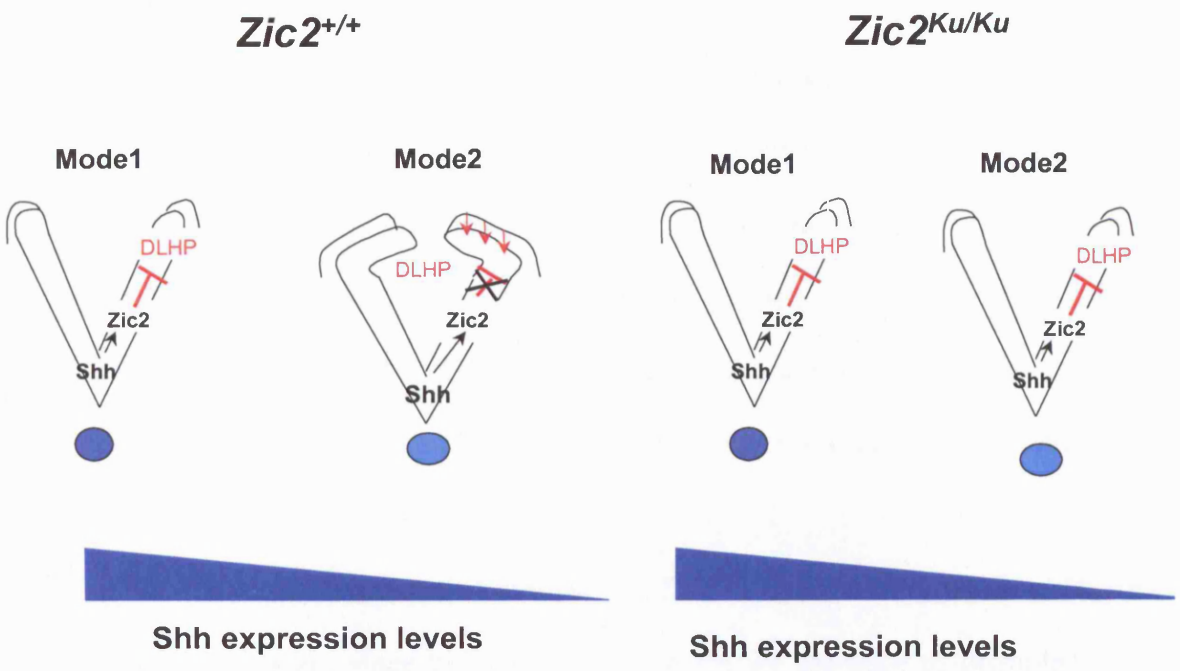

Figure 7.3 Diagram representing a hypothetical model 3 of the function of Zic2 in the formation of DLHPs

In this model the inhibitory effect of Shh signalling on DLHP-inducing signals from the surface ectoderm is mediated through Zic2. During Mode 1 of neurulation, in wild type embryos, Shh is expressed at high levels and inhibits DLHP-inducing signals from the surface ectoderm, resulting in straight neural folds. In Mode 2 of neurulation Shh weakens and its inhibitory function, mediated through Zic2, is reduced so that DLHP-inducing signals from the surface ectoderm result in bending of the neural folds. In this model in *Zic2*$^{Ku/Ku}$ embryos, the mutation acts as a gain-of-function and the inhibition becomes constitutively active irrespective of the levels of Shh present. Hence, the neural folds in *Zic2*$^{Ku/Ku}$ embryos do not progress into Mode 2 morphology.

Further research is required to reveal whether the requirement for Zic2 in DLHP formation is mediated through one of the models described above. An approach that has been initiated during my research time, but has not yet yielded enough conclusive data, is the generation of compound homozygous mutant embryos for *Zic2* and *Shh*. $Zic2^{Ku/Ku}/Shh^{-/-}$ embryos were generated from crosses between compound heterozygotes, $Zic2^{Ku/+}/Shh^{+/-}$. To obtain $Zic2^{Ku/+}/Shh^{+/-}$ mice, $Zic2^{Ku/+}$ males were mated to $Shh^{+/-}$ females resulting in a quarter of the offspring being $Zic2^{Ku/+}/Shh^{+/-}$. In a second generation, crosses between compound heterozygotes produced litters in which one in sixteen embryos were expected to be double homozygote. So far, two double homozygous embryos have been obtained. Interestingly, both of these embryos exhibit spina bifida similar to $Zic2^{Ku/Ku}$ embryos. If this phenotype is observed in further $Zic2^{Ku/Ku}/Shh^{-/-}$ embryos, and no DLHPs are found to be present preceding development of spina bifida, it may be possible to distinguish between the three models presented above.

The first model predicts that abrogation of Shh should lead to rescue of DLHPs in double homozygotes, since the absence of Shh, in the presence of disrupted Zic2, would allow signals from the surface ectoderm to induce DLHPs. In contrast, models 2 and 3 both predict that removal of Shh and disruption of Zic2 will be associated with persistent absence of DLHPs. In model 2, this is because DLHP-inducing signals from the surface ectoderm are not transduced within the neural plate owing to the disruption of Zic2 function, irrespective of the simultaneous loss of the Shh inhibition. Moreover, in model 3, the mutant form of Zic2 functions as a constitutive inhibitor of DLHPs formation, regardless of Shh concentration, so that $Zic2^{Ku/Ku}/Shh^{-/-}$ compound homozygotes lack DLHPs like $Zic2^{Ku/Ku}$ embryos.

At first sight therefore, the *Shh/Zic2* double mutant experiment favours models 2 and 3 over model 1. How can model 2 and model 3 be distinguished? To be able to

answer this question, we need to know something about the nature of the *Kumba* mutation and whether it leads to a loss of function or gain of function, since model 2 predicts that Zic2 functions as an activator of downstream signalling and model 3 views Zic2 as an inhibitor of downstream events.

The mutation identified in the *Kumba* mouse lies in the fourth zinc finger of Zic2. The zinc finger domain region is known to function in both DNA binding and protein-protein interactions. Therefore, the transcriptional activity of $Zic2^{Ku}$ could be hampered by the impairment of mutant $Zic2^{Ku}$ protein to directly bind either to the DNA or to protein co-factors. Two complementary avenues of research can be followed in the future to investigate whether the Zic^{Ku} allele affects DNA binding. Firstly, since it has recently been shown that Zic2 binds to Gli-binding sequences and to the ApoE promoter (Mizugishi *et al.*, 2001a;Salero *et al.*, 2001), an electro-mobility shift assay (EMSA) could be performed to compare the DNA-binding activity of the wild type protein with the mutant $Zic2^{Ku}$ protein. In parallel, a reporter assay using the luciferase gene under control of the Gli-BS or ApoE promoters could also be used to test whether the transcriptional activity of Zic2 is affected by the *Kumba* mutation. These experiments should answer the unresolved question of whether $Zic2^{Ku}$ is a null (loss-of-function) allele of Zic2, or whether a constitutive functional change (gain-of-function) is caused by the *Kumba* mutation. At the present, it is unclear whether model 2 or model 3 best fit the biology of the Zic2 function in mouse neurulation.

During the course of my research Zic2 has been shown to interact with Gli proteins through an interaction that involves the 3^{rd}, 4^{th} and 5^{th} zinc fingers. Since the mutation in *Kumba* lies in the 4^{th} zinc finger, the Gli-Zic2 interaction could be disrupted by the mutation. A speculative idea is that the mutation in Zic2 may affect interactions with other protein co-factors. However, at the beginning of my research, the proteins that interact with Zic2 were not known. To address this question I used the yeast two-

hybrid approach in order to identify several proteins that bind to Zic2 and could be important in mediating Zic2 transcriptional activity. Cic, Glis2, Krox20 and p53bp1 were all shown to interact with Zic2 in the yeast two-hybrid assay (Chapter 5) and in the GST pull- down assay (Chapter 6), providing strong evidence that these interactions might also occur *in vivo*. The identification of these proteins as binding partners provides information on the possible physiological functions of Zic2. For instance, the Krox20-Zic2 interaction although unrelated to neural tube defects could play a role in the regulation of hindbrain segmentation. Cic and Glis2 could directly regulate neurulation and therefore obtaining mutant mouse lines for these genes will be important. To date, no mutant lines or gene trap ES cells lines have been reported.

In the yeast two-hybrid screen I also identified jumonji, Jmj, as a Zic2 interacting protein. Although I have not followed up this protein in subsequent biochemical assays, because of the lack of time, this protein may be of interest in future studies, particularly since the mouse mutant for *Jmj* exhibits cranial neural tube defects (Takeuchi *et al.*, 1999). Therefore, a Zic2-Jmj interaction could be required for cranial neural tube closure. One way to further test the functional relevance of this interaction would be to generate compound heterozygotes for $Zic2^{Ku}$ and *Jmj*. If the interaction occurs physiologically in the embryo, double heterozygous $Zic2^{Ku/+}/Jmj^{+/-}$ embryos might be expected to exhibit NTDs. Hence, the protein interactions identified in this thesis will be useful in designing new experiments to further elucidate the regulation of neurulation by Zic2.

In conclusion, this thesis has strengthened our understanding of the role of Zic2 during neurulation. I have shown that Zic2 is required for the formation of DLHPs at lower spinal levels and that this may be the cause of the neurulation phenotype observed in $Zic2^{Ku}$ mice. At the molecular level, I have identified putative Zic2-interacting

partners that may be involved directly in neurulation. Subsequent studies will be able to build upon these data and further establish the molecular mechanisms by which Zic2 regulates neurulation.

BIBLIOGRAPHY

Abraham,R.T. (2002). Checkpoint signalling: focusing on 53BP1. *Nat. Cell Biol.,* **4,** E277-E279.

Altaba,A.R.I. (1998). Combinatorial *Gli* gene function in floor plate and neuronal inductions by sonic hedgehog. *Development.,* **125,** 2203-2212.

Alvarez,I.S. and Schoenwolf,G.C. (1992). Expansion of surface epithelium provides the major extrinsic force for bending of the neural plate. *J. Exp. Zool.,* **261,** 340-348.

Ang,S.-L. and Rossant,J. (1994). *HNF*-3β is essential for node and notochord formation in mouse development. *Cell,* **78,** 561-574.

Aruga,J., Minowa,O., Yaginuma,H., Kuno,J., Nagai,T., Noda,T., and Mikoshiba,K. (1998a). Mouse Zic1 is involved in cerebellar development. *J. Neurosci.,* **18,** 284-293.

Aruga,J., Minowa,O., Yaginuma,H., Kuno,J., Nagai,T., Noda,T., and Mikoshiba,K. (1998b). Mouse *Zic1* is involved in cerebellar development. *J. Neurosci.,* **18,** 284-293.

Aruga,J., Mizugishi,K., Koseki,H., Imai,K., Balling,R., Noda,T., and Mikoshiba,K. (1999). *Zic1* regulates the patterning of vertebral arches in cooperation with *Gli3*. *Mech. Dev.,* **89,** 141-150.

Aruga,J., Nagai,T., Tokuyama,T., Hayashizaki,Y., Okazaki,Y., Chapman,V.M., and Mikoshiba,K. (1996a). The mouse zic gene family. Homologues of the Drosophila pair-rule gene odd-paired. *J. Biol. Chem.,* **271,** 1043-1047.

Aruga,J., Tohmonda,T., Homma,S., and Mikoshiba,K. (2002). Zic1 promotes the expansion of dorsal neural progenitors in spinal cord by inhibiting neuronal differentiation. *Dev. Biol.,* **244,** 329-341.

Aruga,J., Yokota,N., Hashimoto,M., Furuichi,T., Fukuda,M., and Mikoshiba,K. (1994). A novel zinc finger protein, zic, is involved in neurogenesis, especially in the cell lineage of cerebellar granule cells. *J Neurochem.,* **63,** 1880-1890.

Aruga,J., Yozu,A., Hayashizaki,Y., Okazaki,Y., Chapman,V.M., and Mikoshiba,K. (1996b). Identification and characterization of Zic4, a new member of the mouse Zic gene family. *Gene,* **172,** 291-294.

Bellone,E., Di Maria,E., Soriani,S., Varese,A., Doria,L.L., Ajmar,F., and Mandich,P. (1999). A novel mutation (D305V) in the early growth response 2 gene is associated with severe Charcot-Marie-Tooth type 1 disease. *Hum. Mutat.,* **14,** 353-354.

Benedyk,M.J., Mullen,J.R., and DiNardo,S. (1994). odd-paired: a zinc finger pair-rule protein required for the timely activation of engrailed and wingless in Drosophila embryos. *Genes Dev.,* **8,** 105-117.

Blatter,B.M., Lafeber,A.B., Peters,P.W.J., Roeleveld,N., Verbeek,A.L.M., and Gabreëls,F.J.M. (1997). Heterogeneity of spina bifida. *Teratology.,* **55,** 224-230.

Bork,P., Hofmann,K., Bucher,P., Neuwald,A.F., Altschul,S.F., and Koonin,E.V. (1997). A superfamily of conserved domains in DNA damage-responsive cell cycle checkpoint proteins. *FASEB J,* **11,** 68-76.

Botto,L.D. and Mastroiacovo,P. (1998). Exploring gene-gene interactions in the etiology of neural tube defects. *Clin. Genet,* **53,** 456-459.

Bram,R.J., Lue,N.F., and Kornberg,R.D. (1986). A GAL family of upstream activating sequences in yeast: roles in both induction and repression of transcription. *EMBO J.,* **5,** 603-608.

Brent,R. and Finley,R.L., Jr. (1997). Understanding gene and allele function with two-hybrid methods. *Annu. Rev. Genet.,* **31,** 663-704.

Brent,R. and Ptashne,M. (1985). A eukaryotic transcriptional activator bearing the DNA specificity of a prokaryotic repressor. *Cell,* **43,** 729-736.

Brewster,R., Lee,J., and Altaba,A.R.I. (1998). Gli/Zic factors pattern the neural plate by defining domains of cell differentiation. *Nature,* **393,** 579-583.

Brook,F.A., Shum,A.S.W., Van Straaten,H.W.M., and Copp,A.J. (1991). Curvature of the caudal region is responsible for failure of neural tube closure in the curly tail (ct) mouse embryo. *Development.,* **113,** 671-678.

Brown,L.Y., Hodge,S.E., Johnson,W.G., Guy,S.G., Nye,J.S., and Brown,S. (2002). Possible association of NTDs with a polyhistidine tract polymorphism in the ZIC2 gene. *Am. J. Med. Genet.,* **108,** 128-131.

Brown,L.Y., Odent,S., David,V., Blayau,M., Dubourg,C., Apacik,C., Delgado,M.A., Ha,B.D., Reynolds,J.F., Sommer,A., Wieczorek,D., Brown,S.A., and Muenke,M. (2001). Holoprosencephaly due to mutations in *ZIC2*: alanine tract expansion mutations may be caused by parental somatic recombination. *Hum. Mol. Genet.,* **10,** 791-796.

Brown,S.A., Warburton,D., Brown,L.Y., Yu,C.Y., Roeder,E.R., Stengel-Rutkowski,S., Hennekam,R.C., and Muenke,M. (1998). Holoprosencephaly due to mutations in ZIC2, a homologue of Drosophila odd-paired. *Nature Genet.,* **20,** 180-183.

Cadigan,K.M. and Nusse,R. (1997). Wnt signaling: a common theme in animal development. *Genes Dev.,* **11,** 3286-3305.

Campbell,L.R., Dayton,D.H., and Sohal,G.S. (1986). Neural tube defects: A review of human and animal studies on the etiology of neural tube defects. *Teratology.,* **34,** 171-187.

Campbell,S., Tsannatos,C., and Pearce,J.M. (1984). The prenatal diagnosis of Joubert's syndrome of familial agenesis of the cerebellar vermis. *Prenatal Diag.,* **4,** 391-395.

Carrel,T., Herman,G.E., Moore,G.E., and Stanier,P. (2001). Lack of mutations in ZIC3 in three families with neural tube defects. *Am. J. Med. Genet.,* **98,** 283-285.

Carrel,T., Purandare,S.M., Harrison,W., Elder,F., Fox,T., Casey,B., and Herman,G.E. (2000). The X-linked mouse mutation Bent tail is associated with a deletion of the *Zic3* locus. *Hum. Mol. Genet.,* **9,** 1937-1942.

Carroll,S.B. and Scott,M.P. (1985). Localization of the fushi tarazu protein during Drosophila embryogenesis. *Cell,* **43,** 47-57.

Carter,C.O. (1974). Clues to the aetiology of neural tube malformations. *Dev. Med. Child Neurol.,* **16 (Suppl.32),** 3-15.

Cecconi,F., Alvarez-Bolado,G., Meyer,B.I., Roth,K.A., and Gruss,P. (1998). Apaf1 (CED-4 homolog) regulates programmed cell death in mammalian development. *Cell,* **94,** 727-737.

Chatkupt,S., Hol,F.A., Shugart,Y.Y., Geurds,M.P.A., Stenroos,E.S., Koenigsberger,M.R., Hamel,B.C.J., Johnson,W.G., and Mariman,E.C.M. (1995). Absence of linkage between familial neural tube defects and PAX3 gene. *J. Med. Genet.,* **32,** 200-204.

Chavrier,P., Zerial,M., Lemaire,P., Almendral,J., Bravo,R., and Charnay,P. (1988). A gene encoding a protein with zinc fingers is activated during G0/G1 transition in cultured cells. *EMBO J,* **7,** 29-35.

Chen,C.H., Von Kessler,D.P., Park,W.J., and Beachy,P.A. (1999). Nuclear trafficking of cubitus interruptus in the transcriptional regulation of hedgehog target gene expression. *Cell,* **98,** 305-316.

Chiang,C., Litingtung,Y., Lee,E., Young,K.E., Corden,J.L., Westphal,H., and Beachy,P.A. (1996). Cyclopia and defective axial patterning in mice lacking *Sonic hedgehog* gene function. *Nature,* **383,** 407-413.

Chien,C.T., Bartel,P.L., Sternglanz,R., and Fields,S. (1991). The two-hybrid system: a method to identify and clone genes for proteins that interact with a protein of interest. *Proc. Natl. Acad. Sci. USA,* **88,** 9578-9582.

Chomczynski,P. and Sacchi,N. (1987). Single-step method of RNA isolation by acid guanidinium thiocyanate-phenol-chloroform extraction. *Anal. Biochem.,* **162,** 156-159.

Colas,J.F. and Schoenwolf,G.C. (2001). Towards a cellular and molecular understanding of neurulation. *Dev. Dyn.,* **221,** 117-145.

Copp,A., Cogram,P., Fleming,A., Gerrelli,D., Henderson,D., Hynes,A., Kolatsi-Joannou,M., Murdoch,J., and Ybot-Gonzalez,P. (1999). Neurulation and neural tube closure defects. In Tuan,R.S. and Lo,C.W. (Eds.), *Developmental Biology Protocols, Volume 1,* . Humana Press Inc, Totowa, New Jersey, pp. 135-160.

Copp,A.J. and Bernfield,M. (1994). Etiology and pathogenesis of human neural tube defects: Insights from mouse models. *Curr. Opin. Pediatr.,* **6,** 624-631.

Copp,A.J. and Brook,F.A. (1989). Does lumbosacral spina bifida arise by failure of neural folding or by defective canalisation? *J. Med. Genet.,* **26,** 160-166.

Copp,A.J., Brook,F.A., Estibeiro,J.P., Shum,A.S.W., and Cockroft,D.L. (1990). The embryonic development of mammalian neural tube defects. *Prog. Neurobiol.,* **35,** 363-403.

Copp,A.J., Brook,F.A., and Roberts,H.J. (1988). A cell-type-specific abnormality of cell proliferation in mutant (curly tail) mouse embryos developing spinal neural tube defects. *Development.,* **104,** 285-295.

Copp,A.J. and Cockroft,D.L. (1990). *Postimplantation Mammalian Embryos: A Practical Approach.* IRL Press, Oxford.

Copp,A.J., Greene,N.D.E., and Murdoch,J.N. (2003a). Mouse mutants as models of neural tube defects. In Wyszynski,D.F. (Ed.), *Neural Tube Defects: From Origin to Treatment*, . Oxford University Press, Oxford.

Copp,A.J., Greene,N.D.E., and Murdoch,J.N. (2003b). The genetic basis of mammalian neurulation. *Nat. Rev. Genet.,* **4,** 784-793.

Corrick,C.M., Silvestro,M.J., Lahoud,M.H., Allen,G.J., Tymms,M.J., and Kola,I. (1996). Construction of a mouse blastocyst cDNA library by PCR amplification from total RNA. *Mol. Reprod. Dev.,* **43,** 7-16.

Cossu,G., Tajbakhsh,S., and Buckingham,M. (1996). How is myogenesis initiated in the embryo. *Trends Genet.,* **12,** 218-223.

Costanzo,R., Watterson,R.L., and Schoenwolf,G.C. (1982). Evidence that secondary neurulation occurs autonomously in the chick embryo. *J. Exp. Zool.,* **219,** 233-240.

Criley,B.B. (1969). Analysis of the embryonic sources and mechanisms of development of posterior levels of chick neural tubes. *J. Morph.,* **128,** 465-501.

Croen,L.A., Shaw,G.M., and Lammer,E.J. (1996). Holoprosencephaly: epidemiologic and clinical characteristics of a California population. *Am. J Med. Genet.,* **64,** 465-472.

Curtin,J.A., Quint,E., Tsipouri,V., Arkell,R.M., Cattanach,B., Copp,A.J., Fisher,E.M., Nolan,P.M., Steel,K.P., Brown,S.D.M., Gray,I.C., and Murdoch,J.N. (2003). Mutation of *Celsr1* disrupts planar polarity of inner ear hair cells and causes severe neural tube defects in the mouse. *Curr. Biol.,* **13,** 1-20.

Czeizel,A.E. and Dudás,I. (1992). Prevention of the first occurrence of neural-tube defects by periconceptional vitamin supplementation. *N. Engl. J. Med.,* **327,** 1832-1835.

Dang,D.T., Pevsner,J., and Yang,V.W. (2000). The biology of the mammalian Kruppel-like family of transcription factors. *Int. J Biochem. Cell Biol,* **32,** 1103-1121.

Davidson,L.A. and Keller,R.E. (1999). Neural tube closure in *Xenopus* laevis involves medial migration, directed protrusive activity, cell intercalation and convergent extension. *Development.,* **126,** 4547-4556.

Denis,C.L., Chiang,Y.C., Cui,Y., and Chen,J. (2001). Genetic evidence supports a role for the yeast CCR4-NOT complex in transcriptional elongation. *Genetics,* **158,** 627-634.

Detrick,R.J., Dickey,D., and Kintner,C.R. (1990). The effects of N-cadherin misexpression on morphogenesis in Xenopus embryos. *Neuron,* **4,** 493-506.

Donehower,L.A., Harvey,M., Slagle,B.L., McArthur,M.J., Montgomery,C.A., Jr., Butel,J.S., and Bradley,A. (1992). Mice deficient for p53 are developmentally normal but susceptible to spontaneous tumours. *Nature,* **356,** 215-221.

Edmonds,L.D. and James,L.M. (1993). Temporal trends in the birth prevalence of selected congenital malforamtions in the Birth Defects Monitoring Progam/Commission on Professional and Hospital Activities, 1979-1989. *Teratology.,* **48,** 647-649.

Ehrenberg,L., Fedorcsak,I., and Solymosy,F. (1976). Diethyl pyrocarbonate in nucleic acid research. *Prog. Nucleic Acid Res. Mol. Biol,* **16,** 189-262.

Elms,P., Siggers,P., Napper,D., Greenfield,A., and Arkell,R. (2003). Zic2 is required for neural crest formation and hindbrain patterning during mouse development. *Dev. Biol,* **264,** 391-406.

Epstein,D.J., Vekemans,M., and Gros,P. (1991). splotch (Sp^{2H}), a mutation affecting development of the mouse neural tube, shows a deletion within the paired homeodomain of Pax-3. *Cell,* **67,** 767-774.

Fan,H., Oro,A.E., Scott,M.P., and Khavari,P.A. (1997). Induction of basal cell carcinoma features in transgenic human skin expressing Sonic Hedgehog. *Nature Med.,* **3,** 788-792.

Farese,R.V., Jr., Ruland,S.L., Flynn,L.M., Stokowski,R.P., and Young,S.G. (1995). Knockout of the mouse apolipoprotein B gene results in embryonic lethality in homozygotes and protection against diet-induced hypercholesterolemia in heterozygotes. *Proc. Natl. Acad. Sci. USA,* **92,** 1774-1778.

Fields,S. and Song,O. (1989). A novel genetic system to detect protein-protein interactions. *Nature,* **340,** 245-246.

Fields,S. and Sternglanz,R. (1994). The two-hybrid system: an assay for protein-protein interactions. *Trends Genet,* **10,** 286-292.

Fleming,A. and Copp,A.J. (2000). A genetic risk factor for mouse neural tube defects: defining the embryonic basis. *Hum. Mol. Genet.,* **9,** 575-581.

Franzén,B., Iwabuchi,H., Kato,H., Lindholm,J., and Auer,G. (1991). Two-dimensional polyacrylamide gel electrophoresis of human lung cancer: Qualitative aspects of tissue preparation in relation to histopathology. *Electrophoresis,* **12,** 509-515.

Gebbia,M., Ferrero,G.B., Pilia,G., Bassi,M.T., Aylsworth,A.S., Penman-Splitt,M., Bird,L.M., Bamforth,J.S., Burn,J., Schlessinger,D., Nelson,D.L., and Casey,B. (1997). X-linked *situs* abnormalities result from mutations in *ZIC3*. *Nature Genet.,* **17,** 305-308.

Geelen,J.A.G. and Langman,J. (1979). Ultrastructural observations on closure of the neural tube in the mouse. *Anat. Embryol.,* **156,** 73-88.

Gietz,R.D. and Schiestl,R.H. (1991). Applications of high efficiency lithium acetate transformation of intact yeast cells using single-stranded nucleic acids as carrier. *Yeast,* **7,** 253-263.

Golden,J.A. and Chernoff,G.F. (1993). Intermittent pattern of neural tube closure in two strains of mice. *Teratology.,* **47,** 73-80.

Golden,J.A. and Chernoff,G.F. (1995). Multiple sites of anterior neural tube closure in humans: Evidence from anterior neural tube defects (anencephaly). *Pediatrics,* **95,** 506-510.

Golemis,E.A. and Khazak,V. (1997). Alternative yeast two-hybrid systems. The interaction trap and interaction mating. *Methods Mol. Biol.,* **63,** 197-218.

Goodrich,L.V., Milenkovic,L., Higgins,K.M., and Scott,M.P. (1997). Altered neural cell fates and medulloblastoma in mouse *patched* mutants. *Science,* **277,** 1109-1113.

Goodwin,R.L., Pabon-Pena,L.M., Foster,G.C., and Bader,D. (1999). The cloning and analysis of LEK1 identifies variations in the LEK/centromere protein F/mitosin gene family. *J. Biol. Chem.,* **274,** 18597-18604.

Goto,T. and Keller,R. (2002). The planar cell polarity gene Strabismus regulates convergence and extension and neural fold closure in Xenopus. *Dev. Biol.,* **247,** 165-181.

Greene,N.D.E. and Copp,A.J. (1997). Inositol prevents folate-resistant neural tube defects in the mouse . *Nature Med.,* **3,** 60-66.

Greene,N.D.E., Gerrelli,D., Van Straaten,H.W.M., and Copp,A.J. (1998). Abnormalities of floor plate, notochord and somite differentiation in the *loop-tail* (*Lp*) mouse: a model of severe neural tube defects. *Mech. Dev.,* **73,** 59-72.

Grinblat,Y. and Sive,H. (2001). zic gene expression marks anteroposterior pattern in the presumptive neurectoderm of the zebrafish gastrula. *Dev. Dyn.,* **222,** 688-693.

Gripp,K.W., Wotton,D., Edwards,M.C., Roessler,E., Ades,L., Meinecke,P., Richieri-Costa,A., Zackai,E.H., Massague,J., Muenke,M., and Elledge,S.J. (2000). Mutations in TGIF cause holoprosencephaly and link NODAL signalling to human neural axis determination. *Nat Genet.,* **25,** 205-208.

Gruneberg,H. (1954). Genetical studies on the skeleton of the mouse. VIII. Curly tail. *J. Genet.,* **52,** 52-67.

Gruneberg,H. (1955). Genetical studies on the skeleton of the mouse. XVII. Bent-tail. *J. Genet.,* **53,** 551-562.

Gyuris,J., Golemis,E., Chertkov,H., and Brent,R. (1993). Cdi1, a human G1 and S phase protein phosphatase that associates with Cdk2. *Cell,* **75,** 791-803.

Hahm,K., Cobb,B.S., McCarty,A.S., Brown,K.E., Klug,C.A., Lee,R., Akashi,K., Weissman,I.L., Fisher,A.G., and Smale,S.T. (1998). Helios, a T cell-restricted Ikaros family member that quantitatively associates with Ikaros at centromeric heterochromatin. *Genes Dev.,* **12,** 782-796.

Haigo,S.L., Hildebrand,J.D., Harland,R.M., and Wallingford,J.B. (2003). Shroom induces apical constriction and is required for hingepoint formation during neural tube closure. *Curr. Biol,* **13,** 2125-2137.

Hakem,R., Hakem,A., Duncan,G.S., Henderson,J.T., Woo,M., Soengas,M.S., Elia,A., De la Pompa,J.L., Kagi,D., Khoo,W., Potter,J., Yoshida,R., Kaufman,S.A., Lowe,S.W., Penninger,J.M., and Mak,T.W. (1998). Differential requirement for caspase 9 in apoptotic pathways in vivo. *Cell,* **94,** 339-352.

Hamblet,N.S., Lijam,N., Ruiz-Lozano,P., Wang,J., Yang,Y., Luo,Z., Mei,L., Chien,K.R., Sussman,D.J., and Wynshaw-Boris,A. (2002). Dishevelled 2 is essential for cardiac outflow tract development, somite segmentation and neural tube closure. *Development.,* **129,** 5827-5838.

Hayhurst,M. and McConnell,S.K. (2003). Mouse models of holoprosencephaly. *Curr. Opin. Neurol,* **16,** 135-141.

Herrera,E., Brown,L., Aruga,J., Rachel,R.A., Dolen,G., Mikoshiba,K., Brown,S., and Mason,C.A. (2003). Zic2 patterns binocular vision by specifying the uncrossed retinal projection. *Cell,* **114,** 545-557.

Hildebrand,J.D. and Soriano,P. (1999). Shroom, a PDZ domain-containing actin-binding protein, is required for neural tube morphogenesis in mice. *Cell,* **99,** 485-497.

Hol,F.A., Hamel,B.C.J., Geurds,M.P.A., Mullaart,R.A., Barr,F.G., Macina,R.A., and Mariman,E.C.M. (1995). A frameshift mutation in the gene for PAX3 in a girl with spina bifida and mild signs of Waardenburg syndrome. *J. Med. Genet.,* **32,** 52-56.

Hollenberg,S.M., Sternglanz,R., Cheng,P.F., and Weintraub,H. (1995). Identification of a new family of tissue-specific basic helix-loop-helix proteins with a two-hybrid system. *Mol. Cell Biol.,* **15,** 3813-3822.

Huang,Y., Roelink,H., and McKnight,G.S. (2002). Protein kinase A deficiency causes axially localized neural tube defects in mice. *J. Biol. Chem.,* **277,** 19889-19896.

Hui,C. and Joyner,A.L. (1993). A mouse model of Greig cephalopolysyndactyly syndrome: The *extra-toes*^{J} mutation contains an intragenic deletion of the *Gli3* gene. *Nature Genet.,* **3,** 241-246.

Ishisaki,Z., Takaishi,M., Furuta,I., and Huh,N.-H. (2001). Calmin, a protein with calponin homology and transmembrane domains expressed in maturing spermatogenic cells. *Genomics,* **74,** 172-179.

Jacks,T., Remington,L., Williams,B.O., Schmitt,E.M., Halachmi,S., Bronson,R.T., and Weinberg,R.A. (1994). Tumor spectrum analysis in p53-mutant mice. *Curr. Biol,* **4,** 1-7.

James,P., Halladay,J., and Craig,E.A. (1996). Genomic libraries and a host strain designed for highly efficient two- hybrid selection in yeast. *Genetics,* **144,** 1425-1436.

Jimenez,G., Guichet,A., Ephrussi,A., and Casanova,J. (2000). Relief of gene repression by torso RTK signaling: role of capicua in Drosophila terminal and dorsoventral patterning. *Genes Dev.,* **14,** 224-231.

Joosten,P.H., Hol,F.A., van Beersum,S.E., Peters,H., Hamel,B.C., Afink,G.B., Van Zoelen,E.J., and Mariman,E.C. (1998). Altered regulation of platelet-derived growth factor receptor-alpha gene-transcription in vitro by spina bifida-associated mutant Pax1 proteins. *Proc. Natl. Acad. Sci. U. S. A,* **95,** 14459-14463.

Juriloff,D.M., Gunn,T.M., Harris,M.J., Mah,D.G., Wu,M.K., and Dewell,S.L. (2001). Multifactorial genetics of exencephaly in SELH/Bc mice. *Teratology.,* **64,** 189-200.

Juriloff,D.M. and Harris,M.J. (2000). Mouse models for neural tube closure defects. *Hum. Mol. Genet.,* **9,** 993-1000.

Juriloff,D.M., Harris,M.J., Tom,C., and MacDonald,K.B. (1991). Normal mouse strains differ in the site of initiation of closure of the cranial neural tube. *Teratology.,* **44,** 225-233.

Justice,M.J. (2000). Capitalizing on large-scale mouse mutagenesis screens. *Nat Rev. Genet.,* **1,** 109-115.

Justice,M.J., Noveroske,J.K., Weber,J.S., Zheng,B.H., and Bradley,A. (1999). Mouse ENU mutagenesis. *Hum. Mol. Genet.,* **8,** 1955-1963.

Karfunkel,P. (1974). The mechanisms of neural tube formation. *Int. Rev. Cytol.,* **38,** 245-271.

Kato,N. and Aoyama,H. (1998). Dermomyotomal origin of the ribs as revealed by extirpation and transplantation experiments in chick and quail embryos. *Development.*, **125,** 3437-3443.

Kawasaki,E.S. (1990). *PCR Protocols: A Guide to Methods and Applications.* Academic Press, New York.

Keller,R. (2002). Shaping the vertebrate body plan by polarized embryonic cell movements. *Science,* **298,** 1950-1954.

Keller,R., Shih,J., Sater,A.K., and Moreno,C. (1992). Planar induction of convergence and extension of the neural plate by the organizer of *Xenopus*. *Dev. Dyn.,* **193,** 218-234.

Kibar,Z., Vogan,K.J., Groulx,N., Justice,M.J., Underhill,D.A., and Gros,P. (2001). *Ltap*, a mammalian homolog of *Drosophila Strabismus/Van Gogh*, is altered in the mouse neural tube mutant Loop-tail. *Nature Genet.,* **28,** 251-255.

Kim,Y.-S., Lewandoski,M., Perantoni,A., Kurebayashi,S., Nakanishi,G., and Jetten,A.M. (2003). Identification of Glis1, a novel Gli-related, Kruppel-like zinc finger protein containing transactivation and repressor functions. *J. Biol. Chem.,* **277:34,** 30901-30913.

Kitaguchi,T., Mizugishi,K., Hatayama,M., Aruga,J., and Mikoshiba,K. (2002). Xenopus Brachyury regulates mesodermal expression of Zic3, a gene controlling left-right asymmetry. *Dev. Growth Diff.,* **44,** 55-61.

Kitaguchi,T., Nagai,T., Nakata,K., Aruga,J., and Mikoshiba,K. (2000). *Zic3* is involved in the left-right specification of the *Xenopus* embryo. *Development.,* **127,** 4787-4795.

Kitamura,K., Miura,H., Miyagawa-Tomita,S., Yanazawa,M., Katoh-Fukui,Y., Suzuki,R., Ohuchi,H., Suehiro,A., Motegi,Y., Nakahara,Y., Kondo,S., and Yokoyama,M. (1999). Mouse Pitx2 deficiency leads to anomalies of the ventral body wall, heart, extra- and periocular mesoderm and right pulmonary isomerism. *Development.,* **126,** 5749-5758.

Klootwijk,R., Franke,B., Van der Zee,C.E.E.M., De Boer,R.T., Wilms,W., Hol,F.A., and Mariman,E.C.M. (2000). A deletion encompassing *Zic3* in Bent tail, a mouse model for X- linked neural tube defects. *Hum. Mol. Genet.,* **9,** 1615-1622.

Klootwijk,R., Groenen,P., Schijvenaars,M., Hol,F., Hamel,B., Straatman,H., Steegers-Theunissen,R., Mariman,E., and Franke,B. (2004). Genetic variants in ZIC1, ZIC2, and ZIC3 are not major risk factors for neural tube defects in humans. *Am. J Med. Genet.,* **124A,** 40-47.

Koleske,A.J., Gifford,A.M., Scott,M.L., Nee,M., Bronson,R.T., Miczek,K.A., and Baltimore,D. (1998). Essential roles for the Abl and Arg tyrosine kinases in neurulation. *Neuron,* **21,** 1259-1272.

Koyabu,Y., Nakata,K., Mizugishi,K., Aruga,J., and Mikoshiba,K. (2001a). Physical and functional interactions between Zic and Gli proteins. *J. Biol. Chem.,* **276,** 6889-6892.

Koyabu,Y., Nakata,K., Mizugishi,K., Aruga,J., and Mikoshiba,K. (2001b). Physical and functional interactions between Zic and Gli proteins. *J. Biol. Chem.,* **276,** 6889-6892.

Kühl,M., Sheldahl,L.C., Park,M., Miller,J.R., and Moon,R.T. (2000). The Wnt/Ca^{2+} pathway - a new vertebrate Wnt signaling pathway takes shape. *Trends Genet.,* **16,** 279-283.

Kuida,K., Haydar,T.F., Kuan,C.Y., Gu,Y., Taya,C., Karasuyama,H., Su,M.S., Rakic,P., and Flavell,R.A. (1998). Reduced apoptosis and cytochrome c-mediated caspase activation in mice lacking caspase 9. *Cell,* **94,** 325-337.

Lamar,E., Kintner,C., and Goulding,M. (2001). Identification of NKL, a novel Gli-Kruppel zinc-finger protein that promotes neuronal differentiation. *Development.,* **128,** 1335-1346.

Lander,E.S. (1996). The new genomics: Global views of biology. *Science,* **274,** 536-539.

Lang,D. and Epstein,J.A. (2003). Sox10 and Pax3 physically interact to mediate activation of a conserved c-RET enhancer. *Hum. Mol. Genet.,* **12,** 937-945.

Langman,J., Guerrant,R.L., and Freeman,B.G. (1967). Behaviour of neuro-epithelial cells during closure of the neural tube. *J. Comp. Neurol.,* **127,** 399-412.

Le Douarin,B., Pierrat,B., vom,B.E., Chambon,P., and Losson,R. (1995). A new version of the two-hybrid assay for detection of protein-protein interactions. *Nucleic Acids Res.,* **23,** 876-878.

Lee,C.J., Chan,W.I., Cheung,M., Cheng,Y.C., Appleby,V.J., Orme,A.T., and Scotting,P.J. (2002). CIC, a member of a novel subfamily of the HMG-box superfamily, is transiently expressed in developing granule neurons. *Brain Res. Mol. Brain Res.,* **106,** 151-156.

Lemire,R.J. (1988). Neural tube defects. *JAMA,* **259,** 558-562.

Levi,G., Topilko,P., Schneider-Maunoury,S., Lasagna,M., Mantero,S., Cancedda,R., and Charnay,P. (1996). Defective bone formation in *Krox-20* mutant mice. *Development.,* **122,** 113-120.

Liu,H.Y., Badarinarayana,V., Audino,D.C., Rappsilber,J., Mann,M., and Denis,C.L. (1998). The NOT proteins are part of the CCR4 transcriptional complex and affect gene expression both positively and negatively. *EMBO J.,* **17,** 1096-1106.

Liu,Y.H., Kundu,R., Wu,L., Luo,W., Ignelzi,M.A., Jr., Snead,M.L., and Maxson,R.E., Jr. (1995). Premature suture closure and ectopic cranial bone in mice expressing *Msx2* transgenes in the developing skull. *Proc. Natl. Acad. Sci. USA,* **92,** 6137-6141.

Lorain,S., Quivy,J.P., Monier-Gavelle,F., Scamps,C., Lecluse,Y., Almouzni,G., and Lipinski,M. (1998). Core histones and HIRIP3, a novel histone-binding protein, directly interact with WD repeat protein HIRA. *Mol. Cell Biol.,* **18,** 5546-5556.

Lowe,L.A., Yamada,S., and Kuehn,M.R. (2001). Genetic dissection of *nodal* function in patterning the mouse embryo. *Development.,* **128,** 1831-1843.

MacDonald,K.B., Juriloff,D.M., and Harris,M.J. (1989). Developmental study of neural tube closure in a mouse stock with a high incidence of exencephaly. *Teratology.,* **39,** 195-213.

Mackay,J.P. and Crossley,M. (1998). Zinc fingers are sticking together. *Trends Biochem. Sci.,* **23,** 1-4.

Magnaghi,P., Roberts,C., Lorain,S., Lipinski,M., and Scambler,P.J. (1998). HIRA, a mammalian homologue of Saccharomyces cerevisiae transcriptional co-repressors, interacts with Pax3. *Nature Genet.,* **20,** 74-77.

Marigo,V., Johnson,R.L., Vortkamp,A., and Tabin,C.J. (1996). Sonic hedgehog differentially regulates expression of *GLI* and *GLI3* during limb development. *Dev. Biol.,* **180,** 273-283.

Martinez-Arias,A. and Lawrence,P.A. (1985). Parasegments and compartments in the Drosophila embryo. *Nature,* **313,** 639-642.

Matise,M.P., Epstein,D.J., Park,H.L., Platt,K.A., and Joyner,A.L. (1998). Gli2 is required for induction of floor plate and adjacent cells, but not most ventral neurons in the mouse central nervous system. *Development.,* **125,** 2759-2770.

McCarty,A.S., Kleiger,G., Eisenberg,D., and Smale,S.T. (2003). Selective dimerization of a C2H2 zinc finger subfamily. *Mol. Cell,* **11,** 459-470.

Melton,D.W., Konecki,D.S., Brennand,J., and Caskey,C.T. (1984). Structure, expression, and mutation of the hypoxanthine phosphoribosyltransferase gene. *Proc. Natl. Acad. Sci. USA,* **81,** 2147-2151.

Mendelsohn,A.R. and Brent,R. (1999). Protein interaction methods--toward an endgame. *Science,* **284,** 1948-1950.

Migliorini,D., Denchi,E.L., Danovi,D., Jochemsen,A., Capillo,M., Gobbi,A., Helin,K., Pelicci,P.G., and Marine,J.C. (2002). Mdm4 (Mdmx) regulates p53-induced growth arrest and neuronal cell death during early embryonic mouse development. *Mol. Cell Biol.,* **22,** 5527-5538.

Milenkovic,L., Goodrich,L.V., Higgins,K.M., and Scott,M.P. (1999). Mouse *patched1* controls body size determination and limb patterning. *Development.,* **126,** 4431-4440.

Mitchell,K.J., Pinson,K.I., Kelly,O.G., Brennan,J., Zupicich,L., Scherz,P., Leighton,P.A., Goodrich,L.V., Lu,X.W., Avery,B.J., Tate,P., Dill,K., Pangilinan,E., Wakenight,P., Tessier-Lavigne,M., and Skarnes,W.C. (2001). Functional analysis of secreted and transmembrane proteins critical to mouse development. *Nature Genet.,* **28,** 241-249.

Mizugishi,K., Aruga,J., Nakata,K., and Mikoshiba,K. (2001a). Molecular properties of Zic proteins as transcriptional regulators and their relationship to GLI proteins. *J. Biol. Chem.,* **276,** 2180-2188.

Mizugishi,K., Aruga,J., Nakata,K., and Mikoshiba,K. (2001b). Molecular properties of Zic proteins as transcriptional regulators and their relationship to GLI proteins. *J. Biol. Chem.,* **276,** 2180-2188.

Mlodzik,M. (2002). Planar cell polarization: do the same mechanisms regulate Drosophila tissue polarity and vertebrate gastrulation? *Trends Genet.,* **18,** 564-571.

Mo,R., Freer,A.M., Zinyk,D.L., Crackower,M.A., Michaud,J., Heng,H.H.Q., Chik,K.W., Shi,X.M., Tsui,L.C., Cheng,S.H., Joyner,A.L., and Hui,C.C. (1997). Specific and redundant functions of *Gli2* and *Gli3* zinc finger genes in skeletal patterning and development. *Development.,* **124,** 113-123.

Montcouquioi,M., Rachel,R.A., Lanford,P.J., Copeland,N.G., Jenkins,N.A., and Kelley,M.W. (2003). Identification of *Vangl2* and *Scrb1* as planar polarity genes in mammals. *Nature,* **423,** 173-177.

Moran,D. and Rice,R.W. (1975). An ultrastructural examination of the role of cell membrane surface coat material during neurulation. *J. Cell Biol.,* **64,** 172-181.

Morriss-Kay,G., Wood,H., and Chen,W.-H. (1994). Normal neurulation in mammals. *Ciba. Found. Symp.,* **181,** 51-63.

Morriss-Kay,G.M. (1981). Growth and development of pattern in the cranial neural epithelium of rat embryos during neurulation. *J. Embryol. Exp. Morphol.,* **65 (Suppl.),** 225-241.

Morriss-Kay,G.M. and Tuckett,F. (1985). The role of microfilaments in cranial neurulation in rat embryos: effects of short-term exposure to cytochalasin D. *J. Embryol. Exp. Morphol.,* **88,** 333-348.

Motoyama,J., Liu,J., Mo,R., Ding,Q., Post,M., and Hui,C.C. (1998). Essential function of Gli2 and Gli3 in the formation of lung, trachea and oesophagus. *Nature Genet.,* **20,** 54-57.

Murdoch,J.N., Doudney,K., Paternotte,C., Copp,A.J., and Stanier,P. (2001). Severe neural tube defects in the *loop-tail* mouse result from mutation of *Lpp1*, a novel gene involved in floor plate specification. *Hum. Mol. Genet.,* **10,** 2593-2601.

Murdoch,J.N., Henderson,D.J., Doudney,K., Gaston-Massuet,C., Phillips,H.M., Paternotte,C., Arkell,R., Stanier,P., and Copp,A.J. (2003). Disruption of *scribble* (*Scrb1*) causes severe neural tube defects in the *circletail* mouse. *Hum. Mol. Genet.,* **12,** 87-98.

Nagai,T., Aruga,J., Minowa,O., Sugimoto,T., Ohno,Y., Noda,T., and Mikoshiba,K. (2000). Zic2 regulates the kinetics of neurulation. *Proc. Natl. Acad. Sci. USA,* **97,** 1618-1623.

Nagai,T., Aruga,J., Takada,S.J., Günther,T., Spörle,R., Schughart,K., and Mikoshiba,K. (1997). The expression of the mouse *Zic1, Zic2* and *Zic3* gene suggests an essential role for *Zic* genes in body pattern formation. *Dev. Biol.,* **182,** 299-313.

Nagele,R.G. and Lee,H. (1980). Studies on the mechanisms of neurulation in the chick: microfilament-mediated changes in cell shape during uplifting of neural folds. *J. Exp. Zool.,* **213,** 391-398.

Nakata,K., Koyabu,Y., Aruga,J., and Mikoshiba,K. (2000). A novel member of the *Xenopus Zic* family, *Zic5*, mediates neural crest development. *Mech. Dev.,* **99,** 83-91.

Nakata,K., Nagai,T., Aruga,J., and Mikoshiba,K. (1997). *Xenopus Zic3*, a primary regulator both in neural and neural crest development. *Proc. Natl. Acad. Sci. USA,* **94,** 11980-11985.

Nakata,K., Nagai,T., Aruga,J., and Mikoshiba,K. (1998). Xenopus Zic family and its role in neural and neural crest development. *Mech. Dev.,* **75,** 43-51.

Nanni,L., Schelper,R.L., and Muenke,M.T. (2000). Molecular genetics of holoprosencephaly. *Front Biosci.,* **5,** D334-D342.

Nolan,P.M., Peters,J., Strivens,M., Rogers,D., Hagan,J., Spurr,N., Gray,I.C., Vizor,L., Brooker,D., Whitehill,E., Washbourne,R., Hough,T., Greenaway,S., Hewitt,M., Liu,X.H., McCormack,S., Pickford,K., Selley,R., Wells,C., Tymowska-Lalanne,Z., Roby,P., Glenister,P., Thornton,C., and Thaung,C. (2000). A systematic, genome-wide, phenotype-driven mutagenesis programme for gene function studies in the mouse. *Nature Genet.,* **25,** 440-443.

Nusse,R. (1999). WNT targets - repression and activation. *Trends Genet.,* **15,** 1-3.

O'Rahilly,R. and Müller,F. (2002). The two sites of fusion of the neural folds and the two neuropores in the human embryo. *Teratology.,* **65,** 162-170.

O'Shea,K.S. and Kaufman,M.H. (1980). Phospholipase C induced neural tube defects in the mouse embryo. *Experientia,* **36,** 1217-1219.

Pani,L., Horal,M., and Loeken,M.R. (2002). Rescue of neural tube defects in Pax-3-deficient embryos by p53 loss of function: implications for Pax-3-dependent development and tumorigenesis. *Genes Dev.,* **16,** 676-680.

Park,H.L., Bai,C., Platt,K.A., Matise,M.P., Beeghly,A., Hui,C.C., Nakashima,M., and Joyner,A.L. (2000). Mouse *Gli1* mutants are viable but have defects in SHH signaling in combination with a *Gli2* mutation. *Development.,* **127,** 1593-1605.

Park,M. and Moon,R.T. (2001). The planar cell-polarity gene stbm regulates cell behaviour and cell fate in vertebrate embryos. *Nat. Cell Biol.,* **4,** 20-25.

Pavletich,N.P. and Pabo,C.O. (1993). Crystal structure of a five-finger GLI-DNA complex: new perspectives on zinc fingers. *Science,* **261,** 1701-1707.

Peeters,M.C.E., Shum,A.S.W., Hekking,J.W.M., Copp,A.J., and Van Straaten,H.W.M. (1996). Relationship between altered axial curvature and neural tube closure in normal and mutant (*curly tail*) mouse embryos. *Anat. Embryol.,* **193,** 123-130.

Perdomo,J., Holmes,M., Chong,B., and Crossley,M. (2000). Eos and pegasus, two members of the Ikaros family of proteins with distinct DNA binding activities. *J Biol Chem.,* **275,** 38347-38354.

Pinson,K.I., Brennan,J., Monkley,S., Avery,B.J., and Skarnes,W.C. (2000). An LDL-receptor-related protein mediates Wnt signalling in mice. *Nature,* **407,** 535-538.

Purandare,S.M., Ware,S.M., Kwan,K.M., Gebbia,M., Bassi,M.T., Deng,J.M., Vogel,H., Behringer,R.R., Belmont,J.W., and Casey,B. (2002). A complex syndrome of left-right axis, central nervous system and axial skeleton defects in Zic3 mutant mice. *Development.,* **129,** 2293-2302.

Rajadhyaksha,A., Riviere,M., Van Vooren,P., Szpirer,J., Szpirer,C., Babin,J., and Bina,M. (1998). Assignment of AR1, transcription factor 20 (TCF20), to human

chromosome 22q13.3 with somatic cell hybrids and in situ hybridization. *Cytogenet. Cell Genet.*, **81,** 176-177.

Roach,E., Demyer,W., Conneally,P.M., Palmer,C., and Merritt,A.D. (1975). Holoprosencephaly: birth data, benetic and demographic analyses of 30 families. *Birth Defects Orig. Artic. Ser.*, **11,** 294-313.

Ruiz i Altaba,A. (1999). The works of GLI and the power of hedgehog. *Nat. Cell Biol.*, **1,** E147-E148.

Sadler,T.W. (1978). Distribution of surface coat material on fusing neural folds of mouse embryos during neurulation. *Anat. Rec.*, **191,** 345-350.

Sadler,T.W., Greenberg,D., Coughlin,P., and Lessard,J.L. (1982). Actin distribution patterns in the mouse neural tube during neurulation. *Science,* **215,** 172-174.

Sah,V.P., Attardi,L.D., Mulligan,G.J., Williams,B.O., Bronson,R.T., and Jacks,T. (1995). A subset of *p53*-deficient embryos exhibit exencephaly. *Nature Genet.*, **10,** 175-180.

Salero,E., Perez-Sen,R., Aruga,J., Gimenez,C., and Zafra,F. (2001). Transcription factors Zic1 and Zic2 bind and transactivate the apolipoprotein E gene promoter. *J. Biol. Chem.*, **276,** 1881-1888.

Sambrook,J., Fritsch,E.F., and Maniatis,T. (1989). *Molecular cloning. A labolatory manual.* Cold Spring Harbor Labolatory Press.

Schneider-Maunoury,S., Topilko,P., Seitanidou,T., Levi,G., Cohen-Tannoudji,M., Pournin,S., Babinet,C., and Charnay,P. (1993). Disruption of *Krox-20* results in alteration of rhombomeres 3 and 5 in the developing hindbrain. *Cell,* **75,** 1199-1214.

Schoenwolf,G.C. (1984). Histological and ultrastructural studies of secondary neurulation of mouse embryos. *Am. J. Anat.*, **169,** 361-374.

Schoenwolf,G.C. (1985). Shaping and bending of the avian neuroepithelium: morphometric analyses. *Dev. Biol.*, **109,** 127-139.

Scully,R. and Livingston,D.M. (2000). In search of the tumour-suppressor functions of BRCA1 and BRCA2. *Nature,* **408,** 429-432.

Serebriiskii,I., Khazak,V., and Golemis,E.A. (1999). A two-hybrid dual bait system to discriminate specificity of protein interactions. *J. Biol. Chem.,* **274,** 17080-17087.

Sham,M.H., Vesque,C., Nonchev,S., Marshall,H., Frain,M., Das Gupta,R., Whiting,J., Wilkinson,D., Charnay,P., and Krumlauf,R. (1993). The zinc finger gene *Krox20* regulates *HoxB2 (Hox2.8)* during hindbrain segmentation. *Cell,* **72,** 183-196.

Shum,A.S.W. and Copp,A.J. (1996). Regional differences in morphogenesis of the neuroepithelium suggest multiple mechanisms of spinal neurulation in the mouse. *Anat. Embryol.,* **194,** 65-73.

Skarnes,W.C., Auerbach,B.A., and Joyner,A.L. (1992). A gene trap approach in mouse embryonic stem cells: The *lacZ* reporter is activated by splicing, reflects endogenous gene expression, and is mutagenic in mice. *Genes Dev.,* **6,** 903-918.

Smith,J.L. and Schoenwolf,G.C. (1987). Cell cycle and neuroepithelial cell shape during bending of the chick neural plate. *Anat. Rec.,* **218,** 196-206.

Smith,J.L. and Schoenwolf,G.C. (1988). Role of cell-cycle in regulating neuroepithelial cell shape during bending of the chick neural plate. *Cell Tissue Res.,* **252,** 491-500.

Smith,J.L. and Schoenwolf,G.C. (1997). Neurulation: coming to closure. *Trends Neurosci.,* **20,** 510-517.

Smith,J.L., Schoenwolf,G.C., and Quan,J. (1994). Quantitative analyses of neuroepithelial cell shapes during bending of the mouse neural plate. *J. Comp. Neurol.,* **342,** 144-151.

Sporle,R., Gunther,T., Struwe,M., and Schughart,K. (1996). Severe defects in the formation of epaxial musculature in open brain (opb) mutant mouse embryos. *Development.,* **122,** 79-86.

Stark,G. (1977). *Spina Bifida: Problems and Management.* Blackwell Scientific Publications, Oxford.

Stegmann,K., Boecker,J., Kosan,C., Ermert,A., Kunz,J., and Koch,M.C. (1999). Human transcription factor SLUG: mutation analysis in patients with neural tube defects and identification of a missense mutation (D119E) in the Slug subfamily-defining region. *Mutat. Res.,* **406,** 63-69.

Stegmann,K., Boecker,J., Richter,B., Capra,V., Finnell,R.H., Ngo,E.T.K.N., Strehl,E., Ermert,A., and Koch,M.C. (2001). A screen for mutations in human homologues of mice exencephaly genes *Tfap2α* and *Msx2* in patients with neural tube defects. *Teratology.,* **63,** 167-175.

Strong,L.C. and Hollander,W.F. (1949). Hereditary loop-tail in the house mouse. *J. Hered.,* **40,** 329-334.

Stumpo,D.J., Bock,C.B., Tuttle,J.S., and Blackshear,P.J. (1995). MARCKS deficiency in mice leads to abnormal brain development and perinatal death. *Proc. Natl. Acad. Sci. USA,* **92,** 944-948.

Sun,L., Liu,A., and Georgopoulos,K. (1996). Zinc finger-mediated protein interactions modulate Ikaros activity, a molecular control of lymphocyte development. *EMBO J.,* **15,** 5358-5369.

Swiatek,P.J. and Gridley,T. (1993). Perinatal lethality and defects in hindbrain development in mice homozygous for a targeted mutation of the zinc finger gene *Krox20. Genes Dev.,* **7,** 2071-2084.

Tabin,C.J. and McMahon,A. (1997). Recent advances in Hedgehog signalling. *Trends Cell Biol.,* **7,** 442-446.

Takeuchi,T., Kojima,M., Nakajima,K., and Kondo,S. (1999). *jumonji* gene is essential for the neurulation and cardiac development of mouse embryos with a C3H/He background. *Mech. Dev.,* **86,** 29-38.

Tamai,K., Semenov,M., Kato,Y., Spokony,R., Liu,C.M., Katsuyama,Y., Hess,F., Saint-Jeannet,J.P., and He,X. (2000). LDL-receptor-related proteins in Wnt signal transduction. *Nature,* **407,** 530-535.

Theil,T., Frain,M., Gilardi-Hebenstreit,P., Flenniken,A., Charnay,P., and Wilkinson,D.G. (1998). Segmental expression of the *EphA4* (*Sek-1*) receptor tyrosine kinase in the hindbrain is under direct transcriptional control of Krox-20. *Development.,* **125,** 443-452.

Ting,S.B., Wilanowski,T., Auden,A., Hall,M., Voss,A.K., Thomas,T., Parekh,V., Cunningham,J.M., and Jane,S.M. (2003). Inositol- and folate-resistant neural tube defects in mice lacking the epithelial-specific factor Grhl-3. *Nature Med.,* **9,** 1513-1519.

Topilko,P., Schneider-Maunoury,S., Levi,G., Baron-Van Evercooren,A., Chennoufi,A.B.Y., Seitanidou,T., Babinet,C., and Charnay,P. (1994). Krox-20 controls myelination in the peripheral nervous system. *Nature,* **371,** 796-799.

Triezenberg,S.J., Kingsbury,R.C., and McKnight,S.L. (1988). Functional dissection of VP16, the trans-activator of herpes simplex virus immediate early gene expression. *Genes Dev.,* **2,** 718-729.

Tsang,A.P., Fujiwara,Y., Hom,D.B., and Orkin,S.H. (1998). Failure of megakaryopoiesis and arrested erythropoiesis in mice lacking the GATA-1 transcriptional cofactor FOG. *Genes Dev.,* **12,** 1176-1188.

Van Allen,M.I., Kalousek,D.K., Chernoff,G.F., Juriloff,D., Harris,M., McGillivray,B.C., Yong,S.-L., Langlois,S., MacLeod,P.M., Chitayat,D., Friedman,J.M., Wilson,R.D., McFadden,D., Pantzar,J., Ritchie,S., and Hall,J.G. (1993). Evidence for multi-site closure of the neural tube in humans. *Am. J. Med. Genet.,* **47,** 723-743.

Van der Put,N.M.J., Steegers-Theunissen,R.P.M., Frosst,P., Trijbels,F.J.M., Eskes,T.K.A.B., Van den Heuvel,L.P., Mariman,E.C.M., Den Heyer,M., Rozen,R., and Blom,H.J. (1995). Mutated methylenetetrahydrofolate reductase as a risk factor for spina bifida. *Lancet,* **346,** 1070-1071.

Van Straaten,H.W.M. and Copp,A.J. (2001). Curly tail: a 50-year history of the mouse spina bifida model. *Anat. Embryol.,* **203,** 225-237.

Van Straaten,H.W.M., Hekking,J.W.M., Consten,C., and Copp,A.J. (1993). Intrinsic and extrinsic factors in the mechanism of neurulation: effect of curvature of the body axis on closure of the posterior neuropore. *Development.,* **117,** 1163-1172.

Venter,J.C., Adams,M.D., Myers,E.W., Li,P.W., Mural,R.J., Sutton,G.G., Smith,H.O., Yandell,M., Evans,C.A., Holt,R.A., Gocayne,J.D., Amanatides,P., Ballew,R.M., Huson,D.H., Wortman,J.R., Zhang,Q., Kodira,C.D., Zheng,X.H., Chen,L., Skupski,M., Subramanian,G., Thomas,P.D., Zhang,J., Gabor Miklos,G.L., Nelson,C., Broder,S., Clark,A.G., Nadeau,J., McKusick,V.A., Zinder,N., Levine,A.J., Roberts,R.J., Simon,M., Slayman,C., Hunkapiller,M., Bolanos,R., Delcher,A., Dew,I., Fasulo,D., Flanigan,M., Florea,L., Halpern,A., Hannenhalli,S., Kravitz,S., Levy,S., Mobarry,C., Reinert,K., Remington,K., Abu-Threideh,J., Beasley,E., Biddick,K., Bonazzi,V., Brandon,R., Cargill,M., Chandramouliswaran,I., Charlab,R., Chaturvedi,K., Deng,Z., Di,F., V,

Dunn,P., Eilbeck,K., Evangelista,C., Gabrielian,A.E., Gan,W., Ge,W., Gong,F., Gu,Z., Guan,P., Heiman,T.J., Higgins,M.E., Ji,R.R., Ke,Z., Ketchum,K.A., Lai,Z., Lei,Y., Li,Z., Li,J., Liang,Y., Lin,X., Lu,F., Merkulov,G.V., Milshina,N., Moore,H.M., Naik,A.K., Narayan,V.A., Neelam,B., Nusskern,D., Rusch,D.B., Salzberg,S., Shao,W., Shue,B., Sun,J., Wang,Z., Wang,A., Wang,X., Wang,J., Wei,M., Wides,R., Xiao,C., Yan,C., Yao,A., Ye,J., Zhan,M., Zhang,W., Zhang,H., Zhao,Q., Zheng,L., Zhong,F., Zhong,W., Zhu,S., Zhao,S., Gilbert,D., Baumhueter,S., Spier,G., Carter,C., Cravchik,A., Woodage,T., Ali,F., An,H., Awe,A., Baldwin,D., Baden,H., Barnstead,M., Barrow,I., Beeson,K., Busam,D., Carver,A., Center,A., Cheng,M.L., Curry,L., Danaher,S., Davenport,L., Desilets,R., Dietz,S., Dodson,K., Doup,L., Ferriera,S., Garg,N., Gluecksmann,A., Hart,B., Haynes,J., Haynes,C., Heiner,C., Hladun,S., Hostin,D., Houck,J., Howland,T., Ibegwam,C., Johnson,J., Kalush,F., Kline,L., Koduru,S., Love,A., Mann,F., May,D., McCawley,S., McIntosh,T., McMullen,I., Moy,M., Moy,L., Murphy,B., Nelson,K., Pfannkoch,C., Pratts,E., Puri,V., Qureshi,H., Reardon,M., Rodriguez,R., Rogers,Y.H., Romblad,D., Ruhfel,B., Scott,R., Sitter,C., Smallwood,M., Stewart,E., Strong,R., Suh,E., Thomas,R., Tint,N.N., Tse,S., Vech,C., Wang,G., Wetter,J., Williams,S., Williams,M., Windsor,S., Winn-Deen,E., Wolfe,K., Zaveri,J., Zaveri,K., Abril,J.F., Guigo,R., Campbell,M.J., Sjolander,K.V., Karlak,B., Kejariwal,A., Mi,H., Lazareva,B., Hatton,T., Narechania,A., Diemer,K., Muruganujan,A., Guo,N., Sato,S., Bafna,V., Istrail,S., Lippert,R., Schwartz,R., Walenz,B., Yooseph,S., Allen,D., Basu,A., Baxendale,J., Blick,L., Caminha,M., Carnes-Stine,J., Caulk,P., Chiang,Y.H., Coyne,M., Dahlke,C., Mays,A., Dombroski,M., Donnelly,M., Ely,D., Esparham,S., Fosler,C., Gire,H., Glanowski,S., Glasser,K., Glodek,A., Gorokhov,M., Graham,K., Gropman,B., Harris,M., Heil,J., Henderson,S., Hoover,J., Jennings,D., Jordan,C., Jordan,J., Kasha,J., Kagan,L., Kraft,C., Levitsky,A., Lewis,M., Liu,X., Lopez,J., Ma,D., Majoros,W., McDaniel,J., Murphy,S., Newman,M., Nguyen,T., Nguyen,N., and Nodell,M. (2001). The sequence of the human genome. *Science,* **291,** 1304-1351.

Vidal,M. and Legrain,P. (1999). Yeast forward and reverse 'n'-hybrid systems. *Nucleic Acids Res.,* **27,** 919-929.

Wald,N., Sneddon,J., Densem,J., Frost,C., Stone,R., and MRC Vitamin Study Res Group (1991). Prevention of neural tube defects: Results of the Medical Research Council Vitamin Study. *Lancet,* **338,** 131-137.

Wallingford,J.B. and Harland,R.M. (2002). Neural tube closure requires Dishevelled-dependent convergent extension of the midline. *Development.,* **129,** 5815-5825.

Wallingford,J.B., Rowning,B.A., Vogeli,K.M., Rothbächer,U., Fraser,S.E., and Harland,R.M. (2000). Dishevelled controls cell polarity during *Xenopus* gastrulation. *Nature,* **405,** 81-85.

Wang,Z. and Brown,D.D. (1991). A gene expression screen. *Proc. Natl. Acad. Sci. USA,* **88,** 11505-11509.

Ward,I.M., Minn,K., Van Deursen,J., and Chen,J. (2003). p53 Binding Protein 53BP1 is required for DNA damage responses and tumor suppression in mice. *Mol. Cell Biol.,* **23:7,** 2556-2563.

Warner,L.E., Mancias,P., Butler,I.J., McDonald,C.M., Keppen,L., Koob,K.G., and Lupski,J.R. (1998). Mutations in the early growth response 2 (EGR2) gene are associated with hereditary myelinopathies. *Nat Genet.,* **18,** 382-384.

Weatherall,D.J. (1991). The physician scientist: an endangered but far from extinct species. *Br. Med. J.,* **302,** 1002-1005.

Wechsler-Reya,R.J. and Scott,M.P. (1999). Control of neuronal precursor proliferation in the cerebellum by Sonic Hedgehog. *Neuron,* **22,** 103-114.

Wehrli,M., Dougan,S.T., Caldwell,K., O'Keefe,L., Schwartz,S., Vaizel-Ohayon,D., Schejter,E., Tomlinson,A., and DiNardo,S. (2000). Arrow encodes an LDL-receptor-related protein essential for Wingless signalling. *Nature,* **407,** 527-530.

Wilkinson,D.G. (1992). *In Situ Hybridisation: A Practical Approach.* IRL Press, Oxford.

Wilkinson,D.G., Bhatt,S., Chavrier,P., Bravo,R., and Charnay,P. (1989). Segment-specific expression of a zinc-finger gene in the developing nervous system of the mouse. *Nature,* **337,** 461-464.

Wolfe,S.A., Nekludova,L., and Pabo,C.O. (2000). DNA recognition by Cys2His2 zinc finger proteins. *Annu. Rev. Biophys. Biomol. Struct.,* **29,** 183-212.

Wu,M., Chen,D.F., Sasaoka,T., and Tonegawa,S. (1996). Neural tube defects and abnormal brain development in F52- deficient mice. *Proc. Natl. Acad. Sci. USA,* **93,** 2110-2115.

Xu,W.M., Baribault,H., and Adamson,E.D. (1998). Vinculin knockout results in heart and brain defects during embryonic development. *Development.,* **125,** 327-337.

Xu,X., Li,C., Takahashi,K., Slavkin,H.C., Shum,L., and Deng,C.X. (1999). Murine fibroblast growth factor receptor 1alpha isoforms mediate node regression and are essential for posterior mesoderm development. *Dev. Biol.,* **208,** 293-306.

Ybot-Gonzalez,P., Cogram,P., Gerrelli,D., and Copp,A.J. (2002). Sonic hedgehog and the molecular regulation of neural tube closure. *Development.,* **129,** 2507-2517.

Ybot-Gonzalez,P. and Copp,A.J. (1999). Bending of the neural plate during mouse spinal neurulation is independent of actin microfilaments. *Dev. Dyn.,* **215,** 273-283.

Zhang,F. and Jetten,A.M. (2001). Genomic structure of the gene encoding the human GLI-related, Kruppel-like zinc finger protein GLIS2. *Gene,* **280,** 49-57.

Zhang,F., Nakanishi,G., Kurebayashi,S., Yoshino,K., Perantoni,A., Kim,Y.S., and Jetten,A.M. (2002). Characterization of Glis2, a novel gene encoding a Gli-related, Kruppel-like transcription factor with transactivation and repressor functions. Roles in kidney development and neurogenesis. *J. Biol. Chem.,* **277,** 10139-10149.

APPENDIX

Possible role of *Zic2* in the somite segmentation clock

As shown in Figure 3.3 *Zic2* is expressed in the most rostral presomitic (paraxial) mesoderm that will give rise to the somites. The presomitic mesoderm (PSM) is the unsegmented tissue posterior to the somites, which through gene patterning and changes in cell organisation, buds to form the somites at regular intervals of the body axes. The precise timing, periodicity and positioning of the somites is controlled by the segmentation clock, such that cyclic gene expression in the PSM moves from anterior to posterior axes like a wave keeping the timing of maturation of the most anterior cells (reviewed by Giudicelly, F. *et al.*, 2004; Kiefer, JC. *et al.* 2005). Hence cells that are situated in a most anterior position express genes of somite boundary and differentiation, maturing and developing into the new somites. Genes that control the segmentation clock are characterised by cyclic expression within the PSM. Hence *Axin2* and *lunatic fringe* are strongly expressed in the anterior PSM and their expression is reduced in the most posterior PSM and this domain moves anteriorly with time regulating waves of cell maturation (Aulehla, A. *et al.*, 2003). Since expression of *Zic2* did not show cyclic expression in the PSM, rather the expression was always in the two newly undifferentiated somites, it is possible to hypothisise that *Zic2* does not play a role in regulating the segmentation clock itself. However the possibility that *Zic2* may be downstream of the genes regulating the segmentation clock is possible and intriguing. *Zic2* could specify the domain where somite-differentiating genes are activated. A second hypothetical possibility could be that *Zic2* specifies boundary identity of the newly formed somites by binding to spatially restricted co-factors as has been suggested in the parasegment boundary formation of the *Drosophila* body axis (Benedyk, MJ *et al.*, 1994).

Figure 4.8 *Zic2*$^{Ku/Ku}$ fails to form DLHPs at any axial level

Sections through the posterior neuropore of a 15 somite wild type embryo (A-D) and a *Zic2*$^{Ku/Ku}$ embryo (E-H) at the level of the dotted lines indicated in the schematic drawing of the posterior neuropore. (A-B) Show the presence of DLHPs (arrows). (E-F) Sections through the PNP show that the neural folds have a different morphology compared to equivalent axial levels of the wild type embryos (A, B). The neural folds appear thicker and fail to bend dorso-laterally (arrowhead in E). (F) Further caudally the neural folds of the *Zic2*$^{Ku/Ku}$ embryo appear straight in a V shape (arrowheads in F) in contrast to the wild type neural folds, which start to develop DLHPs (arrows in B). At more caudal axial levels no significant difference in the neural plate is seen between the wild type PNP (C-D) and the *Zic2*$^{Ku/Ku}$ PNP (G-F). Abbreviations: nf, neural folds; np, neural plate; pnp, posterior neuropore. Scale bar in A, B, E and F represents 200 μm and in C, D, G, H represents 100μm. The schematic drawing has been modified from A. Copp 1988.

Figure 4.8

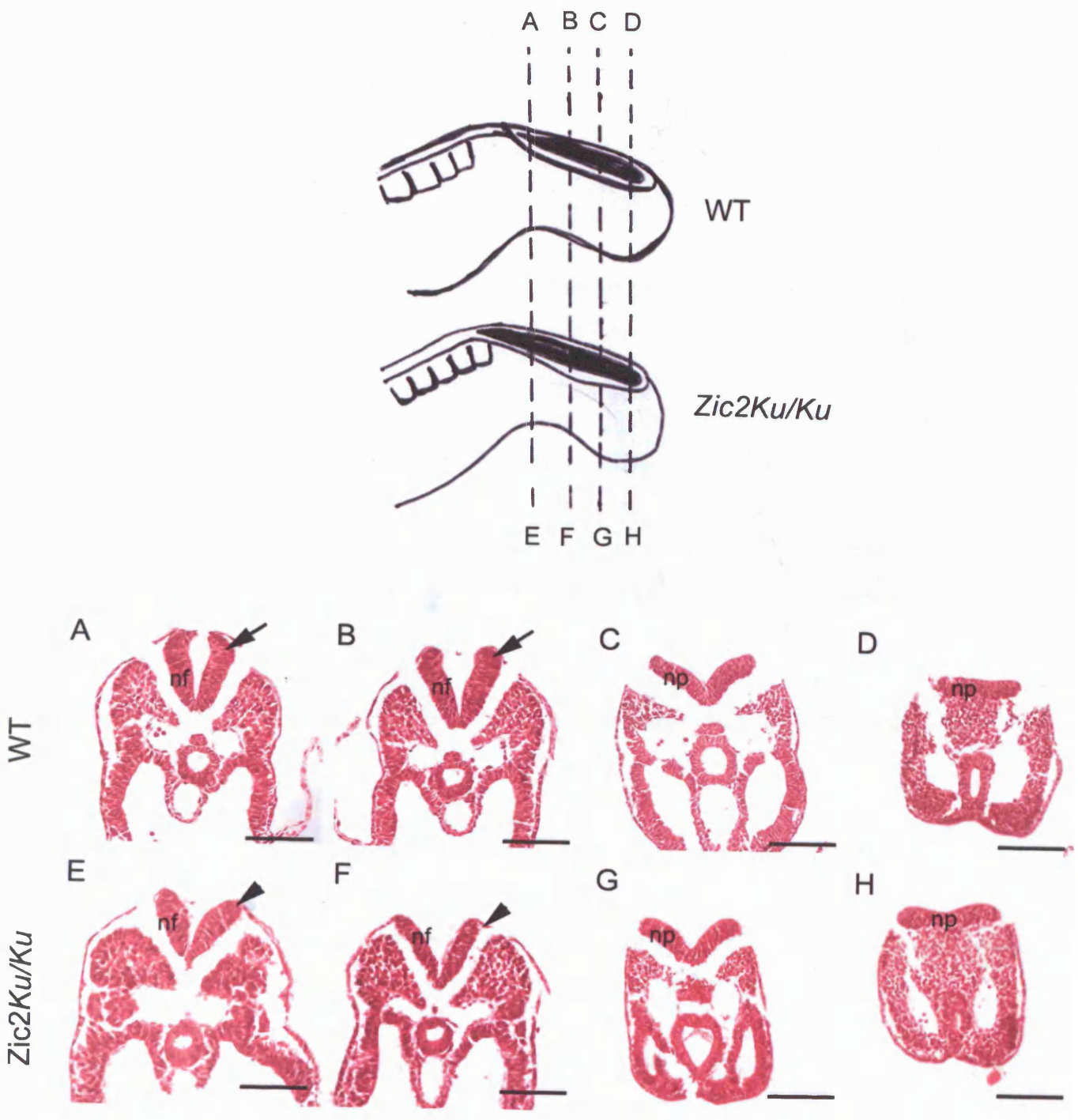

BIBLIOGRAPHY

Aulehla, A., Wehrle, C., Brand-Saberi, B., Kemler, R., Gossler, A., Kanzler, B., Hermann BG. (2003) Wnt3a plays a major role in the segmentation clock controlling somitogensis. *Dev Cell* **4,** 395-406.

Bound, JP., Francis, BJ., Harvery, PW. (1991) Neural tube defects, maternal cohorts, and age: A pointer to aetiology. Ach. Dis. Child. **66,** 1223-1226.

Buccimazza, SS., Tourmente, S., Chapel, S., Sobrier, ML., Couderc, J.L and Dastugue, B. (1994) Prevalence of neural tube defects in Cape Town, South Africa. *Teratology* **50,** 194-199.

Dallaire, L., Melancon, SB., Potier, M., Mathieu, JP., Ducharme, D. (1984) Date of conception and prevention of neural tube defects. *Clin. Gen.*, **26,** 304-307.

EUROCAT Working group (1991) Prevalence of neural tube defects in 20 regions of Europe and the impact of prenatal diagnosis, 1980-1986. *J. Epidimiol. Community Health* 45, 52-58.

Giudicelli, F., Lewis, J.(2004) The vertebrate segmentation clock. *Curr Opin Genet Dev,* **14,** 407-414.

Hunter, AG. (1984) Neural tube defects in Eastern Ontorio and Western Quebec: Demography and family data. *Am. J. Med. Genet.* **19**, 45-63.

Keller-Peck, CR., Mullen, RJ. (1996) Patterns of neuronal differentiation in the neural tube mutant mice: curly tail and Pax3 splotch delay. *J Comp Neurol* **368,** 516-526.

Kiefer, JC. (2005) The somitogenesis segmentation clock: It takes a licking and keeps on ticking. *Dev Dyn* **232**, 519-523.

Nakatsu, T.,Uwabe, C., Shiota, K. (2000) Neural tube closure in humans initiates at multiple sites: evidence from human and implications for the pathogenesis of neural tube degects. *Anat Embryol* **201,** 455-466.

Soler, NG., Walsh, CH., Malins, JM. (1976) Congenital malformations in infants of diabetic mothers. *Q.J. Med.***178**, 303-313.

Sauer F.C. (1935) Mitosis in the neural tube *J. Comp. Neurol.* 62: 377-405.